DISSERTATION

SUBMITTED TO

THE COMBINED FACULTIES FOR

THE NATURAL SCIENCES AND

FOR MATHEMATICS OF

THE RUPERTO-CAROLA UNIVERSITY OF HEIDELBERG, GERMANY

FOR THE DEGREE OF

DOCTOR OF NATURAL SCIENCES

SANDEEP PAUL

INSTITUTE FOR TOXICOLOGY AND GENETICS

FORSCHUNGSZENTRUM KARLSRUHE

Examination Committee:

Prof. Dr. Uwe Strähle

Prof. Dr. Stephan Frings

Prof. Dr. Nicholas Foulkes

Prof. Dr. Gabriele Petersen

Date of the oral exam:……..

DEVELOPING A ZEBRAFISH MODEL FOR MUSCLE REGENERATION

Presented by

SANDEEP PAUL

Institute for Toxicology and Genetics

Forschungzentrum Karlsruhe

DISSERTATION SUBMITTED TO

THE COMBINED FACULTIES FOR THE NATURAL

SCIENCES AND FOR MATHEMATICS OF

THE RUPERTO-CAROLA UNIVERSITY OF HEIDELBERG, GERMANY

FOR THE DEGREE OF

DOCTOR OF NATURAL SCIENCES

For my parents…

Zusammenfassung

Ein besseres Verständnis der Muskelregeneration würde es uns ermöglichen, effektivere Therapien für Patienten zu entwickeln, die unter degenerativen Muskelerkrankungen leiden, wie zum Beispiel muskuläre Dystrophien. Modellorganismen erleichtern das Verständnis von Muskelregeneration, jedoch wurden bis jetzt nur Nagetiere und Hühner entsprechend untersucht.

In der vorliegenden Arbeit wurden drei verschiedene Ansätze angewendet, um ein Modell der Muskelregeneration im Zebrafisch zu erstellen.

Erstens, wurde ein ENU-Mutagenese-Screen durchgeführt, um Mutanten mit defekter Muskelerhaltung zu identifizieren, die möglicherweise auf fehlerhafter Regeneration basiert. Es wurde eine Mutante identifiziert und charakterisiert (*gum*), die einen fortschreitenden Verlust von Beweglichkeit und myofibrillärer Organisation aufweist. Charakterisierung der *gum* Mutanten ließ multiple Defekte in der Muskulatur und in neuronalem und Neuralleisten-Gewebe erkennen.

Zweitens, wurde durch Verwendung eines Acetylcholinesterase-Inhibitors (GAL) ein chemisch induzierbares Modell für Myopathie im Zebrafisch entwickelt. Entfernung von GAL erlaubte es den Muskeln sich zu regenerieren und ihre normale Funktion wiederzuerlangen. Basierend auf Elektronenmikroskopie und Antikörperfärbung wurden vermeintliche Muskelstammzellen (Satellitenzellen) des Zebrafischs identifiziert. Pax7, ein Hauptmarker für Satellitenzellen in allen Wirbeltieren, markiert im Zebrafisch eine Zellschicht, das Dermomyotom, auf der Oberfläche der Somiten ab dem 24 Stunden Stadium (24 hpf). Diese Zellen bilden zunächst FT Muskelfasern (weiße Muskelfasern) und später Satellitenzellen. In dieser Arbeit wurde beobachtet, dass Pax7-positive Dermomyotomzellen erhöhte

Proliferation aufweisen und eine gesteigerte Bewegung in tiefere Schichten des Myotoms nach Beschädigung der Muskulatur.

Drittens, zeigte die Erstellung eines genomweiten Transkriptionsprofils von mit GAL behandelten Zebrafisch-Larven eine Heraufregulierung von zahlreichen Genen als Reaktion auf die Myopathie. Ein Vergleich dieser Gene mit Muskelregenerationsmodellen in der Maus zeigte eine signifikante Übereinstimmung (ca. 25%). Eine Expressionsanalyse einiger dieser Gene (*cmya1*, zgc:100919) deutet darauf hin, dass sie möglicherweise eine Rolle in der Biologie von Satellitenzellen spielen.

Abstract

A better understanding of muscle regeneration would allow us to devise therapies that are more effective for patients suffering from myodegenerative diseases such as muscular dystrophies. Animal models facilitate the understanding of muscle regeneration, but so far, only rodents and chicken have been suitably exploited in this regard.

In the present study, I adopted three different approaches to establish a model of muscle regeneration in zebrafish. Firstly, an ENU mutagenesis screen was performed for mutants with defective muscle maintenance that might result from faulty regeneration. I identified and characterized one mutant (*gum*) showing progressive loss of motility and myofibrillar organization. Characterization of *gum* mutants revealed multiple defects in muscle, neuronal and neural crest derived tissues.

Secondly, using an inhibitor of acetycholinesterase (GAL), I established a chemically inducible model of myopathy in zebrafish. Removal of GAL allowed the muscles to regenerate and restored their normal function. Based on electron microscopy and immunohistochemistry, the zebrafish putative muscle stem cells (satellite cells) were identified. Pax7, a key marker for satellite cells in all vertebrates, labels a layer of cells, the dermomyotome, on the surface of zebrafish somites from 24 hpf onwards. These cells give rise initially, to the fast muscle fibers and later to the satellite cells. In this study, it was observed that the $Pax7^{+ve}$ dermomyotome cells show increased proliferation and migration into deeper myotome upon muscle damage.

Thirdly, unbiased genome wide transcriptional profiling of GAL treated zebrafish larvae showed numerous genes upregulated in response to the myopathy. Comparison of these genes to mouse models of muscle regeneration showed a significant (about 25%) overlap. Expression analysis of some of the genes (*cmya1*, zgc:100919) indicates that they might have a role in satellite cells biology.

"Sandeep, you should be as creative about your sequences as you are about coffee."Uwe

Acknowledgements

This is the most difficult part: to sum up the experience of a few years in a few words, that convention demands but comprehension defies. I would start by thanking Uwe for accepting me as his graduate student, and then forgetting me for large tracts of time. That helped me become independent (I believe, Uwe hopes) to a level where I am now. I would like to thank Lixin for all the initial help in the lab especially for microarray experiments. Yavor made it a lot easier for me to settle down in a new place, both within and outside the lab. Christelle deserves a special mention for being hypercritical of each experiment I did (and still do). Anticipating her questions helps me to improve the quality of my work. I would like to thank Maryam and Sepand, for maintaining the nice social interaction within the lab, and also Maryam for help with microscopy and Sepand for help with especially difficult clonings. I would like to thank Masanari for showing me how to make your data visually appealing and many, many, many discussions/suggestions about labeling and live imaging. Urmas deserves special thanks for maintaining my (in)sanity in trying times with his humor, which I appreciate even more than his skills in photography. I would like to thank Martin for the excellent (I have been told so by native speakers) German translation of the abstract of my thesis. I would also like to thank Olivier for not only all the help with molecular biology, gene ontology, microarrays etc, but also for entertaining us with his adorable French accent. I should also thank the fish facility staff; without their indefatigable care I would have never learned how to take care of my fish.

That this report has so few mistakes is due to the diligent, untiring and (mostly) brutal editing of Thomas. Not that he did it willingly; I had to cajole, beg, grovel, and finally threaten him in equal measure. If it has many mistakes it is due to my confusion between picking corrected copies vs. uncorrected ones.

And finally, I would like to thank Simone, for everything else and more.

Table of Contents

List of Abbreviations

ABCs	Anterior Border Cells
BAC	Bacterial Artificial Chromosome
bHLH	basic helix-loop-helix
bp	base pair
BSA	bovine serum albumin
cDNA	complementary Deoxyribonucleic Acid
DAB	3,3´-diaminobenzidine
DEPC	diethylpyrocarbonate
DMSO	dimethylsulfoxide
Dpf	Days post fertilization
DTT	dithiothreitol
EDTA	ethylenediamine tetraacetic acid
EM	electron microscopy
FACS	fluorescence activated cell sorting
GAL	Galanthamine Hydrobromide
GFP	green fluorescent protein
HGF	hepatocytes growth factor
Hpf	Hours post fertilitzation
IHC	Immunohistochemistry
IRF	interferon regulatory factor
ISH	In situ hybridization
Kb	kilobase
mesab	3-aminobenzoic acid-ethyl ester methanesulfonate
MO	morpholino
MPCs	Myogenic Precursor Cells
mRNA	messenger RNA
myf 6/MRF 4	Myogenic factor 6 /Muscle regulatory factor 4

Myf5	Myogenic factor 5
MyoD	Myogenic Diffrentiation
myog	myogenin
Pax3	paired box gene 3
Pax7	paired box gene 7
PBS	phosphate-buffered saline
PCR	polymerase chain reaction
PFA	paraformaldehyde
PTU	1-phenyl-2-thiourea
RNAi	Ribonucleic Acid interference
RT PCR	reverse transcriptase polymerase chain reaction
SP	side population
TEM	Transmission Electron Microscopy

List of Tables

List of Figures

"Nature must be explained by Nature, not by our own views." Abraham Trembley

1 Introduction

1.1 Regeneration in metazoans

Regenerating body parts has fostered human imagination like few other things. Aristotle (384–322 BC) was perhaps the first scientist to observe that the tails of lizards and snakes, as well as the eyes of swallow-chicks, could regenerate (Peck AL, 1965). In 1712, the French scientist René-Antoine Ferchault de Réaumur turned this fascination into a proper scientific enquiry when he published his seminal work on crayfish limb and claw regeneration (Réaumur, 1712). Soon after, a wide variety of animals were described to show regeneration of different body parts, in the works of Abraham Trembley (Hydra, 1740) (Lenhoff SG, 1986), Peter Simon Pallas (planarians, 1766) (Pallas, 1766), and Lazzaro Spallanzani (tadpole tails; salamander jaws, limbs, tails and eyes, 1768) (Spallanzani, 1769). As for humans, it was shown after two centuries of Trembley's discovery that human liver can regenerate (Widmann JJ 1975).

Despite a long history of reports about regeneration, and the knowledge that understanding regeneration would shed light on issues such as tissue polarity, patterning, and the control of size and proportion in animals, our understanding of regenerative biology is woefully inadequate. The reasons for this are many. For example, one puzzling aspect of regeneration that has limited our understanding is why the regenerative capacity manifests itself during evolution in some organisms and not in others, even within the same phyla. The model organisms such as *Drosophila melanogaster*, *Caenorhabditis elegans*, *Xenopus*, chicken and mice that proved so useful in advancing our knowledge in genetics and developmental biology

and later molecular biology, display either limited abilities to regenerate or were overlooked in the context of studies on regeneration. On the other hand, those model organisms which show tremendous regenerative abilities, such as axolotls, urodeles and salamanders, have been extremely refractory to genetic and molecular manipulations. However, the last twenty years have seen a spurt in growth of our understanding of regenerative processes as basic advances in genetics; genomics, development and molecular biology have been successfully applied to study of regeneration. Moreover, developmental biologists have begun to investigate the so far overlooked regenerative abilities of genetic model systems such as *Drosophila melanogaster* (Bosch et al., 2008; Marsh and Theisen, 1999; McClure and Schubiger, 2007). The introduction of methodologies such as RNA-mediated genetic interference (RNAi) and the introduction of functional genomics and transgenic methodologies in hydra, planarians, and salamanders (Sanchez Alvarado and Tsonis, 2006) have increased the resolution of molecular analyses in those animals species showing a high degree of regenerative ability. The emergence of new vertebrate models such as zebrafish that are highly amenable to genetic manipulations yet show a greater degree of regenerative ability than most mammals has also advanced the acceleration of research in this field (Curado et al., 2007; Lepilina et al., 2006; Stoick-Cooper et al., 2007).

1.2 Mechanism of Regenerations: Stem Cells vs. De-differentiation

1.2.1 Stem cells and stem cell niche

The consensus amongst researchers is that so-called progenitor cells are required for most regenerative processes. However, the origin of these progenitor

cells varies between regenerating systems. The progenitor cell could be either set aside during development or arise *de novo* by a mechanism involving reversal of embryonic development where a terminally differentiated cell reverts to its uncommitted state. This process, termed as cellular dedifferentiation, is especially prominent in animals with exceptional regenerative abilities like salamanders.

The progenitors set aside during development, called "stem cells", are normally mitotically quiescent and respond to normal tissue wear and tear or tissue damage by taking on a program of multiplication and differentiation to lead effective regeneration. The regular turnover or regeneration of skin, blood, muscle and bone in mammals and the replacement of lost tissues in the flatworm planarian are but a few examples of such stem cell mediated regeneration. The quintessential stem cell would be capable of limitless self-renewal and differentiation capability. The closest mammalian stem cells comes to this "ideal" state is the cells of the inner cell mass (ICM) that are found in the blastocyst. These cells from the inner cell mass give rise to the entire embryo (Rossant, 2008) and perhaps some extra-embryonic membranes (Solter, 2006). When taken out and grown in culture these cells give rise to the embryonic stem (ES) cells.

Although it has been show shown that an entire mouse could be generated from a single ES cell, the extra embryonic membrane and the placenta were derived from a tetraploid embryo (Nagy et al., 1993). For this reason an ES cell could not be considered a "totipotent" cell. The terms "stem cell" and "progenitor cell" are sometimes used interchangeably but strictly speaking stem cells, such as the ES cells, are capable of unlimited self renewal and are pluripotent while progenitor cells have a limited capacity to self renew and are only multipotent. "Pluripotent" cells can give rise to derivatives of all three germ layers whereas "multipotent" cells can only give

rise to several cell types which are restricted to the derivatives of a single germ layer or to a specific sublineage (Solter, 2006). By these strict criteria, all adult "stem cells" should rather be termed multipotent progenitor cells which would become increasingly fate restricted as they move through their lineage. Since the term stem cell is now widely used in the literature also describing these cell types, here we include pluripotent cells in this term. Examples of such tissue specific progenitor cells include, in *Drosophila melanogaster*, germline stem cells (Lopez-Onieva et al., 2008; Yamashita et al., 2007), follicle stem cells (Nystul and Spradling, 2007), intestinal stem cells (Ohlstein and Spradling, 2007), and escort stem cells (Gilboa and Lehmann, 2006). In mammals some of the examples of such progenitor cells are haematopoetic stem cells (Adams and Scadden, 2006), the neural "stem cells" in the subventricular zone and the dentate gyrus of the hippocampus in the mammalian adult central nervous system (Taupin and Gage, 2002), skeletal muscle satellite cells (Dhawan and Rando, 2005), and interfollicular epidermis cells (Clayton et al., 2007).

The stem cells reside in restricted tissue microenvironments known as "niches". The niche provides localized signals for the maintenance of the stem cell population and houses one or more stem cell(s) of the same kind. To be definitely qualified as a stem cell niche, a candidate niche must be transiently depleted of its full complement of stem cells and then be shown to take up and maintain a newly introduced stem cell. For example, the demonstration that new *Drosophila* germline stem cells (GSCs) can be introduced and maintained at the gonad tips by local signals provided the clearest evidence of gonad tips acting as GSC niche (Brawley and Matunis, 2004; Tulina and Matunis, 2001; Xie and Spradling, 2000). Other examples of stem cell niches in *Drosophila* are the follicle stem cell niche (Nystul and Spradling, 2007) and the intestinal stem cell niche (Ohlstein and Spradling, 2007). In

vertebrates, the stem cells niches have been defined for haematopoetic stem cells (Adams and Scadden, 2006), central nervous system subventricular zone stem cells (Doetsch, 2003), intestinal epithelium (Barker et al., 2007), hair follicle bulge (Blanpain and Fuchs, 2006), spermatogonial stem cells (Blanpain and Fuchs, 2006; Yoshida et al., 2007a; Yoshida et al., 2007b) and muscle satellite cells (Dhawan and Rando, 2005), among others. Upon sensing tissue damage by local signals such as mechanical stress or secreted signals (for example, from macrophages) the stem cells leave their niche, transiently amplify, generate tissue precursors and finally repair or regenerate the damaged tissue. At the same time, the stem cells must also replenish themselves and repopulate the niche.

1.2.2 Strategies of stem cell propagation: Asymmetric vs. Symmetric division

A stem cell must self renew as well as produce differentiated progeny to achieve these dual tasks and it must do so while maintaining the tissue homeostasis; too much self renewal would lead to cancer and too much differentiation would lead to depletion of the stem cell pool. The mechanisms of how stem cells generate asymmetric progeny have begun to emerge with the discovery of asymmetric cell division. Stem cells maintain a balance between self-renewal and differentiation by employing both asymmetric cell division as well as symmetric cell divisions according to the requirements of the organism. Under normal conditions of tissue maintenance, stem cells can employ asymmetric divisions to produce one daughter stem cell and one cell capable of differentiation. The asymmetry can be “intrinsic” to the stem cell itself in the form of asymmetrically localized proteins during cell division to generate a polarity within the cell. These proteins act as cell fate determinants to give rise to the divergent progeny of stem cells. A good example of a

cell showing intrinsic asymmetric cell divisions is the *C. elegans* zygote, where asymmetry is defined by the sperm entry site (Cowan and Hyman, 2004; Goldstein and Hird, 1996). The *C. elegans* zygote divides into a large blastomere that would give rise to ectoderm and a smaller blastomere that would produce mesoderm, endoderm and germline in a series of asymmetric cell divisions (Doe and Bowerman, 2001). Although the zygote is not a typical stem cell, it uses many of the molecules used by stem cells for asymmetric divisions in a similar manner. These include PAR3, PAR6 and atypical protein kinase C (aPKC) that are all asymmetrically localized during cell cycle. These proteins in turn govern cell fate determinants like ribonucleoprotein particles known as P granules and PIE-1, a transcriptional repressor required for germline fate determination (Mello et al., 1992; Mello et al., 1996; Reese et al., 2000; Shimada et al., 2006; Strome, 2005; Strome and Wood, 1983). Also in *Drosophila* neuroblast cell divisions, Numb, an evolutionarily conserved cell fate determinant is asymmetrically localized to the cells that are destined to differentiate (Spana et al., 1995). Another mechanism to generate asymmetric progeny is via the so-called "extrinsic" asymmetry, where the stem cells divide with a reproducible orientation relative to the niche. In this case the fate acquisition depends on external signals emanating from the niche and loss of contact with the niche can trigger differentiation in one of the progeny. A classic example are the Drosophila germline stem cells (Spradling et al., 2001; Xie and Spradling, 2000; Yamashita et al., 2005). The niche is created by the cap cells in the *Drosophila* ovary (Xie and Spradling, 2000) and the hub cells in the *Drosophila* testis (Kiger et al., 2001; Tulina and Matunis, 2001). In the ovary, the members of Bone Morphogenetic Protein (BMP) family of growth factors, Decapentaplegic (DPP) and Glass Bottom Boat (GBB), emanating from the niche serve to repress the differentiation promoting gene *bag-of-*

marbles (Chen and McKearin, 2003; Song et al., 2004). In the testis, a ligand called Unpaired is expressed by the hub cells. Unpaired activates the JAK-STAT (Janus kinase and signal transducer and activator of transcription) signaling cascade in the germline cells to keep them undifferentiated (Kiger et al., 2001; Tulina and Matunis, 2001; Yamashita et al., 2005).

Asymmetric cell divisions maintain a steady supply of progeny capable of differentiation and stem cells. However, during development or regeneration there is a demand for exponential increase in numbers of both cell types. This demand can be met by the stem cells by switching to a mode of symmetric divisions. Under such conditions stem cells can rapidly multiply either to increase or to replenish a diminished stem cell pool. Once enough stem cells have been generated, some of them would start to differentiate stochastically. For example, mouse haematopoietic stem (HS) cells double in number every day during mid-gestation (Morrison et al., 1995), a rate of expansion that cannot be achieved by asymmetric cell division. Also direct imaging of the divisions of neural progenitors in slice cultures of the developing rodent cerebral cortex (Chenn and McConnell, 1995; Huttner and Kosodo, 2005; Noctor et al., 2004) has revealed an exponential expansion that seems to produce morphologically identical undifferentiated cells. However, it remains possible that these cells retain a divergent developmental potential than their siblings. In the absence of more direct evidence of their developmental fate inferences regarding the involvement of symmetric divisions remain provisional.

1.2.3 Cellular dedifferentiation

In certain cases, the progenitor cells can be created de novo through a process in which fully differentiated cells reverse their normal developmental processes and

revert to proliferating progenitor cells. This alternative regeneration strategy relies on the ability of some post-mitotic cells to dedifferentiate or transdifferentiate to repair damaged organs. Hydra's extreme regenerative capacity is well documented. Hydra does not regenerate by cell proliferation. For example, decapitation of Hydra resets positional information along the remaining body axis, forcing the cells in the gastric column to undergo transdifferentiation and form the missing head (Wolpert et al., 1971). Certain tissues in higher vertebrates such as the mammalian pancreas also employ a similar strategy. Studies in rodents have shown that during acute pancreatitis ß- cells are derived from non-endocrine cells (Adler et al., 1979; Hao et al., 2006). Among vertebrates, cellular dedifferentiation is especially prominent in animals with exceptional regenerative abilities, such as Urodele amphibians like salamanders and newts. The red spotted newt (*Notophthalmus viridescens*) can regenerate entire limbs, brain, jaw, heart, intestines, spinal cord, tail, retina, lens and optic nerve (Jamie Morrison Pers. Comm., MYORES Workshop: Muscle Regeneration and Stem Cells: a multiorganismic approach in Niepolomice, Poland, October 12- 15, 2008). During salamander limb regeneration, cells from muscle, bone, cartilage, nerve sheath, and connective tissues participate in the dedifferentiation process to form a pool of proliferating progenitor cells in the regeneration blastema (Bodemer CW, 1959; Chalkley, 1954; Hay and Fischman, 1961; Kumar et al., 2000; Lo et al., 1993; Wallace et al., 1974). These blastemal cells redifferentiate and give rise to all the internal tissues of the regenerated limb. Therefore, in contrast to hydra, cellular dedifferentiation followed by amplification is the mode of regeneration in salamanders.

1.3 Muscular Dystrophies: The need for understanding Muscle Regeneration

Unlike many other mammalian tissue types, skeletal muscle tissue shows very high regenerative capacity (Charge and Rudnicki, 2004). On one hand, this provides us with an excellent model to study basic processes involved in tissue regeneration. On the other hand, understanding these processes better would help us in designing more effective treatment strategies for patients suffering from heritable muscle wasting diseases such as muscular dystrophies.

Muscular dystrophies range from early onset, debilitating conditions, which confine the patient to a wheelchair and lead to an early death resulting from cardiac or respiratory failure, to late onset conditions (40 years and beyond), in which the patient can lead an almost normal life with varying degrees of muscle loss. The most common muscular dystrophies are the Duchenne, Becker, Limb Girdle, Congenital, Facioscapulohumeral, Myotonic, Oculopharyngeal, distal and Emery-Dreifuss muscular dystrophies. Altogether there are over 25 genes now known to produce various muscular dystrophies (Heydemann et al., 2007). Duchenne muscular dystrophy (DMD), a debilitating X linked disorder, is the most common form of muscular dystrophy (Emery, 1991). It results from mutations in the *dystrophin* gene and is found at a high frequency of 1 in 3500 male newborns (Hoffman et al., 1992). The *dystrophin* gene is the largest human gene to be identified so far (Koenig et al., 1987). It comprises of 79 exons spanning atleast 2,300 kilobases (kb) (Tennyson et al., 1995). Consequently, it is a prime candidate for accumulating mutations. It encodes a 427 kDa protein that becomes strongly glycosylated (Ozawa et al., 1995; Yoshida et al., 1994) and forms a mesh with cytoskeletal intracellular proteins like F-Actin, dystrophin, dystrobrevin and syntrophins, the transmembrane proteins

dystroglycans, sarcoglycans and integrins, and the extracellular matrix proteins such as Laminins and agrins (Ervasti et al., 1990). This meshwork, called the Dystrophin Associated Protein Complex (DAPC), is a major structural link holding the myofibers and the basal lamina together. Mutations in several of these genes result in a weakening of the DAPC complex and can result in a muscular dystrophy. For example, the four recessive limb girdle muscular dystrophies 2D, 2E, 2C and 2F are caused by absence of α, ß, γ or δ sarcoglycans, respectively (Hack et al., 2000; Heydemann et al., 2007; Wagner, 2002). Disrupting the cytoskeletal-ECM connections renders the myofiber membrane fragile, as the contractile forces of the myofiber are not transferred to the ECM. As a consequence of this intense stress the the muscle plasma membrane (sarcolemma) develop tears. Indeed, electron microscopy analysis and biopsies of muscular dystrophy patients have revealed numerous membrane lesions (Mokri and Engel, 1975) and also showed an increased uptake of membrane-impermeable dyes, and presence of non-muscle proteins inside of dystrophic muscle (Pestronk et al., 1982; Straub et al., 2000). Disruption of myofibers by membrane instability probably leads to elevated intracellular calcium levels. Elevated calcium in muscle fibers of muscular dystrophy patients and *mdx* mice (a mouse model of human Duchenne Muscular Dystrophy) has been demonstrated (De Backer et al., 2002; Robert et al., 2001; Turner et al., 1991). A high intracellular concentration of Ca^{+} can lead to activation of Ca^{++} activated neutral proteases such as Calpain3. Calpain3 is a muscle specific calpain that is essential for sarcomeric organization by modulating stability of structural proteins such as myosin light chain 1 (Cohen et al., 2006) and titin (Huebsch et al., 2005). Moreover, Calpain 3 can cleave filamin C and regulate its ability to bind to γ- and δ-sarcoglycans (Guyon et al., 2003). Hyperactive Calpain may thus digest more structural proteins and

dynamics of protein turnover are disturbed thus weakening the muscle further. Increased intracellular Ca^{++} may also cause mitochondrial dysfunction in the muscles, thus resulting in a dystrophy via an alternative pathway (Robert et al., 2001; Vandebrouck et al., 2006). Hence, elevated levels of Ca^{++} ions could lead to a myopathy that could manifest itself as a muscular dystrophy. Additionally, dystrophin-deficient myotubes are susceptible to oxidative damage (Rando et al., 1998). The initial damage to myotubes activates satellite cells and they proceed to repair the dystrophic muscles (Charge and Rudnicki, 2004; Wallace and McNally, 2008). However, repeated rounds of satellite cells activation and muscle repair might cause replicative senescence of the satellite cell pool (Bigot et al., 2008) that may further contribute to the progression of the disease. How this may happen is not understood and is an active area of research.

As of now there are no definite treatments available for muscular dystrophies and they are treated mostly symptomatically. Promising therapeutic avenues of gene replacement, stem cell transplantation, pharmaceuticals, and upregulation of endogenous compensatory proteins have all been explored. Some of these methods are in clinical trials. For example, one of the therapies undergoing clinical trials till recently was based on using an antibody (MYO-029) blocking the activity of myostatin (initially called growth/differentiation factor-8 [GDF-8]), a TGF-ß family member that is a negative regulator of muscle growth. Normally, myostatin activity would regulate the skeletal muscle mass and terminate myofiber growth (Joulia et al., 2003; Langley et al., 2002; McPherron et al., 1997; Rios et al., 2002). Mutations in the myostatin gene result in animals with a huge increase in muscle mass (Kambadur et al., 1997; McPherron and Lee, 1997; Westhusin, 1997). Therefore, using an antibody against myostatin seemed like a promising way to counter muscle wasting

diseases. Unfortunately, even though the use of MYO-029 in adult subjects with muscular dystrophy produced a significant increase in muscle fiber size (10-15%), it did not result in increased muscle strength in a nine month trial period (Wagner et al., 2008). Wyeth pharmaceuticals, Madison, New Jersey, USA, the manufacturers of MYO-029 have decided not to continue development of this recombinant antibody. The details of the clinical trials can be accessed at United States National Institute of Health website at *http://www.clinicaltrials.gov/ct2/show/NCT00104078?term=MYO-029&rank=2*. This study, among others, underscores the importance of having a better understanding of both the diseases themselves and the biology of muscle regeneration and muscle stem cells. Coherent systemic ability to quantitatively manipulate information from a systems biology level understanding of muscle regeneration might be necessary to design therapies that influence multiple processes, just the right amount, at a time in a spatially and temporally coherent manner.

1.4 Embryonic myogenesis and the origin of muscle stem cells

Since any regenerative event may tend to recapitulate an embryonic development paradigm (such as dedifferentiation), let us now take a brief look at the development of musculature in vertebrates. Most of our understanding about vertebrate myogenesis comes from the work done in chick and mouse models, although in recent years zebrafish has emerged as an important contributor to this field. We will first briefly review the basic paradigms of myogenesis in mouse/chick model and then compare these to what is known in zebrafish.

1.4.1 Early mesoderm and its derivatives

In vertebrate embryos, during gastrulation the mesoderm comes to lie underneath the ectoderm. Shortly after gastrulation, during neurulation, the invagination and folding of ectoderm to form the neural tube, the mesodermal cell population is split into two halves on either side of the neural tube. Some mesodermal cells left underneath the ventral section of the neural tube (the chordamesoderm) develop into the notochord. As the embryonic development proceeds, the masses of mesodermal cells placed on either side of the neural tube become organized into somites, transient condensations of mesodermal tissue that form in a metameric fashion as they are pinched off the pre somitic mesoderm (PSM). At this time the mesoderm can be subdivided into five regions. 1) The "chordamesoderm", the tissue that gives rise to the notochord, a transient organ that establishes the anterior-posterior body axis. 2) The "paraxial mesoderm" that forms the somites. The somites give rise to many of the tissues of the back such as muscle, cartilage, bone, and dermis. 3) The "intermediate mesoderm" which forms the urinogenital system, comprising of the kidneys, the gonads and their associated ducts. It also forms the cortical part of adrenal gland. 4) The "lateral plate mesoderm" gives rise to the heart and the circulatory system, blood cells, lining of the body cavities and all the mesodermal components of the limbs except muscle. Finally 5) the "head mesenchyme" gives rise to the connective tissue and muscles of the face. A schematic of mesoderm derived tissues is shown in Fig. 1.

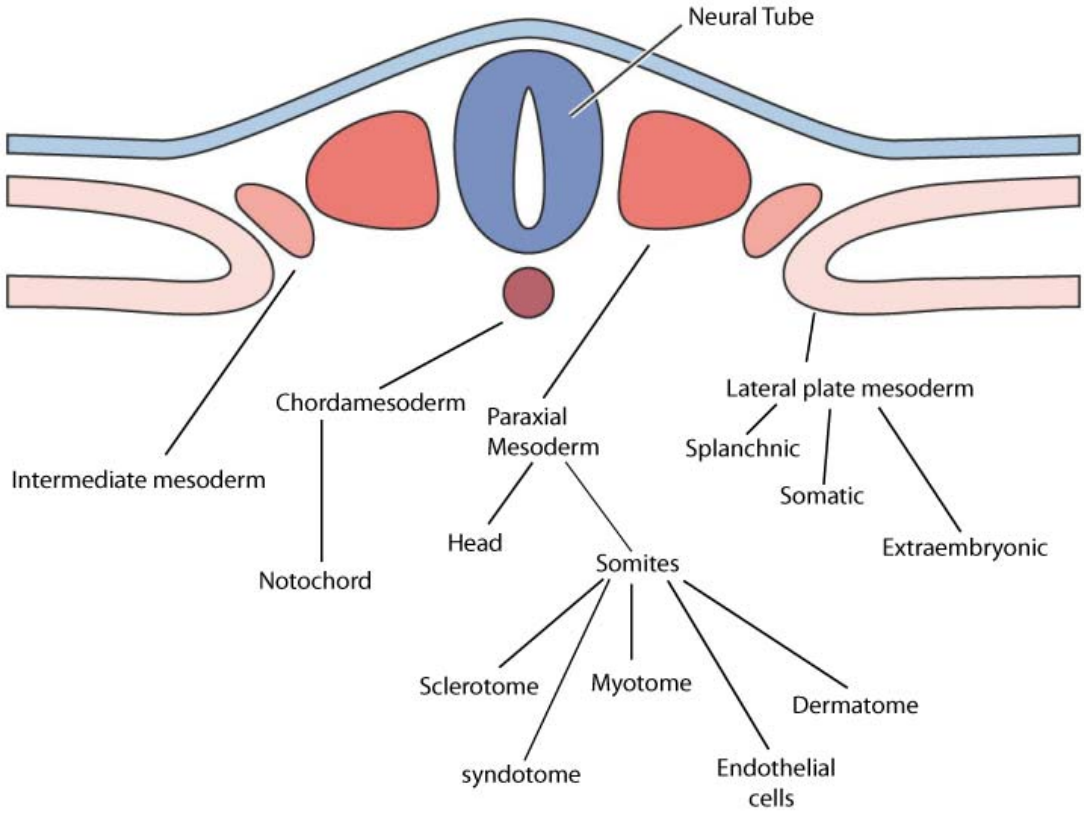

Figure1: Transverse section of an idealized chick embryo showing mesoderm and tissues derived from it (except neural tube). See text for details. Figure adapted from Developmental Biology by Scott F. Gilbert (6th Edition).

Neurulation and the formation of somites proceed in an anterior to posterior manner such that the anterior somites are formed first and the posterior somites later (Fig. 3 and Fig. 4). The segmentation of the PSM is a complex process that depends on complex genetic interactions involving highly dynamic gene expression. Despite identification of several key molecular players in this process it is not understood very well. A few models have been proposed to understand certain subsets of segmentation but a mechanistic understanding of the whole process has not yet been achieved. Since somites form at regular intervals; every 2 hours in mouse, 90 minutes in chick and 30 minutes in zebrafish; it has been proposed that there is a segmentation clock at work during segmentation. . First proposed by Cooke and Zeeman in 1976, the

"clock-and-wavefront model" proposes the existence of a cellular clock that might interact with a slowly progressing wave (wavefront) that moves along the presomitic mesoderm from anterior to posterior at a constant velocity to produce the periodic series of somites (Cooke and Zeeman, 1976). The interaction between the wave and the oscillator was proposed to allocate cells to individual somites in a regular fashion along the anteroposterior axis.

The first evidence for segmentation clock came from the observations that a Notch target gene, *c-hairy 1,* is expressed in rhythmic waves in the PSM in chick embryos with the same periodicity as the somite formation (90 minutes) (Palmeirim et al., 1997). Thereafter, several genes exhibiting a dynamic oscillatory expression pattern in PSM were identifies in fish, frog, chick and mouse embryos, pointing towards a conserved mechanism of segmentation clock in vertebrates. These genes include *lunatic fringe* (*lfng*) (Aulehla and Johnson, 1999; Forsberg et al., 1998), *Hes1* (Jouve et al., 2000), *Hey2* (Leimeister et al., 2000) and *Hes7* (Bessho et al., 2003; Bessho et al., 2001) in mouse; *c-hairy2*, *c-Hey2/HRT2* (Leimeister et al., 2000) and *Lfng* (Aulehla and Johnson, 1999; McGrew et al., 1998) in chick; *her1* (Holley et al., 2000; Sawada et al., 2001), *deltaC* (Jiang et al., 2000) and *her7* (Gajewski et al., 2003; Oates and Ho, 2002) in zebrafish; and *esr9* and *esr10* in Xenopus (Li et al., 2003b). In accordance with the cyclic nature of somitogenesis, these genes oscillate in phase and their expression is driven by Notch signaling (Barrantes et al., 1999; Jouve et al., 2000; Leimeister et al., 2000; Oates and Ho, 2002; Sieger et al., 2003; Takke and Campos-Ortega, 1999). Several of these genes have been demonstrated to form part of a negative feedback transcriptional regulatory loop which keeps the segmentation clock ticking.

Activation of Notch signalling via Delta cleaves the Notch intracellular domain (NICD) (Huppert et al., 2005; Morimoto et al., 2005) and it translocated to the nucleus (Kidd et al., 1998; Kopan et al., 1996; Lecourtois and Schweisguth, 1998; Struhl and Adachi, 1998). Once within nucleus NICD binds to Supressesor of Hairless (SuH)/RBP Jκ (Jarriault et al., 1995; Lu and Lux, 1996) and activates Notch responsive genes including the glycosyltransferase, Lunatic fringe (Lnfg) (Cole et al., 2002; Morales et al., 2002). Lnfg can modulate ligand-receptor affinity of Notch by modification of the extracellular domain of Notch (Bruckner et al., 2000; Moloney et al., 2000; Panin et al., 1997). Since Notch signaling becomes constitutively active in *lunatic fringe* mutants (Morimoto et al., 2005) it is believed that Lunatic Fringe acts to inhibit Notch, forming a negative feedback loop. This would lead to a diminished activity of Notch as Lfng accumulates. The repression on Notch activity is removed as Lfng undergoes degradation and no fresh Lfng is transcribed (due to Notch activity being compromised). A reduction in Lfng causes increased Notch activity which in turn continues the whole cycle again (Fig. 2).

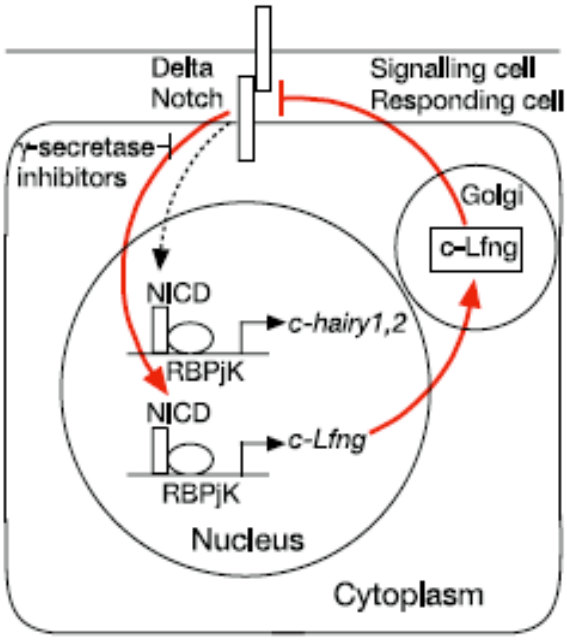

Figure 2: Model of an oscillator mechanism based on negative feedback. Notch signalling activates cyclic gene transcription. Lfng then closes the loop by modifying Notch, thereby inhibiting Notch signalling. This negative effect is transient owing to the rapid turnover of Lfng. NICD, NotchICD. Adapted from (Dale et al., 2003).

The second key component of the model proposed by Cooke and Zeeman was the "wavefront", a maturation wave moving in the anterior to posterior direction (A-P) (Cooke and Zeeman, 1976). It was observed that *fibroblast growth factor 8 (fgf8)* transcripts form an A-P gradient along the PSM (Dubrulle et al., 2001). Increasing the local concentration on FGF8 protein in the PSM caused reduction in somite size, and inhibition of FGF8 signaling resulted in generation of larger somites. Recent work by Dubrulle and colleagues showed that the de novo *fgf8* mRNA synthesis is restricted to the tail bud and that the *fgf8* mRNA as well as the protein gradient is formed as a result of mRNA decay (Dubrulle and Pourquie, 2004). Blocking the FGF signaling in mouse tail explants with SU5402, an inhibitor of the tyrosine kinase activity of the FGF Receptor, resulted in quick loss of cyclic expression of *axin2* and *sprouty2* (an FGF target gene) but *Lfng* oscillations took a day to subside. This clearly shows that

Notch signaling is an indirect target of FGF signaling during segmentation (Wahl et al., 2007).

Although the clock and wavefront model explains some aspects of somitogenesis, it does not explain the anterior-posterior polarity generated within the somite. Other models have been proposed to explain specific aspects of somitogenesis (Collier et al., 2000; Flint et al., 1978; Kerszberg and Wolpert, 2000; Meinhardt, 1986; Polezhaev, 1992) but none of them, as yet, give a holistic explanation of somitogenesis. Finally, depending on their position along the anteroposterior (AP) axis, somite derivatives acquire a defined anatomical identity that is imposed mainly by Hox genes that control their subsequent regional differentiation (Kmita and Duboule, 2003; Wellik, 2007).

1.4.3 Muscle development from the somites: A morphological overview

Different regions in the somite give rise to different kind of cells. The most ventral cells become mesenchymal and form the sclerotome (Fig. 4), which gives rise to the ribs and vertebrae. The dorsal part of the somite forms the dermomyotome (Fig. 4) which gives rise to muscles and the dermis of the skin. The dermomyotome itself is subdivided into medial and lateral halves. The medial part, also called epaxial dermomyotome, is closer to the neural tube and the lateral part (also called hypaxial dermomyotome) is furthest away from the neural tube (Fig. 4). Cells from the medial dermomyotome turn inwards (called the Dorsomedial lip, DML) (Denetclaw et al., 1997) and form the myotome (Fig. 4), from which the muscle progenitor cells called embryonic myoblasts (Fig. 4) will arise and form the axial muscles (Fig. 4) of the body. The cells at the ventral most edge of the hypaxial dermomyotome also turn inwards and the edge is now called the Venterolateral lip, VLL (Denetclaw and

Ordahl, 2000) (Fig. 4). The behavior of cells at the VLL depends on their axial level. At the limb bud level, cells from VLL will delaminate and migrate into the lateral plate mesoderm where they would differentiate to form limb and limb girdle muscles(Chevallier et al., 1977). At interlimb levels, cells at the VLL translocate underneath to produce the hypaxial myotome (Cinnamon et al., 1999; Denetclaw and Ordahl, 2000). The VLL and hypaxial myotome invade the lateral plate mesoderm together as a somitic bud, which gives rise to the body wall and abdominal muscle (Christ et al., 1983).

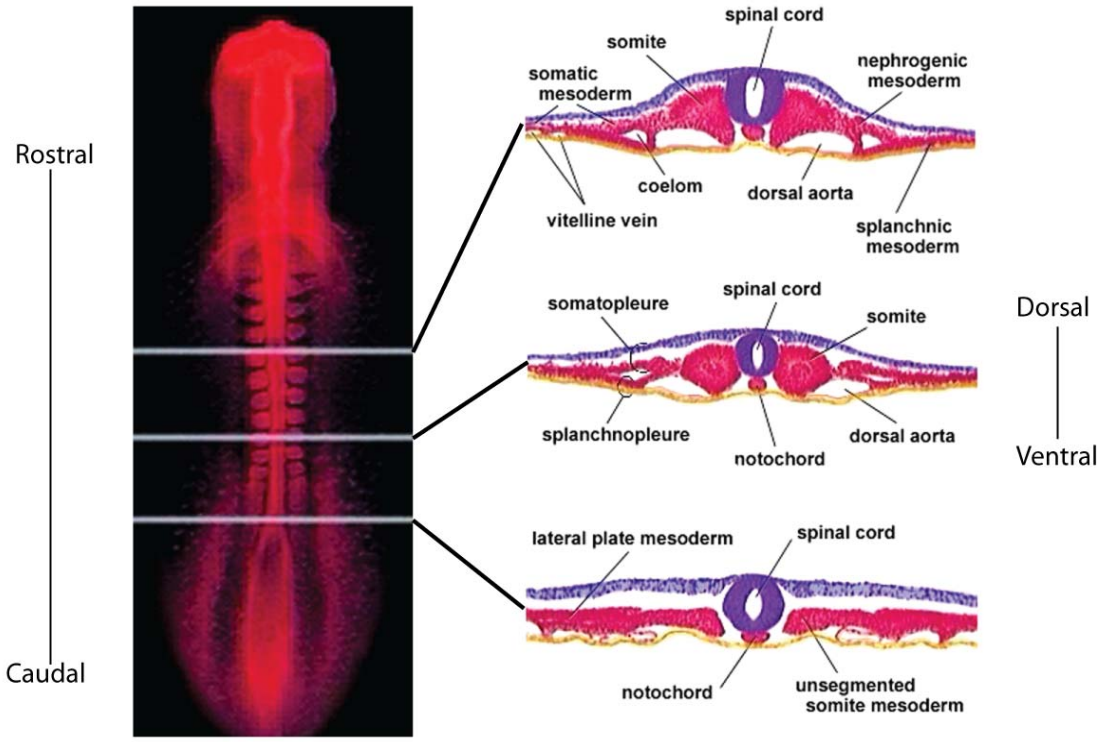

Figure 3: Hamburger Hamilton stage 10 chick embryo showing development of somites. The left panel shows a dorsal view and the right panel shows transverse sections at different axial levels. Note that the rostral somites are more developed than the caudal somites (see text). Adapted from *Vade mecum*, an interactive guide to developmental biology, the CD companion to Developmental Biology by Scott F. Gilbert (6th Edition).

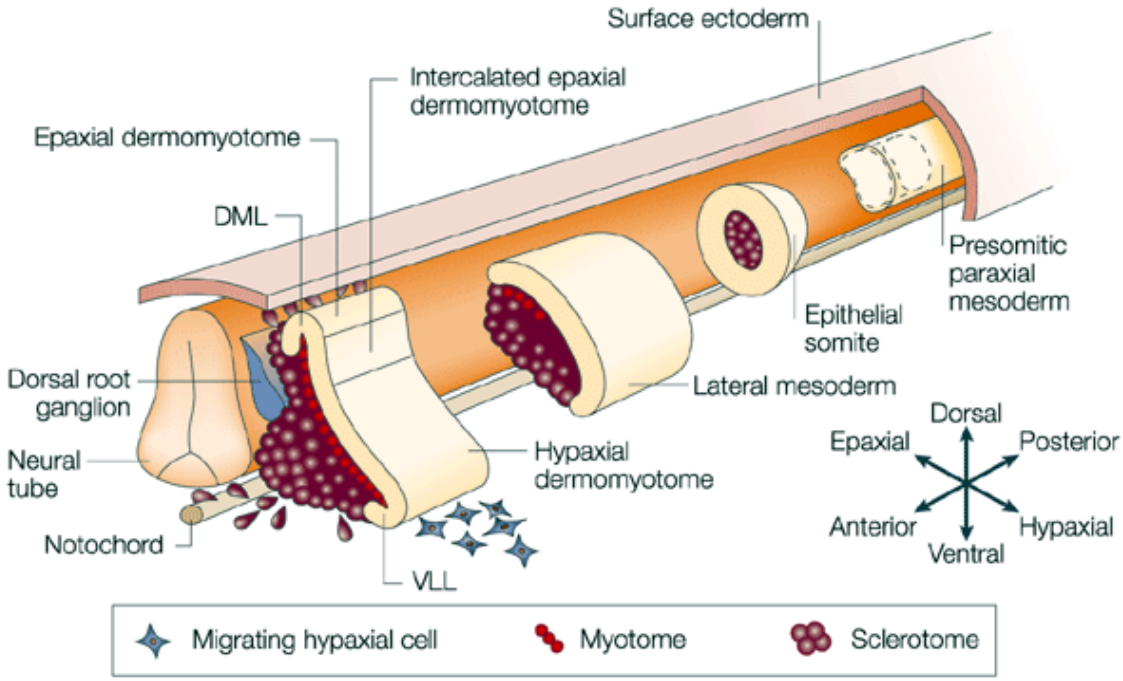

Figure 4: The embryonic origin of limb and trunk skeletal muscle. The presomitic paraxial mesoderm is located on either side of the notochord. The lateral-plate mesoderm is positioned tangentially to the intermediate mesoderm, which in turn is positioned laterally to the paraxial mesoderm. Segmentation of the paraxial mesoderm into somites occurs along the dorsal–ventral axis and in a rostral to caudal direction. In response to signals from the notochord and the neural tube, the somites differentiate and subdivide to give rise to the dermomyotome and the sclerotome. The dermomyotome is subdivided into the hypaxial and the epaxial dermomyotome, and is the source of cells for the lateral trunk musculature and deep back musculature, respectively. Cells of the dorsal medial lip (DML) migrate under the dermomyotome to form the epaxial myotome. A similar event occurs at the ventral lateral lip (VLL), which results in the formation of the hypaxial myotome. Cells of the VLL also undergo an epithelial to mesenchymal transition, delaminate and migrate to regions of presumptive muscle development in the limbs (migrating hypaxial cells). Adapted from (Parker et al., 2003).

Currently, in chick, there are two models proposed to explain the generation of myotome from dermomyotomal cells. The Kalcheim model (Fig. 5A-C) proposes that there are distinct waves of myotomal growth. In the first wave of myogenesis, the myogenic precursors from the DML, instead of translocating directly into the myotome, first migrate to the rostral lip of the dermomyotome and then as they differentiate into the myofibers, elongate along the rostro-caudal axis. Subsequent growth occurs when the second wave of myogenic precursors translocates directly

into the myotome from the rostral and caudal dermomyotome lips, and intercalates with preexisting myofibers (Kahane et al., 1998a; Kahane et al., 1998b). A later, third wave of myotome growth occurs when another mitotically active population of myoblasts enters the myotome from rostral and caudal dermomyotome edges (Kahane et al., 2001) to continue the expansion of myotome. In contrast, Ordhal and colleagues (Fig. 5D-F) state that DML and VLL cells translocate directly underneath the dermomyotome to form the subjacent myotome. Once in the myotome, the myofibers elongate in a rostro-caudal direction, while the myotome expands medio-laterally. In this way older myofibers are displaced laterally as newer myofibers translocate into the myotome medially. Surgical ablation and dye labeling studies reveal that the DML is both necessary and sufficient for formation and growth of epaxial myotome and that DML cells translocate directly into the myotome without prior translational movement (Denetclaw et al., 2001; Ordahl et al., 2001). Shortly afterwards, the central dermomyotomal sheet undergoes epithelial to mesenchymal transition (EMT) (Tosney et al., 1994) and its progeny, composed of at least bipotent cells, forms both the dermis (Olivera-Martinez et al., 2000), and a majority of mitotic muscle progenitors (Ben-Yair et al., 2003; Ben-Yair and Kalcheim, 2005). The final fate of these cells is varied with most of them undergoing myogenesis, but other contributing to muscle fibroblasts, endothelial cells and muscle satellite cells (Gros et al., 2005; Kassar-Duchossoy et al., 2005; Relaix et al., 2005; Scaal and Christ, 2004).

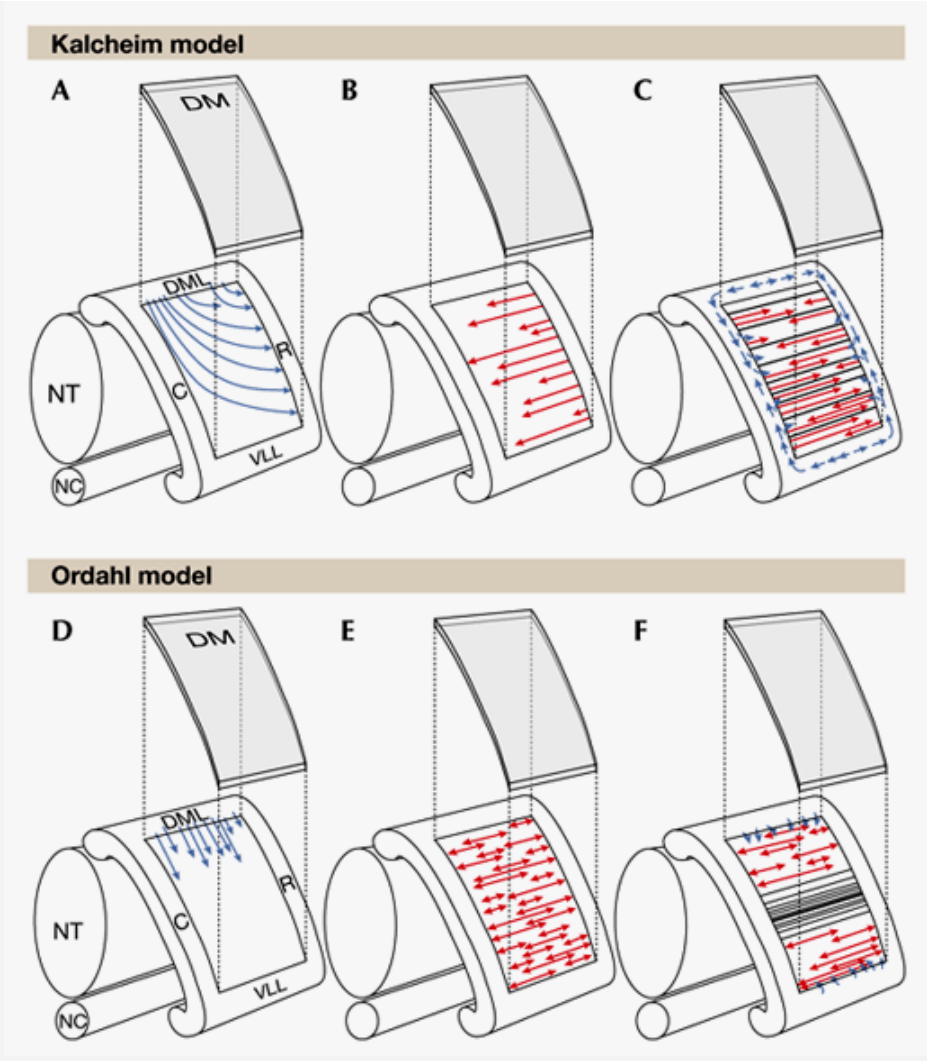

Figure 5: The Kalcheim and the Ordhal models of myoblast migration and myofibre growth during avian myotome formation. The dermomyotome epithelium (DM) has been lifted, leaving the myotome and the dermomyotome edges, the dorsomedial lip (DML), the ventrolateral lip (VLL), the rostral lip (R) and the caudal lip (C). Blue arrows represent migration of myoblasts, red arrows represent growth of myofibres and black lines represent elongated myofibres. (**A**–**C**) In the Kalcheim model (see text for details), the progenitor myoblasts originate along the rostral–caudal extent of the dorsomedial wall, delaminate and migrate to rostral positions (**A**), and the myofibres then grow in a rostral-to-caudal direction (**B**). A second wave of fibres arises from all four myotome edges; the myoblasts from the rostral and caudal edges directly generate myofibres, whereas those from the DML and VLL first migrate to the rostral and caudal edges before entering the myotome (**C**). The second wave causes expansion of the myotome in both the rostrocaudal and dorsoventral directions and also increases the myotome thickness in the transverse plane. (**D**–**F**) In the Ordahl model (see text for details), myoblasts enter from the DML along its rostral–caudal extent (**D**), and myofibres grow out towards the rostral and caudal edges simultaneously from many points along the rostral–caudal extent of the myotome (**E**).Myoblasts continue to be added from the DML, and the VLL, and older fibres are displaced more laterally (**F**). **NC**, notochord; **NT**, neural tube. Figure adapted from (Hollway and Currie, 2003).

1.4.4 The spatial patterning of somite occurs in response to signals emanating from adjacent tissues

One pertinent question in somitogenesis is whether different regions in a somite are lineage restricted or whether they acquire their identity in response to the signals in the range of which they find themselves in. Grafting a part of the somite to another region of the somite or transplantation of a somite rotated through 180° have shown that cells in the newly formed somite are not lineage restricted (Aoyama and Asamoto, 1988; Dockter and Ordahl, 2000; Ordahl and Le Douarin, 1992). Rather, the somatic compartments are determined in response to extrinsic signals emanating from surrounding tissues (Dockter and Ordahl, 1998; Williams and Ordahl, 1997) (Fig. 6). Expression of Sonic hedgehog (Shh) and Noggin in the floorplate of the neural tube and notochord is required for inducing and maintaining the sclerotome (Borycki et al., 1998; Brand-Saberi et al., 1993; Chiang et al., 1996; Dietrich et al., 1997; Fan and Tessier-Lavigne, 1994; Johnson et al., 1994; McMahon et al., 1998; Munsterberg et al., 1995; Munsterberg and Lassar, 1995; Pourquie et al., 1993; Watterson et al., 1954). The Wnts, Wnt1 and Wnt3a from the dorsal neural tube play an inductive role in formation of the epaxial dermomyotome (Capdevila et al., 1998; Christ et al., 1992; Dietrich et al., 1997; Fan et al., 1997; Fan and Tessier-Lavigne, 1994; Ikeya and Takada, 1998; Munsterberg et al., 1995; Munsterberg and Lassar, 1995; Olivera-Martinez et al., 2001; Spence et al., 1996; Wagner et al., 2000), while hypaxial dermomyotome induction requires contact mediated signaling by Wnt4, Wnt6 and Wnt7a from the surface ectoderm (Dietrich et al., 1997; Fan et al., 1997; Fan and Tessier-Lavigne, 1994) and Bmp4 from the lateral plate mesoderm (Pourquie et al., 1996). Thus, the somite is patterned by the dorsalizing influence of Wnts from

the dorsal neural tube and the surface ectoderm and the ventralizing influence of Shh activity from the ventral midline.

Since both Wnts and Shh are morphogens that have been shown to act, *in vitro*, at a distance greater than the diameter of the somite (Fan et al., 1997; Fan et al., 1995; Fan and Tessier-Lavigne, 1994), it is surprising how precisely the range of dorsalizing and ventralizing influences is maintained. It seems that dorsalizing and ventralizing signals not only induce cell fate but that they also induce competitive inhibitors of the opposing signaling molecule. Therefore, a higher concentration of Shh is inhibitory to Wnt influence and a higher concentration of Wnts curbs Shh influence. For example, it has been shown that the Wnt antagonist Soluble frizzled related protein 2 (Srfp2) is expressed in the sclerotome (Lee et al., 2000). It has also been shown that Srfp2 is upregulated in PSM explants in response to Shh and can block the activity of Wnt1 and Wnt4 in these explants (Lee et al., 2000). Similarly, Growth-arrest specific gene1 (Gas1), a glycosyphosphatidylinositol (GPI)-anchored membrane protein, is expressed in the dorsal somite (Lee et al., 2001). In PSM explant cultures, Gas1, induced in response to Wnts, can bind recombinant Shh and reduce the transcriptional read out of Shh target genes like *pax1* and *patched* (Lee et al., 2001). Thus, Shh and Wnts use a combination of induction and competitive inhibition to precisely pattern the somite.

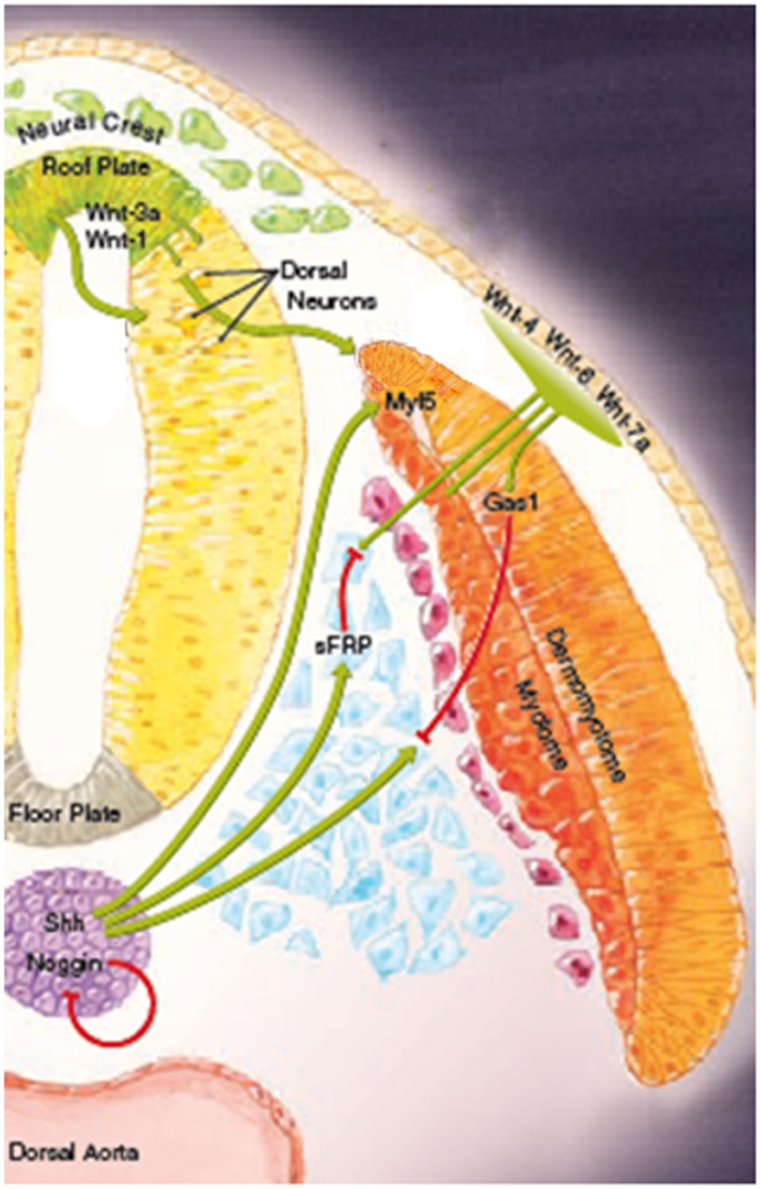

Figure 6: Genetic interactions in the dermomyotome. A schematic showing how Wnts from the dorsal neural tube and the dorsally lying ectoderm and Shh from the notochord and the floor plate pattern the somite by inducing dorsal and ventral fates, respectively, and also limiting the influence of other signaling molecule by inducing inhibitors. See text for details. Figure adapted from "Development of Somitic Lineages" poster from the R&D Systems website (http://www.rndsystems.com/DAM_public/5834.pdf)

Even though the skeletal muscles in the vertebrate body in different locations are quite similar in form and function, there are four distinct muscle groups based on their developmental origins and genetic hierarchies: the trunk muscles, the cranio-facial muscles, the extra-ocular muscles and the pharyngeal arch muscles. For the purpose of this report, the discussion on myogenesis will be limited to the trunk muscles. The common feature during development among all skeletal muscles is the expression of and subsequent impartment of the genetic program driven by members

of basic Helix loop Helix (bHLH) domain containing transcription factors called the Myogenic Regulatory Factors (MRFs). Once a myoblast starts expressing MRFs it is committed to become a skeletal muscle. MRFs include myogenic factor 5 (myf5) (Emerson, 1990; Rudnicki et al., 1993), myogenic differentiation 1 (myod1 also called myod) (Rudnicki et al., 1993), myf6 (also called MRF4) (Montarras et al., 1991) and myogenin (Myog) (Edmondson and Olson, 1989; Emerson, 1990; Wright et al., 1989). MRFs, along with a number of cofactors, are responsible for the expression of genes that are required to make the contractile apparatus of a mature skeletal muscle cell. The upstream genetic regulators of MRFs might vary depending on whether the skeletal muscles being formed are cranio-facial, extraoccular, pharyngeal arch or trunk muscles. For example, mice knockouts of transcription factors Tbx1, Pitx2, Transcription factor 21 (tcf21), and musculin, all show defects in the formation of distinct cranial muscles (Arnold et al., 2006; Dastjerdi et al., 2007; Dong et al., 2006; Kelly et al., 2004; Lu et al., 1999; Lu et al., 2002). For generating trunk muscles though, the MRFs act downstream or in parallel with the paired box transcription factors Pax3 and Pax7 (Kassar-Duchossoy et al., 2005). This is obvious since the loss of Pax3/7 results in loss of all but very early (prior to E10.5) muscles (Fig. 7). Pax3 itself is regulated by the activity of members of sine occulis (six) (Grifone et al., 2005) and eyes absent (eya) (Heanue et al., 1999) protein family members. The Six proteins have also been shown to directly regulate Myf5 and Myogenin in specific contexts (Giordani et al., 2007; Laclef et al., 2003).

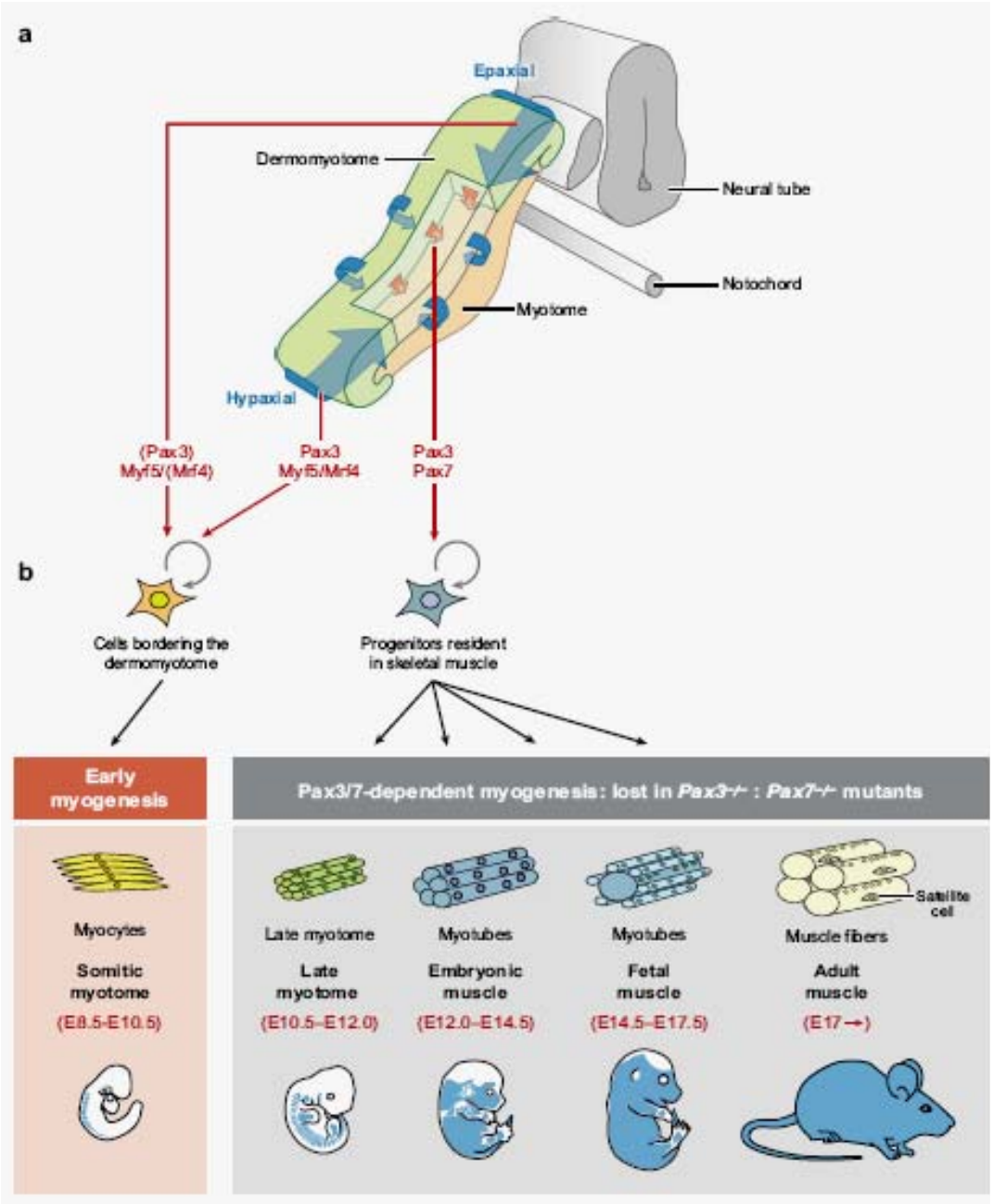

Figure 7: Pax3/7 function during the formation of skeletal muscle. (*a*) The epithelial dermomyotome of a somite (*green*) and the underlying skeletal muscle of the myotome (*beige*) are initially formed by delamination of cells from the edges of the dermomyotome (*blue arrows*). Subsequently, as the central dermomyotome loses its epithelial structure and resident myogenic progenitor cells enter the myotome (*red arrows*). The transcription factors that regulate these events are shown in red. (*b*) A schematic of the progenitor cells and their muscle derivatives, together with the timing of these events in the mouse embryo. Circular gray arrows indicate proliferation. The gray box shows myogenic events that are lost in the absence of Pax3 and Pax7. **E**, embryonic day. Figure adapted from (Buckingham and Relaix, 2007).

In the context of a somitic muscle development, *pax3* is already transcribed in presomitic paraxial mesoderm just prior to segmentation. Thereafter, it is transcribed throughout the epithelial somite before becoming restricted dorsally to the dermomyotome, where its expression extends to the extremities of the epaxial and hypaxial dermomyotomes. In contrast, *pax7* transcripts are concentrated in the central domain. Pax3 is required for the formation of hypaxial muscles of the trunk and for the delamination and migration of myogenic progenitor cells to other sites of myogenesis such as those in the limb (Tajbakhsh and Buckingham, 2000). As cells leave the dermomyotome and enter non-myogenic lineages, Pax3/7 expression is downregulated (Ben-Yair and Kalcheim, 2005; Esner et al., 2006; Gros et al., 2005). As stated above, the differentiation of skeletal muscles is totally dependent on MRFs. Myf5, MyoD and MRF4 govern the acquisition of a myoblast fate whereas Myogenin, MyoD and MRF4 are needed for terminal differentiation (Buckingham et al., 2006). As the myogenic progenitor cells enter the myotome from the extremities of dermomyotome, Myf5 and MRF4 regulate their myogenic program independently of Pax3/7.

In mice, Myf5 and MyoD are activated at different times and in different domains. Myf5 is first expressed in the DML epaxial myotome and later in the myotome itself. MyoD is expressed somewhat later, first in the somitic dorsomedial quadrant and thereafter in the incipient myotome. Till recently it was believed that Myf5 and MyoD can act in a largely redundant manner as mice knockouts for either gene have normal myogenesis but a double knockout was described as completely devoid of trunk musculature (Rudnicki et al., 1993). Since mice mutant for both Pax3 and Myf5 do not show any MyoD expression or trunk muscle formation, two parallel pathways for trunk myogenesis have been proposed in mice. Either Myf5 or MyoD is

sufficient to regulate myogenesis but MyoD is turned on by Myf5 in one pathway and Pax3 in the other pathway (Tajbakhsh et al., 1997) (Fig. 8, black arrows). However, recent data from Kassar-Duchossoy et al. suggest that MRF4 acts as a cell fate determination gene in absence of both Myf5 and MyoD (Kassar-Duchossoy et al., 2004). Kassar-Duchossoy et al. used an allelic series of three *Myf5* mutants that differentially affect the expression of the genetically linked *Mrf4* gene, showing that skeletal muscle is lost in the Myf5:MyoD double null mice only when Mrf4 expression is also compromised (Kassar-Duchossoy et al., 2004). It is likely that Pax3 also regulates Mrf4 expression (Fig. 8, shown as red arrow). In contrast to mice, the evidence for involvement of Notch signaling in the chick, points to a slightly different hierarchy between Pax3, Myf5 and MyoD. Initially Myf5 is co-expressed with Pax3 in the DML, where proliferating cells are believed to reside (Hirsinger et al., 2001). MyoD expression is turned on later when the myoblasts have entered the myotome and are believed to be postmitotic. So here it seems that proliferative cells express Pax3 and Myf5 and once the cells are postmitotic, they express MyoD. Components of the Notch pathway such as the Notch1 receptor and its ligands Delta1 and Serrate2 are expressed in differentiating myoblasts (Hirsinger et al., 2001). Overexpressing Delta1 leads to down regulation of MyoD and results in a complete lack of differentiated muscles, although initial formation of the myotome is unaffected (Hirsinger et al., 2001). Therefore, Notch signaling acts downstream of Pax3/Myf5 and upstream of MyoD to regulate myogenic differentiation.

In the lateral dermomyotome the precursors of hypaxial muscles are demarcated by Pax3 expression as is evident by loss of all hypaxial muscles in Pax3 mutant mice. The first step in migration of muscle precursors is their delamination from the hypaxial dermomyotome. This delamination is mediated by the receptor

tyrosine kinase c-Met and its ligand Scatter Factor/Hepatocyte Growth Factor (SF/HGF) (Bladt et al., 1995; Dietrich et al., 1998). c-Met is expressed throughout the hypaxial dermomyotome, and this is consistent with it being a direct target of Pax3 (Epstein et al., 1996; Relaix et al., 2003). SF/HGF, the ligand of c-Met however, is expressed only at the axial levels of limb buds. Ectopic application of HGF has shown to cause delamination of dermomyotomal cells at axial levels on which these cells never delaminate (Brand-Saberi et al., 1996; Heymann et al., 1996). Once delaminated, the muscle precursors migrate and are guided to their targets by "guidance cues" such as SDF1 (Ratajczak et al., 2003). For details of myoblast migration please see (Vasyutina and Birchmeier, 2006).

Amidst all these myogenic events the proliferating central dermomyotomal population that co-expresses Pax3 and Pax7 undergoes EMT, with cells entering either the myotome or the dermis as the dermomyotome disintegrates (Tosney et al., 1994). Elegant quail-chick chimera experiments have revealed that the majority of the cells in this myotomal population starts expressing Myf5/MyoD and will eventually contribute to muscle growth in late fetal and postnatal life. A quail central dermomyotomal tissue was grafted into a region of the central dermomyotome of chick after chick tissue had been excised. Thereafter, an antibody specifically recognizing quail cells was used to identify the quail cells in post hatch chicks. This lead to the finding that most of the cells derived from the central dermomyotomal region (quail derived) contributed to the post natal muscle.

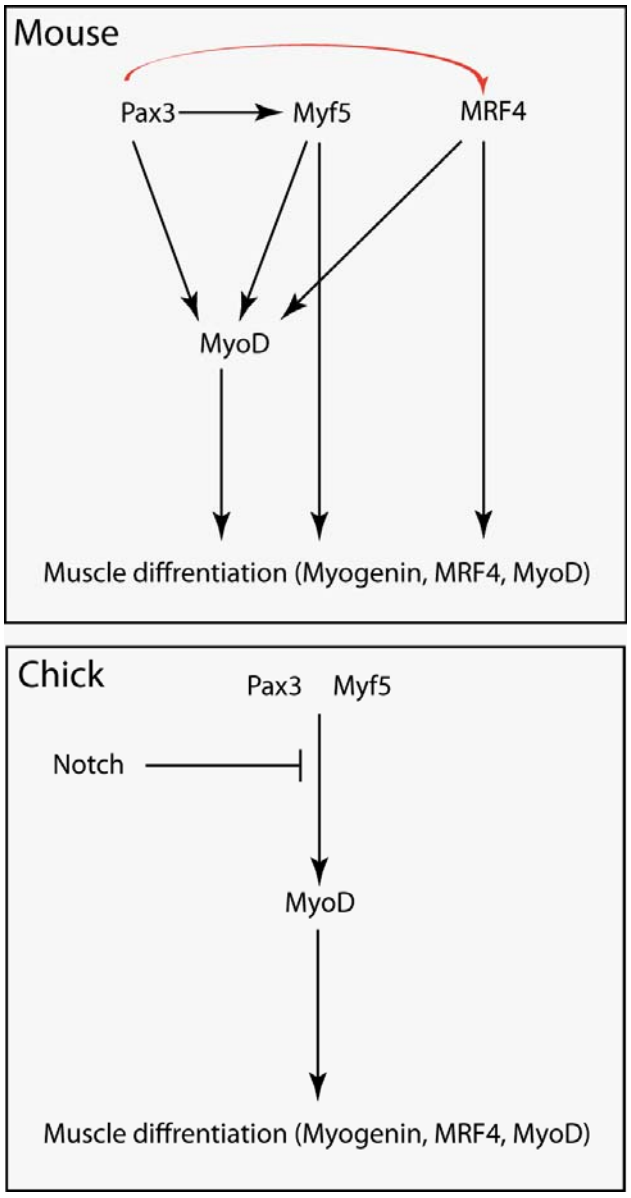

Figure 8: Differences in mouse vs. chick myogenesis. Myogenic pathway is inherently dependent on MyoD in chick where as in mouse MyoD independent pathways can compensate for loss of MyoD activity. See text for details. See text for details (Brent and Tabin, 2002; Kassar-Duchossoy et al., 2004).

1.5 Skeletal muscle regeneration: The role of satellite cells

Mammalian muscle regeneration has been shown to proceed almost exclusively through a "stem cell" population responsible for postnatal muscle growth and regeneration. Although cells from sources other than muscles, such as cell from bone marrow or pericytes, the blood vessel associated mesenchymal like cells (Grounds et al., 2002), might contribute to skeletal muscle regeneration under culture or experimental conditions, the extent of their contribution to regenerating muscles in

physiological conditions remains unknown. In 1961, Mauro described a population of cells lying under the basal lamina, juxtaposed to the myofiber, in a "satellite" position (Fig. 12). He decided to call these cells "satellite cells" and speculated that they "might be" pertinent to the vexing problem of skeletal muscle regeneration" (Mauro, 1961). Mauro also speculated on the origin of these cells and hypothesized that they might be remnants of the embryonic myoblasts and recapitulate embryonic development when the main multinucleated cell is damaged.

Indeed this is the case, as it has been shown with quail chick chimera and long term lineage tracing experiments. Using the quail chick chimera methodology, in conjunction with Pax7 antibody staining to mark satellite cells, it was shown that over 90% of the satellite cells identified in the graft region came from quail (Gros et al., 2005). Hence most of the satellite cells found in postnatal muscle are dermomyotomal in origin and share a common origin with embryonic myoblasts.

Much of the research focused on satellite cells has been performed on single fiber cultures, where satellite cells are isolated with their associated fibers still covered by the basal lamina that surrounds each muscle fiber (i.e., within their niche). Isolated myofibres provide an accessible means to study the activation, proliferation, and differentiation of satellite cells in their native position. This model preserves potentially important interactions between satellite cells and/or myofiber.

The general mechanism of muscle repair via satellite cell has now been established, although the details of several of the processes are not understood very well. Normally quiescent satellite cells lie under the basal lamina adjacent to the myofiber. Following activation, satellite cells, now termed skeletal myoblasts, leave their niche and undergo repeated rounds of self replication (Fig. 9). The skeletal myoblasts have to survive and proliferate initially in a severe inflammatory response

from immune cells and macrophages as the degraded muscle fibers around them become necrotic and are cleared away by the immune cells (not shown in Fig. 9). When the skeletal myoblasts have amplified to a sufficient number, most of these cells start expressing markers committing them to differentiation (Fig. 9). Some myoblasts however do not proceed to differentiation and go back to expressing markers of quiescent satellite cells and populate the satellite cell niche (not shown in Fig. 9). Finally they fuse forming multinucleated myofibers and start expressing genes encoding for sarcomeric proteins (Fig. 9). The entire process is highly dynamic and is tightly regulated by genetic networks, the details of which have begun to emerge only in last 10 years. For a review see (Charge and Rudnicki, 2004). In the subsequent sections we would take a look at these events and the underlying mechanisms in more detail.

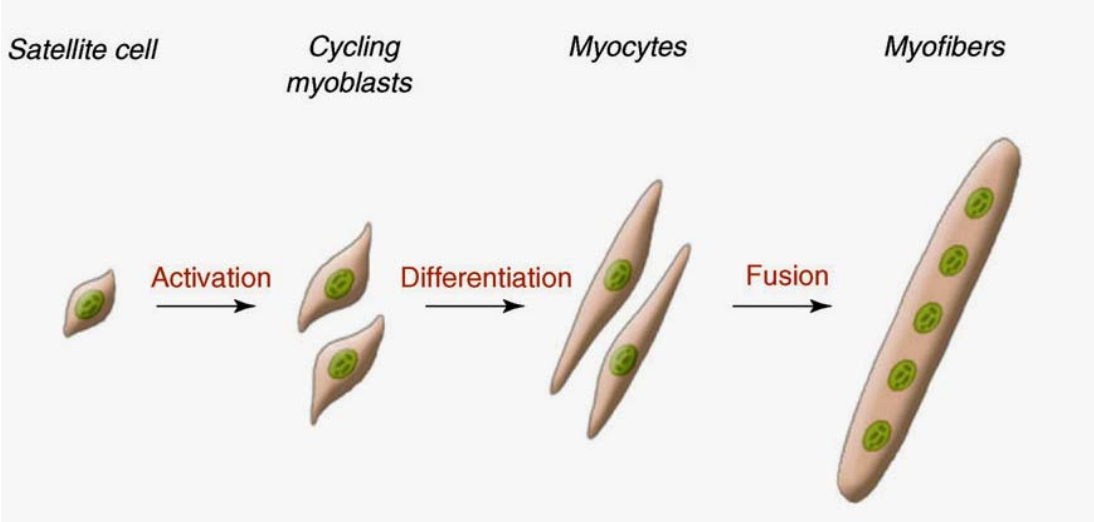

Figure 9: A satellite cell progressing from quiescence, through activation to fully mature myofiber. See text for details. Figure adapted from (Le Grand and Rudnicki, 2007).

1.5.1 The role of *pax3/7* genes in satellite cell biogenesis and function

Pax7 is the key genetic regulator required for satellite cell generation and function. Pax7 is expressed by all satellite cells (Kuang et al., 2006; Seale et al., 2000) and has been the most commonly used marker for their study. Although neonatal Pax7 null mice have a significant number of satellite cells, a major fraction of these cells is lost via apoptosis as the mice reach adulthood (Relaix et al., 2005; Seale et al., 2000). A few Pax3 positive satellite cells are observed in some muscles, but Pax3 is mostly downregulated before birth and is unable to substitute for the anti-apoptotic effects of Pax7. Posttranscriptional regulations also differentially affect Pax3 and Pax7 stability. Specific lysine residues at the C-terminal region of Pax3 protein get mono-ubiquitinated, leading to proteasome mediated degradation (Boutet et al., 2007). However, Pax7 lacks such lysine residues and therefore escapes this degradation, as it has been shown that addition of these lysine residues to the Pax7 protein can cause mono-ubiqitination and subsequent proteasomal degradation (Boutet et al., 2007). Since Pax3 null mice are embryonic lethal, a true evaluation of the role of Pax3 in regulation of satellite cell biology must await the generation of a conditional null allele of Pax3. The mechanism by which Pax7 governs adult myogenesis has been under intense investigation. Recent work has suggested a direct regulation of Myf5 by Pax7 binding a paired domain motif containing enhancer and driving expression in myoblasts derived from satellite cells (Buchberger et al., 2007). Another recent study demonstrated that Myf5 is regulated by Pax7 through a histone methylation mechanism when ChIP analysis and Mass spectrometry revealed that Pax7 in a complex with Wdr5 and Ash2L, members of a histone methyl transferase complex, binds to -57.5 kb region of myf5 gene (McKinnell et al., 2008).

These results suggest a sequential activation of Myf5 by Pax7 that directs the subsequent myogenic program via MyoD and other MRFs till finally muscle differentiation genes are expressed. However they do not explain the heterogeneity that exists within satellite cell pools in vivo, and the cross-inhibitory interaction between Pax7 and certain MRFs that seems to be independent of the transcriptional regulatory ability of Pax7 (Olguin et al., 2007) (discussed in Fig. 10 and accompanied text).

1.5.2 Satellite cell activation

The adult skeletal muscle satellite cells are normally quiescent and exhibit limited gene activity and protein synthesis. Upon muscle injury, such as those induced by load bearing exercise, by trauma, or by myo-degenerative diseases, such as muscular dystrophies, the satellite cells are activated and enter the cell cycle (Charge and Rudnicki, 2004). It remains largely unknown which signal triggers this activation, although recent reports point towards involvement of both intrinsic as well as extrinsic signals. A signal intrinsic to the cell itself, sphingosine-1-phosphate (S-1-P), synthesized from sphingomyelin from the inner leaflet of the satellite cell plasma membrane, seems to be required for satellite cell entry into the cell cycle, and inhibition of its synthesis drastically abrogates muscle regeneration (Nagata et al., 2006b). However it is not clear what extracellular signals regulate generation of S-1-P from sphingomyelin. Extracellular signals such as stretch induced nitric oxide synthesis that results in release of hepatocyte growth factor (HGF) can lead to activation of satellite cells via the HGF receptor c-MET (Wozniak and Anderson, 2007). Nitric oxide also induces expression of Follistatin (Pisconti et al., 2006), a fusigenic (causing membrane fusion) secreted molecule, known to antagonize

myostatin. Myostatin, expressed by quiescent satellite cells, is a negative regulator of myogenesis. Thus nitric oxide may contribute to the satellite cells' exit from quiescence. Microenvironment-secreted growth factors are another stimulus for satellite cell activation. Fibroblast growth factors (FGF) are known to induce promyogenic Mitogen Activated Protein Kinases (MAPK) signaling cascades and the p38α/ß MAPK acts as a molecular switch by activating satellite cells when it is activated and by maintaining quiescence when it is inactivated (Jones et al., 2005).

A conundrum related to satellite cell activation is why there is a decrease in regenerative potential during senescence. Satellite cells from aged mice show reduced proliferative potential and a decline in numbers. It was shown that satellite cells from aged rats can proliferate and lead to effective regeneration when transplanted into a younger host while satellite cells from a young donor are unable to do the same when transplanted into a senescent host (Carlson and Faulkner, 1989). This has been attributed to a shift of balance between Notch and Wnt signaling pathways during aging. Satellite cells from aged muscles fail to upregulate the Notch ligand Delta, resulting in a lower level of Notch activation in muscles of senescent animals (Conboy et al., 2003). This hypothesis is supported by the evidence that forced activation of Notch restored the regenerative potential of aged muscle and that blocking Notch signaling impairs muscle regeneration in young mice (Conboy et al., 2003). Satellite cells from aged animals upregulate the canonical Wnt signaling pathway, thereby acquiring an increased tendency to differentiate into a fibrogenic lineage (Brack et al., 2007). Presence of Klotho, a secreted protein with glucosidase activity that is capable of binding and antagonizing Wnts, seems to be a likely component in the young systemic milieu leading to an effective regeneration (Liu et

al., 2007a). Indeed, mice mutant for Klotho exhibit premature aging like phenotype (Kuro-o et al., 1997), however, a direct role for Klotho in muscle is yet to be tested.

1.5.3 Myogenic progression of satellite cells

The myogenic potential of the satellite cells relies on their ability to sequentially express Pax3/7 genes and subsequently express the MRFs (myoD, Myf5, myogenin, and MRF4). As mentioned before, Pax7 is expressed by all satellite cells and Pax3 by a subset of satellite cells. After activation, however, Pax3 can be detected in most skeletal myoblasts (Relaix et al., 2006) but its role in muscle regeneration is not clear as Pax3 knock outs die *in utero* and a conditional knock out of Pax3 does not exist. Pax3 and Pax7 both can activate myogenic genes like *myoD* but only Pax7 possesses the antiapoptotic function (Relaix et al., 2006). Therefore, continued expression of Pax7 after their activation ensures that satellite cells survive a massive surge in production of free radicals and the inflammatory response that digests the necrotic myofibers after injury. It has recently been shown that signaling via erbB receptors, members of the EGF receptor tyrosine kinase family, is involved in mediating this anti-apoptotic role (Golding et al., 2007) although it is not known if Pax7 plays a direct role in this process. Pax3 expression prevents differentiation of skeletal myoblasts, and proteasomal degradation of Pax3 by mono-ubiquitination paves the way for their differentiation (Boutet et al., 2007). This is evident from the observation that expressing a mutant form of Pax3 that is resistant to this ubiquitination and thus proteasomal degradation leads to inhibition of differentiation in skeletal myoblasts (Boutet et al., 2007). Pax7 induces myoblast proliferation and delays their differentiation by decreasing MyoD protein stability (Olguin et al., 2007). This activity of Pax7 however, seems to be independent of its function as a

transcriptional activator (Olguin et al., 2007). Therefore Pax7 can act both at a transcriptional level as well as at protein level.

In contrast to the Pax proteins, MyoD and Myf5 have very well defined roles in satellite cells. MyoD is essential for the differentiation potential of skeletal myoblasts (Cornelison et al., 2000; Sabourin et al., 1999) while Myf5 regulates their proliferation rate and homeostasis (Gayraud-Morel et al., 2007; Ustanina et al., 2007). Unlike in embryonic myogenesis, Myf5 and MyoD cannot effectively compensate for the loss of each other in adult context. This is evident from the fact that *mdx* mice, when crossed into either Myf5 null or MyoD null mice, did not show efficient muscle regeneration (Gayraud-Morel et al., 2007; Megeney et al., 1996; Ustanina et al., 2007). After several rounds of cell proliferation a majority of skeletal myoblasts start expressing myogenin. The expression of myogenin is not only essential and sufficient for formation of myotubes and myofibers but also for downregulating pax7 expression (Olguin et al., 2007) (cells with red nucleus, Fig. 10).

In single fiber cultures, a small proportion of skeletal myoblasts downregulate *myoD*, upregulate *pax7* and eventually leave the cell cycle and reenter the niche under the basal lamina (Olguin and Olwin, 2004; Zammit et al., 2004). It has been shown, especially by clonal analysis of Pax7+ve/MyoD+ve expressing skeletal myoblasts, that some cells in the clone could downregulate MyoD expression. These Pax7+ve/MyoD-ve skeletal myoblasts could only arise from Pax7+ve/MyoD+ve cells and have thus been postulated to form the self-renewing fraction of satellite cells (cells with green nucleus, Fig. 10).

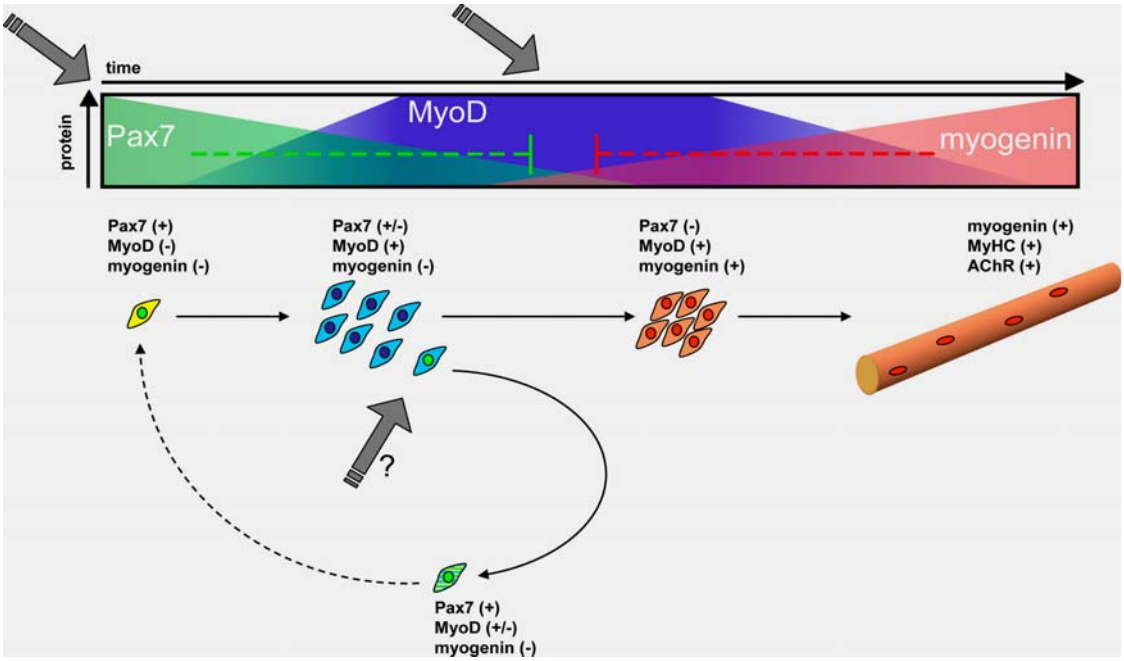

Figure 10: Reciprocal regulation of Pax7 and MRFs during myogenic cell fate commitment. Satellite cells ($Pax7^{+}/MyoD^{-}/myogenin^{-}$) must commit to proliferate, differentiate, or renew the progenitor population to maintain muscle function. Commitment to proliferation requires environmental cues (gray arrows) that activate satellite cells and up-regulate MyoD (blue) with a concomitant decline in Pax7 expression (green). Upon commitment to terminal differentiation, up-regulation of myogenin (red) down-regulates Pax7. In a small cell population, up- regulation of myogenin is prevented; Pax7 is up-regulated by unknown mechanisms, resulting in MyoD down-regulation (green nucleus and dashed cytoplasm cell) leading to the commitment to a quiescent, undifferentiated phenotype. In this model, the Pax7/MRF expression ratio is critical and integrates with environmental signals (gray arrows, question mark) to regulate cell fate commitment. Figure adapted from (Olguin et al., 2007).

Several markers have been identified that label the different stages during the course of satellite cells' journey from muscle progenitor to a fully formed myotube (Fig. 11). CD34, Pax7, and Myf5/ß-gal, among others, are expressed in quiescent satellite cells. Myf5/ß-gal denotes the fusion protein product of the targeted allele of the Myf5nlacZ/1 mouse (Tajbakhsh et al., 1997). Satellite cell activation is marked by the rapid onset of MyoD expression, whereas myogenin later marks the commitment to differentiation. MLC3F-tg is the product of the 3F-nlacZ-E transgene (Kelly et al.,

1995). The temporal expression pattern of MLC3F-tg is typical of many structural muscle genes such as skeletal muscle actin and MyHC, which mark sarcomeric assembly in the later stages of differentiation.

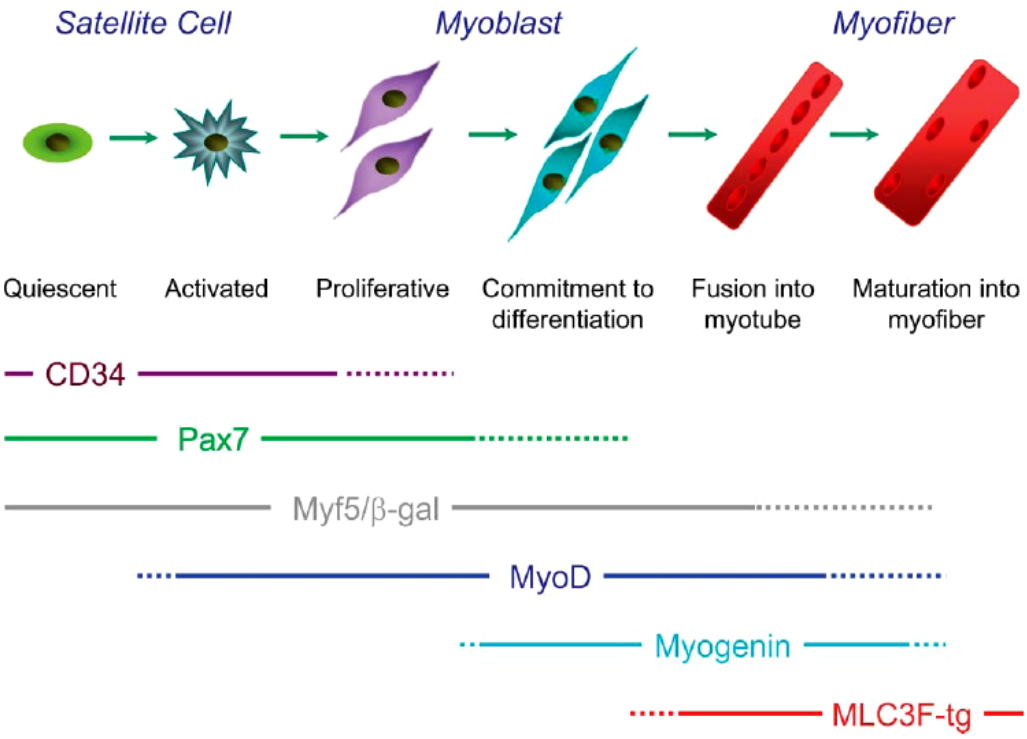

Figure 11: Schematic of satellite cell myogenesis and markers typical of each stage. Satellite cells are quiescent in normal adult muscle and can be activated by muscle damage. Once activated, satellite cells divide to produce skeletal myoblasts that further proliferate, before committing to differentiation and fusing to form myotubes, which then mature into myofibers (for clarity, satellite cell self-renewal is not included). See text for details. Figure adapted from (Zammit et al., 2006).

Marker	Species[a]	Expression			Function
		Q	A	D	
Cell surface					
c-met	m, h	+	+	+	HGF receptor (reviewed in [1])
Caveolin-1	m	+	-	-	Cell-cycle arrest [43,44]
CD34	m	+	+	+	Unknown, isotype switching during activation (reviewed in [1])
CTR	m	+	-	-	Regulation of quiescence [41]
CXCR4/SDF-1[b]	m, h	+	+	+	Migration [52,102,103]
ErbB receptor	m	-	+	+	Anti-apoptotic [46]

Igsf4a	m	+	+	-	Unknown [104]
Integrin a7	m, h	+	+	+	ECM signaling, fusion [104,105]
Integrin b1	m, h	+	+	+	ECM signaling, fusion [106,107]
M-cadherin	m, h	+	+	+	Anchoring (reviewed in [1])
Necdin	m	-	+	+	Promotes differentiation [45]
Megf10	m	+/ -	+	-	Regulation of quiescence [108]
NCAM	m, h	+	+	+	Adhesion (reviewed in [1])
Neuritin-1	m	+	+	-	Unknown [104]
p75NTR/BDNF[c]	m	+	+	-	Inhibition of differentiation [109]
Pb99	m	+	+	-	Unknown [104]
SM/C-2.6	m	+	+	-	Unknown [110]
Sphingomyelin	m	+	-	-	Cell-cycle entry [42]
Syndecan 3/4	m	+	+	+	ECM signaling [111]
TcRb	m	+	+	-	Unknown [104]
VCAM-1/VLA-4[d]	m	+	+	+	Myoblast fusion [104,112]
Transcription factor					
Foxk1	m	+	+	+	Proliferation or cell cycle [113,114]
HoxC10	m	+	+	+	Unknown [104]
Lbx1	m	-	+	+	Forcing activated cells to quiescence [47]
Myf5	m, h	+	+	+	Myogenic commitment and transient amplification [18,115]
MyoD	m, h	-	+	+	Activation and myogenic differentiation (reviewed in [1])
Msx1	m	+	-	-	Inhibition of differentiation [116,117]
Pax3	m	+/-	+/-	-	Multiple roles (see text)
Pax7	m, h	+	+	-	Multiple roles (see text)
Sox8/9	m	+	+	-	Inhibition of differentiation [118]
Other					
Desmin	m, h	+/-	+	+	Cytoskeleton [40,119]
Myostatin/ACVR2	m, h?	+	+	+	Inhibit satellite cell activation and muscle growth [73,120]
Nestin	m, h	+	-	-	Cytoskeleton, nuclear organization? [40,104,121]

Table 1. Satellite cell markers
Abbreviations: A, activated (cycling) satellite cell; ACVR2, activitin receptor type 2; CTR, calcitonin receptor; D, differentiating myoblast; ECM, extracellular matrix; Q, quiescent satellite cell.
[a] Species column only includes mouse (m) and human (h).
[b] CXCR4/SDF-1: stromal derived factor 1 (SDF-1) is a ligand for CXCR4 receptor.
[c] p75NTR/BDNF: p75NTR is a neurotrophin receptor for BDNF (brain-derived neurotrophic factor).
[d] VCAM-1/VLA-4: very late antigen-4 (VLA-4) or integrin a4b1 is a receptor for vascular cell adhesion molecule 1 (VCAM-1).

The references in the brackets refer to the ones from (Kuang and Rudnicki, 2008) from where the table is adapted from.

1.5.4 Satellite cell self renewal and the stem cell potential: the role of the niche and the heterogeneity within

Satellite cell self renewal and stem cell potential is one of the most intensely researched topics in muscle regeneration research. Several lines of evidence point towards a mechanism of self renewal of satellite cells. For example, satellite cells that comprise only 3-5.5% of the myonuclei of their associated fiber can produce enough myoblasts to replace all the myonuclei of the myofiber within 4-5 days (Zammit et al., 2002). More importantly, the satellite cell pool continues to replace more myonuclei when the muscle is subjected to repeated severe damage (Luz et al., 2002; Sadeh et al., 1985). Transplantation of myoblasts has shown that grafted myoblasts not only generate myonuclei (Lipton and Schultz, 1979) but also give rise to viable myogenic precursors(Cousins et al., 2004; Gross and Morgan, 1999; Heslop et al., 2001; Morgan et al., 1994; Yao and Kurachi, 1993). Later it was shown that engrafting a single extensor digitorum longus myofiber, containing approximately 7 satellite cells, produced about 11 times as many new satellite cells in addition to many more myonuclei (Collins et al., 2005).

So how do satellite cells self renew? One line of evidence for satellite cell self renewal came from clonal analysis of single fiber associated satellite cells 24 hours after isolation and culture of single myofibers most satellite cells are activated, as revealed by their co-expression of Pax7 and MyoD (Zammit et al., 2002). By 48 hours, these cells proliferated, as revealed by uptake of BrdU, and continued to express both Pax7 and MyoD. Beyond 48 hours however, some cells lost MyoD expression while others gained myogenin expression. A significant proportion of satellite cell progeny were pax7 +ve but devoid of MyoD and they withdrew from the

cell cycle (Zammit et al., 2004). Since such cells could only have arisen from Pax7+ve/MyoD+ve cells, the authors concluded that this fraction that downregulates MyoD while maintain Pax7 expression must constitute the self renewing fraction of satellite cell progeny (Zammit et al., 2004). The re-entry of such cells in quiescence was proven by their re-expression of a *nestin* transgene (Day et al., 2007) and increased levels of sphingomyelin (Nagata et al., 2006a), definite markers of satellite cells quiescence. In such a scenario all satellite cells are homogenous to start with but with time acquire heterogeneity based on extrinsic cues that force some of the progeny of satellite cells to adopt divergent fates and some to retain the stem cell fate.

An alternate scenario has been proposed by studies of Kuang and colleagues based on lineage tracing of Myf5 expressing satellite cells (Kuang et al., 2007). The authors used *Myf5-Cre* expressing mice to permanently label satellite cells that have expressed Myf5 at any stage by driving constitutive expression of YFP under the Rosa 26 locus in response to Cre. Thus, such YFP labeled cells would have had a 'myogenic experience' at some point in their life. Using this method the authors reported that about 10% of satellite cells have never ever expressed Myf5 (Kuang et al., 2007). The authors hypothesize this to be the stem cell fraction of the satellite cell population and support their hypothesis by showing that the YFP^{-ve} satellite cells can give rise to both YFP^{+ve} and YFP^{-ve} cells (thus myogenic and stem cell lineage) by asymmetric cell division or only YFP^{-ve} cells by symmetric cell division (Kuang et al., 2007). Furthermore, their data suggest that the plane of cell division decides whether the division is symmetric or asymmetric: the divisions parallel to the myofiber being symmetric and the divisions perpendicular to the myofiber being asymmetric (Fig. 12). They show an involvement of Notch signaling in this process; the YFP^{+ve} cells showing a higher expression of Notch ligand Delta1 (Fig. 12) (Kuang

et al., 2007). When grafted into Pax7 null mice, the YFP^{-ve} cell fraction was able to give rise to 3 times as many $Pax7^{+ve}$ satellite cells as the YFP^{+ve} fraction (Kuang et al., 2007). In this study the transient amplifying progenitors (YFP^{+ve} cells) were defined by the ability of Cre to effectively cause recombination at the ROSA 26 locus. However, effective recombination may not occur in case of too brief an expression (or too little) of Myf5-Cre or an inability of the ROSA 26 locus to drive the expression of YFP in all quiescent satellite cells. More importantly, the YFP^{+ve} population gives rise to $Myf5^{-ve}$ cells (that would still express YFP). Indeed it was shown that YFP^{+v}e cells give rise to satellite cells when grafted into Pax7 null mice, although at a lower frequency than YFP^{-ve} population.

As mentioned before, the balance between self-renewal and differentiation is crucial for stem cell maintenance and tissue homeostasis, and satellite cells are no exception to this. Recent findings, in addition to the lineage tracing study of Kuang et al. have pointed towards an involvement of asymmetric cell division in maintaining this balance. Asymmetric co-segregation of parental and daughter DNA strands into different daughter cells was reported in a fraction of satellite cells (Conboy et al., 2007; Shinin et al., 2006). Newly synthesized DNA strands were labeled using a short BrdU pulse during the S phase while a longer pulse of BrdU was used to label all DNA strands cells during consecutive rounds of S phase. This was followed by a chase period where no BrdU was present to allow the segregation of labeled strands. These experiments demonstrated that the older "immortal" DNA strands (Immortal strand hypothesis, (Cairns, 1975)), co-segregated into the self renewing daughter cell, that expresses the stem cell marker Sca1 and the younger "replication error prone" DNA strands cosegregated into the daughter cells fated for differentiation and expressing the differentiation marker Desmin (Conboy et al., 2007; Shinin et al.,

2006). One of these studies also showed that the cell fate determinant Numb cosegregated with the older DNA strand into the stem cell (also consistent with its role in repressing Notch (Shinin et al., 2006). This data fits in with the study from Kuang et al. where Notch was repressed in the self renewing (YFP^{-ve}) and consequently Delta1 was upregulated in the differentiation prone (YFP^{+ve}) cell during asymmetric cell division (Fig.12) (Kuang et al., 2007). It is worth noting that cosegregation has been shown in some (epithelial and neural) (Karpowicz et al., 2005; Smith, 2005) but not in other (haematopoietic) stem cells(Kiel et al., 2007). This ability to asymmetrically coseggregate DNA is dramatically reduced with time in vitro (Conboy et al., 2007; Shinin et al., 2006) implying that stem cell niche mediated influence might be imperative in maintaining this ability of the satellite cells for asymmetric division. Also, since asymmetric cosegregation occurs only in a limited number of satellite cells (Conboy et al., 2007; Shinin et al., 2006), it is tempting to speculate whether this is a property of a subpopulation of satellite cells. As a caveat to these arguments, it should be noted that BrdU can act as a negative repressor of MyoD expression (Ogino et al., 2002) and inhibit myogenic differentiation (Bischoff and Holtzer, 1970). It might then be that the real reason for non-random segregation of DNA strands is to enable differential gene expression-the “silent sister” hypothesis (Lansdorp, 2007).

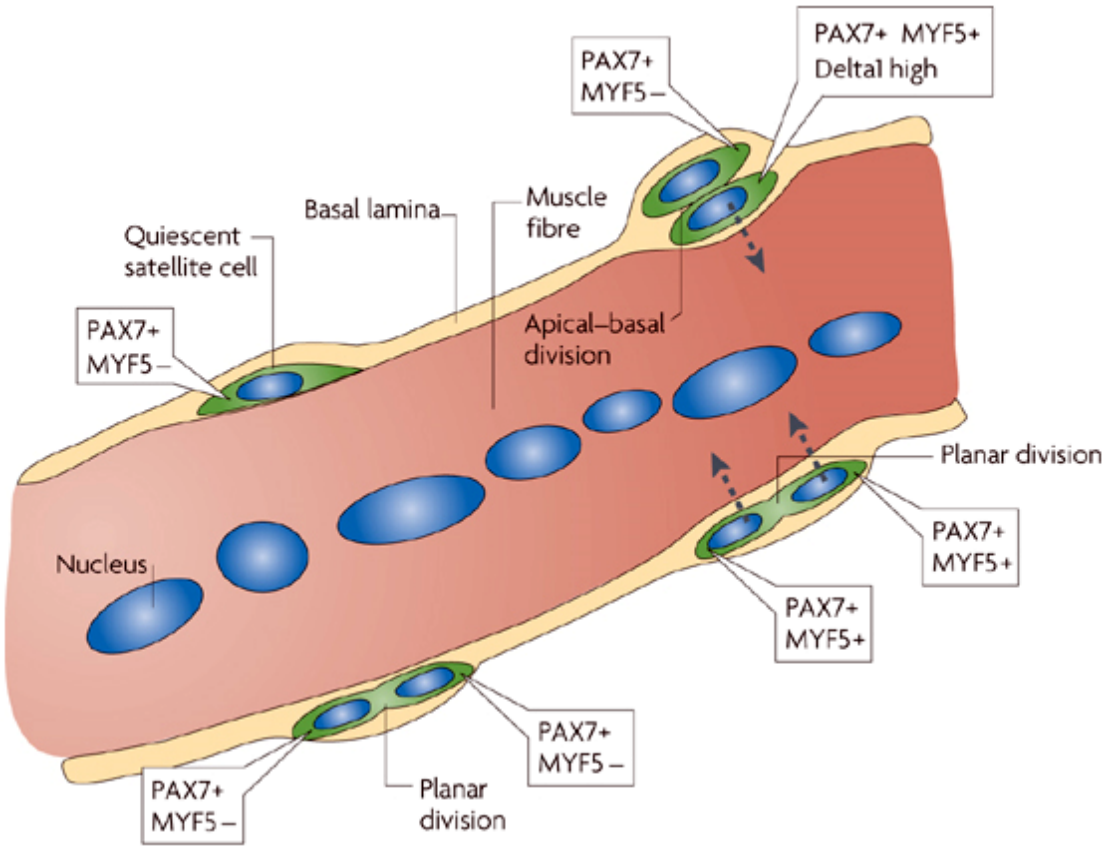

Figure 12: Adult myogenesis. Quiescent satellite cells are marked by the expression of paired box gene 7 (PAX7), met proto-oncogene (MET), M-cadherin and other satellite-cell markers, and differ from cells that are committing to a muscle-progenitor fate, which begin to express myogenic factor 5 (MYF5). More recently, analysis of cultured fibres has identified that the plane of satellite-cell division determines the fate of the daughter cells. Satellite cells (green) carrying out planar division (parallel to the myofiber) generally give rise to daughter cells with symmetric MYF5 expression. Cells dividing along an apical–basal plane (perpendicular to the myofiber) generally have asymmetric expression of MYF5. In this way, a satellite cell can divide and give rise to committed progenitors (MYF5 positive) as well as maintain a pool of uncommitted satellite cells (MYF5 negative). Figure adapted from (Bryson-Richardson and Currie, 2008).

Stem cell niches have come to be recognized as a crucial component of stem cell maintenance and function and regulate, in particular, the generation of the asymmetry so critical for asymmetric (or asymmetric outcome of) cell division. Satellite cells possess a very well defined anatomical niche, sandwiched between the host muscle fiber and the ensheathing basal lamina. There is increasing evidence that the niche and the systemic environment also regulate the regenerative potential of

satellite cells (Shefer et al., 2006). Mechanical, chemical and electrical signals have all been shown to be involved in regulation of satellite cell function (Charge and Rudnicki, 2004; Molgo et al., 2004; Tatsumi et al., 2006). On the other hand, extracellular matrix associated proteins such as laminin, collagen, and proteoglycans from the basal lamina anchor the satellite cell (Fuchs et al., 2004). A large majority, up to 70-80% of satellite cells in mice and humans reside within 5mm of the microvasculature that is a constant source of various extrinsic signals (Christov et al., 2007). Since satellite cell activation accompanies their vacation of the niche, it is possible to speculate whether the two events are linked. Recent evidence shows that Caveolin-1 and sphingomyelin, both are specifically localized to the caveolae, membrane invaginations composed of lipid rafts, of quiescent satellite cells (Nagata et al., 2006b; Schubert et al., 2007; Volonte et al., 2005). Caveolin-1 regulates internalization of caveolae (Navarro et al., 2004) and thus might activate sphingomyelin signaling, converting sphingomyelin into sphingosine-1-phosphate, known to activate satellite cells. It has been observed that caveolin-1 dependent internalization of caveolae occurs concomitantly with cell detachment from the ECM and regulates the integrin mediated Erk MAP kinase, PI3K, and Rac signaling pathways (del Pozo et al., 2005). It is therefore tempting to speculate that laminin-integrin adhesions might regulate the quiescence of satellite cells by inhibiting caveolin-1 dependent endocytosis of sphingomyelin signaling. Fig. 13 summarizes the different signals a satellite cell is subjected to from various niche components. Both the daughter cell of a satellite cell undergoing planar division would get exposed to both apical and basal signals in equal measure. However the progeny of a satellite cells undergoing apical-basal cell division would be subjected to either apical *or* basal signals and could therefore influence the cell fate decision. This line of discussion is

supported by the evidence from Kuang et al. who showed that the apical cell gives rise to the self renewing stem cell and the basal cell gives rise to differentiation destines progeny (Kuang et al., 2007). Such a progeny being apposed to a muscle fiber is also likely to fuse to the host myofiber more readily. However, the key signals that organize the satellite cell polarity and the mitotic spindle orientation need to be determined.

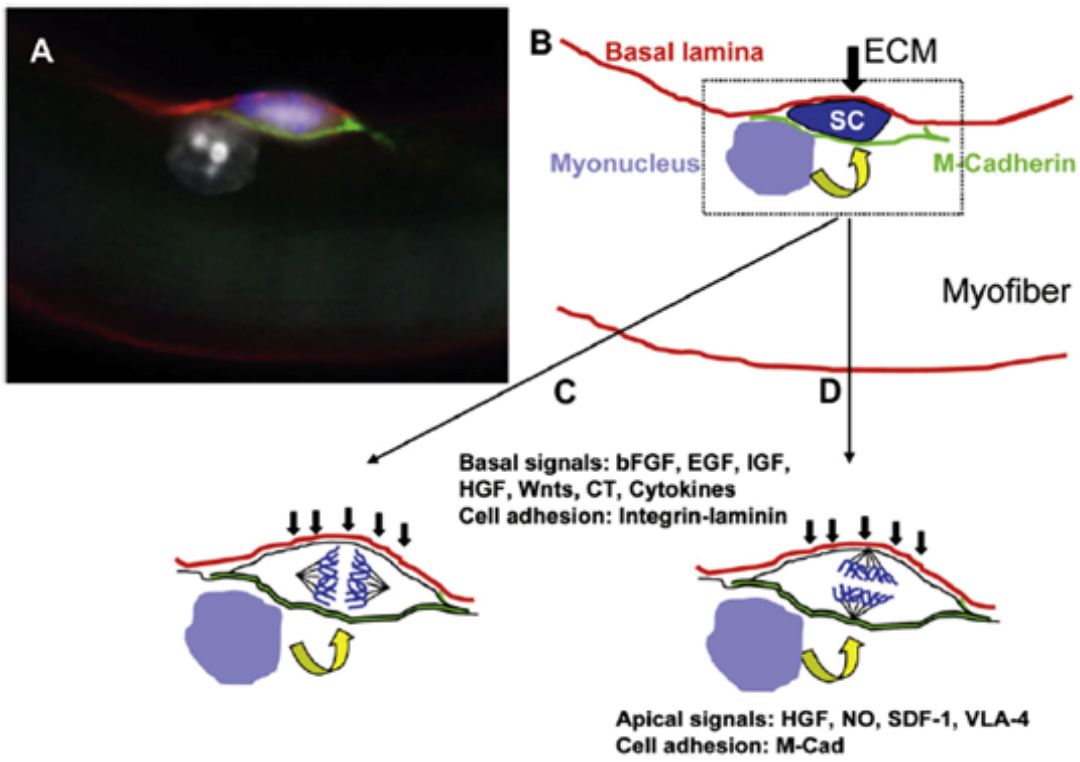

Figure 13: Regulation of Satellite Cell Polarity and Daughter Cell Fate by Niche (A) Immunostaining of a freshly isolated single myofiber showing some key components of a satellite cell niche. The satellite cell is labeled with Pax7 (in blue). Red, laminin; green, M-cadherin; white, nuclei revealed with DAPI.(B) A diagram redrawn from (A) showing how differential signals from the extracellular matrix (ECM) (black arrow) and the host myofiber (yellow arrow) might impose on the satellite cell to establish a polarity. (C) A planar-oriented division would deposit both daughter cells under identical influence of apical and basal signals.(D) In contrast, an apical-basal-oriented division(the mitotic spindle is perpendicular to the basal laminin) would result in a situation where the daughter cell attached to the basal lamina and the one attached to the host myofiber are exposed to different signals. Figure adapted from (Kuang et al., 2008).

1.5.5 Therapeutic Potential of Satellite cells

The report in 1989, that cultured myoblasts can restore dystrophin in muscles of *mdx* mice stimulated great interest and clinical trials (Partridge et al., 1989). However it was soon offset by the realization that autologous satellite cells cannot produce dystrophin and to lead effective muscle regeneration large numbers of myoblasts would need to be transplanted. The grafted cells suffer from poor survival, self renewal and migration and incompatibility with systemic delivery methods. It was argued that a very small number of the self renewing fraction of muscle precursors could solve the problem, as the self renewing myoblasts will give rise to both regenerated muscle tissue as well as future satellite cells. Several recent studies have indicated that freshly isolated or single fibers harboring quiescent satellite cells when transplanted give rise to new satellite cells in the host (Cerletti et al., 2008; Collins et al., 2005; Kuang et al., 2007; Montarras et al., 2005; Sacco et al., 2008). Of particular note is the study from Cerletti and colleagues reporting Fluorescence-Activated Cell Sorting (FACS) of a subset of satellite cells based on their expression of certain markers. This $CD45^{-}Sca\text{-}1^{-}Mac\text{-}1^{-}CXCR4^{+}ß1\text{-}integrin^{+}$ (CSM4B) fraction was designated as Skeletal Muscle Precursors (SMPs). These cells were verified to be highly enriched in the expression of markers for quiescent satellite cells, expressed no markers characteristic of differentiation and were in the G_0 phase of the cell cycle (Cerletti et al., 2008). These SMPs (isolated from a GPF^{+ve} donor) were then injected into the muscles of *mdx* mice and the number of GPF^{+ve} fibers was used as readout of the regeneration ability. Quantification of the results showed that purified SMPs contributed to up to 94% of the myofibers in the host animals, restored dystrophin expression to these fibers and significantly improved the contractile function of the muscle. Furthermore, these SMPs inhabited satellite cell compartments and continued

to contribute to muscle growth and regeneration till four months after transplantation (the longest stage till the study was carried to) (Cerletti et al., 2008).

1.5.6 Non-satellite cell mediated muscle regeneration

Although satellite cells are the most prominent species of progenitors leading to muscle regeneration, a number of other sources contributing to muscle regeneration have been reported (Price et al., 2007). The most prominent amongst these are the "side population" (SP) cells, first identified as a sub-fraction of mouse haematopoetic stem cells by their ability to exclude the DNA binding dye Hoechst 33342 (Goodell et al., 1996; Goodell et al., 1997). SP cells possess long term multilineage reconstitution abilities and exist in diverse organs such as bone marrow, skeletal muscle, liver, brain, lung, skin and heart (Asakura et al., 2002; Goodell et al., 1996; Goodell et al., 1997; Montanaro et al., 2003). Bone marrow derived or muscle derived SP cells do not possess an intrinsic ability to differentiate into myocytes, yet upon injection into muscle or coculture with satellite cells they give rise to myocytes (Asakura et al., 2002; Gussoni et al., 1999). The muscle derived SP cells from Pax7 null mice can undergo myogenic specification, thereby indicating that SP cells and satellite cells constitute distinct populations (Seale et al., 2000). In contrast to satellite cells, SP cells are suitable for systemic delivery via bloodstream, have been reported to take up satellite cell position (Asakura et al., 2002; Bachrach et al., 2006; Gussoni et al., 1999) and provide dystrophin to diseased muscle via arterial transplantation (Bachrach et al., 2004; Bachrach et al., 2006). It is therefore puzzling why they do not contribute to long term muscle regeneration.

Cell populations other than satellite cells and SP cells have also been observed to contribute to muscle regeneration. These include the multipotent mesenchymal

stem cells capable of producing skeletal muscle in addition to osteoblasts, chondroblasts, and adipocytes (Caplan, 1991; Friedenstein et al., 1966; Prockop, 1997). Blood vessel derived mesangioblasts were recently shown to restore expression of α-sarcoglycan when injected into α-sarcoglycan deficient mice, to improve muscle fiber morphology and to ameliorate muscle function in dystrophic dogs (Sampaolesi et al., 2006; Sampaolesi et al., 2003). Pericytes have also been reported to form a class of myogenic precursors distinct from satellite cells (Dellavalle et al., 2007; Sampaolesi et al., 2006; Sampaolesi et al., 2003).

1.6 Myogenesis in zebrafish

Zebrafish is an ideal model system to study motility behavior and muscle development. In addition to the general advantages outlined above there are several advantages specific to muscle development. Motility develops relatively early at around 18 hpf and the embryo exhibits spontaneous twitching of the body axis. By 48 hpf, the larva responds to touch by swimming away from the stimulus, the so called 'escape response'. Within this period all the muscle lineages are established in the trunk musculature. Furthermore, the zebrafish myotomal structure is well studied and in contrast to chick and mouse, consensus about cell structure and cell migration has been achieved. As the zebrafish myotome continues to expand, it exhibits two types of growth; hyperplasia, an increase in cell numbers that occurs in larval stages and hypertrophy, an increase in the size of existing fibers that occurs in the juveniles and adults (Rowlerson A, 2001). In teleosts, the addition of new fibers initially occurs at the dorsal and the ventral edges of the myotome (Galloway et al., 1999). This type of regional growth is termed stratified hyperplasia and is reminiscent of the growth that occurs in chick myotome (Amthor et al., 1999; Rowlerson A, 2001).

1.6.1 Somite patterning in zebrafish

Unlike amniotes, zebrafish do not need a robust skeleton as they live in an aquatic habitat. However, to traverse the relatively viscous medium (water) they require substantial musculature. Therefore most of the zebrafish somite is composed of the myotome, with sclerotome forming a minor proportion. Consequently the fish sclerotome, although still ventral to myotome (like amniotes), does not lie adjacent to the notochord. The zebrafish sclerotome could be first identified, either morphologically, as a cluster of cells under on the venteromedial surface of the somite (. 14 A), or by the expression of markers such as *pax9* and *twist1a* (Germanguz et al., 2007; Morin-Kensicki and Eisen, 1997; Nornes et al., 1996). Many of these cells would migrate to encircle the spinal cord and the notochord (Fig. 14B) to give rise to the vertebrae.

In zebrafish, muscle fibers fall into two broad anatomical subclasses, slow twitch fibers and fast twitch fibers depending on expression of the genes that encode lineage specific isoforms of sarcomeric structural proteins such as Myosin Heavy Chain (MyHC) and troponin. Slow twitch fibers are required for slow swimming that the fish employ most of the time and fast twitch fibers are necessary for rapid bursts of speed as required when escaping a predator or chasing a prey. Anatomically, the slow fibers are located at the periphery of the myotome and in the adult they form a triangular wedge shape at the horizontal myoseptum. Being heavily vascularized the slow fibers are darker in color. Fast muscle fibers are located deeper in the myotome and are lighter in color than slow fibers.

The slow and the fast muscle cells are lineage restricted and their lineages are established very early in development (Devoto et al., 1996). Fate mapping has

revealed that cells that ultimately form skeletal muscles are present in the marginal zone of the embryo (Kimmel et al., 1990) and even at this early stage the slow and fast muscle precursors have different locations (Hirsinger et al., 2004). By the time gastrulation ends, the muscle precursor are arranged either side of nascent notochord as a monolayer of cuboidal cells, adaxial cells, called so by the virtue of their position (Fig. 12) (Devoto et al., 1996). Adaxial cells are the precursors of all slow muscles and form the earliest muscle fibers to develop, the muscle pioneer cells (van Raamsdonk et al., 1982; Waterman, 1969). These are a subset of embryonic slow muscle fibers, are formed at the level of horizontal myosepta, and were later shown to express the homeodomain transcription factor Engrailed (Hatta et al., 1991). As the somite matures the adaxial cells undertake a remarkable journey to migrate radially towards the somite periphery (Fig. 14C-E) (Devoto et al., 1996). This journey is completed in two phases: in the first phase the adaxial cells migrate dorso-ventrally and elongate while they are still medially located, in the second phase the elongated adaxial cells migrate radially outwards to the somite surface (Devoto et al., 1996). As the slow muscle fibers migrate outwards they induce differentiation and elongation of fast muscle fibers in their wake (Henry and Amacher, 2004). By 24 hpf the muscle pioneer cells become separated from the notochord and by 36 hpf slow muscle migration is complete (Devoto et al., 1996). By 24 hpf, Engrailed protein could be detected not only in muscle pioneer cells but also at a lower level in nuclei of fibers surrounding the muscle pioneers (Hatta et al., 1991; Wolff et al., 2004). Because these cells lack expression of slow MyHC (characteristically expressed by muscle pioneers and slow muscle cells) they are designated as medial fast fibers (Wolff et al., 2004). So far no specific function has been ascribed to them.

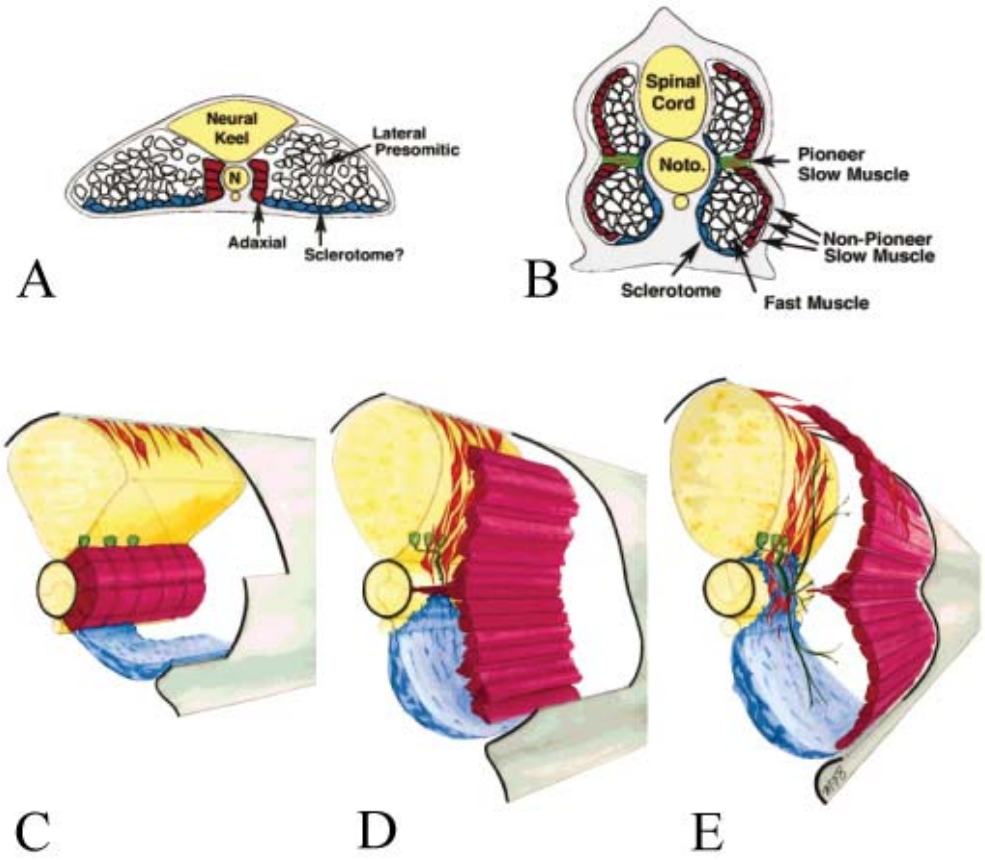

Figure 14: (A-B) Schematic representation of a transverse section of zebrafish somite at 13hpf (A) through the anterior PSM, and at 24hpf (B), showing relative positions of fast muscle precursors (lateral presomitic), *twist 1a* expressing (sclerotome) and slow muscle precursors (adaxial cells, A) that form pioneer slow muscles and non-pioneer slow muscles (B). (C-E) Multiple populations of cells move at similar times. (C-E) Schematic views of a developing posterior trunk somite. Adaxial cells (in C)/slow muscle (in D and E) cells are depicted in red, and sclerotome in blue. The clear, 3-dimensional space in the somite represents fast muscle cells. (C) At 12 hr adaxial cells are positioned adjacent to the notochord medial to both fast muscle and the sclerotome. (D) At about 18 hr, slow muscle cells are migrating toward the surface with fast muscle precursors positioned both medial and lateral to them. Muscle pioneer cells, however, remain adjacent to the notochord. (E) Muscle pioneer cells become separated from the notochord at about 24 hr. The sclerotome is now adjacent to the notochord. Fast muscle is completely medial to the slow muscle fiber monolayer. Neural crest cells in orange and motor neurons in green are also depicted though and undergoing migration at the same time but are not discussed here. Figure adapted from (Stickney et al., 2000).

1.6.2 Patterning of the zebrafish myotome

In zebrafish, availability of gamma ray and ENU induced mutants (Fritz et al., 1996; Haffter and Nusslein-Volhard, 1996; Whitfield et al., 1996) have provided new insights and has implicated novel genes in myogenesis.

The expression of *myoD* is first observed at 75% epiboly (Weinberg et al., 1996) in a triangular patch of cells on either side of the embryonic shield and the expression of *myf5* slightly later, at 80% epiboly (Coutelle et al., 2001) in the strips of PSM adjacent to the notochord. The expression of *myogenin* is not detected till segmentation period (Weinberg et al., 1996) and the expression of Mrf4 (*myf6*) has not been reported. The zebrafish MRFs have not been studied as extensively as their chick or rodent homologs so their roles in muscle specification and differentiation are as yet unclear. The current body of knowledge suggests that the myogenesis in zebrafish relies on the interplay between FGF and Hh signaling pathways and members of Tbx family of transcription factors, *notail* (*ntl*) and *spadetail* (*spt*).

The zebrafish *fgf8* mutant (*acerebellar*) embryos show reduced myoD expression in adaxial cells but somite expreesion of myoD is normal (Reifers, Bohli et al. 1998). However, blocking *fgf24* expression in *fgf8* mutant background completely abolishes myoD expression (Draper et al., 2003) indicating critical importance of FGF8 and FG24 for zebrafish myotome formation.

Mutations in zebrafish T-box family member genes *notail* (*ntl, brachyury*) (Kimmel et al., 1991) and *spadetail* (*spt*, *Tbx16*) (Kimmel et al., 1989) result in absence of or a great reduction in the size of tail due to failure of somite formation (Griffin et al., 1998; Halpern et al., 1993). In either of the *ntl-/-* or *spt-/-* single mutants, myoD expression is not initiated until the end of gastrulation but recovers

partially during segmentation (Amacher et al., 2002; Weinberg et al., 1996). In contrast the *ntl/spt* double mutants are completely lacking in myoD expression (Amacher et al., 2002). Therefore *ntl* and *spt* are both required for zebrafish myogenesis.

In zebrafish, Hedgehogs plays a critical role in muscle development. For a review see (Ingham and Kim, 2005). Hedgehogs (Hh) are secreted signaling molecuales that are essential for a number of developmental processes. They can act as morphogens and mediate their effects through the receptor complex consisting of Patched (Ptc) and Smoothened (Smo) transmembrane proteins. In the absence of Hh, Ptc represses Smo so that Smo cannot signal. When Hh binds to Ptc the repression on Smo is removed and Smo can transduce the signal. In vertebrates this signal is mediated through Gli proteins that can act as transcriptional activators of repressors. The whole process is complicated by the fact that usually there are several paralogs of Hh, Ptc and Gli proteins. For a review of Hedgehog signaling see (Ingham and Placzek, 2006).

In zebrafish, Hh activity from midline is necessary and sufficient to induce slow muscle and muscle pioneer cells, both *in vivo* and *in vitro* (Du et al., 1997; Norris et al., 2000; Weinberg et al., 1996; Wolff et al., 2003). An entire class of mutants, called *you*-type (because of the U-shaped somites that they have) include *you-too* (*yot*)*, sonic-you* (*syu*), *you* (*you*), *u-boot* (*ubo*) and *chameleon* (*con*) have been shown to have muscle defects (van Eeden et al., 1996). These mutations show muscle defects and the genes disrupted by these mutations were shown to encode components of the hedgehog pathway (Baxendale et al., 2004; Hollway et al., 2006; Karlstrom et al., 1999; Nakano et al., 2004; Schauerte et al., 1998; van Eeden et al., 1996). Analysis of these mutants as well as chemical inhibitor experiments have led to a

consensus that a near complete loss of Hh activity results in almost complete absence of the adaxial cell derived slow muscles (Barresi et al., 2000) but the fast muscle cells, that derive from paraxial mesoderm, remain relatively unaffected (Barresi et al., 2000; Chen et al., 2001).

Genetic and embryological analysis in zebrafish has revealed novel regulators of Hh pathway in vertebrates. Two such mutants are *you* (encoding Scube2) and *iguana* (encoding Dzip) (Hollway et al., 2006; Kawakami et al., 2005; Sekimizu et al., 2004; van Eeden et al., 1996; Wolff et al., 2004; Woods and Talbot, 2005). Epistatic and molecular analysis suggests that Scube2 is functions upstream of Smoothened (the signal transducer in the Smoothened-patched complex) (Hollway et al., 2006). The Dzip1 protein is expressed ubiquitously throughout the embryo through the segmentation state (Sekimizu et al., 2004; Wolff et al., 2004). It has been shown that Dzip1 shuttles between the nucleus and cytoplasm and may regulate Hh signaling both positively and negatively (Sekimizu et al., 2004; Wolff et al., 2004). The Hh dependent muscle cell types form aberrantly in *dzip1* (*iguana*) mutants (Wolff et al., 2004). Hedgehog interacting protein (Hhip) is another vertebrate specific Hh activity regulator required for formation of muscle pioneers (Ochi et al., 2006). Hhip, a type I transmembrane protein was originally identified in a biochemical screen for finding out interacting partners of Shh (Chuang and McMahon, 1999). Genetic and biochemical evidence suggests that Hhip sequesters Hh thus acting as a negative regulator to modulate the amount of Hh present on the cell surface (Chuang et al., 2003; Kawahira et al., 2003; Treier et al., 2001). In zebrafish, Hhip is first expressed by adaxial cells and later by muscle pioneers and a subset of fast muscle cells (Ochi et al., 2006). Gain and loss of function experiments have revealed a requirement of Hhip

for myoD expression in adaxial cells, and subsequently slow muscle and muscle pioneer development (Ochi et al., 2006).

In zebrafish, *prdm1* (also called *blimp-1*) expression comes on in adaxial cells after *myoD* and *myf5* expression (Baxendale et al., 2004; Wilm and Solnica-Krezel, 2005). Prdm1 expression is lost in *smo* mutants and overexpression of *shha* can lead to ectopic expression of prdm1 (Baxendale et al., 2004). Therefore *prdm1* expression is believed to be Hh dependent in adaxial cells. In prdm1 mutants (*u-boot*) slow muscles fail to express the slow muscle specific marker Prox1 and instead express fast MyHC (Roy et al., 2001). It is therefore believed that prdm1 expression functions as a point of choice in slow or fast muscle differentiation program. How Prdm1 governs slow muscle identity remained unknown till recently when it was shown that Prdm1 represses the transcription of *sox6* in adaxial cells (von Hofsten et al., 2008). Repression of *sox6*, a known repressor of slow muscle fate allows adaxial cells to adopt a slow muscle identity. Moreover, analysis of DNA sequences recovered after performing ChIP with an antibody against Prdm1 revealed that putative promoters of several of the fast-fibre-specific isoforms of sarcomeric proteins, including those encoding fast MyHC and troponins, were enriched while no slow muscle specific gene promoter were found (von Hofsten et al., 2008). Taken together, this data strongly suggest that Prdm1 promotes slow muscle fate in adaxial cells by repression of *sox6*, a repressor of slow muscle fate and repressing activation of atleast some fast muscle specific isoforms of sarcomeric proteins.

1.6.3 Gene networks in skeletal muscle development in zebrafish

Having looked at the various genetic pathways that are responsible for muscle development in zebrafish we can integrate and summarize them in the schematic depicted in Fig. 15. Unlike chick and mouse, in zebrafish myogenesis the roles of Pax3 and pax7 are not understood very well. Instead, as indicated above, T-box genes and FGF are implicated in the expression of myoD (and hence myogenesis) (Fig. 15A). Although it is accepted that the interactions between FGF and Ntl are important for myoD expression, both these genes are expressed are earlier (30% epiboly) that the time that myoD expression is initiated (75% epiboly) (Griffin et al., 1998; Rodaway et al., 1999; Schier and Talbot, 2005). Thus it is not clear if FGFs and T-box genes function in an inductive or a permissive way for muscle induction.

It has now been established that the precursors of slow muscles are formed independent of Hh signaling but Hh signaling is required later for the commitment to slow muscle fate (Du et al., 1997; Hirsinger et al., 2004; Norris et al., 2000; Wolff et al., 2003). Furthermore it is the concentration of Hh activity that decides the ultimate fate of muscle cells. Adaxial cells that express high levels of Ptc (Lewis et al., 1999a; Lewis et al., 1999b) and Hhip (Ochi et al., 2006), thus sequestering Shh emanating from the notocord. Thus local high concentration of Shh leads to formation of muscle pioneers from adaxial cells and medial fast fibers from fast muscle precursors immediately adjacent to them (Fig. 15B and D). Another member of Hh pathway; Fused (Fu), a serine/threonine kinase, is required for cells to respond to maximum levels of Hh signaling (Ingham and McMahon, 2001). Inhibition of Fu activity in zebrafish causes a loss of muscle pioneers without affecting other cell types in the myotome (Wolff et al., 2003) indicating that Fu might function as a choice point in

the differentiation of muscle pioneers (Fig. 15D) (Ingham and Kim, 2005). In *iguana* (Dzip) mutants, both muscle pioneers (requiring high levels of Hh activity) and slow muscle fibers (requiring high levels of Hh activity) that are specified by early Hh signaling are reduced in numbers (Wolff et al., 2004), whereas the number of medial fast fibers that require intermediate levels of Hh, at a later time, are substantially increased (Wolff et al., 2004). Therefore, it is believed that Dzip may act on Hh activity as a positive regulator for early developing slow muscle fibers or negative regulator for later developing fast medial fibers (Fig. 15D) (Sekimizu et al., 2004; Wolff et al., 2004). The role of prdm1 in choice of slow/fast muscle fate has already been outlined above (Fig. 15D).

As described before, slow muscle fiber migration induces differentiation and elongation of fast muscle fibers in their wake (Henry and Amacher, 2004). During segmentation, Fgf8 regulates myoD expression thereby regulating terminal differentiation of a subset of fast muscle cells (non-medial fast fibers) (Groves et al., 2005). Fgf8 itself might be induced by retinoic acid that has been shown to inhibit proliferation and promote terminal differentiation of myoblasts in cell culture experiments (Alric et al., 1998). In zebrafish, the main retinoic acid synthesizing enzyme, Retinaldehyde dehydrogenase 2, is expressed in the somites where it activates *fgf8* expression thus inducing fast muscle differentiation (Fig. 15C and D) (Hamade et al., 2006).

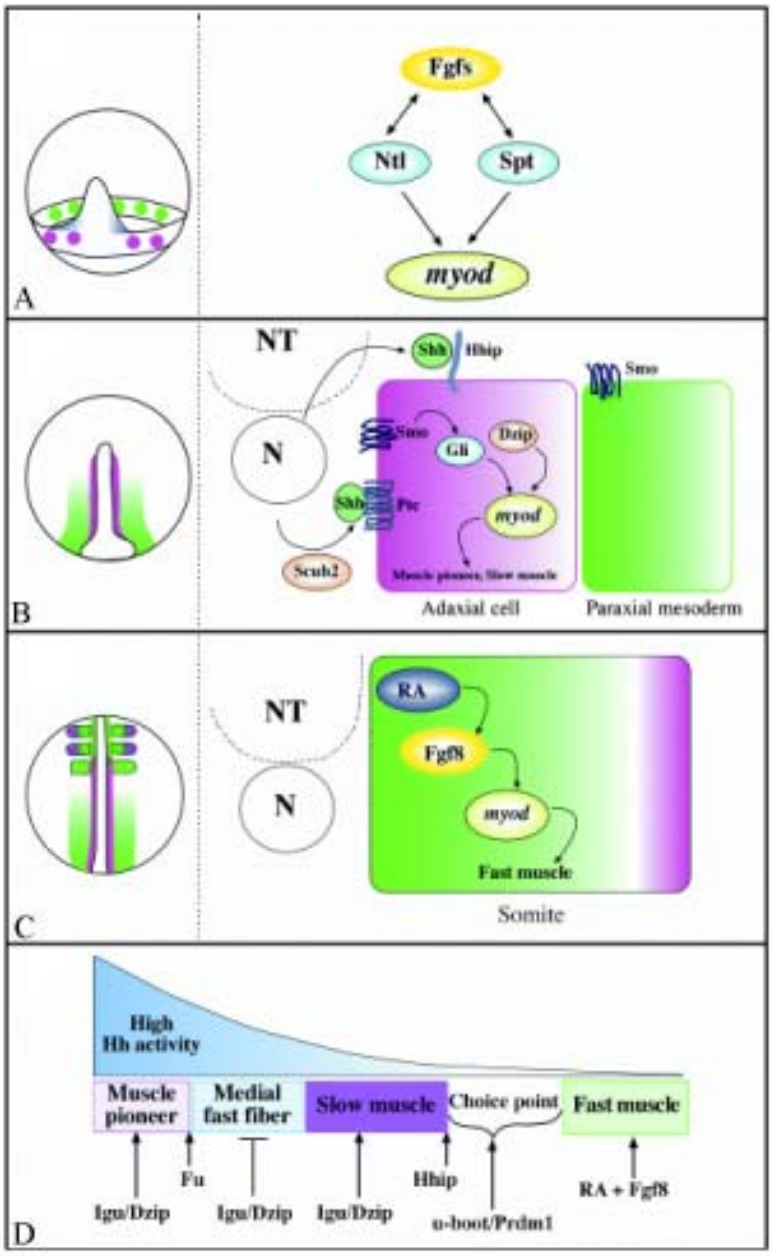

Figure 15: Model of skeletal muscle development in zebrafish. (A) Schematic illustration of the genetic regulation of early myogenesis in zebrafish. Both fibroblast growth factor (Fgf) signaling and T-box genes are required for early *myod* expression. (B) Molecular mechanisms that specify the formation of slow and muscle pioneer cells from adaxial cells. Expression of Patched (Ptc) may allow adaxial cells to respond to high levels of Hh activity and, together with Hedgehog interacting protein (Hhip), prevent the lateral diffusion of Hh proteins. (C) Specification of fast muscle cells. A combination of Retinoic acid (RA) and Fgf8 regulates *myod* expression in the somites and promotes fast muscle differentiation. (D) Model explaining how Fgf and Hh signal pathways function in the specification of zebrafish skeletal muscle cell types. **NT**, neural tube; **N**, notochord. Figure adapted from (Ochi and Westerfield, 2007)

1.7 Zebrfaish as a model for developmental genetics

In the last twenty years zebrafish has emerged as an important model system to study genetics, genomics and developmental biology. Zebrafish are small (3-4 cms in length) and easily housed in aquaria at relatively high densities, are highly fecund (produce up to 150-200 embryos per mating pair), develop *ex utero*, and are optically transparent at embryonic and larval stages. The embryonic development of zebrafish is quite fast and within 24 hours all major organ systems have started to form. They have a short generation time (3-4 months) and live up to 3-5 years with optimal fertility between 6-18 months.

1.7.1 Genetic methods to study zebrafish muscle development and regeneration

1.7.1.1 Forward genetics approaches to study zebrafish

Zebrafish possess a diploid genome and are the rare vertebrate model system in which large scale forward genetic screens have been possible. Large scale mutagenesis screens such as the Boston and Tübingen screens of 1996 (Driever and Fishman, 1996; Haffter et al., 1996; Haffter and Nusslein-Volhard, 1996) brought zebrafish to the forefront of developmental biology research. In these screens the premeiotic germ cells of the male fish were mutagenised using ethyl nitrosyl urea (ENU). The mutagenized males (founders) were crossed with wildtype fish to produce F1 progenies that contained heterozygotes for mutations within the zebrafish genome at a rate of 100-200 mutations per fish. The F1 fish were mated to wildtype fish to obtain the F2 generation. Siblings from F2 generation were incrossed and their progeny, the F3 generation, were screened in a Mendelian manner (Fig. 16) (Haffter et al., 1996). These screen produced more than 4000 embryonic lethal mutants that were characterized (Driever and Fishman, 1996; Haffter et al., 1996).

An alternate approach to chemical mutagenesis has been the retroviral vector mediated insertional mutagenesis approach. This method does away with the painstaking positional cloning to identify the mutagenized gene as the sequence of the insert is known and could be used to determine the site of insertion. However the efficiency of insertional mutagenesis is reported to be only as much as about 10% of ENU based mutagenesis (Amsterdam et al., 1999; Amsterdam and Hopkins, 2004; Golling et al., 2002) Another disadvantage of insertional mutagenesis is that it is less likely to produce subtle phenotypes, such as temperature sensitive mutations, than ENU mutagenesis could produce due to point mutations.

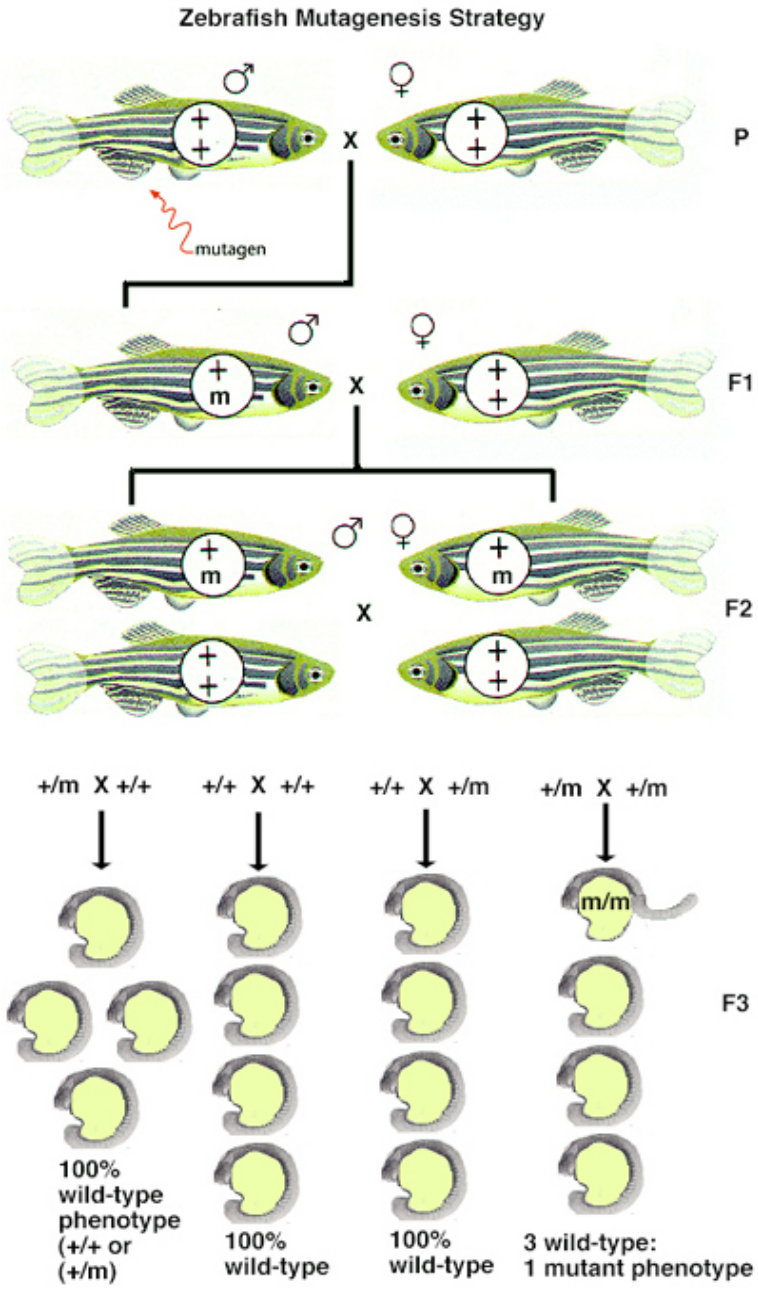

Figure 16: Screening protocol for identifying mutants of zebrafish development. The male parent is mutagenized, such that some of its sperm contains a mutant allele. It is then mated with a wild-type female. The F1 progeny of this mating (here shown as a male carrying the mutant allele *m*), are mated with wild-type partners. This creates an F2 generation wherein some males and some females carry the recessive mutant allele. When the F2 fish are mated, some of their progeny will show the mutant phenotype. Figure adapted from (Haffter et al., 1996)

1.7.1.2 Reverse genetics approaches to study zebrafish

The most common reverse genetics approach used in zebrafish is based on use of antisense morpholino oligos (MOs), first developed for clinical therapeutic applications, later introduced into developmental biology, and have been in use since 2000 in organisms as diverse as sea urchin, ascidians, frog, chick, and mouse besides

zebrafish (Heasman, 2002; Nasevicius and Ekker, 2000). MOs act by blocking translation of mRNA into polypeptide or by interfering the splicing of mRNA. Unlike DNA analogs they are resistant to enzymatic degradation. The advantages of MOs are their ease of use, high specificity and simple delivery methods; in case of zebrafish: microinjection. The disadvantages are that they become diluted as development persists and their effect does not last beyond 3-6 days (Heasman, 2002).

Recent advances in techniques, such as TILLING (**T**argeting **I**nduced **L**ocal **L**esions **IN** **G**enomes) or development of methods such as engineering zinc finger nucleases to generate targeted heritable gene inactivation promise to expand the repertoire of reverse genetics approaches in zebrafish. TILLING allows the identification of single-base-pair allelic variation in a target gene, screened from a library generated from (mutagenised zebrafish sperm) in a high-throughput manner (Draper et al., 2004). The use of zinc finger nucleases (ZFNs) to cause targeting disruption of genes relies on the ability of ZFNs to induce targeted double-strand break that is repaired to generate small insertions or deletions (Doyon et al., 2008; Meng et al., 2008).

1.7.2 Zebrafish genomics

The Sanger Institute started sequencing zebrafish genome from February 2001. The zebrafish genome is about 1977Mb, spread over 25 chromosomes. Of this about 1,475Mb of genome is sequenced (http://www.sanger.ac.uk/Projects/D_rerio/). To obtain the genome sequence clones from BAC libraries are being used for mapping and sequencing with a whole genome shotgun (WGS) assembly. The finished clones are manually annotated and are accessible in Vega (http://vega.sanger.ac.uk/Danio_rerio). Sequences release from Vega, as of now (Nov

2008), cover around 1,290 Mb of zebrafish genome, of which about 420 Mb has been manually annotated. The assembly is generated based on the integration of the finished clone sequences and WGS sequences which are filled in the gaps between these clone contigs. The assembly is automatically annotated and can be browsed on the Ensembl wesite at http://www.ensembl.org/Danio_rerio/Info/Index. Currently the Sanger centre has released the seventh assembly of the zebrafish genome (Zv7) in Ensembl, which includes 17,330 known protein-coding genes, 1,177 projected protein-coding genes, 2,815 novel protein-coding genes and 98 pseudogenes. Having a well annotated genome greatly facilitates the mapping of mutant genes and the reverse genetics approaches mentioned above.

1.7.3 Transgenic reporters: live imaging possibilities

Microinjection of DNA constructs into one cell stage zebrafish embryos has been successfully used to generate transgenic zebrafish carrying reporters such as green fluorescent protein (GFP). By selecting the right promoter (and other cis-regulatory) elements precise spatio-temporal expression pattern of a gene could be mimicked (de Jong and Zon, 2005). Any regenerative process is highly dynamic and their study would benefit greatly from an *in vivo* model. The development of new fluorophores with wide spectral range, photoswitchability, and photoconversion from one spectral range to another coupled with the optical clarity of young zebrafish embryos or larvae could be harnessed to generate an impressive array of tools for following regeneration processes in vivo. The fluorescent transgenic fish could also be used in mutant screening, cellular defect analysis in mutants, cell fate mapping and cell transplantation experiments (Langenau et al., 2004; Traver et al., 2003).

1.7.4 High throughput analysis

Zebrafish is perhaps a unique vertebrate in that it can be adapted easily for high throughput analyses. The analyses can itself widely range from a small molecule treatment screens (MacRae and Peterson, 2003), toxicology screens (Hill et al., 2005) or pharmaceutical screens (Zon and Peterson, 2005). The high fecundity and small size of zebrafish embryos makes it easy to raise 1-3 embryos per well in a 96 well microtiter plate. The liquid handling for introduction of small biomolecules/toxicants/pharmaceuticals could be performed by a robot. Similarly a robotic arm can grip and place the microtiter plate on the stage of a microscope for imaging and remove it afterwords. The automated stage would move from well to well either capturing the whole well or specific features of embryos using an autofocus camera. In this way multiple plates could be used for generating a large amount of data in a very short time. This approach would definitely supplement existing methods of drug screens and would greatly speed up the same.

1.8 The need for a new model: using zebrafish to study muscle regeneration

All the above mentioned reasons make zebrafish an ideal model to study a regenerative event *in vivo*. To be able to develop a systemic approach towards treatment of muscle degenerative diseases we need to approach the challenges of muscle regeneration from a whole organism level. Traditionally most of the studies performed on satellite cells were performed in single fiber culture system. Such a model ignores valuable information from the systemic environment and the extracellular matrix. The dynamic nature of regeneration could best be understood in

the context of a whole organism. Therefore, with this study we aimed to develop a zebrafish model to study muscle regeneration, establish similarity with other models and identify putative genes involved in this process.

2 Materials and Methods

2.1 General Procedures

2.1.1 Fish breeding and maintenance

Zebrafish (Danio rerio) were maintained at 28° C, according to The Zebrafish Book (Westerfield, 2000). Wild-type embryos were obtained by pairwise matings of adult zebrafish (AB, AB202 or leo strains) raised in the fish facility of the FZK. Mutant embryos were obtained by crossing heterozygote carriers. were identified based on published descriptions and mendelian inheritance. The stages in hours post fertilization (hpf) or days post fertilization (dpf) were identified using the morphological features described by (Kimmel et al., 1995). Embryos were collected in a fine plastic mesh and raised in egg water (Westerfield, 2000) with 0.01% methylene blue to prevent fungal growth and treated at 18 hpf with PTU (Sigma, 30 mg/ml) to block pigment formation. Bulk de-chorionation was performed using pronase and MESAB (0.5 mM 3-aminobenzoic acid ethyl ester, 2 mM Na2HPO4) was added to the egg water at a final concentration of 0.5 mg/ml for anesthesia.

2.1.2 Using the escape response as an assay for motility

At 48 hpf, wild-type embryos exposed to a tactile stimulus at the side of the trunk responded with a strong bend of the body axis away from the source of stimulation, followed by an extended episode of swimming (Behra et al., 2002). I used this “escape response” in thr assay for motility mutant screen or as an assay for recovery from chemically induced myopathy. Larvae were touched by a blunt needle on their flank and observed under a stereo microscope. The embryos showing diminished or uncoordinated movement were counted to ascertain the Mendalian ratio of 1:4 for

recessive mutants. These observations were followed by daily observation for progressive motility loss as well as observation under polarized light for reduction or loss of muscle birefringence.

2.1.3 Birefringence assay to assess the myofibrillar structure

The integrity of muscles can be assayed by illuminating embryos with plane polarized light. Since muscles contain Anisotropic (A-) band, they shine when illuminated with plane polarized light, just like anisotropic crystals. This property was used to assay the muscle integrity in zebrafish larvae as in previous studies (Behra et al., 2002; Behra et al., 2004).

2.1.4 Galanthamine treatment

Viable embryos were sorted and raised in batches of 50 embryos, per 6 cm petri dish, in embryo medium. At 60-80% epiboly all embryo media was aspirated using a fine Pasteur pipette and 10mL of GAL solution of various concentrations was added. If blockage of pigmentation was desired for microscopy or ISH/IHC methods, GAL stocks were made in 1x PTU. For microarray analysis, PTU was omitted as it could induce off target genes. The embryos were monitored daily until harvesting at the desired stage and dead embryos/larvae were promptly removed.

2.2 Molecular Biology Methods

Unless otherwise stated all molecular biology methods were performed according to standard procedures (Sambrook, 2001). The following protocols, described briefly, were most commonly used.

2.2.1 PCR, semi-quantitative RT-PCR, and cDNA Cloning

Primers were designed using Primer3 (Table 5) and/or oligo calculator and were purchased from Metabion (Germany). Regular PCR was performed using *GoTaq* DNA polymerase or with *pfu* DNA polymerase (Promega, Germany) for high fidelity amplification from the BAC. Standard cycling conditions were: an initial denaturation at 94 ºC for 2 mins, 25 to 32 cycles of denaturation at 94 ºC for 30 secs, annealing at 55 ºC (dependent on primer melting point) for 30 secs and extension at 72 ºC for 1 min/target Kb, followed by a final extension at 72 ºC for 10 mins. Sequencing was performed by GATC (Germany) using RUN24. cDNA was generated from reverse transcribed total RNA.

2.2.2 Restriction Digestion and Ligation of DNA

The digestion of DNA with restriction endonucleases was performed according to the instructions of the enzyme supplier (Promega or Fermentas, Germany). Approximately one unit of enzyme per 1µg DNA in appropriate buffered digestion reaction was used. Unless otherwise specified by the manufacturer, the reaction was incubated for 1-4 hours at 37 °C, depending on the amount of DNA. Ligation was performed either, for two hours at room temperature (25°C) or overnight at 16°C with 3-5 units of T4 DNA ligase (Promega, Germany) and insert:vector molar ratios of 1:3, 1:1 or 3:1.

2.2.3 Extraction of DNA from agarose gel

For cloning or homologous recombination of BACs, the DNA fragments were separated by agarose gel electrophoresis. The band containing the desired DNA fragment was cut out from the gel and the DNA was extracted with the SV Gel and

PCR Clean-Up System or with the QIAquick Gel Extraction kit according to the manufacturer's instructions.

2.2.4 TOPO-cloning of genes perturbed in microarray studies

TOPO TA cloning kit (Invitrogen) was used for fast direct cloning of PCR amplified fragments with T overhangs (fragments amplified with Taq polymerase or Taq polymerase based enzyme blends). When the PCR amplification resulted in one specific band 2-4 µl from the PCR were used directly (without any purification) for the cloning reaction. After 5-10 min. incubation at room temperature, the cloning reaction was transformed into XL1 blue chemically competent cells (see below).The set of primers used for generating probes for the genes described in this study are given in the Table 2, along with restriction enzyme used to digest the vector and RNA polymerase used to synthesize the riboprobe.

Probe for ISH	Primer used for amplification	Vector	Restriction enzyme/ RNA Pol. used for antisense probe
hspb1	FP:CATCCCATTCTCCTTCATGC RP: GGCAATCCAGCCTCTCATAC	pCR Topo II	Hind III/ T7
zgc:103408 (MIBP)	FP:GGGAGATTCTGGGAGAAAGG RP:GATCAGCCCAGAGAGTGAGG	pCR Topo II	Not I/ SP6
L-threonine dehydrogenase	FP:GAAACAGCTGCCTGACCTTC RP:GATGTGGATGCAAAGCTTGA	pCR Topo II	BamH I; T7
Agxt	FP:CTCGGAAATGTTCGGGATTA RP:GGCTCCATTTCACCAACTGT	pCR Topo II	Not I/ SP6
zgc:100919	FP:CGCAATGCGAGTATGAGAAA RP:TGGCAGAAAAACATCAACCA	pCR Topo II	Hind III/ T7
hspb11	FP:CCAAACAGCTCAACAGCAAA RP:CTCCAATTTGCAACTTCACAA	pCR Topo II	EcoR V; SP6

Table 2: Primers used for the cloning genes upregulated in GAL microarray with restriction enzyme and RNA polymerase used for generating riboprobe

2.2.5 Transformation of competent E. coli cells and electroporation of targeting vector fragment in electrocompetent BAC containing EL250 cells

The chemo-competent XL1 blue cells were thawed on ice for 5 minutes. Subsequently 10-50 ng plasmid DNA or 5 µl of a ligation reaction was added and the cells incubated with the DNA for 35 minutes on ice, heat shocked at 42°C for 40 seconds and placed again on ice for 5 min. Then the cells were incubated in SOC medium without antibiotics at 37°C and 200 rpm for 30 minutes (ampicillin as selectable marker) and 1 hour (kanamycin or chloramphenicol as selectable marker) before plating them on LB-agar plates with appropriate antibiotics. The plates were incubated overnight (12-16 hours) at 37°C. The concentration of the used antibiotics was 100 µg/ml for ampicillin and 50 µg/ml for kanamycin and chloramphenicol.

For EL250 cells harbouring BACs, the following differences were followed: The culture of EL250 cells, with or without BAC was always performed on or below 32°C to prevent premature expression of recombinase. Subsequently the culture times for these cells were increased for upto 24-32 hours.

The targeting vector fragment was electroporated in the EL250 cells containing specific BAC. The cells were made electrocompetent by raising a fresh culture (at 32°C, 200 RPM) to the log phase ($O.D._{600}$ = 0.4 to 0.6). The recombinase was induced by incubating the culture as 42°C for exactly 15 minutes with periodic vigorous shaking. The culture was then chilled in ice-water slush for 30 minutes. Thereafter the cells were precipitated (2000 RPM, 30 minutes) at 4°C and the supernatant discarded. The cells were washed three times with ice cold autoclaved, distilled water and finally resuspended in appropriate volume of water. Final concentration of electrocompetent cells was adjusted to $2x10^{10}$ cells/ml.

100-300ng of targeting vector fragment (maximum 4µl) was placed in a chilled electroporation cuvette with 2mm gap. To this, 42µl of freshly made, electrocompetent, BAC containing EL250 cells were added. Electroporation was performed at 2.5 kilovolt as 500µl of SOC media was added to the cells immediately after electroporation. The cells were then incubated at 32°C for 2 hours before being plated on LB-agar plates containing chloramphenicol and kanamycin.

2.3 Histological Methods

2.3.1 Whole mount *in-situ* hybridization (WISH)

Dixoxigenin whole mount *in-situ* hybridisation was performed as described (citation). Zebrafish embryos were dechorionated manually using two pairs of sharp forceps at the desired stage and were fixed in BT fix (4% paraformaldeyde, 4% sucrose, 0.12mM CaCl2, 0.1M NaPi pH 7.4) at 4°C overnight. After fixation, embryos were rinsed with PBS, 2x5 min. For storage, embryos were dehydrated stepwise through a series of methanol-PBS, from 25%, 50%, 75% and 100% methanol gradient, and stored at -20°C till desired. Prior to staining embryos were rehydrated through the methanol series and then washed 4x5 minutes in PTW (1xPBS, 0.1% Tween-20). Embryos were then treated with Proteinase K (10 µg/ml) in PTW for 2-6 mins (for 24 hpf) 30 min (for 48hpf) and 60 minutes (for 72 hpf), followed by two washes in PTW, re-fixation in BT fix for 20 mins and washes in PTW 2x5 mins. After this treatment, embryos were transferred to hybridisation buffer (HYB: 50% Formamide, 5x SSC, 0.5 mg/ml yeast RNA, 50 µg/ml heparin, 0.1 % Tween 20.9 mM citric acid). After pre-hybridisation for 3-4 hrs at 65°C, the buffer was replaced by fresh HYB containing 1/400 dilution of the dixoxigenin labelled

antisense RNA probe and embryos were incubated overnight at 65°-70°C. Embryos were washed serially 2x30 min in 50% formamide/50% 2xSSC, 0.1% Tween 20; 1x15 min in 2x SSC, 0.1% Tween 20 ; 2x30 min in 0.2x SSC, 0.1% Tween 20 and 2x 5 min blocking buffer(1x PBS, 0.1% Tween 20, 5% sheep serum, 0.2% BSA, 1% DMSO). The embryos were kept in blocking buffer at room temperature for 2 hours and then incubated in 1/4000 dilution of the anti- dixoxigenin alkaline phosphatase Fab fragments. The antibody incubation was done overnight at 4°C. Embryos were then washed in PTW 6x20 mins followed by 2x5 mins rinsing in staining buffer (100 mM Tris-HCl pH 7.9, 100mM NaCl, 0.1% Tween 20, 50mM MgCl2). The bound antibody was revealed by adding the substrates, NBT and BCIP (0.34 mg/ml and 0.175 mg/ml). Reaction was stopped by repeated rinses in PTW.

2.3.2 Plastic sections of epon mounted WISH embryos

Wholemount *in situ* hybridized larvae were fixed and stored in Karnovski fixative (0.5 mL 20% PFA, 2.5 mL 25% Glutaraldehyde, 40 mL 0.2 M Sodium Cacodylate pH7.3, 7 mL water) over night at 4°C. For embedding, several larvae were collected in 1.5mL microfuge tube and washed in 0.2M Sodium Cacodylate buffer. The samples were then dehydrated in a dilution series of water and ethanol (50%, 70%, 95%, 100% ethanol, 1 hour each), followed by rinsing in propylene oxide. For a better penetration of the embedding resin the tissue was serially incubated in a 30% EPON (36.8 g Glycid ether 100, 21.8 g 2-Dodecenyl succinic anhydride, 24.4 g Methylnadicanhydrate)/70% propylene oxide solution, with a dilution of 70% EPON/30% propylene oxide solution and finally 100% EPON for 1 hour each. Thereafter the tissue was embedded in shallow molds and the samples incubated for two to three days at 65°C till the resin solidified. 5µm thin sections were cut using a

diamond knife (ultra 35°, MA 4693 DiATOME) on a *Leica RM 2065* microtome following the trimming of the tissue blocks (performed on *Leica (Reichert) Ultratrim*).

2.3.3 Immunohistochemistry

The primary antibodies and their concentration used in this study have been listed in the Table 3. The secondary antibodies used were coupled to either Cy3, Cy5 (Vector labs) or the Alexa series of fluorophores (Molecular Probes).

Manually dechorionated larvae were fixed with BT fix for 1 hour at room temperature after which they were washed with 1x PTw (0.1% Tween-20 in 1x PBS) or 1x PBST (0.7% TritonX-100 in 1x PBS) 4x30 minutes to remove traces of fixative left in the buffer. The fixed larvae were stored at 4°C in 1x PBS till required (no longer than 1 week). Larvae were washed with 1x PTw (if less than 50hpf) or 1x PBST (if more than 50hpf) 6x30 minutes and were then immersed in pre-chilled (-20°C) acetone and incubated at -20°C for exactly 7 minutes. The larvae were then rehydrated in autoclaved deionized water till they swell and finally sank to the bottom of the glass vial. Then 3 mL of 1x PTw or 1x PBST was added. Finally they were washed 4x15 minutes with PTw or PBST, 2x10 min. with 1x BDP (1% BSA, 1% DMSO in 1x PBS), and were blocked overnight in 1x BDP. The next day the larvae were distributed to 24 well plates and primary antibodies at required concentrations were added. The incubation with primary antibody was carried out over night at 4°C. On day 3, the primary antibody was retrieved and the embryos were washed with 1x BDP 6x30 minutes and the secondary antibody was added. Following a 2 hour incubation period at room temperature, the secondary antibody solution was aspirated and the embryos washed with 1x PTw or 1x PBST 6 time every 15 minutes. The

larvae were then mounted on Super Frost Plus glass slides (Menzel-Glaeser, cat. No. J1800AMZZ) in Aqua polymount (Polyscience) for imaging.

Marker	Antigen	Species of origin (conc. used)	Source
PH3	Phosphorylated histone H3	Rabbit (1:1000)	Upsate biotechnology
HuC/D	RNA binding protein, marker for differentiating neurons	Mouse (1:50)	Molecular Probes
Pax7	chick Pax7 a.a. 352-523	Mouse (1:20 to 1-200, depending on batch)	Developmental Studies Hybridoma Bank
F59	Slow muscle myosin	Mouse (1:10)	Developmental Studies Hybridoma Bank
Laminin	Laminin	Rabbit (1:50)	Sigma-Aldrich, Inc.
znp-1	recognizes nuronal processes	Mouse (1:50)	Zebrafish Information Resourse Centre (ZIRC)

Table 3: Primary antibodies and the concentrations used in this study.

2.3.4 Tissue preparation for Electron Microscopy

For electron microscopy, the larvae were embedded and sectioned in a similar way as for epon embedding and sectioning for WISH larvae (section 2.3.2) with the following exceptions. Following the Sodium cacodylate buffer wash the larvae were incubated in 1% Osmium tetroxide (diluted in 0.1M Sodium Cacodylate) solution. The larvae were then washed twice with 0.1 M Sodium Cacodylate buffer before proceeding with ethanol series dehydration. Following embedding and trimming, 70 nm thin sections were cut from the larvae, using a *Leica EM UC6* microtome and collected on gold grids (Gilder grids/Plano G300HH).

For contrast staining, each grid was incubated on a drop of 50% Uranyl acetate (2g Uranyl acetate in 60ml water)/50% methanol mixture for three minutes. Thereafter the grids were rinsed once in 50% methanol (in water) and three times in water, incubated two minutes on a drop of lead citrate (1.33g $Pb(NO_3)_2$ 1.76g $C_6H_5Na_3O_7$ x $2H_2O$ in 30ml dH_2O) and rinsed three times in water. Transmission

electron microscopy was performed on a *Zeiss EM 109* at the magnification various magnifications.

2.4 Optical Microscopy and Image Acquisition

Visualization of the expression pattern of *in-situ* hybridized embryos or epifluorescence of transgenic animals was performed using a stereomicroscope (Leica, MZ16F) equipped with a CCD digital camera (DFC320). For higher magnification and detailed analyses of embryos or plastic sections, an upright compound microscope (Leica, DM5000B with DFC300FX digital camera) equipped with DIC optics was used. Images in TIFF format were acquired using IrfanView. Co-localization of multiple fluorophores was performed using Leica SP2 laser-scanning microscope, equipped with the optics described in Table 4. Subsequent image processing, color channel overlays projections and 3D reconstructions were performed with Photoshop CS2 or CS3 (Adobe), ImageJ (NIH) or Volocity 4 (Improvision).

Model	Lens Type	Magnification	Numerical aperture
HC PL APO	Dry	10X	0.4
HC PL APO	Oil, water, glycerol	20X	0.7
HCX PL APO CS	Oil	40X	1.25
HCX PL APO CS	Oil	63X	1.4
HCX APO	Dip In	63X	0.9

Table 4: Objectives used for confocal analysis in this study

2.5 Microarray Procedure

2.5.1 Sigma Compugen Microarray

Printing of microarrays chips; RNA isolation and labeling; hybridization, washing and scanning chips; data preprocessing, quality control, transformation, and normalization was all performed as previously described by Yang *et al.* (Yang et al., 2007). The number of effective 65mer oligos on this microarray was about 10,000.

2.5.1.1 RNA extraction, cDNA synthesis, probe labeling and hybridization

Total RNA was isolated from GAL treated and control embryos in every experiment in parallel using the Nucleospin RNA L Kit (Macherey-Nagel, Düren, Germany) and mRNA was extracted with the Ambion Purist Kit (Austin, TX). Labelled cDNA was synthesized from 1-2 μg mRNA using the Amersham direct cDNA labeling kit (Amersham Europe, Freiburg, Germany). Upon removal of unincorporated nucleotides over Microcon 30 spin columns (Millipore, Bedford, MA), the concentrated probes were hybridized to the microarray in 1× DIG Easy-Hyb buffer (Hoffmann-La Roche, Basel, Switzerland) overnight at 42°C. Coverslips were removed from the slides by flushing with 4× SSC and slides were washed in prewarmed wash buffer 1 (2× SSC, 0.1% SDS) for 5 min at 42°C, then in buffer 2 (0.1× SSC, 0.1% SDS) for 10 min at room temperature, and finally in 0.1× SSC four times for 1 min at room temperature. The slides were briefly dipped into 0.01× SSC at room temperature before centrifugation for 7 min at 800 rpm in an Eppendorf 5810R centrifuge.

Arrays were scanned using the Axon model 4000B dual-laser scanner and the corresponding GenePix 6 software (Molecular Devices, Union City, CA). Both channels (532 nm for Cy3 and 635 nm for Cy5) were scanned in parallel and stored as

16-bit TIFF files. Each array was scanned three times (low, medium, and high scan) with different signal-amplification factors (voltage settings of the photomultiplier tubes), but with the same laser power. The channels for Cy3 and Cy5 were balanced in each scan for approximately the same intensity range. For the low scan no spot was saturated; in the high scan the signal amplification for Cy5 was set to approximately 80% of maximum and Cy3 amplification was adjusted to this. The settings used in the medium scan lie between the low and the high scan. The absolute intensity values span the range from 0 to 65536. The scans were performed with a resolution of 10 µm. From each spot with a mean diameter of 100 µm, 70-80 pixels were recorded. Individual local background areas around the spots were defined, which comprised approximately 400 pixels. For each channel, the spot signals were calculated as the median intensity of all foreground pixels minus the median intensity of all background pixels.

2.5.1.2 Data preprocessing, quality control, transformation, and normalization

Raw data was derived from the result files generated by the GenePix 6 suite and analyzed with the R software (The R Project for Statstical Computing, http://www.r-project.org/). Preprocessing of data comprises mapping of scans, quality control, transformation, and normalization steps. Signal intensities from low, medium, and high scans are mapped onto the same scale by an affine transformation. Transformation parameters are estimated based on a least-squares optimization. Averaging the transformed intensities gives the consensus signals, which are independent of the voltage settings of the photomultiplier tube. Quality control was performed on a spot and array level. Spots ideally have a diameter of 100 µm. Diameters less than 70 µm and greater than 140 µm are indicative of scratches and printing problems and the corresponding data was discarded. In addition, inconsistent

spots with a coefficient of variance of pixels bigger than 0.7, and weak spots with a foreground signal less than 175% of the background signal were removed from further analyses. Strong but unreliable signals with at least 20% of pixels in saturation were discarded. Quality control on array level determined the overall quality of each single chip. Therefore, results from different arrays were compared with each other on the basis of correlation parameters, scatterplots and chi-plots for all combinations of arrays for a particular treatment (Fisher, 1985; Fisher, 2001). Raw intensities were transformed with the natural logarithm. A locally weighted regression smoother (LOESS) was applied to correct intensity dependent signal patterns (Cui et al., 2003). The regression is a first-order polynomial that takes into account the subset of 25% of spots that yield a signal with similar intensities. Variance stabilization for weakly expressing genes was not performed as such effects were not apparent. All chips hybridized for a particular treatment were scaled to a common median absolute deviation from median (MAD) of the logarithmic fold change (M value) (Yang et al., 2002). Statistical analysis was based on the assumption that the majority of genes are not changed in their expression and that the overall up- and down regulations compensate each other in sum. Each individual gene was tested for difference in expression under toxic conditions with a *t*-test where an adjusted *p* value (p_{adj}) of less than 0.025 indicated significant differential expression. Statistical requirements of normal distribution and homoscedasticity are tenable. A robust variance estimation was derived by balancing gene-specific and pooled variance Baldi, 2001 #633}. The number of false positives due to multiple testing was reduced by adjusting the resulting *p* values by controlling the Benjamini-Hochberg false discovery rate (Benjamini, 1995). Multivariate analysis was based on a subset of genes of interest. Genes that remain unchanged under all conditions were ignored. Marker genes that

are significantly changed by exposure to a particular toxicant were taken into account. In addition, the selected subset included genes that showed a global response across many chemicals. The selected subset included: the top 20 up- or downregulated genes based on fold change (minimum fold change > 2); the top seven genes with the highest correlation among at least two toxicants (minimum correlation > 0.7); the top 100 genes with the highest MAD across all treatments; and the marker genes that are regulated at least threefold for just one treatment. Most multivariate approaches require a complete dataset without missing values. Under the condition that more than 80% of the data for a particular gene is available, missing data for gene *g* are imputed by a k-nearest-neighbor algorithm (Troyanskaya et al., 2001). Missing values are estimated as weighted average of the values for the *k* genes with the closest Euclidean distance to gene *g*.

2.5.2 Agilent Microarray

2.5.2.1 RNA extraction, cDNA synthesis, probe labeling and hybridization

In order to perform the technique reproducibly with enhanced sensitivity, proprietary reagents and an optimized procedure for a two-color gene expression platform based on the zebrafish 22K 60-mer oligonucleotide microarray (G2518A-001, Agilent Technologies, Santa Clara, CA, USA) was acquired and adapted.

Pooled galanthamine treated or untreated larvae, snap-frozen in liquid nitrogen, were homogenized using an 18 gauge needle followed by a rotor stator homogenizer. Total RNA from the homogenate was extracted using “Nucleospin RNA L” RNA extraction kit (Macherey-Nagel), following the manufacturers protocol. The yield and quality of the RNA was assessed using a NanoDrop spectrophotometer and by formaldehyde gel electrophoresis.

For the synthesis of cDNA, the low RNA input linear amplification kit (Agilent), which produces an initial RNA amplification of at least 100-fold, was used. This strategy utilizes an adapter T7 primer for first-strand cDNA synthesis with MMLV reverse transcriptase, followed by in vitro transcription using T7 RNA polymerase to simultaneously amplify target material and incorporate Cy3 or Cy5-labeled CTP (Perkin Elmer). Removal of unincorporated dye and purification of the amplified cRNA was performed with RNeasy mini columns (Qiagen), followed by quantification and determination of the specific activity of the labeled dye with NanoDrop (absorbance at 260 nm with either 550 nm for Cy3 or 650 nm for Cy5). Typically, the yield is above 750 ng and the specific activity is greater than 8 pmol Cy3 or Cy5 per μg of cRNA.

In order to obtain high specificity with low background, the labeled cRNA was treated with blocking agent and fragmented prior to hybridization. The hybridization mixture was then applied to a gasket slide, on which the oligo microarray is placed to form a 'sandwich slide'. This unit was sealed with a hybridization assembly and transferred to a rotisserie in a hybridization oven set to 65 ºC for 17 hours. The next day, the microarray 'sandwich' was disassembled and rinsed in three changes of wash buffer before scanning.

2.5.2.2 Scanning, quality control, normalization and evaluation

Differential gene expression was assessed by scanning the hybridized arrays using a high-resolution laser scanner (GenePix 4000B, Molecular Devices), capable of acquiring data at two wavelengths simultaneously at 532 nm and 635 nm. For each array, scanning was performed at a constant laser power but with two different voltage settings of the photomultiplier tubes to obtain a high (~80% PMT power) and a low range (~60% PMT power) scan image. The pixel intensity histogram at the

scanned wavelengths was used to balance the signal in each channel by adjusting the Cy5:Cy3 count ratio to 1. The absolute intensity values span the range from 0 to 65536 and the scans were performed with a resolution of 10 μm. From each spot with a mean diameter of 100 μm, 70-80 pixels were recorded. Individual local background areas around the spots were defined, which comprised ~400 pixels. For each channel, the spot signals were calculated as the median intensity of all foreground pixels minus the median intensity of all background pixels. The scanned 16-bit tiff image was then analyzed using the embedded functions of the accompanying GenePix Pro 6.0 software.

Raw data from the replicates were analyzed with the R software (Fisher, 1985). Signal intensities from the low and high scans were mapped onto the same scale by an affine transformation, based on Least Square optimization. Averaging the transformed intensities gives the consensus signals, which are independent of the voltage settings of the photomultiplier tube. Quality control was performed on the spot and array level. The spots representing the arrayed genes were identified with a grid and spurious signals or irregularities were flagged. In addition, inconsistent spots with a coefficient of variance of its pixels bigger than 0.7 and weak spots with a foreground signal less than 175% of the background signal were removed from further analyses. Strong but unreliable signals with at least 20% of its pixels in saturation were discarded. Quality control on array level determined the overall quality of each single chip. Therefore, results from different arrays were compared to each other based on correlation parameters, scatter plots and chi-plots (Fisher, 1985; Fisher, 2001). Raw intensities were transformed with the natural logarithm. A locally weighted regression smoother (LOESS) was applied to correct intensity-dependent signal patterns (Cui et al., 2003). The regression is a first order polynomial that takes

into account the subset of 25% of spots that yield a signal with similar intensities. All the hybridized chips for age group or mutant versus wild type comparisons were scaled to a common median absolute deviation from median (MAD) of the logarithmic fold change (M value) (Altman, 2005).

Following normalization, the spots were referenced to Agilent's 22K gene list to identify the genes that are differentially expressed. Three independent microarray assays (biological repeats) for Galanthamine treatment experiment, starting from independent Galanthamine treatment and total RNA isolations, were performed to exclude stochastic changes and to identify the genes that are truly differentially expressed. Genes with p-value fold change > |1.7|, were uploaded to The **D**atabase for **A**nnotation, **V**isualization and **I**ntegrated **D**iscovery (**DAVID**) (http://david.abcc.ncifcrf.gov/) for gene ontology analysis.

2.6 Generation of Tol2 based constructs

The Tol2 arms containing vector used was pT2KXIGΔin (Urasaki et al., 2006), that contained an EF1 promoter, a ß-globin intron, eGFP, and finally an SV40 late poly A signal, within the two Tol2 arms. I replaced the EF1 promoter and ß-globin intron with the putative promoter sequences of *pax7*, *met*, and *myoD*. The web based resource ECR browser Ovcharenko *et al.* (2004) (http://ecrbrowser.dcode.org/) (Fig. 17) was used to identify evolutionary conserved regions upstream of the transcription start site of these genes in zebrafish. Subsequently, these sequences (-3.3kb region for *pax7*, -5.3kb region for *met*, and -5kb region for *myoD)* were PCR amplified using primers containing *Xho I* and *BamH I* sites and were cloned into the pT2KXIGΔin vector (Fig. 18). The promoter:reporter construct were then co-injected

with the *in-vitro* transcribed transposase mRNA to allow for integration of the tol2 repeat flanked sequences into the genome.

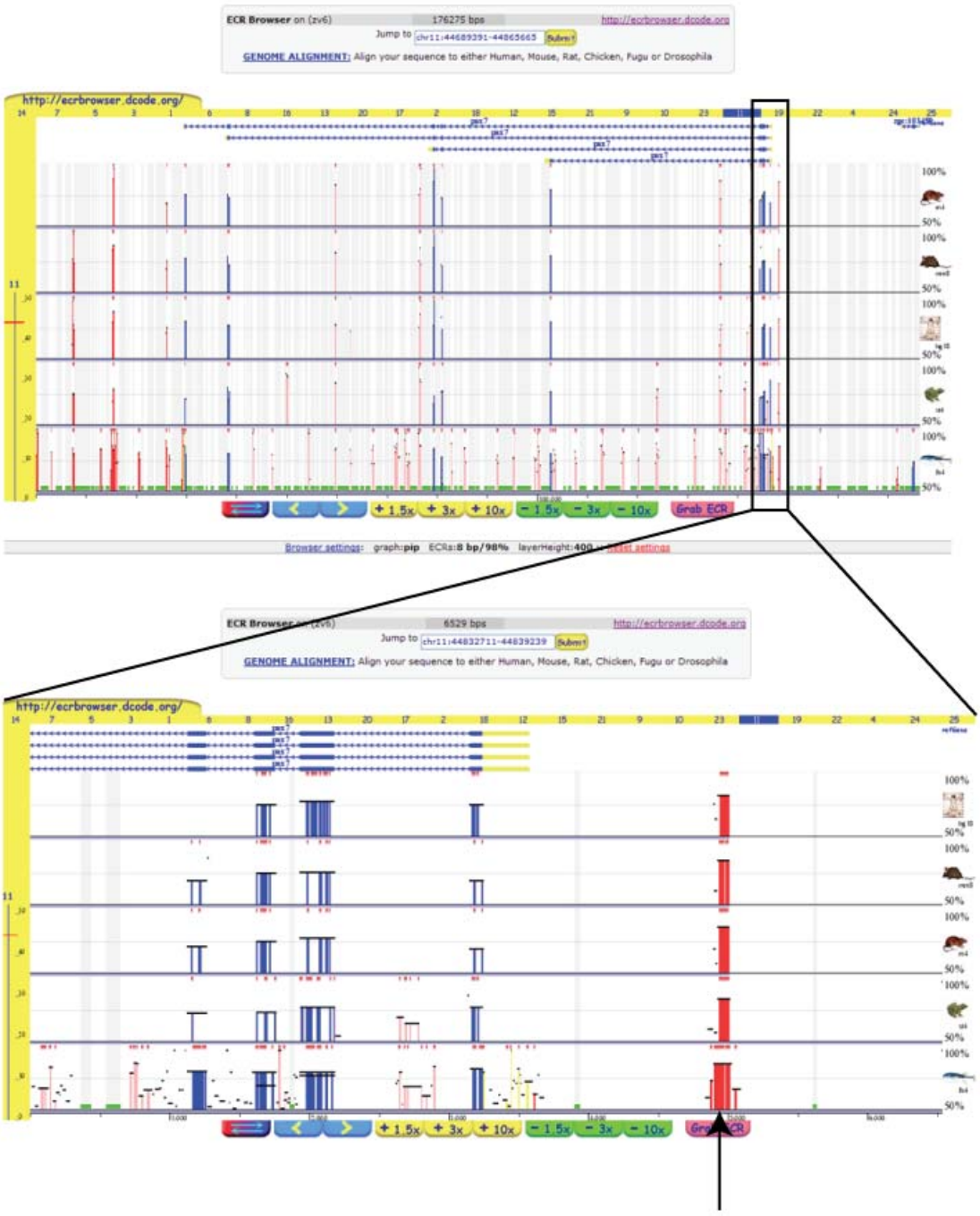

Figure 17: The ECR browser comparision of zebrafish Pax7 genomic region with fugu, xenopus, mouse, rat and human (top panel). The lower panel represents the boxed area in the top panel, showing the first four exons and about 2 kb upstream region. A highly conserved sequence (arrow) is observed 1 kb upstream of the first exon. Blue lines represent the known exons, yellow ones show the non-coding exons while pink/red depict non-coding, non-genic evolutionary conserved elements which represent the putative cis-regulatory elements. Width in the conservation panel tells the size, while the height shows the degree of conservation.

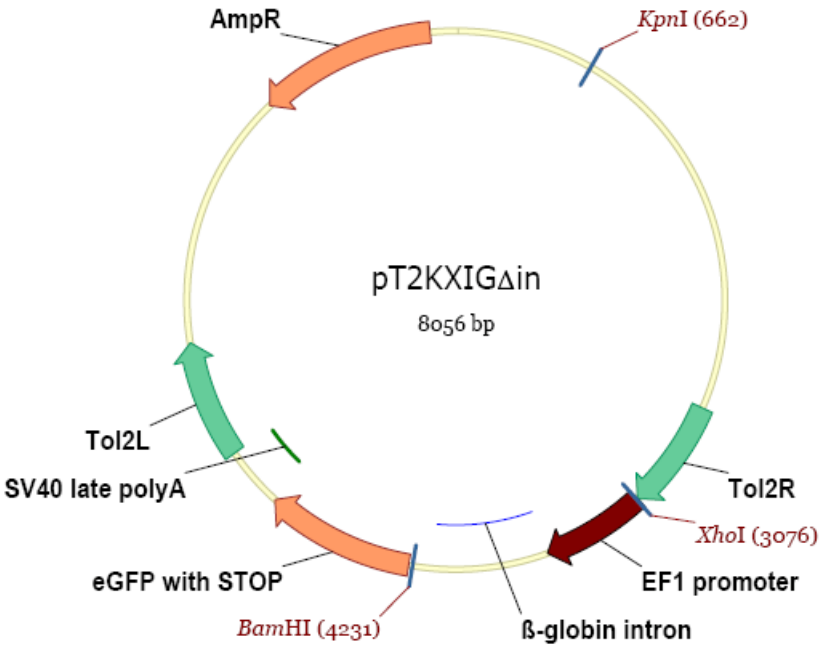

Fig. 18: pT2KXIGΔin vector used as a base for construction of Tol2 constructs harboring *pax7*, *met* and *myoD* promoter regions. See text for details.

2.7 Generation of BAC s modified with fluorescent reporters

2.7.1 Identification and verification of Pax7, Pax3, and Myf5 containing BACs

Pax7, Pax3 and Myf5 BACs were identified from zebrafish information network (www.zfin.org) and ordered from either BACPAC resources (Children's Hospital Oakland Research Institute, California, USA) or from Imagenes GmbH (previously called RZPD). The presence of gene of interest in the BAC was verified by PCR approach using set of primers described below (also Fig. 20).

2.7.2 Generation of Targeting Vectors for BACs

2.7.2.1 The choice of fluorescent reporter proteins

For Pax7 and Pax3 BACs the fluorescent proteins chosen was KikGR1. KikGR1 was isolated from the stony coral, *Favia favus* and green-to-red photoconvertibility was conferred to it by in vitro, semi-rational, mutagenesis of the amino acids surrounding the chromophore (Tsutsui et al., 2005). KikGR1 contains the tripeptide chromophore, His 62-Tyr 63-Gly 64, that is photoconvertible to red following (ultra-) violet irradiation (Tsutsui et al., 2005). This allows it to be used as an efficient highlighter for labeling specific cells using photoconversion of kikGR1 in single cell using two photon microscopy (Hatta et al., 2006). The excitation and emission spectra for native kikGR1 is 507 and 517 nm respectively. A brief pulse of violet/ultraviolet light (350-410 nm) will irreversibly convert the yellow/green fluorescent kikGR1 to Red kikGR1. The photoconversion could also be achieved using two photon laser at 780nm. Although the use of two photon requires over 1000 times more scanning (over several minutes) than conventional confocal microscopy, it does improve the resolution especially along the z-axis and it is possible to label single cells in a tissue expressing (Hatta et al., 2006). This allows labelling and tracking the fate of single cell in the whole organism.

For Myf5 BAC a Nuclear localization signal (NLS) sequence, a 9 amino acid peptide (MAPKKKRKV), was generated by using primers containing the sequence to amplify monomeric Teal fluorescent protein (mTFP1). The restriction sites XmaI and BglII were also incorporate in the 5' and 3' region of NLS-mTFP via these primers. Finally, NLS-mTFP was cloned into pPCR-eGFP$_{kan}$ after excision of 5'-XmaI-eGFP-BglII-3' fragment.

2.7.2.2 Generation of targeting vectors for individual BACs

The kikGR1/NLS-mTFP containing vectors (designated as a generic 'Fluorescent Reporter' in the Fig. 19) were used as base vectors to incorporate the BAC 5' and 3' homology arms. PCR generated 5' and 3' homology arms were cloned in KpnI/HindIII and SacII/SacI restriction sites respectively. The BAC targeting strategy is illustrated in Fig. 20 for the Pax7 BAC (CH211-119A10). Since the sequence between primers C and D would be lost in the recombination step, primers C and D was designed to lose as little of non coding region as possible.

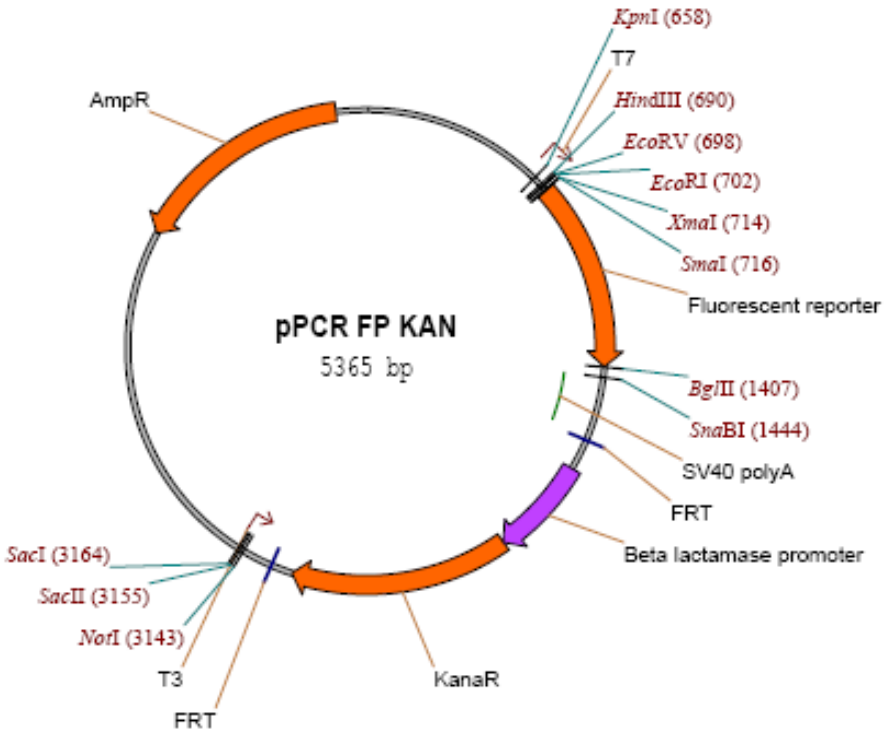

Fig. 19: Depiction of a generic fluorescent protein containing vector used for generating targeting vectors for BAC transgenesis. KikGR1/nlsTeal were used as reporters and cloned in XmaI/BglII site. The 5' homology arm was PCR amplified from BAC and cloned into KpnI/HindIII site and the 3' homology arm was cloned into SacII/SacI site after PCR amplification. The completed targeting vector was digested with KpnI and SacI to liberate the fluorescent reporter flanked by homology arms that was subsequently electroporated into BAC containing EL250 cells to cause homologous recombination. See text for details.

The strategy to modify a BAC clone for transgenesis was adapted from (Shin et al., 2003). KikGR1 was targeted to the translation start site of Pax7 gene (schematic depicted in Fig. 20).

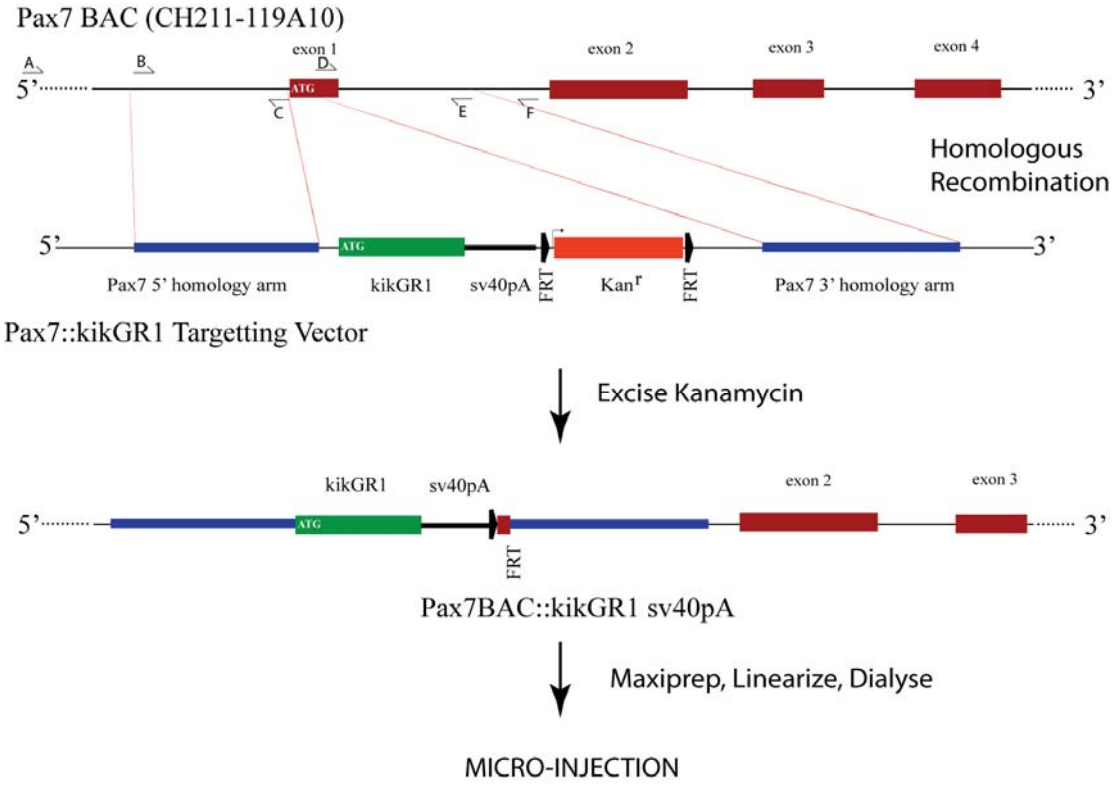

Figure 20: Strategy for homologous recombination for BAC modification. Primers B and C were used to amplify the 5' homology arm and primers D and E were used to amplify 3' homology arm. These arms were cloned into a targeting vector either side of the sequence containing kikGR1, polyA, FRT-Kan-FRT, by conventional molecular biology. This targeting vector fragment was electroporated into Pax7 BAC containing EL250 cells and homologous recombination performed, followed by kanamycin cassette excision via induced Flippase activity by arabinose treatment. The modified BAC was verified by PCR and sequencing and used for microinjection.

Briefly, the 5' and the 3' homology arms were PCR amplified from the BAC and restriction sites, KpnI and HindIII (5' homology arm) and SacII and SacI (3' homology arms) restriction digested and cloned into the respective sites of pPCR-kikGR1$_{kan}$ vector to genetare a targeting vector for Pax7 BAC. The pPCRkikGR1$_{kan}$

vector was earlier generated by cloning PCR amplified kikGR1 from AM-V0084 phKikGR1-S1 (MBL international) into the XmaI and BglII sites of $pPCReGFP_{kan}$ vector (Shin et al., 2003). The Pax7 BAC (CH211-119A10) was electroporated into the EL250 cells, the recombinase induced by placing the cells in 42°C water bath for 15 minutes, and the cells made electrocompetent again. Gel purified targeting vector fragment was electroporated into the BAC containing, recombinase induced EL250 cells and the cells were plated over LB plates containing both kanamycin and chloramphenicol. The colonies were picked and verified for recombination by PCR. Finally, kanamycin cassette was excised by inducing Flippase by addition of arabinose to the recombinant BAC culture. Flippase causes FRT mediated recombination and thus excision of kanamycin cassette. The culture was again plated, on LB plates with chloramphenicol only, and colonies verified for kanamycin excision by PCR. Glycerol stock of such positive prep was made to keep the recombined BAC from getting lost. The integration of fluorescent reporter was further confirmed by sequencing using a BAC specific primer. Pax3 and Myf5 BACs were modified in a similar manner with fluorescent reporters.

2.8 Preparation of DNA/mRNA for microinjection

2.8.1 Preparation of mRNA

Capped mRNA was synthesized using mMessage mMachine High Yield Capped RNA Transcription Kit from Ambion following the manufacturer's recommendation. For Tol2 mediated transgenesis mRNA was injected with the plasmid at 25ng/µl.

2.8.2 Preparation of BAC DNA

BAC DNA was isolated using the Qiagen Large construct kit (Qiagen) using the manufacturer's instructions. Supercoiled BAC was resuspended in nuclease free water and digested with PI-SceI for 6 hours at 37°C. BAC thus linearized was dialyzed overnight against 1L 0.5X TE buffer at 4°C on 0.025 µm Millipore membrane filters (Millipore, Cat. No. VSWP04700). Dialyzed BAC was injected into fertilized zebrafish embryos at 30-50ng/µl concentration. The injected larvae were screened for transgene expression and those showing specific expression were raised to adulthood.

2.9 ENU mutagenesis

The ENU mutagenesis was performed according to the standard protocol with minor modifications (Mullins et al., 1994; Solnica-Krezel et al., 1994). Ten male of AB* strain fish were placed in a plastic cylindrical container with a fine mesh bottom and immersed in 300 ml of ENU working solution (3mM ENU in 10mM sodium phosphate buffer) at 22.5°C and left for 1 hour in dark. The fish were transferred to a cylinder with 50% 10mM sodium phosphate buffer and 50% fish water. After one hour the fish were transferred to fish water and kept for another hour. Finally, the fish were transferred to mouse cages and returned to fish room at 28°C. The treatment was repeated 3 times within 1-3 weeks. The ENU working solution was inactivated by incubating with equal amount of 2x inactivating solution (20% sodium thiosulphate, 1% NaOH) before discarding.

2.9.1 Generation of F1 fish and F2 families

After three weeks of last round of ENU treatment, the mutagenised fish were crossed with wildtype females every week till viable embryos were obtained. The viable progeny were raised to generate F_1 fish, which were then crossed with each other to produce F_2 families.

2.10 Reagents

2.10.1 Solutions, Buffers and media

Unless otherwise specified, all solutions and buffers have been prepared in autoclaved, deionized water.

Buffer/Solution	**Composition**
TAE Buffer	40 mM Tris-Base, 1 mM EDTA, 5 mM Acetic acid; pH=7,8
TBE-Buffer	90 mM Tris-Base, 1 mM EDTA, 44 mM Boric acid; pH=8,0
TE-Buffer	10 mM Tris-HCl (pH = 7,4), 1mM EDTA; (pH = 8)
Pancreatic ribonuclease A (RNase A) stock solution	20 mg/ml RNase A in 1 mM sodium acetate; pH=4,5
Proteinase K stock solution	10mg/ml in PBS
LB-Agar	1,5% Bacto-Agar in LB-Medium
LB-Medium	1% Bacto-Trypton, 0.5% Yeast extract, 1% NaCl; pH=7.0
SOC–Medium	2% Bactotrypton, 0.5% Yeast extract, 10 mM NaCl, 25 mM KCl
Hank´s solution	0,14 M NaCl, 5.4 mM KCl, 0.25 mM Na2HPO4, 0.44 mM KH2PO4, 1.3 mM CaCl2, 1 mM MgSO4, 4,2 mM NaHCO3.
System water in the fish facility	120 mg/l “Ocean Sea Salt”, 45 mg/l NaHCO3 in desalted water
Phenol red solution (10x)	10% Phenolred, 0,2 M KCl; pH=7,5
Methylene blue solution (2000x)	0,1% methylene blue in distilled water
ENU working solution	3 mM in 10 mM sodium phosphate buffer

ENU inactivating solution	20% sodium thiosulphate, 1% NaOH

2.10.2 Chemicals, enzymes, kits and equipment

Reagent	**Supplier**
Acetic acid	Merck, Darmstadt
Agarose	Sigma, Taufkirchen
Ammonium acetate	Merck, Darmstadt
Ampicillin	Roche, Mannheim
Bacto-Agar	Roth, Karlsruhe
Bacto-Trypton	Roth, Karlsruhe
Bacto-Yeast extract	Roth, Karlsruhe
Boric acid	Roth, Karlsruhe
BSA	Serva, Heidelberg
Calcium chloride	Merck, Darmstadt
Calf intestine alkaline phosphatase	Promega, Mannheim
Disodium hydrogen phosphate	Roth, Karlsruhe
DNA-Ladder (1 kb)	New England Biolabs, Frankfurt a.M.
DNA-Ladder (100 bp)	New England Biolabs, Frankfurt a.M.
DNA-Ladder (Mix)	Peqlab, Erlangen
dNTPs	Promega, Mannheim
EDTA	Roth. Karlsruhe
Ethanol	Roth. Karlsruhe
Ethidium bromide	Roth. Karlsruhe
Gentamicin	Sigma, Taufkirchen

Isoamyl alcohol	Roth, Karlsruhe
Isopropanol	Merck, Darmstadt
Magnesium sulphate	Merck, Darmstadt
Methanol	Roth, Karlsruhe
Nuclease free water	Ambion, Huntigdon, UK
Ocean Sea Salt	Kölle-Zoo, Karlsruhe
Oligonucleotides	Metabion, Planegg
Pancreatic ribonuclease A	Sigma, Taufkirchen
PBS	Invitrogen, Karlsruhe
Phenol	Roth, Karlsruhe
Phenol red	Roth, Karlsruhe
Potassium acetate	Roth, Karlsruhe
Proteinase K	Sigma, Taufkirchen
QIAGEN Plasmid Maxi Kit	Qiagen, Hilden
QIAquick Gel Extraction Kit Qiagen, Hilden	Qiagen, Hilden
QIAquick PCR Purification Kit Qiagen, Hilden	Qiagen, Hilden
QuickLyse Miniprep Kit Qiagen, Hilden	Qiagen, Hilden
Restriction endonucleases	Promega, Mannheim or New England Biolabs, Frankfurt a.M.
SDS	Roth, Karlsruhe
Sodium acetate	Roth, Karlsruhe
Sodium chloride	Roth, Karlsruhe
Sodium dihydrogen phosphate	Roth, Karlsruhe
Sodium hydrogen carbonate	Roth, Karlsruhe
Sodium hydroxide	Sigma, Taufkirchen
T4 DNA ligase	Promega, Mannheim

T4 DNA polymerase	Promega, Mannheim
GoTaq DNA polymerase	Promega, Mannheim
TOPO TA Cloning Kit	Invitrogen, Karlsruhe
Triple Master PCR System	Eppendorf, Hamburg
Tris-Base	Roth, Karlsruhe
Tris-HCl	Roth, Karlsruhe
Wizard SV Gel and PCR Clean-Up System	Promega, Mannheim

Equipment and materials	**Supplier**
Bacteria incubators	Heraeus, Hanau
Borosilicate glass capillaries	Harvard Ltd., Kent, UK
Cooling centrifuge J2-HS	Beckman, Stuttgart
Digital camera DFC300 FX	Leica, Bensheim
Electrophorese chambers	Peqlab, Erlangen
Eppendorf microcentrifuge tubes	Eppendorf, Hamburg
Falkon tubes	Greiner, Nürtingen
FemtoJet microinjector	Eppendorf, Hamburg
Flaming-Brown Needle puller	Sutter Instruments, USA
Fluorescent stereomicroscope MZ FLIII	Leica, Bensheim
Gas microinjector Tritech research inc.	L.A., USA
Incubator for fish embryos	Heraeus, Hanau
Magnetic thermomixer	Heidolph, Rosenfeld
Microcentrifuge 5417 R and C	Eppendorf, Hamburg
Microcentrifuge Biofuge pico	Heraeus, Hanau
Microfiltration columns	Pall, Ann Arbor, USA

NanoDrop ND-1000	Peqlab, Erlangen
PCR-Thermocycler	MJ Research Biozym, Oldendorf
Petri dishes	Greiner, Nürtingen
Pipette tips	Corning, Corning
Spectrophotometer	Eppendorf, Hamburg
Stereomicroscope SMZ645	Nikon, Düsseldorf
Sterile filters	Renner, Darmstadt
Thermomixer	Eppendorf, Hamburg
UV Transilluminator	Saur, Reutlingen
Vac-Man Vacuum manifold	Promega, Mannheim
Vortex	Bender & Hohbein, Karlsruhe
Water bath	Kötterman, Uetze-Hänigsen
Leica Confocal Microscope TCS SP2	Leica, Bensheim
Transmission Electron Microscope (TEM) Zeiss EM 109	Carl Zeiss MicroImaging GmbH, Göttingen

3 Results

3.1 ENU mutagenesis screen to identify motility mutants

An ENU mutagenesis screen was performed to identify motility mutants using the escape response and measurement of muscle birefringence by plane polarized light as assays for motility and for muscle integrity, respectively. Specifically, I screened for progressive loss of motility and birefringence, which would indicate that the development of muscles is normal, but maintenance is defective. Such defective maintenance could result from mutations in genes required for muscle regeneration.

I performed mutagenesis on males of AB* wild type fish. Three mutagenised males (founders) were crossed with 12 golden WT fish to give rise to the F1 generation. 238 families, each containing around 50 individuals, were established from the mating of siblings from the F1 generation. Out of these, 84 families, with 224 egg lays were screened in a seven week period. Seven motility mutants were identified based on a reduced or aberrant escape response and reduced birefringence. The numbers of mutant embryos were always in accordance with the Mendelian ratio of 1:4 for recessive mutants. Out of the seven mutants, I selected ENU-Gold 202.1 for further analysis as it showed a gradual loss of motility (Fig. 21). Based on its morphological phenotype and expression of certain markers I decided to call this mutant, *gumrah* (Hindi for someone or something that has lost its path).

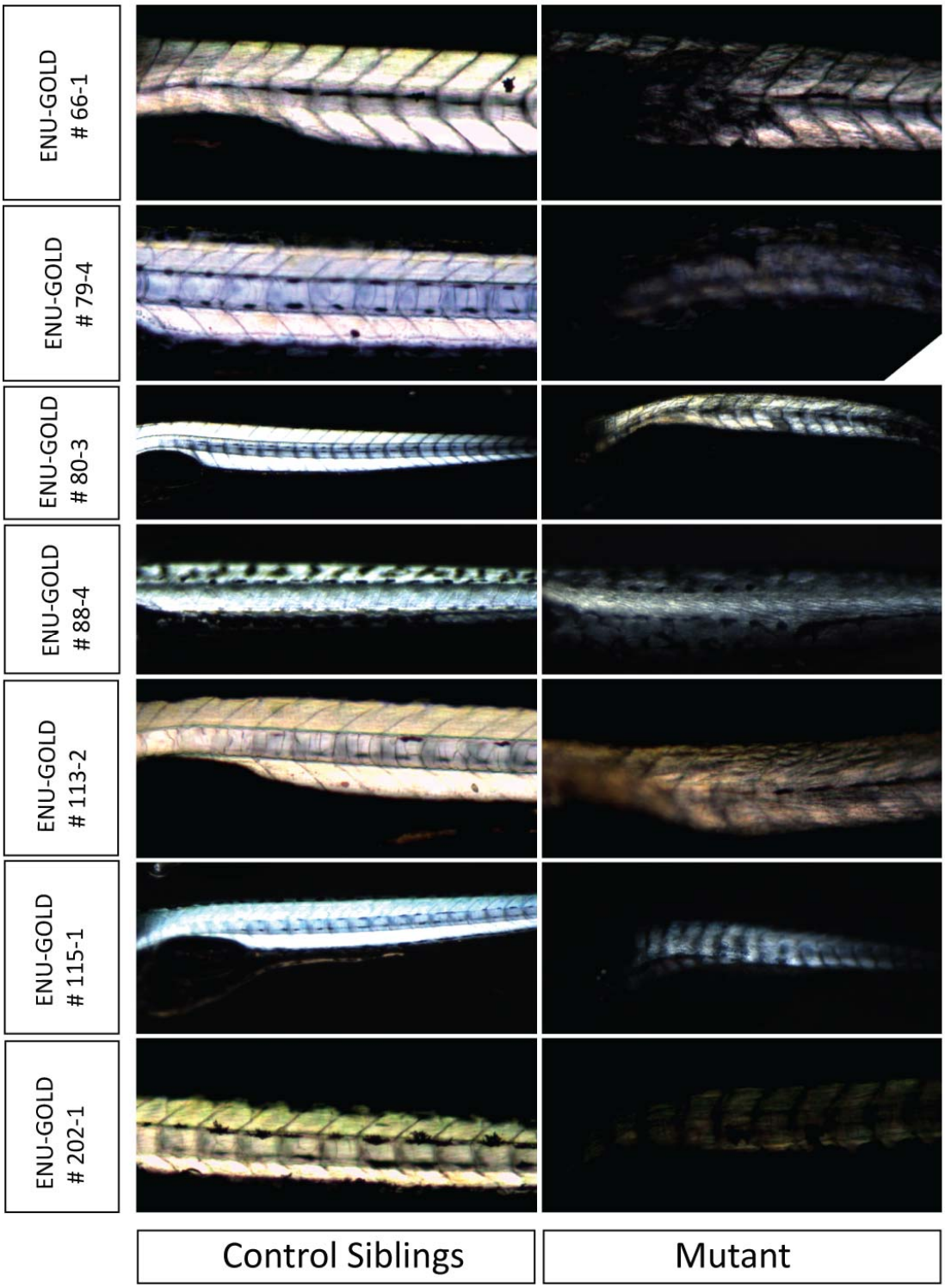

Figure 21: The seven mutants obtained after screening of 84 families. Polarized light images of 3 dpf larvae show severely reduced birefringence, indicative of muscle damage. The number of embryos with reduced birefringence was always in the Mendelian ratio of 1:4 for recessive mutants.

3.1.1 Characterization of the *gumrah* mutant

3.1.1.1 Morphological phenotype of the *gumrah* mutant

At 24 hpf *gumrah* (*gum*) embryos are slightly smaller than the wildtype siblings, sometimes have a kink in the tail and have a smaller head which is pointed like a beak. Around 30 hpf necrosis (darkened area) is observed in the hindbrain, just after the midbrain-hindbrain boundary, which is sometimes pinched. The yolk is more rounded and the yolk extension is thinner when compared to the non-mutant siblings. The somites are U-shaped rather than chevron shaped (Fig. 22 and Fig. 24) and the motility of the *gum*$^{-/-}$ embryos is reduced.

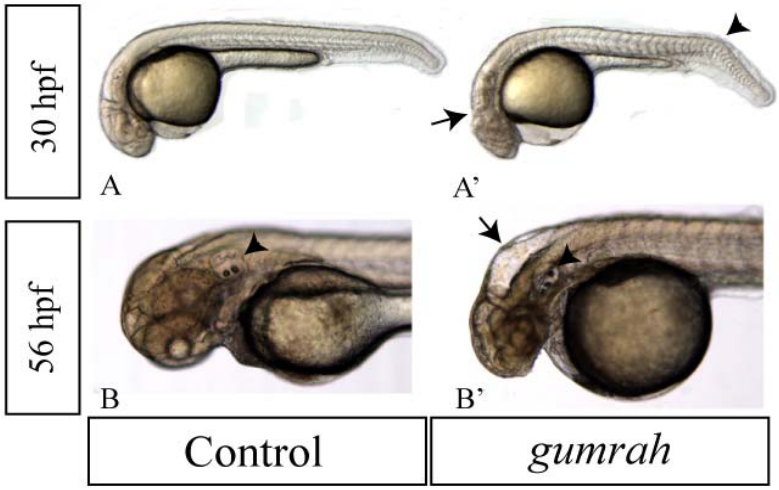

Figure 22: Control (A) and mutant (A') *gum* embryos showing reduced size, necrosis in the hindbrain (arrow) and a kink in tail (arrowhead) at 30 hpf. 56 hpf control (B) and *gum* embryo (B') showing hindbrain edema (arrow) and a reduced size of the otic vesicle (arrowhead).

During the second day of development, the smaller size of the head becomes very apparent and the hindbrain develops edema. The size of the otic vesicle is also reduced. The embryo movement is uncoordinated. By the fourth day post fertilization (4 dpf) the size of the head and the eyes is severely reduced, membrane blebs appear

on the cornea of some embryos and the jaw is malformed. The motility is drastically affected by now and the birefringence (a measure of muscle fiber integrity) goes down significantly. Sometimes, the location and/or size of one or both lenses is effected in the *gum* mutant embryos. The pigmentation pattern is also abnormal and the mutant embryos develop cardiac edema (Fig. 23).

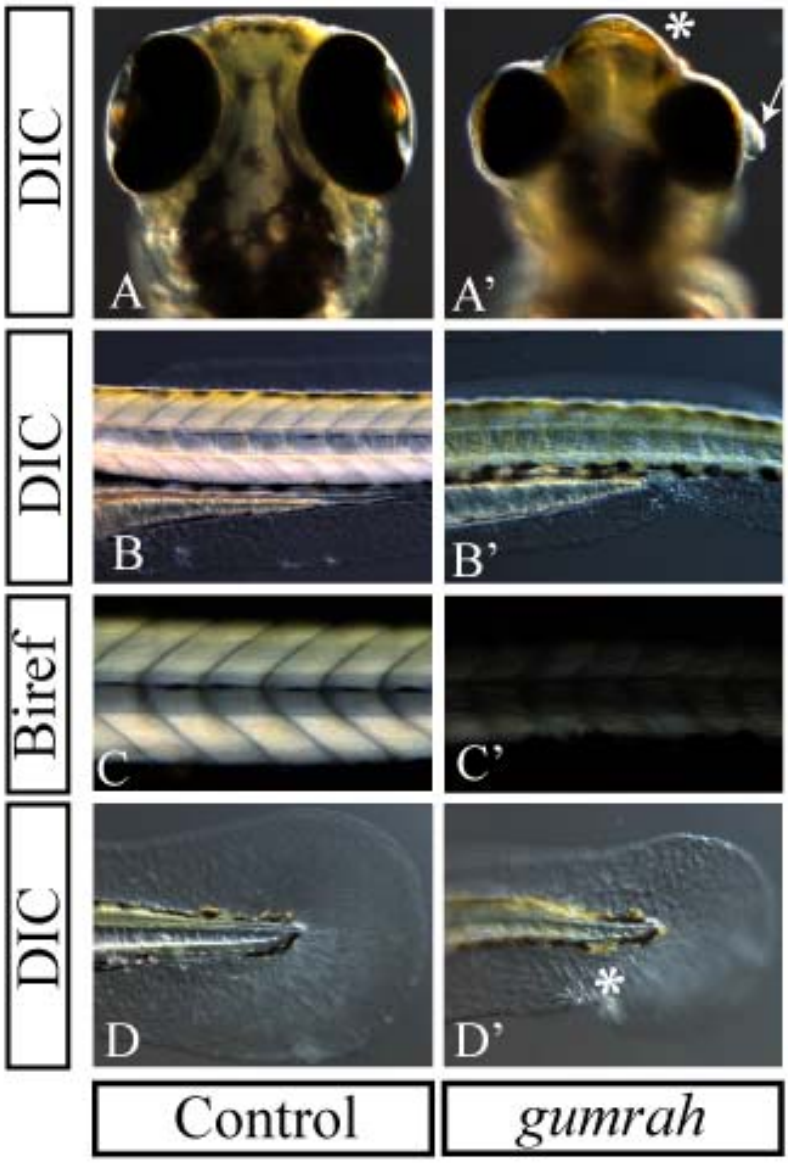

Figure 23: 4 dpf DIC images of control (A, B, D) or *gum* mutant (A', B', D') embryos showing blebbing on the corneal surface (arrow, A'), pointed snout (asterisk, A'), thinner and curved trunk (B') and aberrant pigmentation resulting in the shortening of the pigmentation gap in the tail fin (asterisk, D'). Plane polarized light images of the control (C) and the *gum* mutant embryos show reduced birefringence (C')

3.1.1.2 Muscle fibers are generated but not maintained normally in *gumrah* mutants

Loss of motility could result from a mutation leading to a defect in either muscle development or neuronal development. To distinguish between the two possibilities I employed immunohistochemical (IHC) analysis to check for the presence of various molecular markers for neuronal and myofibrillar organization.

U-shaped somites are a characteristic feature of *sonic hedgehog* (*shh*) pathway mutants (van Eeden et al., 1996). Loss of Shh activity results in an almost complete absence of slow muscle fibers (Barresi et al., 2000; Blagden et al., 1997; Lewis et al., 1999b). Therefore, I stained *gum* embryos with the F59 antibody that specifically labels slow muscle myosin in zebrafish (Miller et al., 1989). F59 staining revealed the presence of muscle pioneer cells and slow muscle fibers that are lost in the absence of Shh activity. The slow muscle fibers were present in *gum* mutants but they developed gaps around 50 hpf (Fig. 24) and these gaps increased with age. Slow muscle fibers also tended to separate from the edges of the myosepta at the somite boundaries. The angle between the vertical myosepta is around 120° in the mutant embryos compared to around 90° in the wildtype embryos (Fig. 24). F59 staining, as well as staining with anti-titin, anti-troponin and anti α-actinin (Costa et al., 2002) showed that the myofiber specification and the sarcomeric organization is correct by 50 hpf (data not shown) in the *gum* embryos but their maintenance is defective, as the structures are progressively disorganized by 5 dpf.

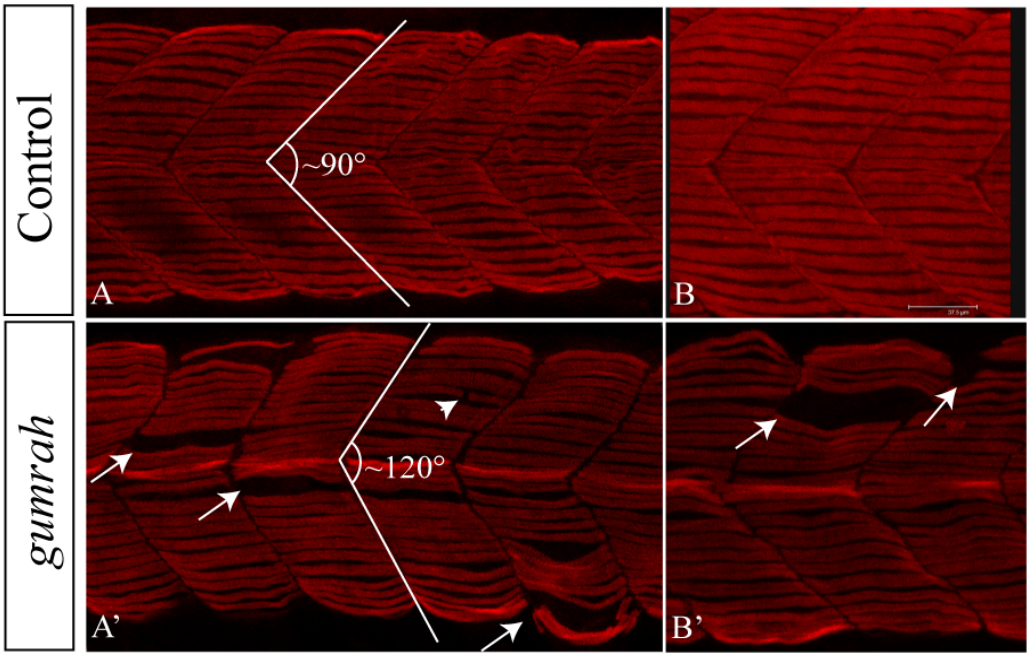

Figure 24: 50hpf *gum* (A', B') and control embryos (A, B).Slow muscles are formed normally (F59 staining) but develop gaps (arrows, A') as the larva ages. Sometimes the muscle fibers show breaks (arrow head, A'). The angle between the vertical myosepta is around 120° in *gum* compared to around 90° in the control larvae. Panels B and B' are different areas from the same larvae in panels A and A' respectively.

Laminins form a sheet-like matrix that is a major component of basal lamina. They form an important component of proteins linking the myofiber to the basement membrane providing mechanical stability. Gaps within myofibers/myosepta might result from a loss of laminin. I therefore performed IHC with an anti-laminin antibody (Sigma, Cat. No. L9393).This reveals that the gaps in F59 staining along the myosepta correlate with gaps in laminin staining implying a loss of myosepta in that region (Fig. 25). Also, laminin immunoreactivity is absent or greatly reduced in the horizontal myosepta (Fig. 25).

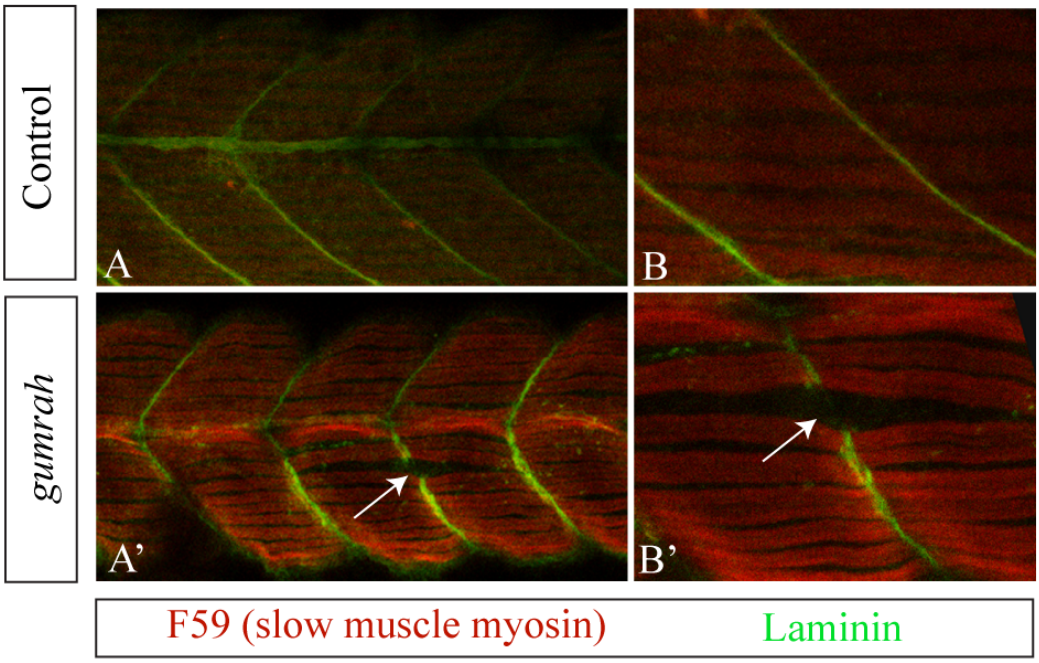

Figure 25: F-59 and anti laminin co-staining of 50 hpf control (A, B) and *gum* (A', B') larvae shows that gaps in laminin expression coincide with gaps in muscle fibers (arrows A' and B'). Anterior is to left and dorsal to top.

To further characterize the muscle structure I performed electron microscopy on *gum* mutant embryos at 5 dpf. Electron microscopy confirmed the observation that muscle fibers are formed normally but huge gaps appear between the fibers as the embryo ages. Sometimes remnants of myofibers are seen in these gaps (Fig. 26). The thickness of myofibers is also lesser compared to the fibers of the wildtype controls.

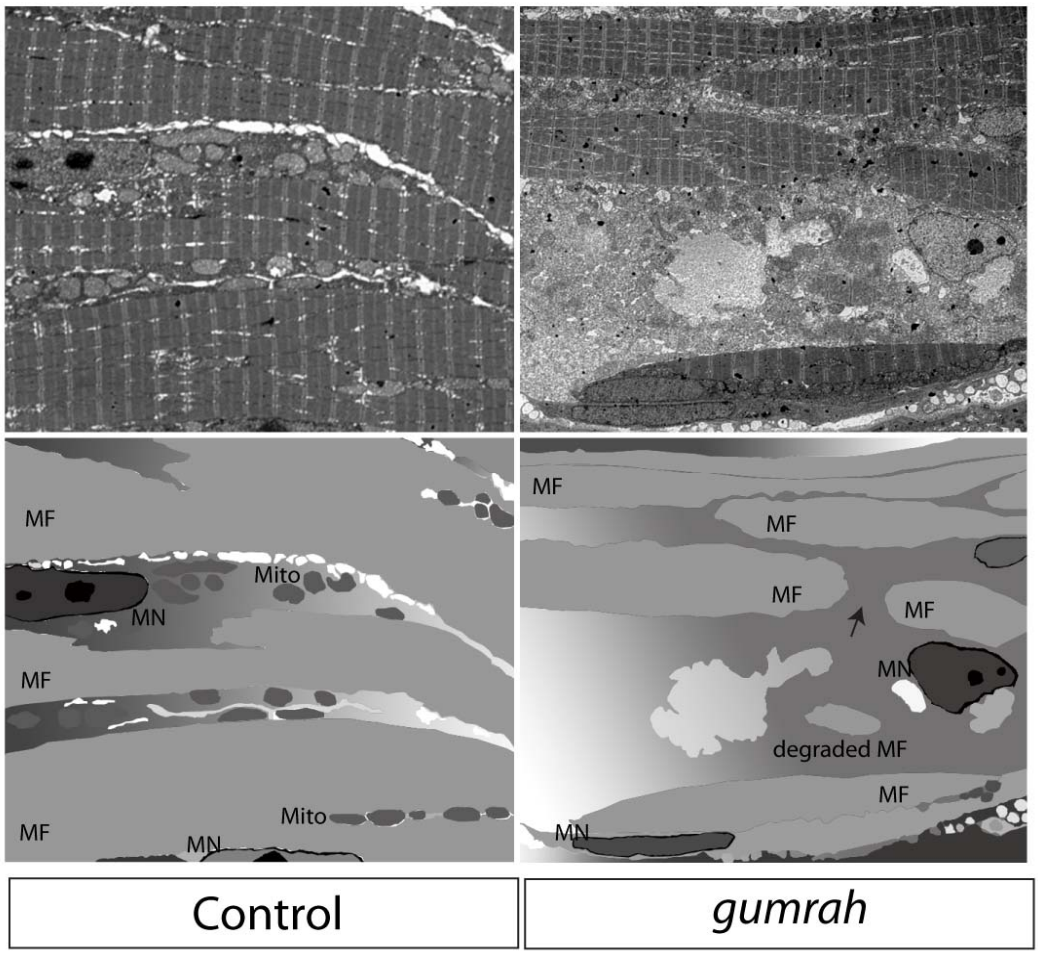

Figure 26: Transmission Electron Micrographs of the coronal sections of the 5 dpf old control and the *gum* mutant embryos. Myofibers in the *gum* larvae are thinner, with huge gaps, where the remnants of degraded myofibers can be observed. Sometime breaks in the myofibers are also observed (arrow). **MF** myofiber, **MN** myoneuclei, **Mito** mitochondria.

3.1.1.3 *gumrah* mutants have multiple neuronal defects

To check if the motility defect in the *gumrah* embryos is due to the neuronal defects, antibodies staining the secondary neurons (Anti Hu-C) as well as the neuronal processes (znp-1) were employed (Fashena and Westerfield, 1999). To visualize whether the clustering of nicotinic acetylcholine receptors (nAChR) takes place, α-bungarotoxin (which binds to the nAChRs) coupled to the fluorophore FITC was used.

Staining with anti Hu-C antibody revealed that the dorsal root ganglia (DRG) are either missing or located at an ectopic location in the *gum* embryos. In *gum* mutants certain neurons (arrows, Fig. 27B') are observed almost at the level of midline. These could be the missing or ectopic DRG although specific markers for DRG would have to be used to confirm this. Enteric neurons are almost completely absent in the *gum* mutants (asterisk, Fig. 26B') when compared to the control larvae (arrowheads, Fig. 27B). Staining with the Znp-1 antibody revealed gaps in neuronal processes in the posterior half of the somite (asterisk, Fig. 27A') when compared to the wildtype sibling (Fig. 27A). This aberrant staining of znp-1 might reflect the gaps in muscle fibers in *gum* mutants. However, α-bungarotoxin, that binds to the nicotinic acetylcholine receptors (nAChR), co-staining with znp-1 revealed that nAChRs are correctly assembled (Fig. 28).

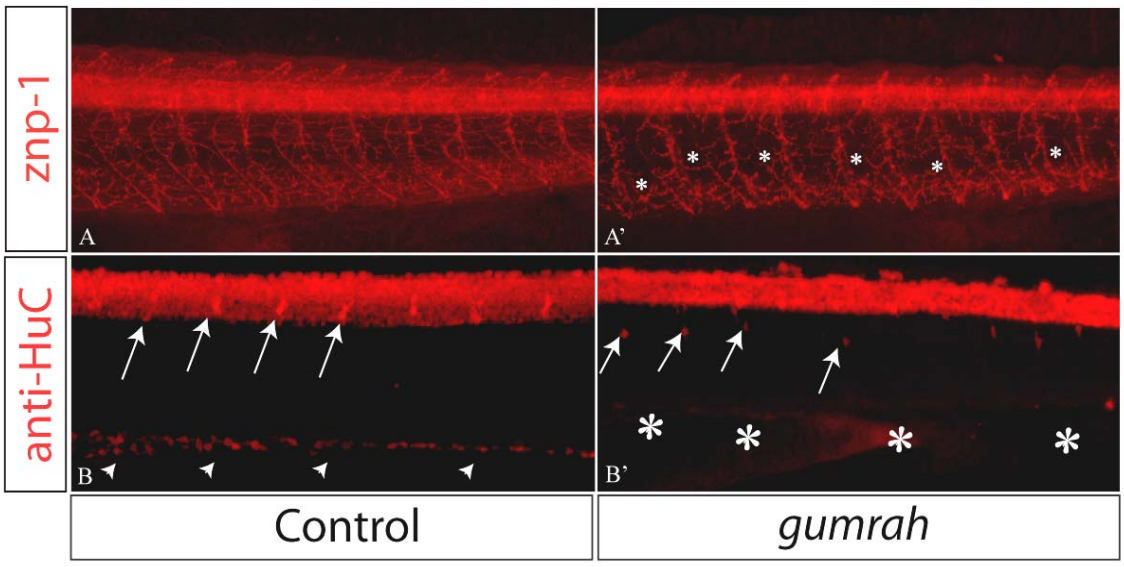

Figure 27: znp-1 staining shows gaps in the posterior half of the somites (asterisks, A') and anti-HuC staining reveals ectopic location of dorsal root ganglia (arrows) and loss of enteric neurons (asterisks, B'). Stage 72 hpf.

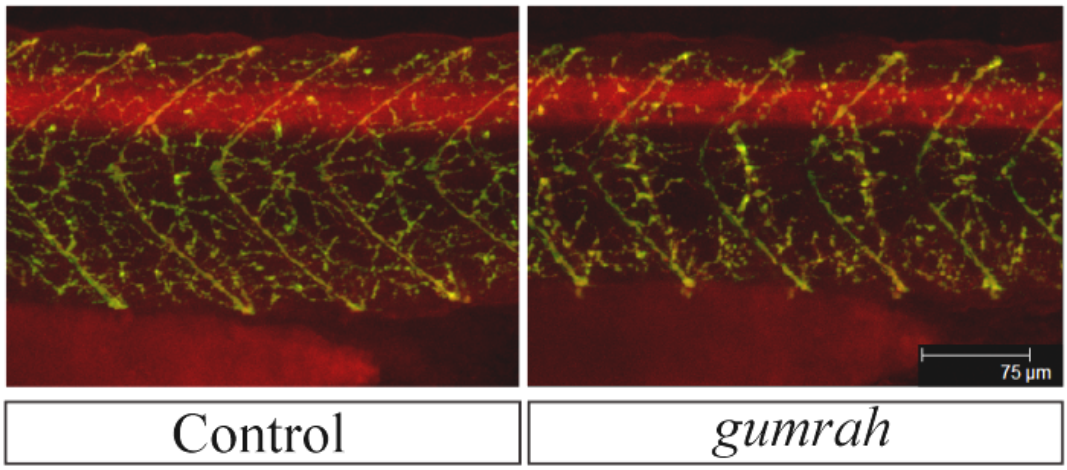

Figure 28: FITC tagged α-bungarotoxin (green) and znp-1 (red) co-staining shows that the nAChRs are present and correctly assembled.

3.1.1.4 *gumrah* mutants have defects in neural crest derived tissues

Since dorsal root ganglia as well as enteric neurons are neural crest derived tissues and since *gum* mutants show a near complete loss of the jaw (as shown by alcian blue staining, Fig. 29), another neural crest derived tissue, it is feasible to speculate that *gum*$^{-/-}$ mutants might be defective in the specification and/or the migration of the neural crest cells. I also observed an almost complete absence of placodal derived neuromast cells. DASPEI stain, a vital dye that stains the sensory hair cells of the neuromasts, was used to visualize neuromasts in 5 day old embryos. *gum* mutants had almost nonexistent posterior neuromast hair cells and very weakly stained anterior neuromast hair cells (Fig. 30).

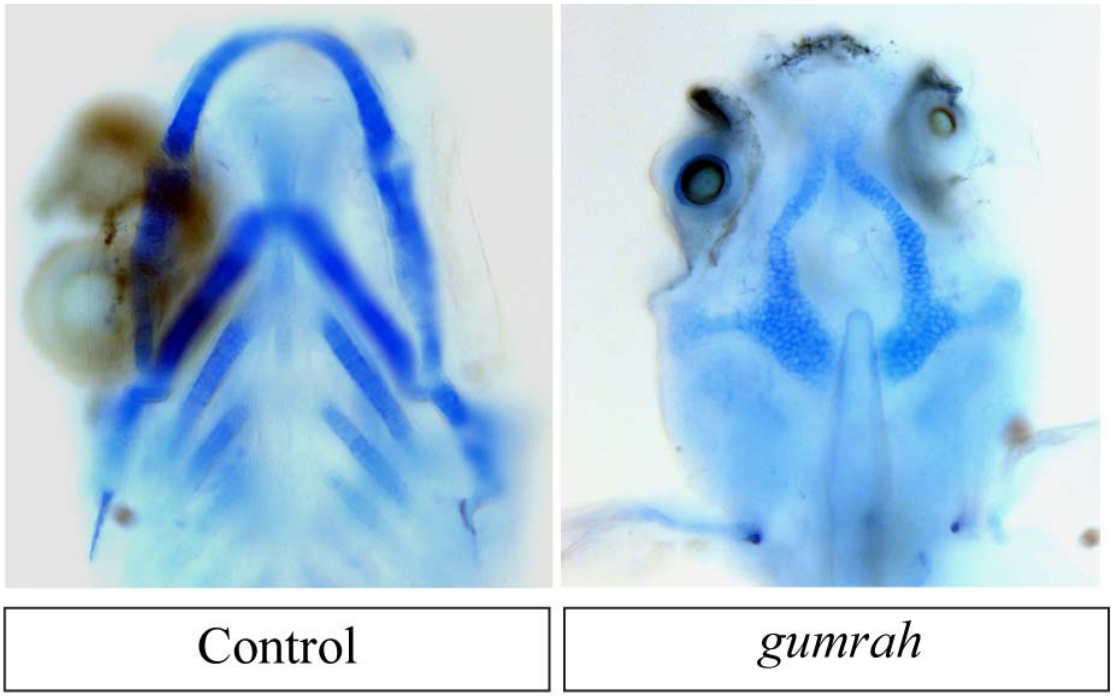

Figure 29: Alcian Blue staining for cartilage shows severely malformed cartilage. Ventral view of 5dpf old larvae, anterior is to the top.

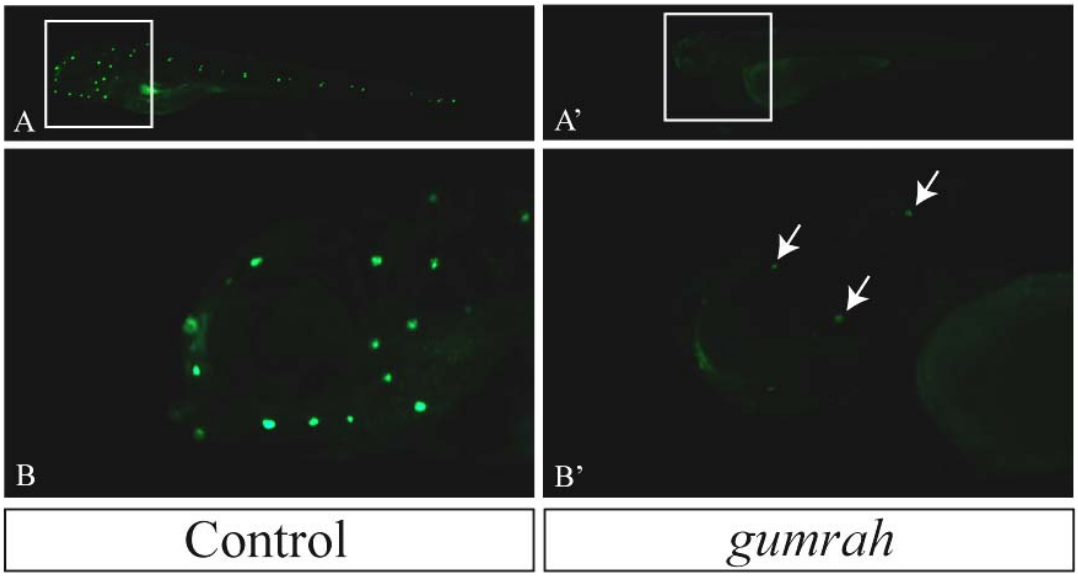

Figure 30: DASPEI staining for the control (A, B) and the *gum* (A'B') 5dpf larvae. *gum* mutants have very few anterior neuromast hair cells (arrows B') and almost no posterior neuromast hair cells. B and B' represent the boxed areas in A and A' respectively.

Therefore whole mount *in situ* hybridization (WISH) was performed on *gum*$^{-/-}$ mutant embryos with an antisense probe against the neural crest marker *crestin* (Luo et al., 2001). *crestin* Dorsal views of the *gum* larvae whole mount in situ hybridized for *crestin* staining at 28hpf, 31hpf and 33hpf revealed that the migratory neural crest cells over the yolk sac had not migrated as far as their wildtype siblings (arrows, central panel, Fig. 31). The number of neural crest cells on the yolk sac is also reduced although it is not clear whether this is because of delayed development or loss of hind brain tissue due to necrosis that occurs around the same time (Fig. 22A').

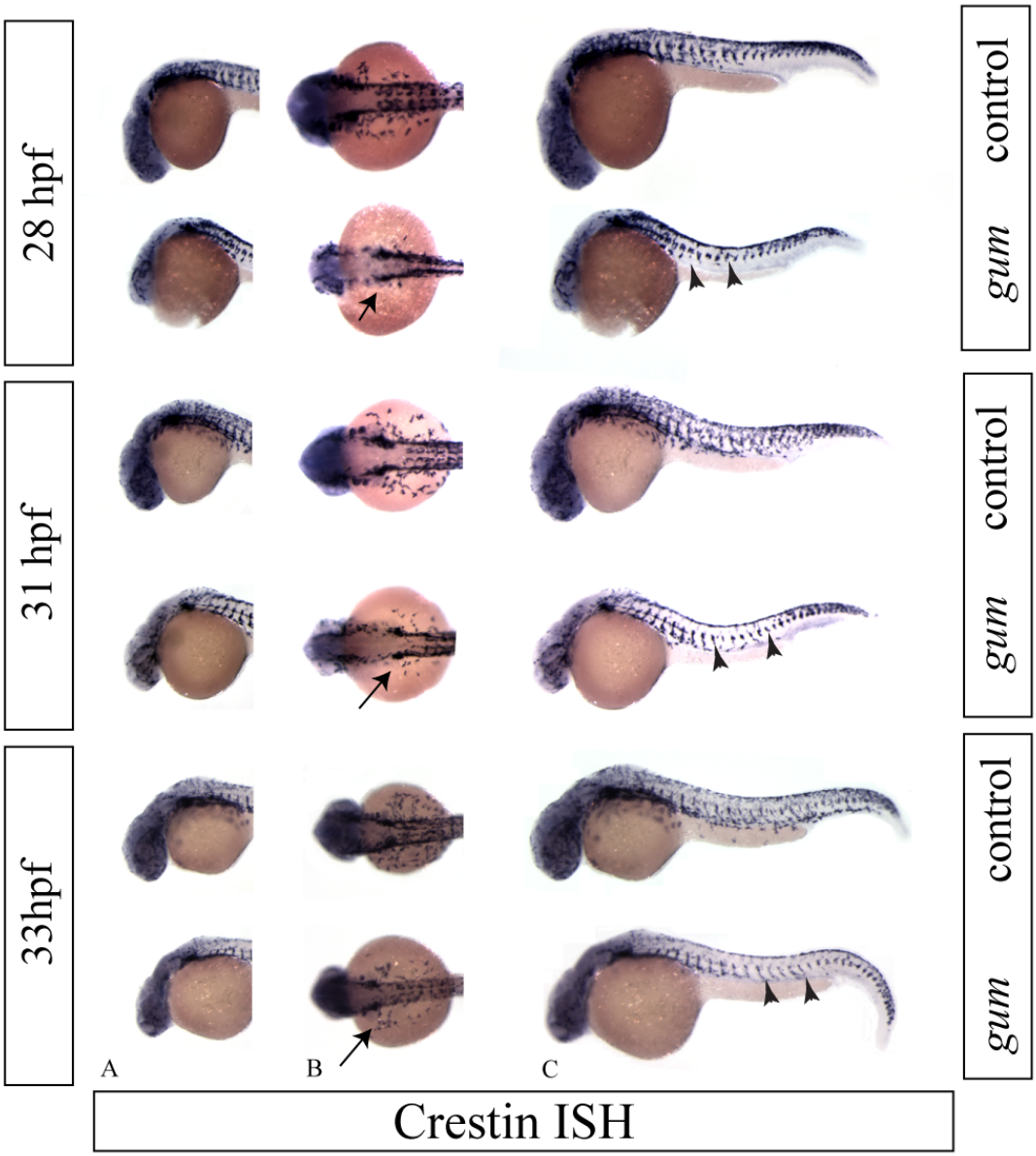

Figure 31: Time course of *crestin* staining for control and *gum* larvae of 28, 31 and 33 hpf stages. In both the dorsal (B) as well as the lateral (C) views *crestin* positive cells seem to be reduced and/or migrate less in the *gum* larvae (arrow, B) relative to the control larvae. In the trunk the *gum* larvae form a single stripe (arrowheads, C) of *crestin* positive cells rather that a speckled appearance of the control larvae.

Transverse sections (at the level of the yolk extension) performed on *crestin* stained embryos revealed that indeed the migratory trunk neural crest cells tended to stay adjacent to neural tube and do not take the sub-dermal migratory route while migrating ventrally. In the *gum* mutants the trunk neural crest cells were observed

only adjacent to or abutting the neural tube as opposed to a sub-dermal path followed by wildtype trunk neural crest cells (arrowheads, Fig. 32). The missing enteric neuron precursors are also evident in the *gum* mutant larvae (asterisk, Fig. 32) while they are abundant in control larvae (arrows, Fig. 32).

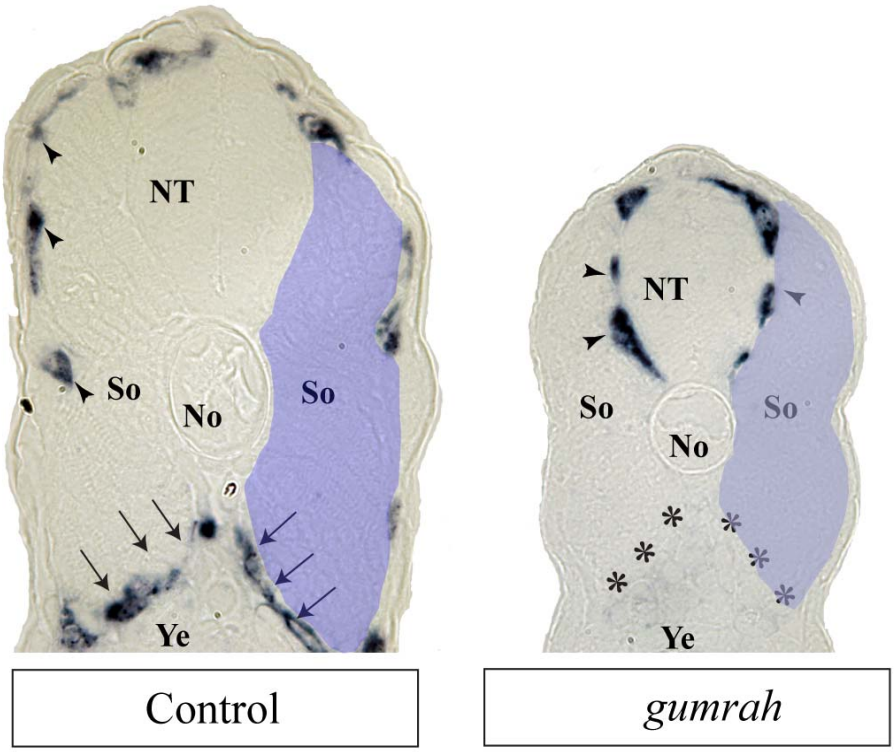

Figure 32: Transverse section of *crestin* stained *gum* embryos at 31hpf reveals that the trunk neural crest cells in the *gum* mutants do not undertake the sub-dermal migratory route and prefer to stay abutting the neural tube. Absence of neural crest derived enteric neuronal precursors (asterisks) is also evident. **NT**, Neural tube, **No**, Notochord, **So**, somite (half of which is depicted in blue shaded area), **Ye**, Yolk extension.

I also performed ISH for another neural crest marker *pax7*. The 33hpf *gum* embryos have a huge reduction in *pax7* expressing cells in the brain (arrow, Fig. 33) although the posterior neural crest (arrowheads, Fig. 33) as well as myotomal expression of pax7 was not affected (Fig. 33).

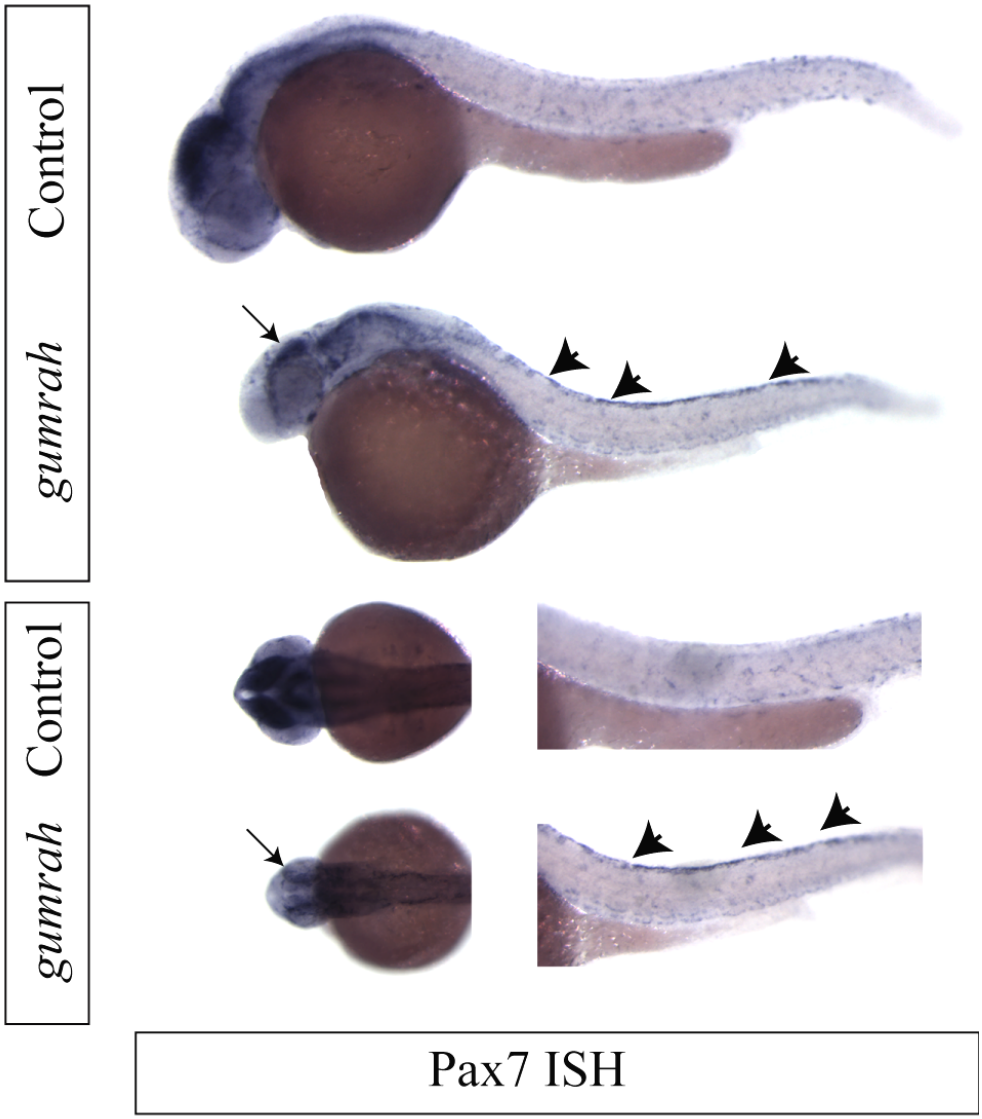

Figure 33: *pax7* ISH on 33 hpf *gum* embryos shows reduced expression levels in the brain of the *gum* embryos (arrows) although the trunk neural crest (arrowheads) appears to be normal. The higher levels of trunk neural crest staining in *gum* embryos could be a result of a lag in development.

To identify the genetic defect and molecular mechanism underlying the *gum* mutant phenotype, we are currently mapping the mutation by a positional cloning approach (collaboration with Dr. Christelle Etard). At the time of writing this report the mutation was localized to a 2 Mb region on chromosome 14 (Ensembl ZV 7).

3.2 Developing an inducible zebrafish model for muscle regeneration

I also looked at the previously isolated progressive myopathy mutants from earlier mutagenesis screens in the lab. One such mutant, with a mutation in the *acetylcholinesterase (ache)* gene, develops a progressive myopathy (Behra et al., 2002). Homozygous *ache* mutant embryos are motile at 24 hours post-fertilization (hpf) but become almost paralyzed by 72 hpf. Further work showed that the mutant phenotype could be mimicked with bath application of acetylcholinesterase inhibitors such as eserine (ESE), tacrine (TAC), edrophonium (EDRO) and Galanthamine hydrobrobide (GAL) (Behra et al., 2004).

Galanthamine hydrobromide was found to phenocopy the mutant best, without inducing secondary effects. Galanthamine is an alkaloid which occurs naturally in various plant species of *Galanthus* and *Narcissus*, including the Caucasian snowdrop, *Galanthus woronowii* (*Amaryllidaceae*), and *Narcissus confusus* (Lopez, Bastida et al. 2002). It is a reversible inhibitor of cholinesterase activity and has been used in studies of nicotinic receptors (Pereira et al., 2002).

3.2.1 Galanthamine treatment causes an inducible myopathy

The *ache* mutant shows decrease of birefringence and galanthamine treatment is able to reproduce this effect (Behra et al., 2004)**.** Lack of AchE activity, whether genetic or chemically induced, can cause an accumulation of acetylcholine since the acetylcholine scavenger is missing. This excessive acetylcholine in the neuromuscular junction can render the nicotinic acetylcholinesterase receptors (nAChRs), ligand

gated ion channels required for muscle excitation, open constitutively. nAChRs are permissive to Na^{+} and K^{+} but can also allow Ca^{++} ions into the muscle fiber. A high intracellular concentration of Ca^{++} can lead to activation of Ca^{++} activated neutral proteases such as Calpain3. As described in earlier work, an increased activity of Calpain 3 could lead to a myopathy such as the one observed in *ache* mutants or galanthamine treated embryos (Behra et al., 2004).

3.2.2 Galanthamine treatment induced myopathy is reversible

Galanthamine treatment gives us an exciting possibility of generating a conditional myopathy at specific time points. This is a major advantage of using a chemical inhibitor approach that is not possible with the genetic mutants, where developmental defects might overshadow more direct effects of acetylcholine excess. Furthermore, withdrawal of the drug might allow for recovery from the induced muscle damage and allow us to examine the process of regeneration. Therefore, we asked next whether the galanthamine induced myopathy was reversible. We treated the embryos with 10^{-3}M galanthamine for 48 hours which causes them to become paralytic and then transferred the larvae back to embryo medium. We observed that the larvae recovered motility gradually over a period of the next 48 hours and were then virtually indistinguishable from untreated larvae. The recovery was very robust, as 96% (n = 144/150 in three different repeats of 50 embryos each, Tab. 1) of the treated embryos completely recovered from galanthamine treatment. The remaining 6 embryos died. The survival rate was comparable to the wild type, untreated control embryos (145/150 survivors). Continued treatment of embryos with galanthamine resulted in death for all embryos (150/150) presumably because of extensive muscle damage and cardiac edema. This is in accordance with the life expectancy for *ache*

mutants that rarely survive beyond 5 days. Thus, the zebrafish embryos can recover from a severe paralysis induced by galanthamine treatment.

	GAL –ve Control (Untreated)			**GAL +ve control (continuous treatment for 96 hours)**			**GAL Treatment (48 hours)-Recovery (48 hours)**		
Sets	I	II	III	I	II	III	I	II	III
Total number of embryos	50	50	50	50	50	50	50	50	50
Immobile after 48h treatment	0	0	0	50	50	50	50	50	50
Regained motility after 48h recovery period	NA	NA	NA	0	0	0	50	50	50
Survival	48 Alive	48 Alive	49 Alive	All Dead	All Dead	All Dead	48 Alive	49 Alive	47 Alive

Table 5: Recovery from galanthamine treatment is very robust and reproducible. 150 embryos were treated with GAL in three sets of 50 embryos each. 48 hours of treatment resulted in a severe loss of motility that was reversed after removal of galanthamine and subsequent recovery of another 48 hours. Continued treatment with galanthamine resulted in death of all embryos (similar to the longevity of *ache* mutants). The survival rate among the experimental group was similar to the untreated controls.

Since the recovery of galanthamine embryos was quite rapid, we decided to repeat the birefringence results from Behra et al. (Behra et al., 2004). It is possible that galanthamine tretment had caused a temporary blockage of electrical activity in the skeletal muscle (similar to the way conotoxin or tetrodotoxin cause paralysis) thus leading to a lack of motility while no structural damage was endured. To rule out this possibility we confirmed the motility findings with birefringence images of galanthamine treated larvae. Embryos at 80% epiboly were treated with 10^{-3}M or 10^{-4}M GAL for 48 hours. Following this treatment birefringence images were acquired and larvae were transferred to fresh embryo medium. After another 48 hour

period, the same larvae were imaged again for birefringence. We found that the birefringence of GAL treated larvae to be indeed diminished in a concentration dependent manner similar to previous report. Upon removal of galanthamine and following the subsequent recovery period, the birefringence levels increase dramatically (Fig. 34). Although the birefringence was not back to the same levels as the wildtype untreated controls there was not much difference in the motility levels of the larvae, indicating substantial functional regeneration. Thus, it is obvious that GAL treatment leads to disruption of higher order muscle structure and that the larvae are able to mount a very rapid repair/regeneration response after galanthamine induced muscle damage.

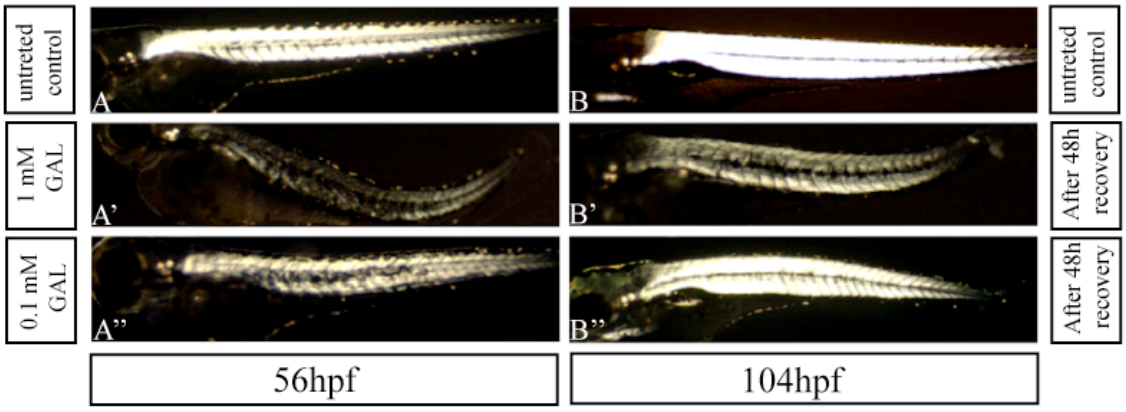

Figure 34: Plane polarized light images of 56 hpf (A, A', A'') and the same embryos at 104 hpf (B, B', B''). Galanthamine treatment reduces birefringence intensity in a dose dependent manner (10^{-3} M for A', 10^{-4} M for A'', untreted control A). GAL treatment was from 8 hpf to 56 hpf. Upon removal of GAL and subsequent recovery period of 48 hours birefringence intensity increases (B', B'', untreated control B)

In order to gain more insight about the precise nature of the structural defects, I next carried out electron microscopy of galanthamine treated embryos as well as recovered embryos to assess the muscle ultrastructure before and after recovery.

56hpf embryos that were treated with galanthamine for the past 48 hours had totally fragmented myofibers that were mis-oriented (Fig. 35A and A'). Following a 48 hour recovery period the myofibers of these larvae were virtually indistinguishable from untreated controls of the same age (Fig. 35B and B'). Thus electron microscopy confirms the birefringence data and reveals a striking regeneration by the larvae at the ultrastructural level within two days.

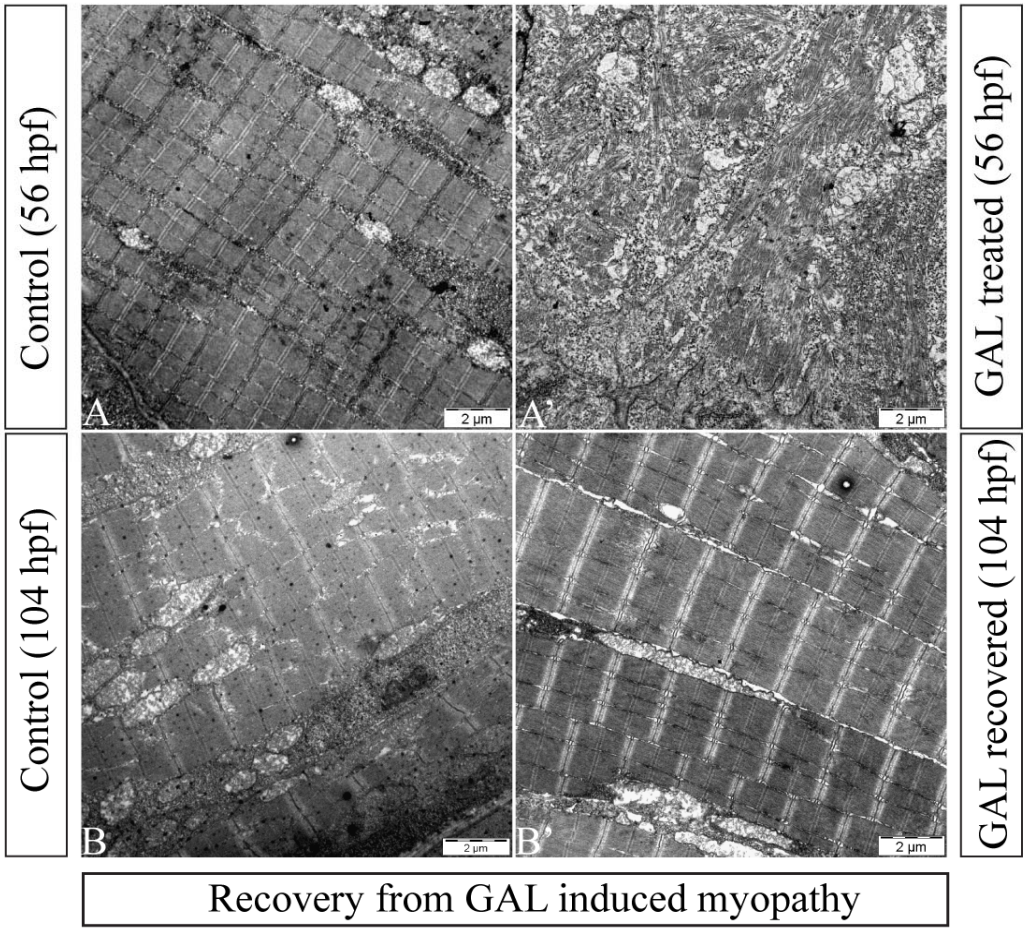

Figure 35: Electron Micrographs of coronal sections of zebrafish larvae showing regeneration from GAL treatment at the ultrastructural level. 10^{-3} M GAL treatment from 8 to 56 hpf (A') leads to severe loss of myofibers at an ultrastructural level, in comparison to wildtype 56 hpf (A) larvae. When the treated embryos are allowed to recover for 48 hours in absence of GAL their muscles regenerate very robustly (B') and are almost indistinguishable from untreated control embryos (B). Scale bar is 2 µm.

3.2.3 What is the cause of this repair/regeneration?

Skeletal muscle is a post-mitotic, terminally differentiated tissue. Regeneration in this tissue would require; a) a specialized population of cells capable of generating new myofibers, or b) the ability of injured myofibers to de-differentiate into mononuclear cells which can amplify and then fuse together and differentiate into new myofibers. As outlined in the introduction, it seems that both these mechanisms were employed in evolution. To understand what mechanism is at work in zebrafish muscle regeneration we would have to distinguish between the two alternatives, the stem cell vs. the de-differentiation model.

During the course of the electron microscopy studies we observed certain cells that based on their morphology and location could be prime candidates for being classified as satellite cells. These cells were adjacent to the myofibers, generally at the myosepta, had large nuclei and a large nuclear to cytoplasmic ratio, and lay under the basement membrane, characteristic morphological hallmarks of satellite cells (Fig. 36) as outlined in the introduction. Over the last decade identification of several molecular markers has provided genetically amenable tools for the study of satellite cells. The spatio-temporally restricted expression pattern of these markers has also revealed that the satellite cells are a heterogeneous population consisting of at least two classes, *Myogenic precursor cells* (*MPCs*) that undergo several rounds of self duplication and ultimately differentiate to muscles, whereas the *real stem cells* can repopulate the satellite cell niche when transplanted into dystrophic animals and give rise to differentiated muscle fibers, yet maintain the satellite cell compartment after a long period (Cerletti et al., 2008; Kuang et al., 2007). In order to develop the zebrafish as a model for the study of muscle regeneration it is very important to

understand the basic biology of satellite cells in zebrafish. Therefore we need to establish the similarities and differences in zebrafish versus rodent/avian models: whether they express the same makers, whether they are also a heterogeneous population, and ultimately whether they can lead to efficient muscle regeneration and repopulate the satellite cell niche.

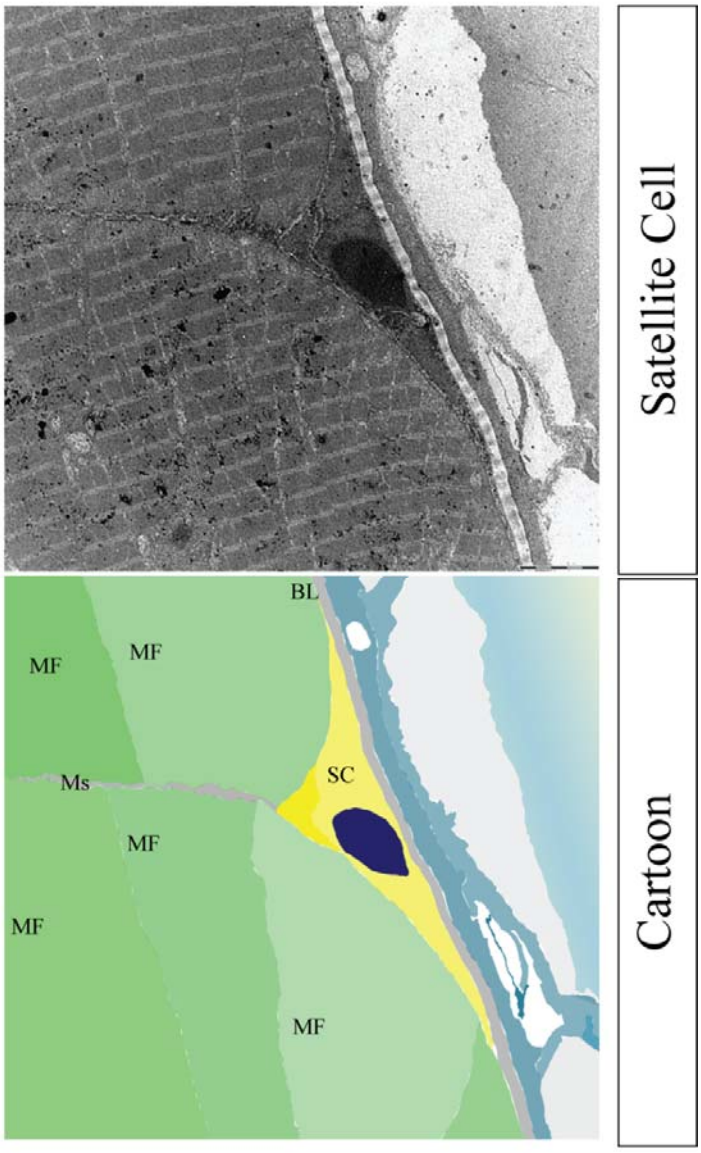

Figure 36: Electron micrograph (top) of a coronal section of a 104 hpf zebrafish larva, and a scheme of the micrograph (bottom), showing a putative satellite cell. The satellite cell is adjacent to the myofibers, lies under the basal lamina, and has a large nuclear to cytoplasmic ratio. **SC**, satellite cell; **BL**, Basal Lamina; **MF**, Myofiber; **Ms**, Myoseptum. The scale bar in the top panel is 5 microns long.

3.2.4 Markers for satellite cells

Although electron microscopy is the most unambiguous way to distinguish a satellite cell it is not a good tool for functional studies as it is slow and laborious and the animal has to be sacrificed. Therefore we decided to look for molecular markers that could facilitate investigation of satellite cell involvement in the regenerative process and allow us to image them in vivo.

In addition to Pax7, various markers such as Pax3, Myf5, MyoD, and Met have been used to label satellite cells in rodents. Pax7 and Pax3 label a vast majority of satellite cells, both uncommitted ones and those committed to muscle fate (myogenic precursors). Myf5 and MyoD are myogenic regulatory factors (MRFs) that are expressed by satellite cells committed to a myogenic fate. To determine whether the same markers label satellite cells in zebrafish we decided to do in situ hybridizations for Pax3 and Pax7 and look at their expression pattern in developing zebrafish larvae.

3.2.5 ISH for Pax3 and Pax7

3.2.5.1 Pax3 expression pattern

At 22hpf, Pax3 is highly expressed in the midbrain (green arrows, Fig. 37A), the hindbrain (red arrows, Fig. 37A), neural crest cells and the dorsal neural tube (black arrows, Fig. 37A). Migratory neural crest cells in the trunk also express pax3, along with the myogenic precursors (black arrowheads Fig. 37A). By 48hpf the trunk expression has ceased although the midbrain expression and hindbrain expression is still robust for Pax3. Additionally, Pax3 is expressed in the precursors of the pectoral fin muscles (Fig. 37C arrowheads, also in the inset). This is in accordance with Pax3's

role in regulating limb muscle progenitor migration to distal parts of the limbs in rodents (Birchmeier and Brohmann, 2000). By 72hpf, Pax3 expression in the brain is diminished, but it is expressed in the newly forming jaw and cranial muscles.

3.2.5.2 Pax7 expression pattern

At 22hpf Pax7 is highly expressed in midbrain (green arrows, Fig. 37B), hindbrain (red arrows, Fig. 37B), neural crest cells and dorsal neural tube (black arrows, Fig. 37B). Migratory neural crest cells in the trunk also visible in the trunk, along the myogenic precursors (black arrowheads, Fig. 37B). By 48hpf the trunk expression has ceased although the midbrain expression (green arrows Fig. 37D) is still robust for Pax7 and hindbrain expression is lost, after the isthmus (black arrow, Fig. 37D). By 72hpf Pax7 is still robustly expressed in the midbrain (green arrow, Fig. 37F) and the newly forming jaw and cranial muscles (black arrowheads, Fig. 37F).

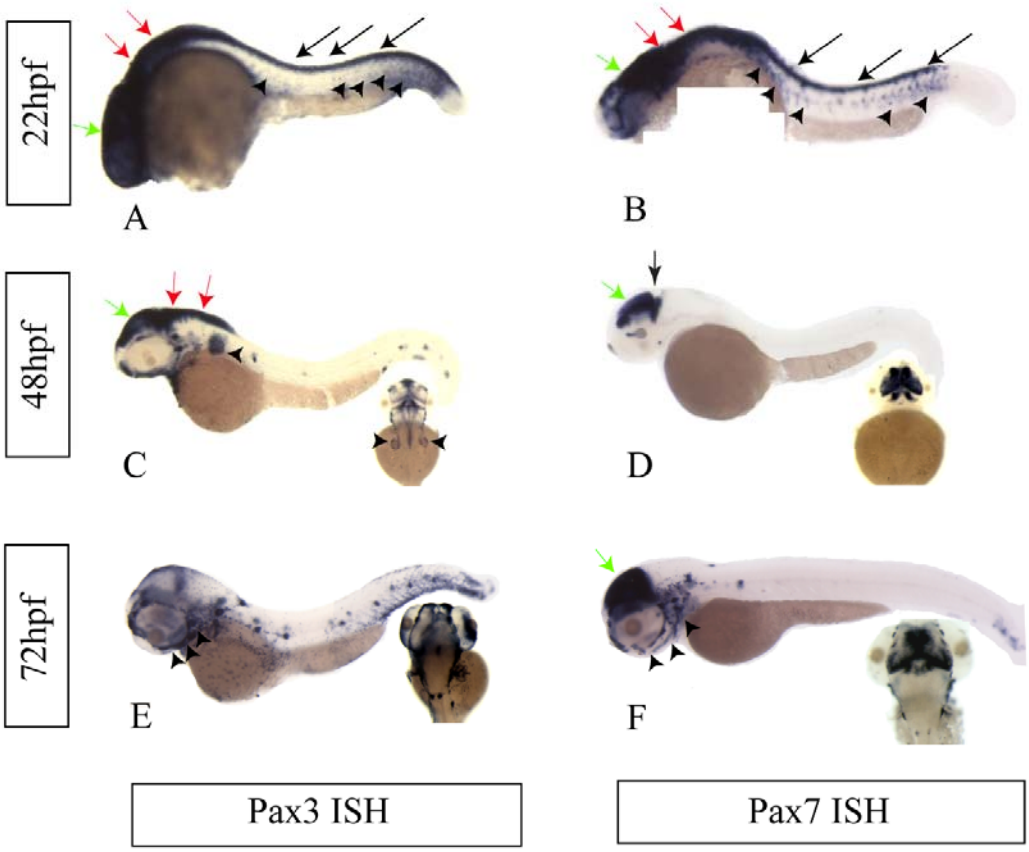

Figure 37: Wholemount ISH for *pax3* (A, C, E) and Pax7 (B, D, F) at 22 hpf (A, B), 48 hpf (C, D) and 72 hpf (E, F). Insets in C-F show dorsal views of the same embryo. At 22 hpf, predominantly the midbrain (green arrows in A and B), the hindbrain (red arrows in A and B), neural crest and the dorsal spinal cord (black arrows in A and B) are stained by both *pax3* as well as *pax7* (black arrow in A and B), although migratory trunk neural crest and myogenic precursors are also evident in the staining (arrowheads in A and B). At 48 hpf, the trunk expression is not evident for both *pax3* and *7*, presumably due to very low level of expression of the transcript, although brain expression is robust in the midbrain (green arrows in C and D) for both and in the hindbrain (red arrows in C) for *pax3* only. *pax7* expression is not observed behind the isthmus (black arrow in D). Additionally, *pax3* expression is also seen in myogenic precursors of the pectoral fin (arrowheads in C). At 72 hpf newly formed jaw muscle precursors also express *pax3* and *7* (arrowheads in E and F). *pax3* brain expression has mostly subsided but *pax7* continues to be expressed at high levels in midbrain (green arrows in F).

We next carried out immunohistochemistry for the Pax7 protein to better characterize Pax7 expression, as protein expression might show a lag relative to mRNA expression and also because immunohistochemistry can provide information on the subcellular localization of the protein.

3.2.6 IHC for Pax7

At 26 hpf, the Pax7 protein is expressed in the trunk in two distinct populations of cells that differ by the intensity of staining (Fig. 38). The weakly stained $Pax7^{+ve}$ nuclei are spread all over the somite whereas there are fewer strongly stained nuclei. When the confocal stacks were used to generate a 3D reconstruction and the reconstruction rotated through 90°, we found that all the $Pax7^{+ve}$ cells are restricted to the external surface of the somite, the so-called "external cell layer". By 75 hpf most of the $Pax7^{+ve}$ nuclei are lined along the dorsal and the ventral edges of the myotome and along the horizontal and the vertical myosepta (Fig. 39; Supplementary movie S1). Most of the $Pax7^{+ve}$ cells though are still in the external layer and it is very rare to find a $Pax7^{+ve}$ nucleus in the deeper myotome. Having thus established the location of $Pax7^{+ve}$ cells, we examined whether myopathic states change the expression pattern of Pax7.

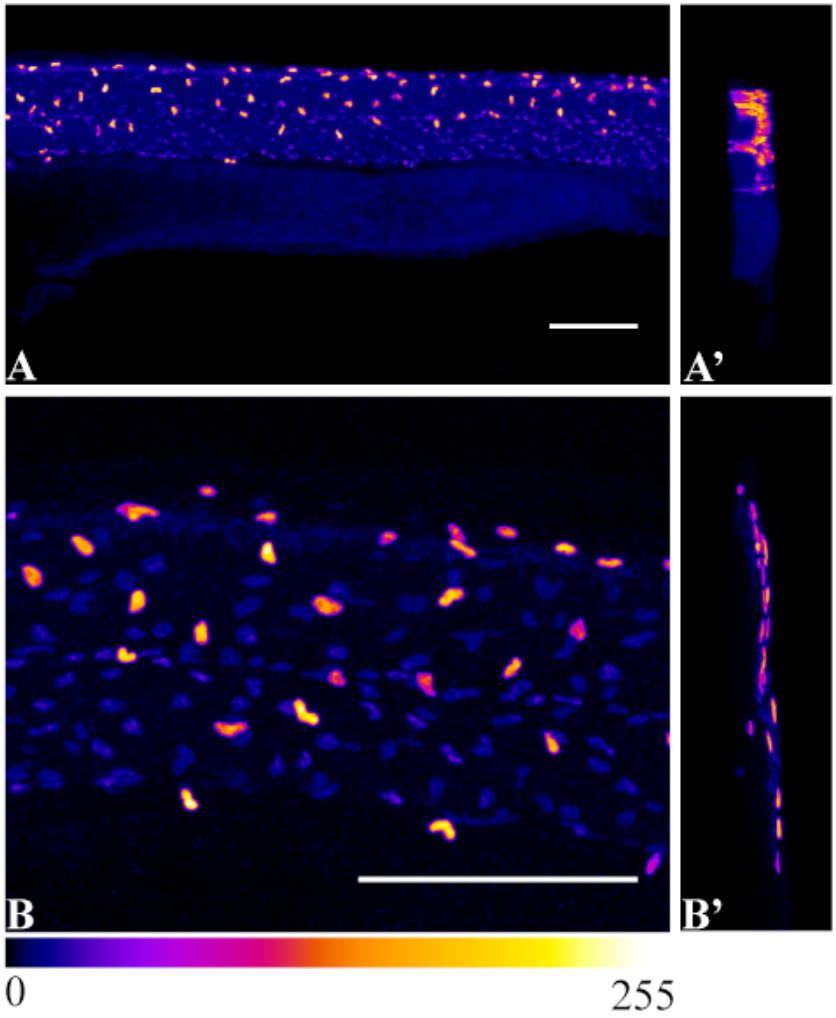

Figure 38: IHC for Pax7 at 26 hpf. Maximum projection images of confocal sections scanned by a 20x objective (A) and a 63x objective (B) through the trunk region. The right panels (A' and B') show 3D reconstructions of z-stacks from corresponding panels on the left rotated through 90°, to reveal the presence of Pax7 positive nuclei in a layer external to the somites. The image has been pseudo colored, with black as minimum and white as maximum intensity, to highlight the two distinct sub populations of Pax7 +ve nuclei based on their level of expression. Anterior is to the left and dorsal is towards the top. Scale bar is 100µm.

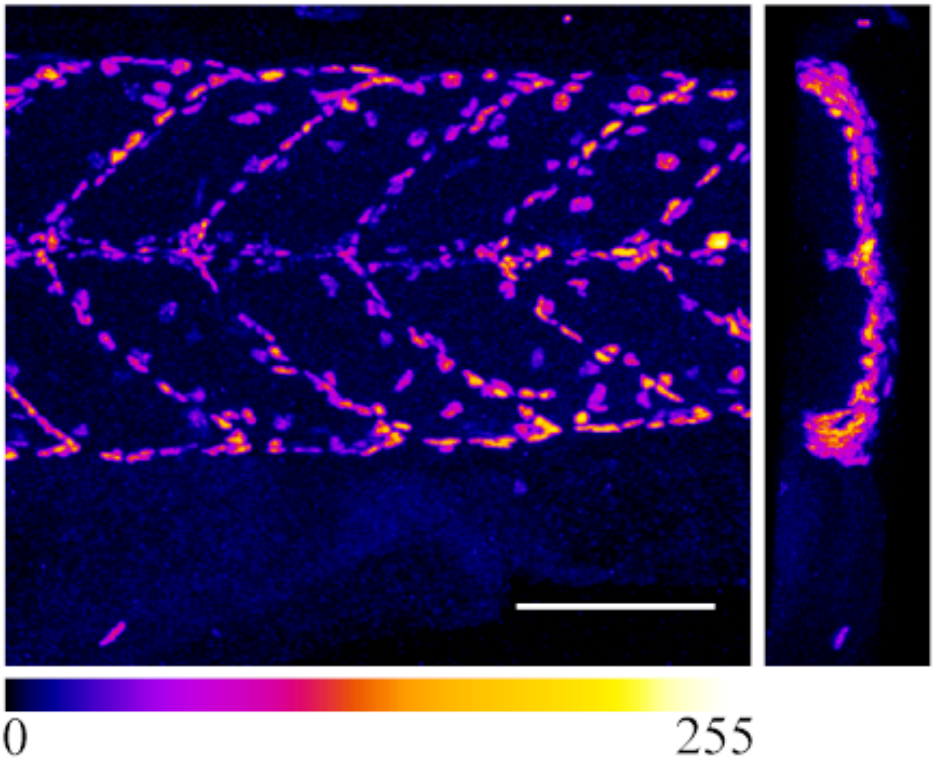

Figure 39: IHC for Pax7 at 75 hpf. Maximum projection images of confocal sections scanned by a 20x objective with a zoom factor of 2x through the trunk region. By this stage most Pax7 +ve nuclei are localized to the edges of the somites. The right panel shows 3D reconstruction of the z stack rotated through 90°, to show that the Pax7^{+ve} nuclei are still found in an external layer (also see Supplementary movie S1). Anterior is towards the left and dorsal is towards the top. Scale bar is 100µm.

3.2.7 Pax7 expression in myopathic states

I performed IHC for Pax7 on galanthamine treated embryos (Fig. 41A, A') to examine if there was a change in satellite cell localization or numbers. The regular arrangement of Pax7^{+ve} nuclei along the myosepta is disturbed in embryos treated with GAL. More Pax7^{+ve} nuclei seem to be in the inter-myosepta region (arrowheads Fig. 41A') than in untreated controls. Also the number of Pax7^{+ve} cells appeared to be higher in the GAL treated group than in the control group. To determine whether

there is really an increase in number of Pax7^{+ve} cells we decided to quantify the numbers of Pax7^{+ve} nuclei upon GAL treatment vs. untreated controls. We found an increase of 8.7% in the number of Pax7^{+ve} nuclei in GAL treated embryos (Fig. 40) when we counted Pax7^{+ve} nuclei in 4 somites of 6 embryos in each condition. However after taking into account the standard deviation, the increase in the number of Pax7^{+ve} nuclei is insignificant.

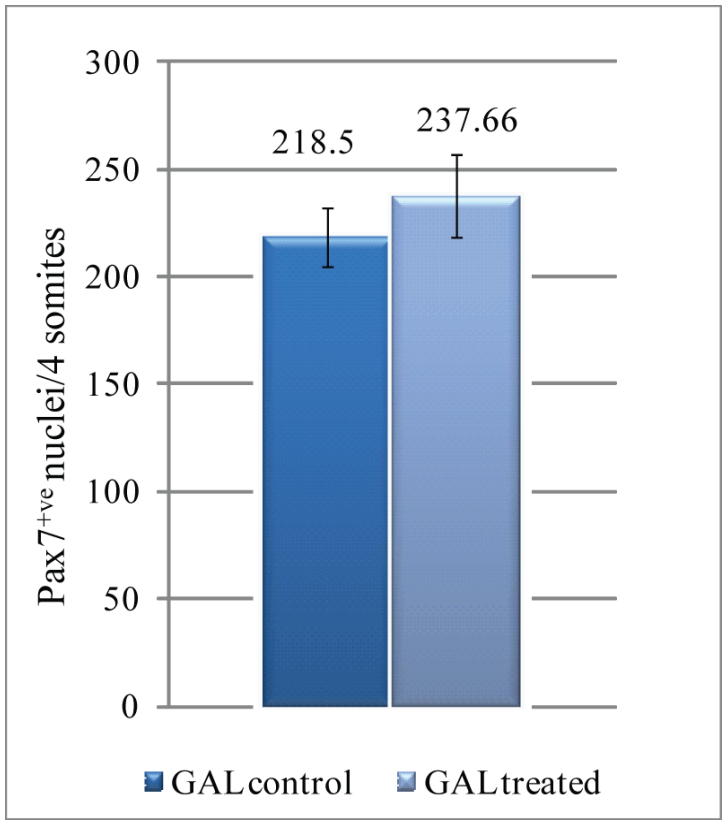

Figure 40: Quantification of Pax7+ve nuclei upon GAL treatment. GAL treatment causes a slight increase in the number of Pax7^{+ve} cells. Pax7^{+ve} cells were counted in 2 somites either side of anus (4 somites in total) in 6 embryos for each state (n=6). Error bars indicate standard deviation. Since the error bars overlap, the increase in number of Pax7+ve nuclei in GAL treated condition was deemed insignificant.

In order to examine whether the changes in number or localization of Pax7^{+ve} cells constitute a hallmark of myopathy, or if they are specifically caused by galanthamine, we decided to repeat the Pax7 IHC staining with two more myopathic

mutants, *steif* and *gumrah*. *Steif* encodes Unc-45b, an Hsp90 co-chaperone required for correct folding of myosin heads, the loss of which causes a myopathy more severe than galanthamine treatment, with the embryos being completely immotile and without any birefringence (Etard et al., 2007). In contrast, *gumrah* is the as yet unidentified motility mutant, described in section 3.1 that develops myopathy gradually and shows diminished motility and birefringence as the larva ages. Comparison of pax7 expressing cells in these slightly different motility mutants should thus reveal whether the phenotype observed in galanthamine treated larva reflects a common mechanism in development of the myopathy. In *steif* mutants the pax7^{+ve} nuclei are scattered all over the surface of the somite (arrowheads, Fig. 41B'). In contrast, in the case of *gumrah* mutants the Pax7^{+ve} nuclei seem to be clustered around the edges of myosepta (arrowheads, Fig. 41C'). It has been shown in section 3.1.1.2 that the muscle fibers tend to break off from the myosepta in *gum* mutants, especially at the edges of the somite (Fig. 24). The Pax7^{+ve} cells therefore may be attracted to such damaged fibers in order to repair them. Comparing three slightly different myopathic states showed that the localization of Pax7^{+ve} nuclei is perturbed in all of them. Thus we hypothesize that a myopathy resulting from chemical treatment or mutation can cause Pax7^{+ve} cells to become migratory and/or mitotic. To verify these hypotheses we performed co-staining of phosphorylated Histone H3, a mitosis marker, with Pax7.

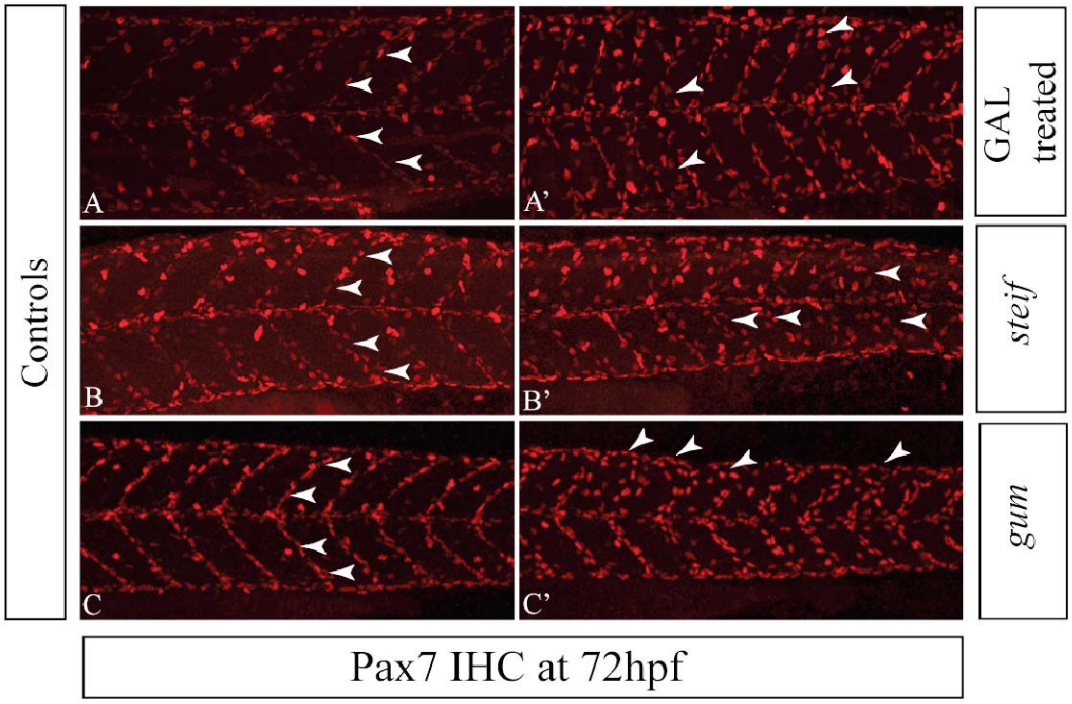

Figure 41: Pax7+ve nuclei in myopathic states. Anti-Pax7 staining on wildtype untreated (control) and Galanthamine treated (A, A') *steif* (unc45b) wildtype sibling (control) and mutant (B, B') and *gumrah* wildtype sibling (control) and mutant (C, C') larvae at 75 hpf. The images in the right panel are myopathic states that show a greater tendency of pax7^{+ve} nuclei to occur in the "inter-myosepta" regions. In addition, the myosepta boundaries are not as clearly defined by Pax7^{+ve} nuclei as in the control group, the left panel. Anterior is to the left and dorsal up.

3.2.8 GAL induced myopathy increases the number of mitotic satellite cells

Co-staining of Pax7^{+ve} cells with Phospho Histone H3 revealed an increased number of satellite cells entering mitosis (arrowheads, Fig. 42B; Supplementary movie S3) as compared to untreated control (arrows Fig. 42A; Supplementary movie S2). I quantified the Pax7^{+ve}/Phospho Histone H3^{+ve} nuclei as described earlier. I found a 79% increase in the mitotic satellite cells based on the co-expression of the two markers (Fig. 43). This showed us that although there is hardly any increase in satellite cells (Pax7^{+ve} nuclei) upon GAL treatment (Fig 40), the number of mitotic satellite cells (Pax7^{+ve}/Phospho Histone H3^{+ve} nuclei) is dramatically increased (Fig. 43).

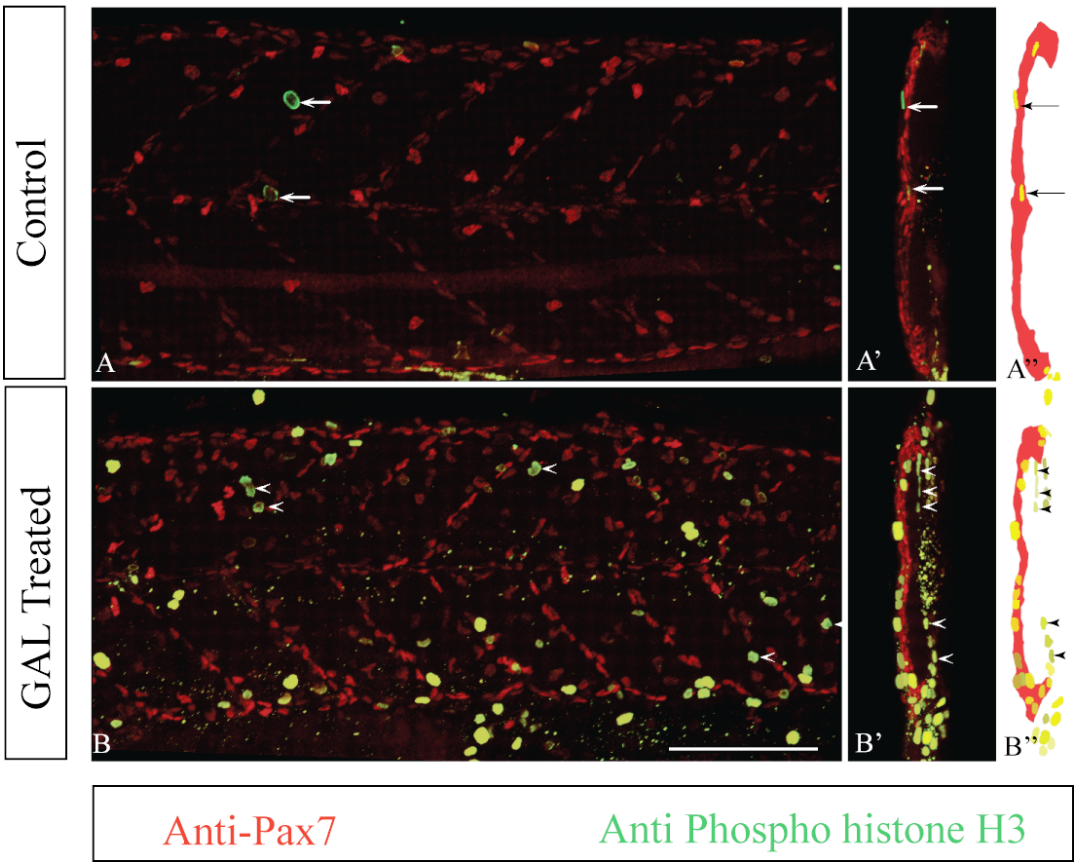

Figure 42: Mitotic Pax7^{+ve} cells are found deeper in the myotome in regenerating muscles. Pax7 (red) and Phospho Histone H3 (green) co-localization in Control (A, A') and GAL treated (B, B') embryos. Maximum projection images of confocal sections scanned by a 20x objective with a zoom factor of 1.5x. GAL treatment causes more Pax7^{+ve} cells to enter the cell cycle (arrowheads, B; supplementary movie S3) than in the control embryos (arrows, A; supplementary movie S2). The middle panel (A', B') shows maximum projection images of 3-D reconstructions rotated through 90° to reveal mitotic Pax7^{+ve} cells located deeper in the myotome (arrowheads, B'') that are very rare in untreated embryos. The scheme in the right panel (A'', B'') indicates the positioning of mitotic pax7^{+ve} cells (yellow, arrowheads, B'') relative to the somite surface (red) compared with control embryos (arrows, A''). The anterior is towards left and the dorsal towards top. The scale bar is 100µm.

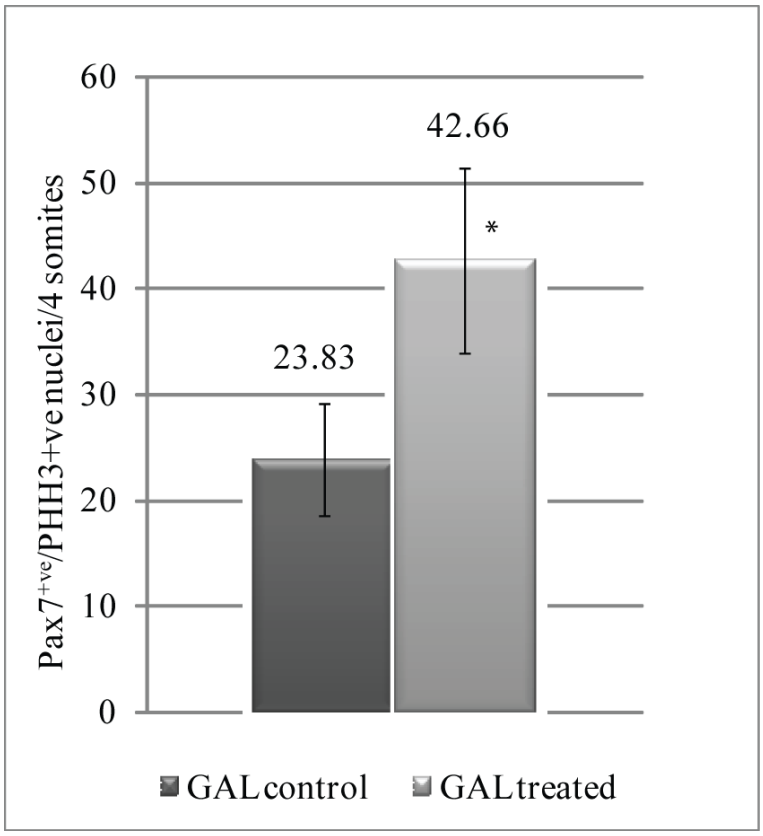

Figure 43: Quantification of mitotic Pax7+ve nuclei upon GAL treatment. GAL treatment causes 79% increase in the number of $Pax7^{+ve}/PHH3^{+ve}$ cells. $Pax7^{+ve}/PHH3^{+ve}$ nuclei were counted in 2 somites either side of the anus (4 somites in total) in 6 embryos for each state (n=6). Error bars indicate standard deviation. * indicates that the results are statistically significant with a p value of ≤ 0.05.

Rotating 3D reconstructions generated from confocal stacks through 90° shows that many of these mitotic $Pax7^{+ve}$ cells in GAL treated embryos are found deeper in myotome (arrowheads, Fig. 42B'; Supplementary movie S3) than in the untreated embryos (arrows, Fig. 42A'; Supplementary movie S2). This implies that the mitotic satellite cells migrate deeper into the myotome upon injury, presumably to repair damaged myofibers. Thus we observed that a myopathic state causes satellite cells to enter the cell cycle at a greater rate and also causes them to become migratory.

To assess the migratory behavior of activated satellite cells we would need tools for in vivo imaging such as transgenic lines fluorescently labeling satellite cells.

3.2.9 Generating tools for in vivo imaging of satellite cell

All the above mentioned data led us to conclude that an in vivo analysis of satellite cells, by live imaging, during normal development and during myopathic conditions would be very advantageous for understanding how they migrate. Therefore, we decided to generate transgenic animals expressing fluorescent proteins that would label satellite cells. We would thus be able follow satellite cell fate during quiescence, activation, migration to the site of injury and differentiation into myofibers. Having a transgenic line would also allow us to FACS sort the satellite cells to obtain a very pure population which could be used for analyzing gene function by RT-PCR or microarrays.

3.2.9.1 The Tol2 Strategy

As a first approach we used the Tol2 transposon mediated transgenesis (for a review see Kawakami, (Kawakami, 2007), Fig. 44) to generate fish carrying promoter driven reporter constructs that would drive gene expression specifically in satellite cells. The Tol2 element is a naturally occurring transposable element found in vertebrate genomes. An autonomous member of the Tol2 element has been identified (Kawakami et al., 1998), which contains a gene encoding a fully functional transposase that is capable of catalyzing transposition (Kawakami and Shima, 1999; Kawakami et al., 2000). Tol2 element is about 4.7 kilobases (kb) in length and contains a gene encoding a transposase protein of 649 amino acids. The transposase protein causes the excision of sequence within the Tol2 flanking sites (the Left and the Right Tol2 arms) and inserts it into another location in the genome (i.e. causes

Transposition) (Kawakami et al., 2000). For transgenesis, the transposon encoding gene is replaced by the foreign DNA, such as the promoter::reporter sequence, to be integrated into the zebrafish genome, yielding a vector construct with the DNA of interest flanked by tol2 repeats. The modified Tol2 plasmid is co-injected with in vitro transcribed transposase mRNA into one cell stage zebrafish embryos. Germ cells, as other cells, of the injected fish, show mosaic transgene expression; therefore, after outcrossing the injected fish (founder) with wild-type fish, non-transgenic fish and transgenic fish heterozygous for the *Tol2* insertion are obtained in variable ratios, depending on insertion efficiency.

We used the web based resource ECR browser (Ovcharenko, Nobrega et al. 2004) (http://ecrbrowser.dcode.org/) (Fig. 44) to identify evolutionary conserved regions upstream of the transcription start site of the *pax7*, *met*, and *myoD* genes in zebrafish and cloned a -3.3kb region for *pax7*, a -5.3kb region for *met*, and a -5kb region for *myoD* into the Tol2 vector.

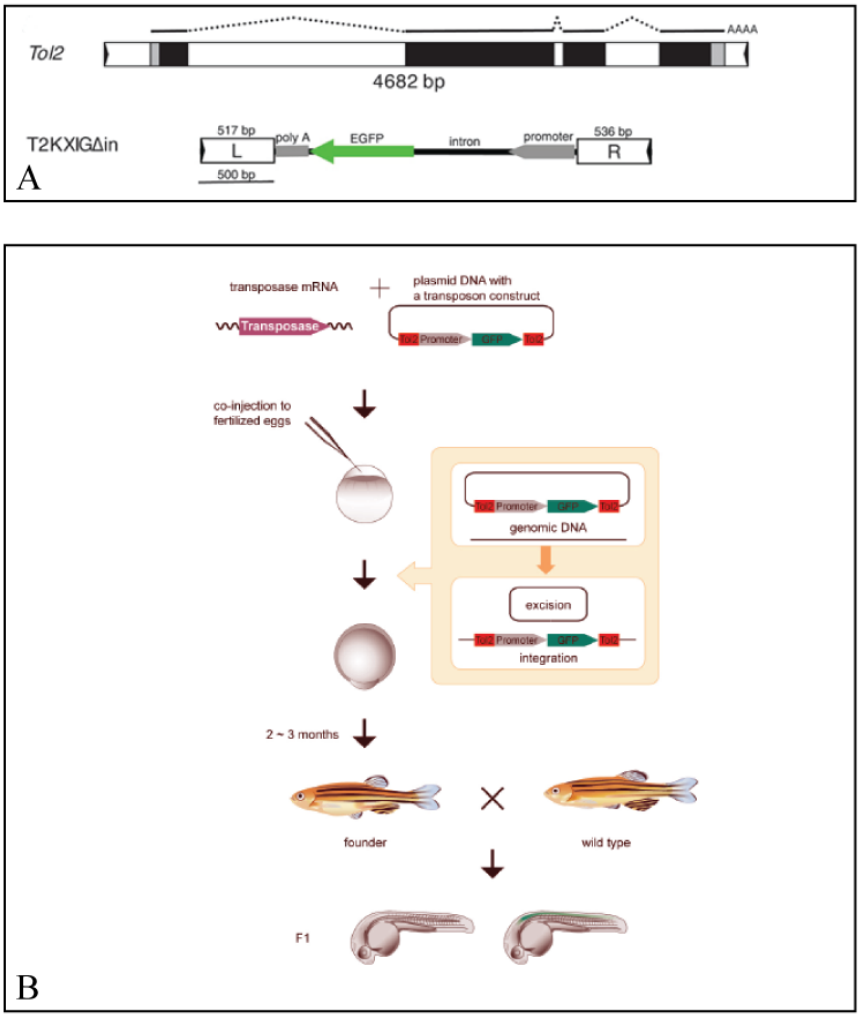

Figure 44: Construction of a Tol2 vector from the original Tol2 (A). The full-length *Tol2* (4682 bp) encodes the transposase gene. Exons are shown in gray (untranslated region) and black (translated region) boxes. Lines (exons), dotted lines (intron), and AAAA (polyadenylation) above Tol2 indicate mRNA for the transposase. The left end (5'-end) and the right end (3'-end) are designated with respect to orientation of the transcript.
Transgenesis in zebrafish (B).The synthetic transposase mRNA and a transposon donor plasmid containing a *Tol2* construct with a promoter and the gene encoding green fluorescent protein (GFP) are co-injected into zebrafish fertilized eggs. The *Tol2* construct is excised from the donor plasmid [2] and integrated into the genome. *Tol2* insertions created in germ cells are transmitted to the F1 generation. Germ cells of the injected fish are mosaic for the transgene, and, by crossing the injected fish (founder) with wild-type fish, non-transgenic fish and transgenic fish heterozygous for the *Tol2* insertion are obtained. In this figure, the promoter is a spinal cord specific enhancer/promoter and the spinal cord of the embryo is depicted in green. Figure (part A) adapted from Urasaki et.al. (Urasaki et al., 2006) and (part B) (Kawakami, 2007).

The -5.3kb *met*::eGFP construct drove expression in heart, muscle fibers, spinal neurons, and liver (Fig. 45). This is in accordance with the reported expression pattern of *met* in the mouse (Yang et al., 1996). In the zebrafish, the expression of *met* has been reported in spinal neurons (Tallafuss and Eisen, 2008). At 6 dpf, there are some eGFP expressing cells localized to the vertical myosepta. These are the locations where $Pax7^{+ve}$ cells are normally found and hence these might be satellite cells.

We observed similar persistent muscle fiber specific expression of eGFP with the -5kb *myoD*::eGFP construct (data not shown) and the -3.3kb *pax7*::eGFP construct (data not shown). The eGFP expression in muscle fibers could be from the eGFP that was expressed by satellite cells before they fused to form muscle fibers, since the half-life of eGFP is quite long. However, the persistence of eGFP during later stages could also mean that the upstream regions of these genes are lacking in enhancer elements that might be required to shut down gene expression after progression of the satellite cell through differentiation and maturation into a muscle fiber.

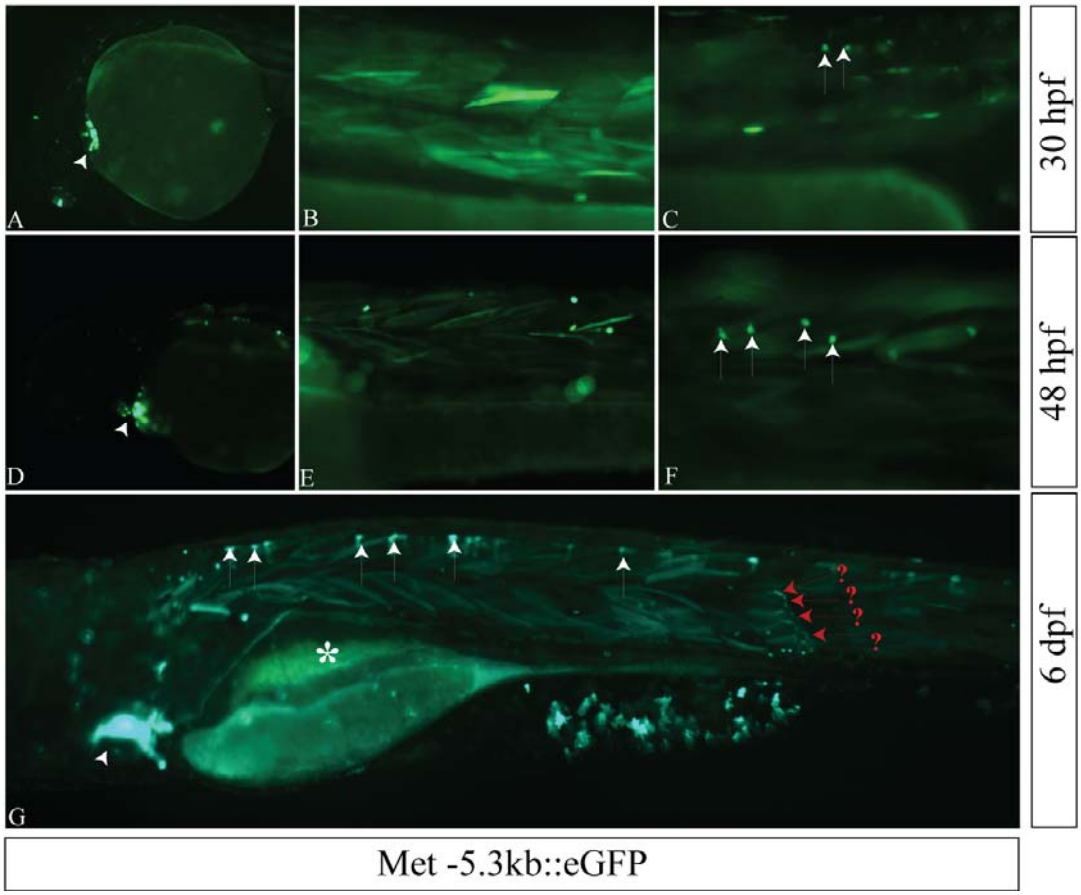

Figure 45: eGFP expression driven by 5.3 kb region upstream of the *met* transcription start site. The expression is most notable in the heart at 30 hpf, 48 hpf and 6 dpf (white arrowheads A, D, G), muscle fibers (B, E, G), and spinal neurons (white arrows C, F, G). At 6 dpf some cells at myosepta (red arrows) express eGFP that could be satellite cells. At this stage expression is also observed in the liver (white asterisk). The strong expression in the ventral fin-fold in figure G is an artifact resulting from ectopic expression.

3.2.9.2 Generation of a *pax7* containing BAC tagged with fluorescent protein reporters

The use of traditional transgenic approaches such as the ones employing basal promoters and upstream elements has several disadvantages. In vertebrates enhancer elements could be scattered over large distances and basal promoter::reporter constructs missing these elements may not properly reflect the dynamics of gene

expression, especially as alternative promoters/enhancers may be involved in regeneration as opposed to normal development (Catherina Becker, pers. Comm.). Indeed, zebrafish *myf5* has been shown to be regulated by enhancer elements located 80 kb upstream from the transcription start site (Chen et al., 2007). Moreover, the fluorescent protein most commonsly used as a reporter (GFP or eGFP) is cytoplasmic and would diffuse throughout the muscle fiber when satellite cells fuse during repair or development making it quite difficult to pick out single cells or count the number of cells in a fluorescent haze. Therefore we decided to approach this problem by using two different approaches; first by adding a nuclear localized signal before the fluorescent protein, and second, by using a photo-convertible fluorescent protein (marketed under the tradename of Kikume Green-Red, kikGR1).

KikGR1 is a green to red photoconvertible fluorescent protein. A photoconvertible protein (such as kikGR) undergoes an irreversible structural change upon irradiation with a particular wavelength of light, converting its absorption/emission spectra from one wavelength to another (usually longer) wavelength. This allows it to be used as an efficient highlighter for labeling specific cells using photoconversion of kikGR1 in single cell using two-photon microscopy (Hatta et al., 2006). The excitation and emission spectra for native kikGR are 507 and 517 nm (GFP/YFP filter) respectively. A brief pulse of violet/ultraviolet light (350-410 nm, CFP filter) will irreversibly convert the yellow/green fluorescent kikGR to Red fluorescent form. The photoconversion can also be achieved using two photon laser at 780nm. Although the use of two photon requires over 1000 times more scanning time (over several minutes) than conventional confocal microscopy, it does improve the resolution especially along the z-axis and it is possible to label single cells in a tissue expressing kikGR (Hatta et al., 2006). Two photon microscopy can

target a single cell buried deep in the tissue without illuminating the plane above or below it (unlike conventional confocal microscopy) thus it would allow labeling a single satellite cell in a mass of closely located satellite cells This would allow us to not only label and follow the fate of single satellite cells in regenerating animals but also to study the dynamics of transcriptional response of pax7 to a muscle injury.

I modified the *pax7* containing BAC by replacing the start codon of the first exon with the start codon of kikGR1 as described in section 2.7.3 (Fig. 20). This modified BAC should express kikGR1 under the regulatory region of the *pax7* gene after injection into the zebrafish embryos. We tested the photoconvertiblity of kikGR1 by subjecting a green fluorescent region to irradiation by standard mercury lamp under a CFP filter (Fig. 46).

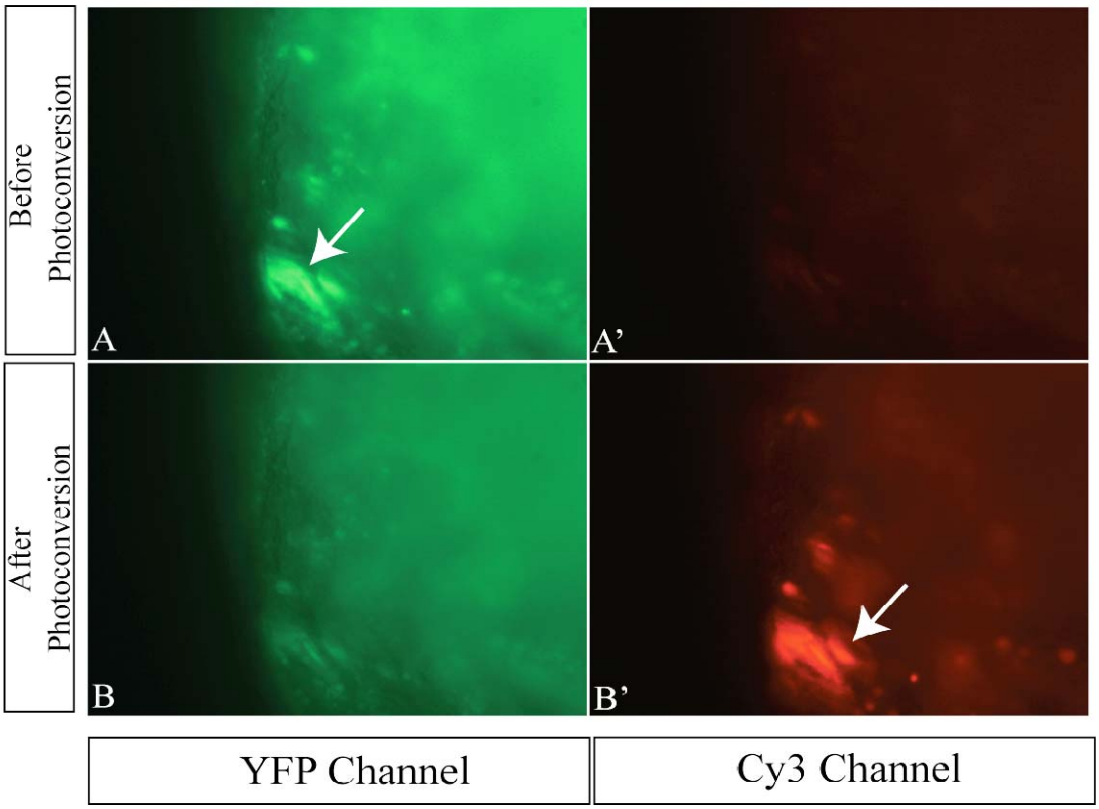

Figure 46: kikGR1 expression in YFP and Cy3 channels before (A, A') and after photoconversion (B, B'). Photoconversion was achieved by illuminating the embryos with illumination from standard mercury arc lamp using a CFP filter for 6 seconds.

Next I decided to check whether the *pax7*BAC::kikGR1 faithfully recapitulates the expression of endogenous *pax7* gene. Therefore I injected the *pax7*BAC::kikGR1 into fertilized one-cell staged zebrafish embryos and reaised the embryos. At 3 dpf, I photoconverted the entire embryo, from green to red, using the technique mentioned above. After another two days (5 dpf) I again observed the embryos for expression of kikGR1 in the YFP and Cy3 channels. I found that the fiber associated satellite cells in these embryos expressed freshly synthesized kikGR1 as evident from the observed signal observed in the YFP channel (Fig. 47). The fiber itself, however, did not show any freshly synthesized kikGR1 (yellow/green), although a low level of photoconverted kikGR1 (red) was visible in the Cy3 channel. Thus, *pax7*Bac::kikGR1 seems to report transcription of Pax7 effectively, although a more thorough analysis with a stable transgenic line will be required to confirm these results.

Therefore, I am currently screening the *pax7*BAC:kikGR1 injected embryos to screen for germline transmission. So far I have found 14 positive larvae from a group mating of these fish indicating that at least one adult out of two females and one male used for mating is positive. Once the founder is identified, it would be outcrossed to the wildtype fish and the kikGR1^{+ve} larvae raised to adulthood to generate a stable transgenic line.

In addition to *pax7*, I have also modified BACs containing *myf5*, *pax3* and *met* genes and I am currently injecting these BACs into embryos and raising these larvae to adulthood. These BACs have been modified with different fluorescent proteins such as nuclear localized signal-Teal (NLS-Teal) (cyan), cytoplasmic kikGR1, NLS-mCherry (red), membrane tagged-mCherry and NLS-Venus (yellow). Once stable transgenic lines have been established for these reporters, I would intercross them to

generate multi-colour double or triple transgenic fish to establish the inter relationship of these genes in satellite cell function during normal development and regeneration.

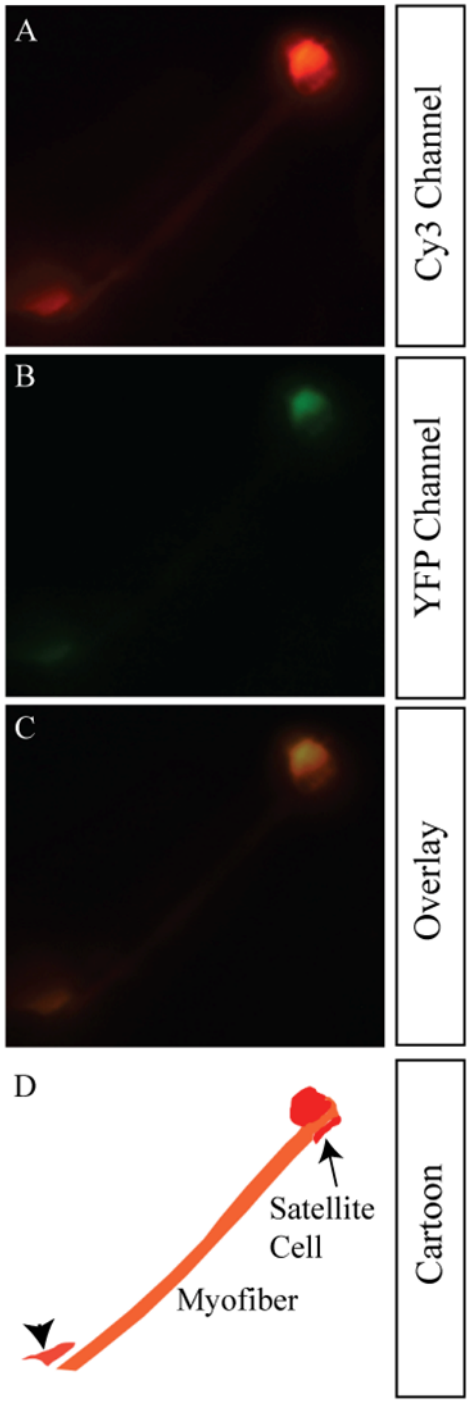

Figure 47: Transient expression of pax7BAC::kikGR1. At 3dpf the whole embryo was photoconverted from green to red. At 5 dpf (time of imaging) only the satellite cells (arrow, arrowhead in cartoon, D) express freshly synthesized kikGR1. The fiber retains red "residual" kikGR1 that it may have received from the pax7^{+ve} cells that gave rise to it.

3.3 Microarray analysis of Galanthamine induced myopathy

To get a holistic view of the gene expression changes induced by a myopathic state I performed an unbiased genome wide expression profile of the galanthamine treated embryos vs. untreated controls using microarray technology. Based on the hypothesis that myopathic animals would express transcripts encoding for proteins involved in the muscle regeneration pathway at an increased level as opposed to non-myopathic animals, comparison of the two transcriptomes may reveal novel potential candidates responsible for muscle regeneration.

The embryos were treated with 10^{-3}M galanthamine for 48 hours and 64 hours from the 8 hpf stage on in two separate experiments. Because chemical treatments can produce a varying degree of phenotypes, even within the same batch, around 600 embryos were pooled together to extract RNA at any given stage. I used entire embryos for the microarray analysis. Although this would dilute the readout of specific RNA transcripts, since the starting sample would not just contain muscle tissue but a multitude of other tissue types, this approach would provide a more accurate representation of the *"in vivo"* trancriptome of a myopathic animal rather than a tissue enriched one.

3.3.1 Sigma Compugen Microarrays

Initially I used 10K zebrafish microarrays produced by the ITG Microarray facility as previously described (Yang et al., 2007). I selected genes with a p-value of ≤ 0.05 and a fold change of $\geq \left|2.0\right|$ in either the 48 hour (56 hpf) or the 64 hour (72 hpf) GAL treatment group. Unfortunately, the number of transcripts perturbed in this range was only 13 (Table 1); substantially smaller than expected. However, one of the transcripts upregulated in the GAL treatment group was *desmin*, a well known marker

of satellite cell differentiation and for regenerating/neonascent myofibers (for a review see (Charge and Rudnicki 2004). This is evident from the phenotype of *desmin* knock-out mice that show slight degeneration of adult muscles but have delayed muscle regeneration following injury (Li et al., 1997; Smythe et al., 2001). Most of the genes upregulated seem to be rather ubiquitous or widely expressed ones (*atf3, SOCS-3, ucp4*). However, one of the genes to be upregulated in both 48 hour and 64 hour treatment groups was *cardiomyopathy associated 1* (*cmya1*), known to be expressed specifically in striated muscles and described in more detail in the following section.

Gene name	FC at 56 hpf (P-value)	FC at 72hpf (P-value)	Reference
zgc:92069 (Protein phosphatase 1 regulatory subunit 3C)	2.19 (0.0038)	1.71 (0.0154)	
Q6PBK2_BRARE	2.05 (0.0160)	1.88 (0.0182)	
zgc:92851	4.83 (0.0016)	2.00 (0.0133)	
phosphoenolpyruvate carboxykinase 1	1.62 (0.0189)	2.07 (0.0070)	
coagulation factor XIII, A1 polypeptide	2.00 (0.0156)	2.19 (0.0065)	
uncoupling protein 4	1.44 (0.0283)	2.23 (0.0048)	
activating transcription factor 3	2.14 (0.0060)	2.43 (0.0066)	
cardiomyopathy associated 1	3.32 (0.0021)	3.22 (0.0023)	(Hawke, Atkinson et al. 2007)
Desmin	1.61(0.0141)	3.38 (0.0013)	(Charge and Rudnicki 2004)
complement component 6	2.06 (0.0156)	3.67 (0.0022)	
SOCS-3b	2.53 (0.0025)	3.94 (0.0019)	
fibronectin 1b	2.37 (0.0023)	8.46 (0.0004)	
SOCS-3a	6.89 (0.0008)	8.57 (0.0007)	

Table 6: Genes upregulated after GAL treatment for 48 hours or 64 hours (on Sigma-Compugen Oligonucleotide arrays). FC, Fold Change.

3.3.1.1 ISH verification of cmya1 upregulation upon GAL treatment

cmya1, initially called *xin*, is a striated muscle specific gene (Wang, Hu et al. 1996) with multiple actin binding domains called Xin repeats (Jung-Ching Lin et al.,

2005; Pacholsky et al., 2004; Wang et al., 1999). Therefore it is believed to play an important role in cytoskeletal organization of skeletal and cardiac muscle.

The zebrafish Cmya1 is a 2297 amino acid protein and the ORF is contained within a single exon (according to Ensembl version Zv7). It contains 25 Xin repeats in the N-terminal half (Fig. 48B). In situ hybridization against cmya1 mRNA shows that it is expressed in nascent myofibers, the heart and the lens (top panel, Fig. 48A) at 30 hpf stage. By 72 hours the expression can be still seen in the lens and the heart and newly forming jaw and ocular muscles also start expressing cmya1, but the expression in the trunk muscles is lost (lower panel, Fig. 48A). The ventral view of the head shows that the expression in the lens is limited to the proximal part of the lens only (black arrows, lower panel, Fig. 48A).

Upon GAL treatment, 72 hpf larvae showed increased staining in the head and trunk (Fig. 48B and C). The increase in staining is most evident in the trunk musculature of GAL treated larvae whereas no staining is present in control embryos. Cross sections of the larvae reveal the presence of *cmya1* transcripts into deeper myotome tissue in a punctuate manner (Fig. 49D). Therefore by wholemount ISH it is clear that cmya1 transcripts are upregulated in the muscles of GAL treated larvae possibly as a repair mechanism. Since mouse Cmya1 has been shown to bundle actin filaments (Choi et al., 2007), it might have a role in cytoskeletal organization and therefore be required for nascent/regenerating myofibers.

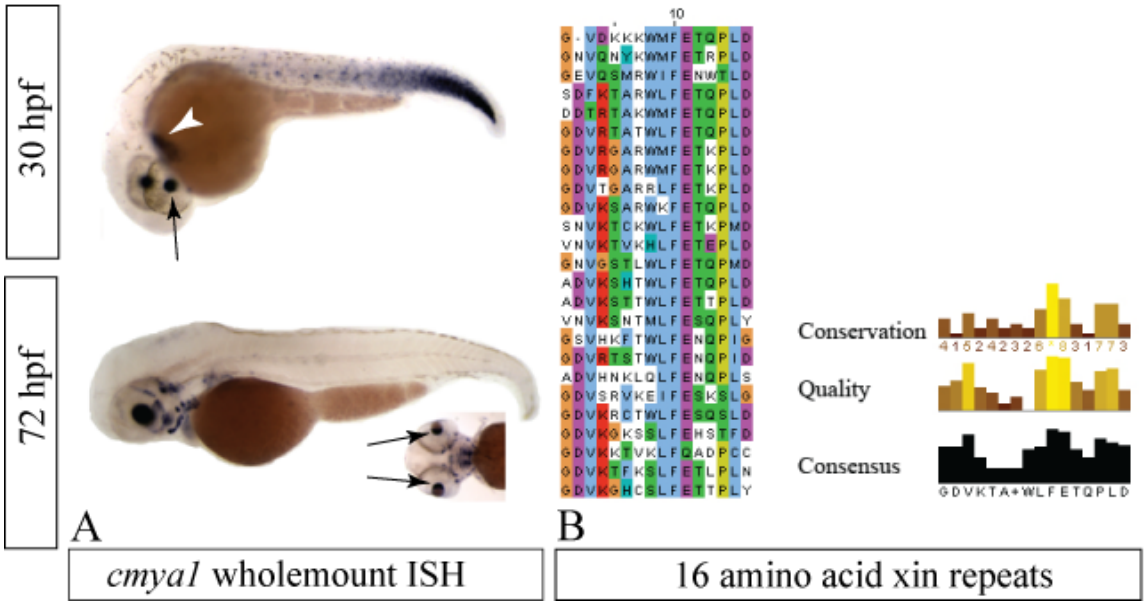

Figure 48: (A) *cmya1* WISH at 30 hpf and 72 hpf. *cmya1* is expressed in nascent myofibers as is evident from staining in the posterior somites that are formed later than the anterior ones. It is also expressed in the heart (white arrowhead) and the lens (black arrow). At 72 hpf, *cmya1* expression can be detected in newly forming muscles of jaw and ocular muscles, but not in the trunk muscles. The expression in the lens is limited to the proximal part of the lens. (B) The N terminal half of the Cmya1 protein contains 25 highly conserved actin binding XIN repeats, containing 16 amino acids each.

To investigate the role of *cmya1* in muscle regeneration, we next injected an anti-sense morpholino against the translations start site of *cmya1* mRNA (MO-cmya1). Blockage of *cmya1* translation resulted in the appearance of huge gaps in the muscles at the 48 hpf stage, but unfortunately the control morpholino (with 5 bp mismatch) tended to produce a much more severe (though unrelated) phenotype (data not shown). One possible reason for this could be that the control morpholino blocks non-specific targets, although the morpholino sequence did not show homologies to any known zebrafish gene. We therefore ordered a targeted TILLING mutant from the Sanger Institute to be able to perform a loss of function analysis of the *cmya1* gene.

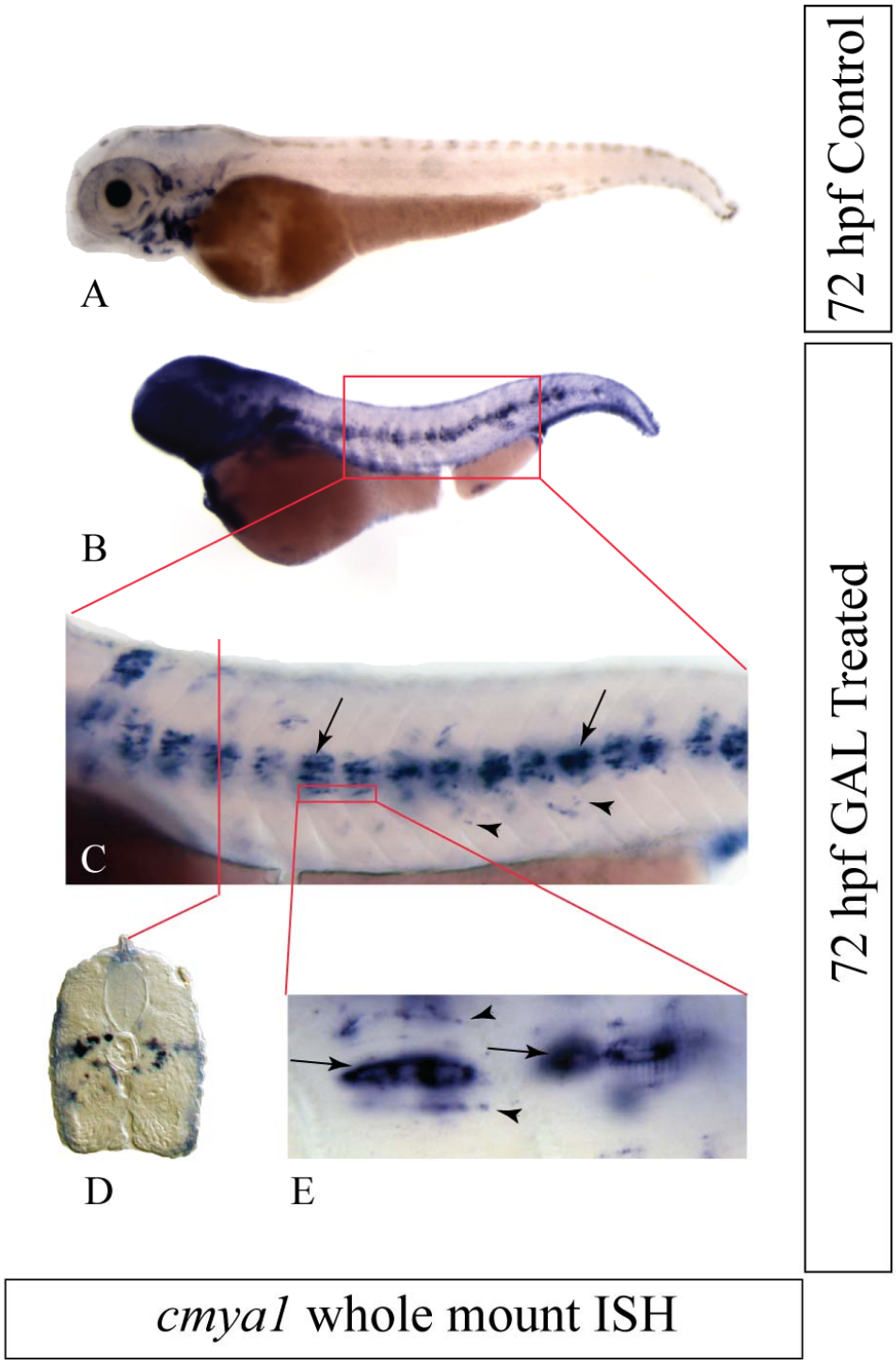

Figure 49: 72 hpf wildtype control (A) and GAL treated (B) larvae. GAL treatment causes robust upregulation of *cmya1* transcripts (B, C, D, and E). The expression in regenerating larvae can be seen in regenerating fibers (arrows, C and E) as well as punctuate staining that could be satellite cells (arrowheads, C and E). See text for details.

3.3.2 Agilent Microarrays

Since the number of differentially expressed genes in galanthamine treated larvae was quite low using the in house spotted microarrays from the Sigma-Genosys-Compugen library, I decided to use Agilent 22k zebrafish microarrays. Since two different durations of GAL exposure microarrays upregulated almost the same genes on the Sigma Compugen chips, I performed microarray analysiss with agilent chips only on embryos that were treated with GAL for one of the previously used durations, namely 64 hours (ie 8-72 hpf). I selected genes with a p-value of ≤ 0.05 and a fold change of $\geq \left| 1.7 \right|$.

3.3.2.1 Genes upregulated upon galanthamine treatment

There were a total of 95 genes upregulated in response to galanthamine (Appendix A1). First and foremost, I looked to verify whether the genes those are upregulated in the Sigma Compugen microarrays are also upregulated in the Agilent microarrays. We found that 9 of the 13 genes are also upregulated in Agilent microarrays (Table 2). These are *Suppressor of cytokine signaling 3a* (*Socs3a)*, *Socs3b*, *Fibronectin 1b*, *complement component 6*, *desmin*, *activating transcription factor 3 (atf3)*, *uncoupling protein 4 (ucp 4)*, zgc:92851, and zgc:92069. Unfortunately, *cmya1* was not represented in the 22,000 oligo set spotted on the microarrays. We performed gene ontology (GO) analysis on the upregulated genes and were able to assign GO categories to 95 of these genes (Fig. 50). Where gene ontology was not available for zebrafish genes, we used human or mouse orthologs to retrieve the GO categories.

The largest category was the one with genes involved in 'receptor/signal transduction' with 15 candidates. The members included *socs3a* and *socs3b*, the genes

that are known to be expressed by activated satellite cells in mouse single fiber cultures (Jonathan Beauchamp, Pers. Comm., MYORES Workshop: Muscle Regeneration and Stem Cells: a multiorganismic approach in Niepolomice, Poland, October 12- 15, 2008). Another gene to be upregulated in this category is ZGC:92886 (calcitonin/calcitonin-related polypeptide, alpha), the ligand for the calcitonin receptor, known to be expressed by, and correlated with the quiescence/activation state of satellite cells (Fukada, Uezumi et al. 2007). Another interesting candidate in this class is *angiopoietin-like 7*. The name and the expression (at the borders of the somites, along myosepta) (ZFIN *in situ* expression database) both suggest a role in angiogenesis. It should be noted that mammalian satellite cells are always found in close proximity to blood vessels (Christov et al., 2007).

The second largest category was 'regulators of transcription' with 13 genes. The most prominent of these genes is the myogenic regulatory factor *myogenin*. As mentioned in section 1.4.4, *myogenin* is the MRF that acts during terminal differentiation of myoblasts by not only activating muscle specific genes but also by downregulating *pax7* in *myogenic progenitor cells* (MPCs) thus pushing them towards differentiation. Upregulation of myogenin therefore is a conclusive proof that muscle regeneration is occurring in GAL treated embryos. Two of the genes upregulated in this category belong to the interferon regulatory factor family, IRF7 and IRF11, pointing towards activation of an immune response to the myopathic condition.

The third largest group belongs to the category 'enzymes', with 10 members. This category contains two members of cathepsin family of cystein proteases; Cathepsin La and zgc:103438 (a paralog of the human Cathepsin W), along with Complement factor B; further evidence of a strong immune response to the myopathic condition. An interesting member of this category is zgc:56376 (human paralog of

Murf3). MuRF3 (**Mu**scle specific **R**ing **F**inger 3) also called TRIM54 is a cardiac and skeletal muscle specific E3 ubiquitin ligase that functions in striated muscle maintenance and remodeling and the loss of which leads to a predisposition for cardiac rupture after myocardiac infarction (Fielitz et al., 2007b). Together with MuRF1, MuRF3 is required for sarcomeric protein turnover and their loss leads to a myopathy characterized by accumulation of myosin (Fielitz et al., 2007a).

The next two categories are those of genes encoding for 'kinase/phosphatases' and genes involved in 'cell death', both with 8 members. Six of the eight genes included in the kinase/phosphatase category are uncharacterized, the other two being dual specificity phosphate 5 and pyruvate dehydrogenase kinase, isoenzyme 2. Dual specificity phosphatases are a subclass of the protein tyrosine phosphatase gene superfamily, which appears to be selective for dephosphorylating the critical phosphothreonine and phosphotyrosine residues within MAP kinases (for a review see (Camps et al., 2000)).

The most prominent gene upregulated in the cell death category is *BCL2-associated athanogene 3* (*bag3*). *bag3* is an anti-apoptotic gene expressed primarily in striated muscles and the Bag3 protein is localized to the Z-discs in skeletal muscles (Homma et al., 2006). Loss of *bag3* expression in cultured C2C12 myoblasts increases apoptosis upon induction of differentiation, revealing a role for *bag3* in myotube survival in a cell autonomous manner. *bag3* is essential for maintenance but not development of myofibers, as is evident from the fact that Bag3 deficient mice generate muscles, but develop a severe myopathy characterized by neonatal disruption of Z-disk architecture followed by myofibrillar degeneration (Homma et al., 2006).

Of the remaining upregulated genes the most interesting members are from the category of genes involved in 'cell adhesion' with 5 genes. Two of these genes, ZGC:103425 and ZGC:103408, the zebrafish homologues of human CD151 and Integrin beta-1-binding protein 3 or Muscle integrin binding protein (MIBP), interact with integrins (Baldwin et al., 2008; Li et al., 2003a; Liu et al., 2007b; Yamada et al., 2008; Yang et al., 2008). As stated in the section 1.3, integrins are important scaffolding proteins involved in myofiber attachment to the extracellular matrix and therefore play a critical role in cell migration. In addition MIBP functions in the control of myogenic differentiation by regulating α7ß1 integrin-mediated cell interactions with the laminin matrix and intracellular signaling through paxillin (Li et al., 2003a). Another interesting gene in this category is matrix metalloproteinase 9 (MMP9). The matrix metalloproteinases (MMPs) are zinc dependent endopeptidases, believed to play a major role in cell proliferation, migration (adhesion/dispersion), differentiation, angiogenesis, apoptosis and host defense. Specifically MMP9 has been shown to be expressed by regenerating but not healthy muscle tissue where it has been suggested to play a role in the inflammatory response and activation of satellite cells.

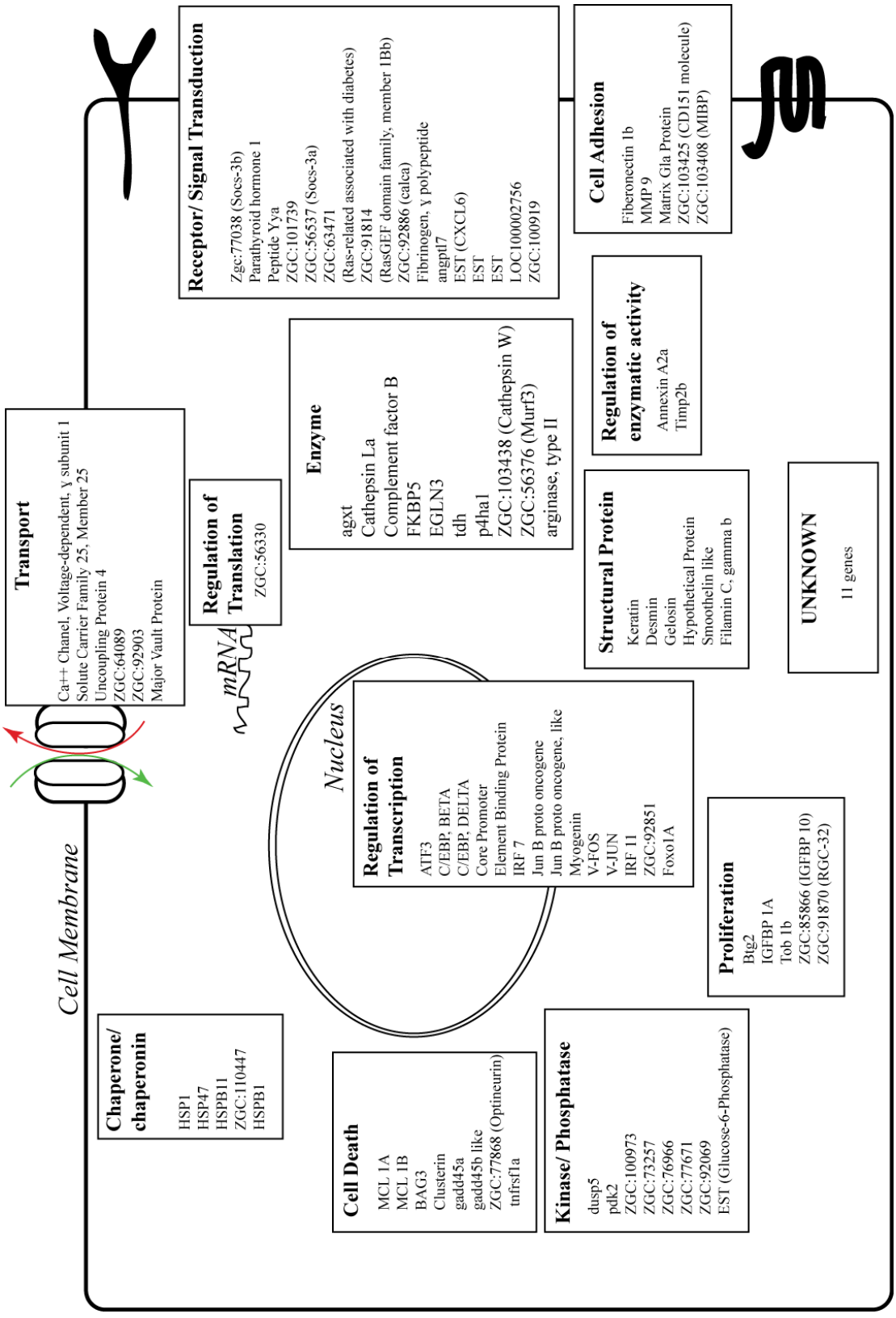

Figure 50: Gene ontology categorization of genes upregulated by GAL treatment. See text for description of the categories.

3.3.2.2 Verfication of upregulated genes by *in-situ* hybridization

To verify the microarray results we cloned the 30 highest upregulated genes and performed wholemount *in-situ* hybridization to look at changes in expression pattern and expression level upon GAL treatment.

Zgc:100919

Zgc:100919 is a four pass transmembrane protein belonging to the tetraspannin family. Tetraspanins are transmembrane proteins with both N- and C-terminus lying on the intracellular side of the membrane. Tetraspanins are involved in diverse processes such as cell adhesion, proliferation and migration. They can form clusters forming a multimolecular network via multiple dimerization domains. Zgc:100919 is expressed in neural crest cells at 28 hpf (arrows, Fig. 51A) and the expression is restricted to the dorsal and ventral edges of the myotome and horizontal myosepta by 48 hpf (arrows Fig. 51B). By 72 hpf the expression is maintained at these sites (black arrows, Fig 51C), but in addition expression is also visible in single cells along vertical myosepta (red arrows, Fig. 51C). Upon GAL treatment, the expression is greatly increased in muscle fibers (Fig. 51D).

To gain a better spatial resolution of expression, I performed transverse sections of embryos for which wholemount *in-situ* hybridized embryos at the level of the yolk extension. In the untreated control 72hpf larvae, zgc:100919 transcripts could be observed in single cells in a sub-dermal location or along the myosepta (Fig. 52A, A') and also in the dorsal and the ventral zones showing stratified hyperplasia (as mentioned in section 1.6) (Fig. 52A). In contrast, GAL treated embryos show much more extensive staining with zgc:100919 antisense probe. The staining is also

observed in deeper myotome (boxed area, Fig. 52B, arrowheads, Fig. 52B') that in uninjured larvae contained mature muscle fibers.

Thus it is clear that GAL treatment leads to increased expression of zgc:100919 in injured muscles and that this gene could have a role in regeneration process.

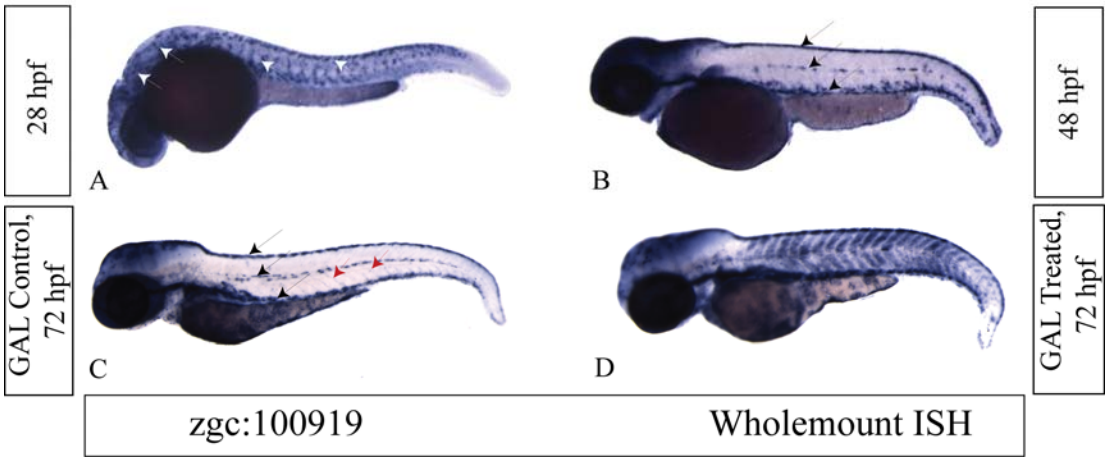

Figure 51: zgc:100919, a member of the tetraspannin family of transmembrane proteins, is expressed in neural crest cells at 28 hpf stage (white arrows, A). By 48 hpf the expression is limited to the dorsal and ventral edge of the myotome and also along the horizontal myosepta (black arrows, B). In wildtype 72 hpf larvae the expression is similar to the 48 hpf larva except that the expression could also be seen in vertical myosepta (red arrows, C) in individual cells. Upon GAL treatment the regenerating muscles upregulate the expression significantly, validating the microarray results (D).

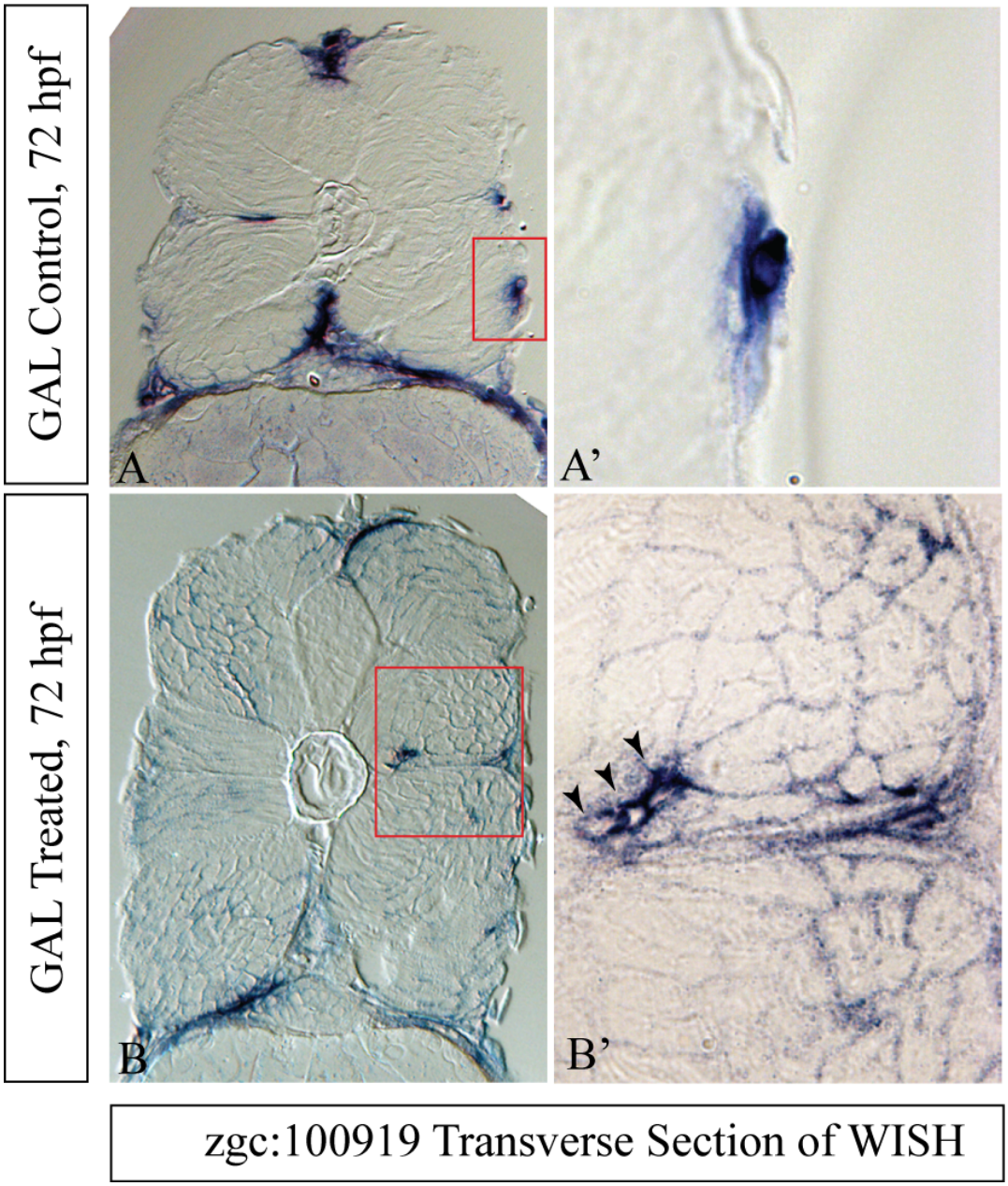

Figure 52: Transverse section of zgc:100919 wholemount *in-situ* hybridized larvae through the level of yolk extension at 72 hpf control (A, A') and GAL treated larva (B,B'). In the control larvae most of the staining is limited to the areas that show stratified hyperplasia i.e., the dorsal and the ventral edge of the myotome. A few cells expressing the gene can be seen at the surface of the somite and horizontal myosepta. The GAL treated larvae show staining deeper within the myotome. The right hand panels (A', B') show the boxed area in the left hand panels (A, B) at a higher resolution. The cells expressing zgc:100919 seem to have migrated deeper into the myotome upon GAL treatment (arrowheads, B'). Note the relatively small diameter of the stained cells (B'), indicating that they are myoblasts or newly forming myofibers.

l-threonine dehydrogenase (tdh)

At 28hpf *tdh* is expressed in the midbrain (arrowhead, Fig. 53A), spinal neurons (arrows, Fig. 53A and B) and the myotome (Fig. 53A and B). By 48hpf the myotomal expression is not detected anymore, but spinal neuron expression is maintained (arrows, Fig. 53C, and D). The developing pectoral fin precursors also show expression of *tdh* at this stage (arrowheads, Fig. 53C, inset). By 72hpf, expression is also observed in individual cells in the trunk (arrowheads, Fig. 53E). On GAL treatment, 72hpf larvae show expression of *tdh* in trunk muscles and the number of small spherical cells expressing *tdh* also increases (arrowheads, Fig. 53F inset).

Zgc:103408

Zgc:103408 is the zebrafish homologue of human Integrin beta-1-binding protein 3, also known as **M**uscle **I**ntegrin **B**inding **P**rotein (MIBP). At 28hpf zgc:103408 is expressed in the axial muscles of the larvae (Fig. 54A and B). By 48hpf the expression in axial muscles continues (Fig. 54C) and it is also observed in pectoral fin muscles (arrows, Fig. 54D) and the heart (arrowheads, Fig. 54D inset). 72hpf larvae show a decrease in expression of zgc:103408 expression in axial muscles (Fig. 54E) but the newly formed jaw muscles (black arrows, Fig. 54E) start expression. Strong expression is also visible in muscles of the pectoral fins (asterisk, Fig. 54E) and hypaxial muscles (red arrows, Fig. 54E, inset). GAL treated 72hpf larvae show increased levels of zgc:103408 expression not just in axial muscles (Fig. 54F), but also in jaw muscles (black arrows, Fig. 54F), pectoral fin muscles (asterisk, Fig. 54F) and hypaxial muscles (red arrows, Fig. 54F inset).

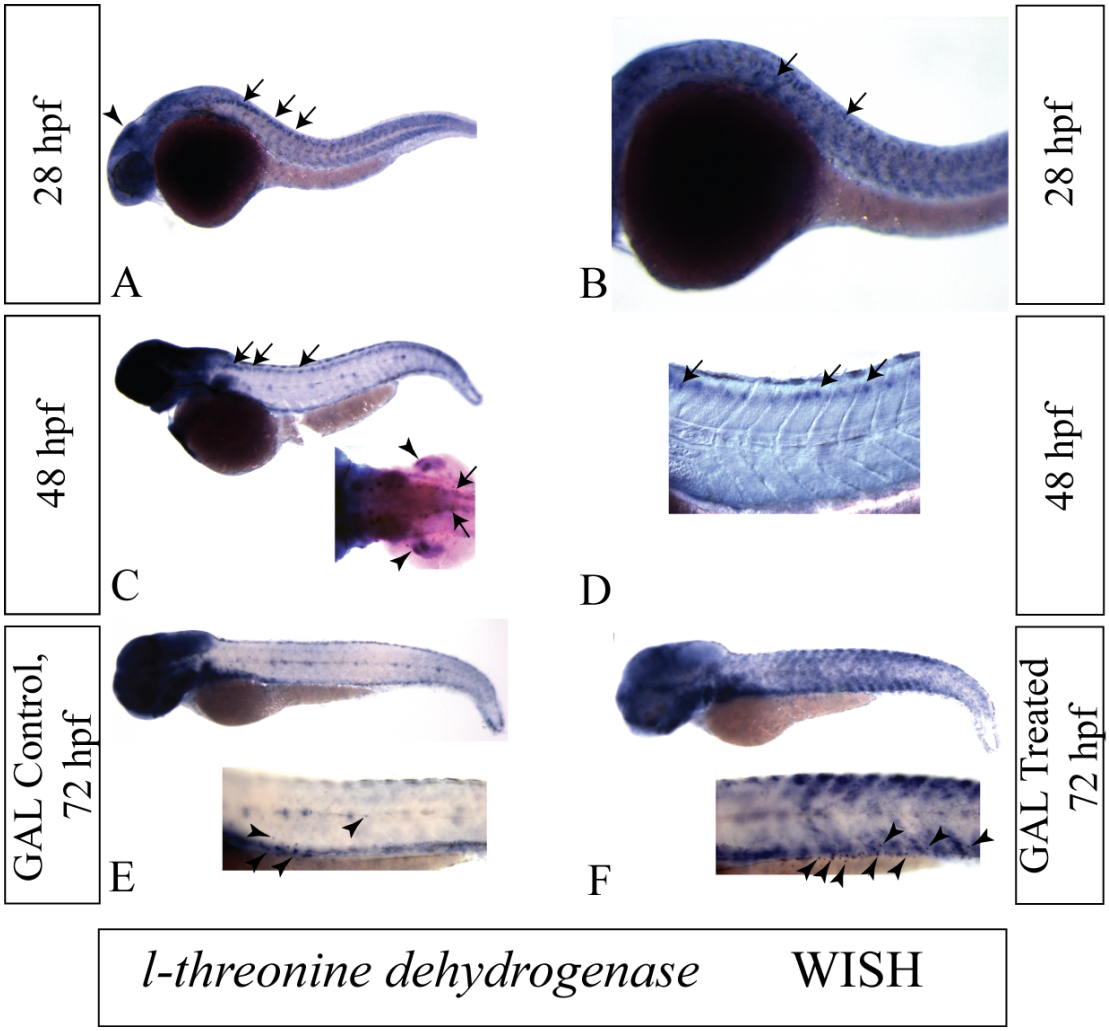

Figure 53: Expression pattern of *l-threonine dehydrogenase (tdh)*. 28 hpf larvae show express *tdh* in the midbrain (arrowhead, A), spinal neurons (arrows, A and B) and the myotome. By 48hpf expression is maintained in spinal neurons (arrows, C and D) and pectoral fin muscles (arrowheads inset, C) also start expressing tdh. By 72 hpf the wildtype larvae express *tdh* at the ventral and dorsal edges of the myotome and horizontal myosepta, besides individual roundish cells (arrowheads, E). GAL treatment increases the expression of *tdh* significantly in the myotome and also a number of small round cells (arrowheads, F).

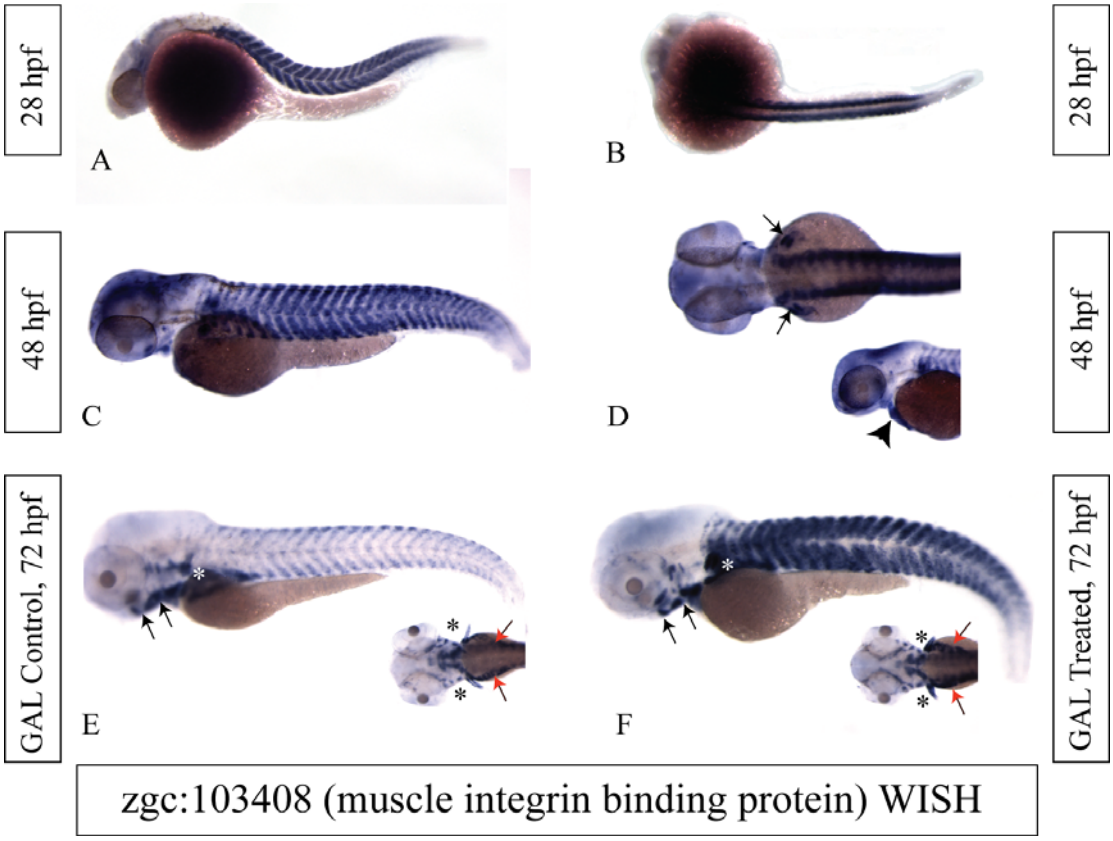

Figure 54: Expression pattern of zgc:103408 (Muscle Integrin Binding Protein, MIBP). At 28 hpf (A and B) MIBP is expressed in the axial muscles of the larvae. By 48 hpf the expression continues in axial muscles (C) and is also visible in pectoral fin musculature (arrows, D) and the heart (arrowhead inset, D). At 72 hpf the wildtype larvae show faint expression in axial muscles but newly forming jaw muscles start expressing MIBP. At this time hypaxial muscles (red arrows, inset, E) and pectoral fins muscles (asterisk, main figure and inset, E) also start expressing MIBP. GAL treated embryos express MIBP transcripts at an elevated level not just in the axial muscles, but also in the jaw muscles (black arrows, F), pectoral fin muscles (asterisk, main figure and inset, F) and hypaxial muscles (red arrows, inset, F).

heat shock protein, alpha-crystallin-related, 1 (hspb1)

Hspb1, also called Heat-shock 27-KDa protein 1 is a stress induced chaperone that is suggested to have a protective role against oxidative stress (Wyttenbach et al., 2002). At 24 hpf, *hspb1* is expressed in the midbrain-hindbrain boundary (MHB) (arrow, Fig.55A and B), in axial muscles, the heart, and fin folds of the tail fin (arrowhead, Fig. 55A). By 72 hpf the expression in the MHB is weak (arrow, Fig.

55C) and the extra-ocular muscles start expressing *hspb1* (arrowhead, Fig. 55C''). The expression in the axial muscles has become reduced by now, the heart expression is maintained, and the hypaxial muscles start to express *hspb1* (arrowhead, Fig. 55C). In 72hpf GAL treated larvae the axial muscles show a very intense staining and the increase in staining is also noticeable in the MHB (arrow, Fig. 55D), the hypaxial muscles (arrowhead, Fig. 55D) and the-extra ocular muscles (arrowhead, Fig. 55D'').

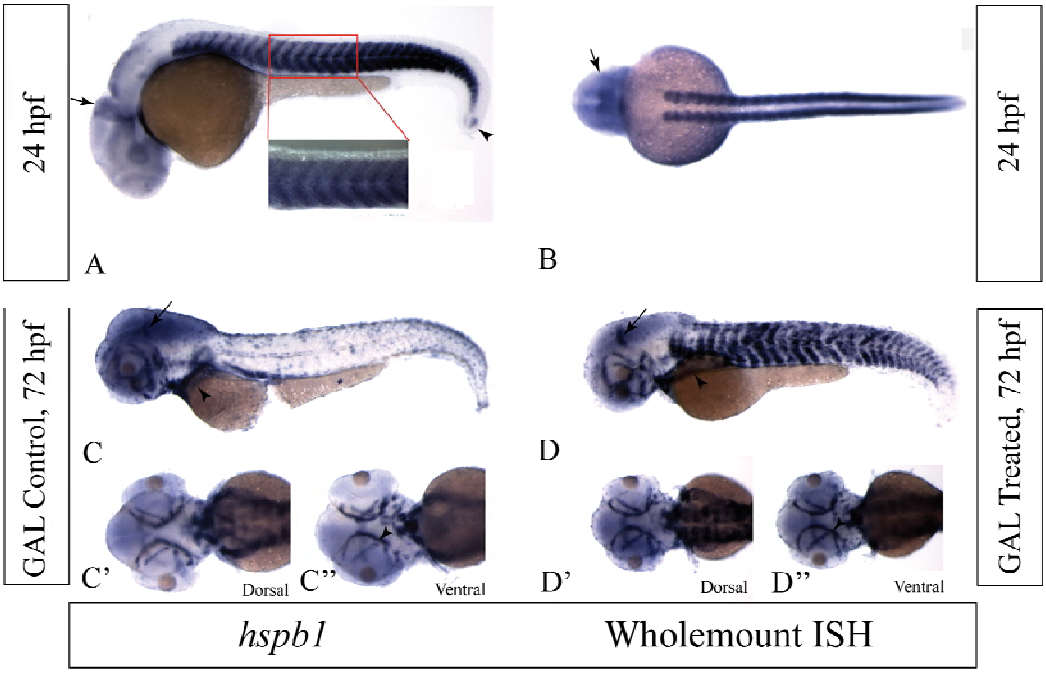

Figure 55: Expression pattern of *hspb1*. Please see text for details.

heat shock protein, alpha-crystallin-related, b11 (hspb11)

At72 hpf very faint *hspb11* expression was observed in the in the extra-ocular muscles and muscles of the jaw (Fig. 56A and A'). Upon treatment with GAL there is a massive upregulation of hspb11 expression in the somites and also in the extra-ocular muscles (Fig. 56B and B').

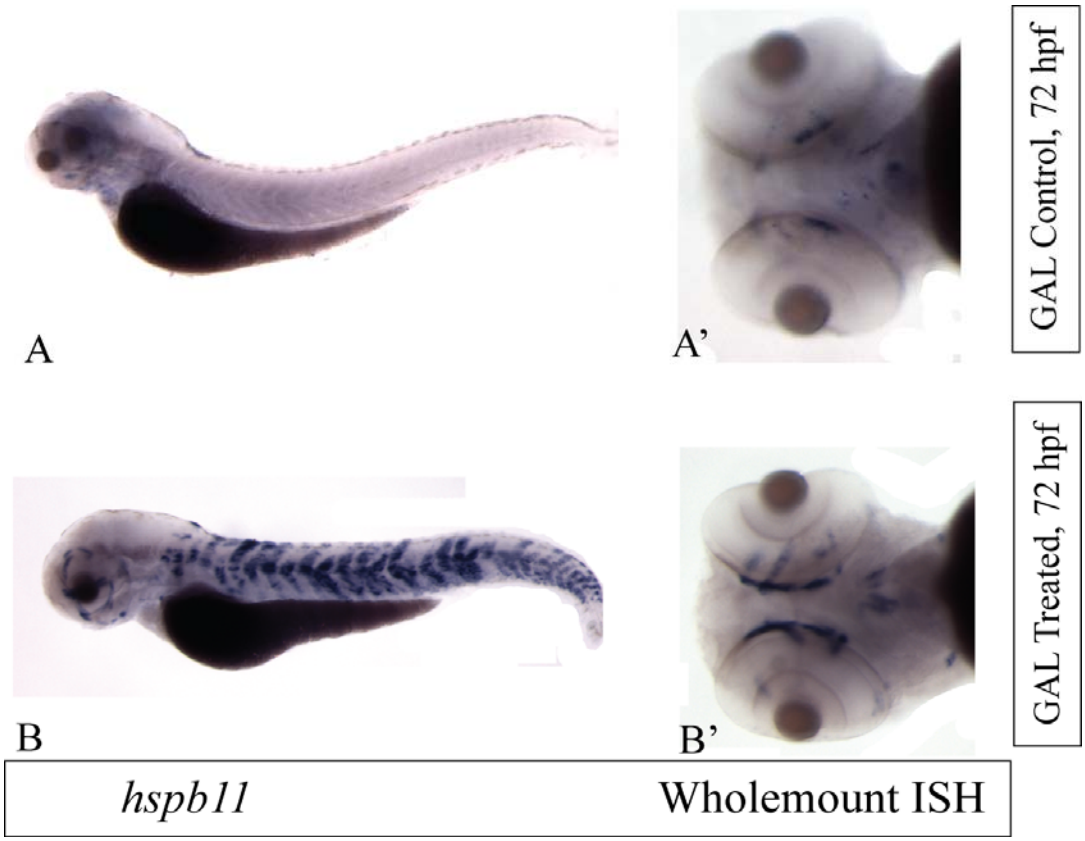

Figure 56: 72 hpf larvae show very low level expression of *hspb11* in the developing cranial muscles (top panel). The expression in the somites was not detected. However, upon treatment with GAL, 72 hpf larvae show a robust expression in somitic muscles in a mosaic manner and the cranial muscles also upregulate the expression.

alanine-glyoxylate aminotransferase (agxt)

agxt is a liver-specific, pyridoxal-phosphate-dependent enzyme. It is localized to the peroxisomes of normal hepatocytes and is known to catalyze the transamination of the intermediary metabolite, glyoxylate, to glycine. This can be considered as a detoxification reaction because the loss of function of Agxt allows glyoxylate to escape from the peroxisomes into the cytosol where it is oxidized to oxalate, and then reduced to glycolate (Danpure and Rumsby, 2004). In humans, at least, oxalate cannot

be further metabolized and its increased synthesis and urinary excretion leads to the progressive deposition of insoluble calcium oxalate in the kidney and urinary tract, resulting in development of kidney stones and subsequent renal failure.

The zebrafish *agxt* is expressed in the liver (white arrowhead, Fig. 57A and A') at 72hpf. Treatment with GAL not only results in an increase in expression in the liver (white arrowhead, Fig. 57B and B') but the expression is now also visible in large cells over the surface of the yolk (Fig. 57B and B') where staining is not detected in untreated controls (asterisk, Fig. 57A and A').

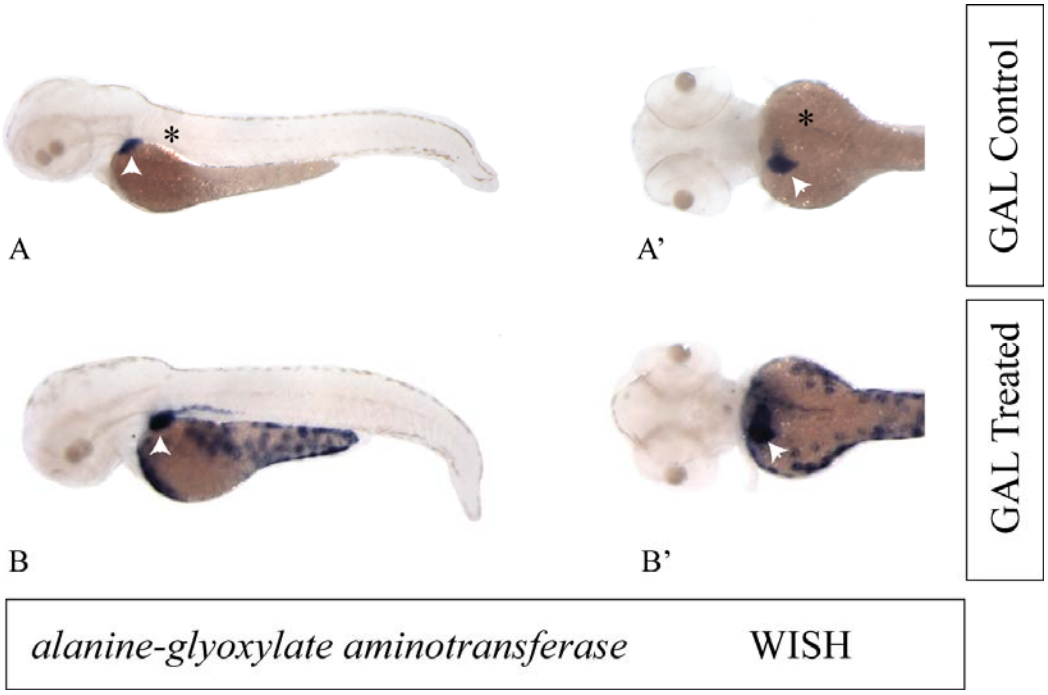

Figure 57: 72 hpf larvae reveal *alanine-glyoxylate aminotransferase* (*agxt*) expression in liver (white arrowhead, A, A'). GAL treatment causes not only increased staining in liver (white arrowheads, B, B') but also expression in large cells over the surface of the yolk (B, B') where staining is not detected in untreated controls (asterisk, A,A').

In summary, of the initial 30 genes cloned, expression analysis has been performed for six genes while expression analysis of the rest is currently in progress.

However, already based on the results so far, the expression analysis of above mentioned genes has generally validated the microarray data. Of the six genes analyzed, five genes showed an increased muscle specific expression when treated with GAL and the sixth showed increased expression in liver, an organ involved in detoxification of the body. This, at least partially, validates our initial hypothesis that microarrays of GAL treated larvae should upregulate muscle specific genes. Further investigation of these genes shall reveal their specific roles in the regenerative pathway.

4 Discussion

4.1 A genetic screen for motility mutants

An ENU induced mutagenesis screen was performed to identify mutants with progressive loss of motility. Additionally, birefringence was used as an assay to assess muscle integrity. Such mutants would develop musculature or nervous system normally, but the muscle or neuronal maintenance might be defective. This defective maintenance could result from a lack of functional regeneration. Seven motility mutants displaying reduced birefringence were found in the screen.

4.1.1 *gumrah* mutant shows multiple defects muscles, neurons and neural crest derived tissues

Isolation and characterization of one such mutant (*gumrah*) that shows progressive loss of motility and concomitant muscle degeneration was performed. *gum* mutants seem to move normally at 24hpf, but develop uncoordinated movements over next few days, ultimately leading to death by the 5^{th} or 6^{th} dpf. In addition, the *gum* mutants develop necrosis in the hindbrain that leads to a severe reduction of the size of the head. The mutants also develop U-shaped somites, an aberrant pigmentation pattern and cardiac edema.

The presence of U-shaped somites is a characteristic feature of Shh pathway mutants. However, *gum* mutants develop slow muscles that are typically absent or severely reduced in mutants lacking Shh activity, arguing that *gum* does not act in the Shh pathway. *gum* mutants also show normal organization of sarcomeric proteins, but muscle maintenance seems to be defective. As the *gum* mutant larvae age, the

myofibers tend to detach from the myosepta, especially at the dorsal and ventral borders of the somites (Fig. 24 and 25). Sometimes myosepta/myofibers also develop gaps (section 3.1.1.2).

Detachment of myofibers from myosepta is a characteristic feature of many myopathies in zebrafish. Fiber detachment could result either from a loss of sarcolemmal integrity or from loss of a component of extracellular matrix at the attachment site. One example of the former is the *sapje* mutant (the zebrafish orthologue of the human *Duchenne muscular dystrophy* gene) (Bassett et al., 2003), while an example of the latter scenario is the *candyfloss* mutant (zebrafish *laminin α2* gene) (Hall et al., 2007). The observation that gaps in myosepta and muscle fiber detachment sites coincide with gaps in anti-Laminin staining suggests that *gum* embryos might suffer from a loss in a component of the ECM at the fiber attachment site and thus may belong to the latter category. Once the fibers are detached from myosepta, they undergo degeneration. This is obvious from the decrease in birefringence of *gum* larvae over time, as well as from the electron micrographs taken at 5 dpf that show large gaps between the muscle fibers, muscle fibers with reduced thickness, and remnants of many fibers in the gaps. Therefore it appears that the maintenance of contact (and possibly signaling) between sarcolemmal and ECM components, such as laminin and integrins, is essential for maintenance of muscle fibers. For example, in both mouse and humans, loss of *α7 integrin* function causes a myopathy that is distinct from those caused by the loss of dystrophin-dystroglycan complex (Hayashi et al., 1998; Mayer et al., 1997). Other ligands of integrins include fiberonectin, vitronectin and collagen, and signaling mediated by these might regulate growth, cell adhesion, cell migration and differentiation (for a review see (Harburger and Calderwood, 2009)). Loss of function of certain other integrins such as *αV*

integrin can be ameliorated by concomitant loss of p53 function, indicating a role for integrin signaling in programmed cell death (Stromblad et al., 2002). Hence, in the context of *gum* mutants, it would be important to find out whether the fiber detachment seen is a primary or a secondary event of the mutation.

IHC analysis with antibodies labeling various neuronal structures revealed several neuronal defects in *gum* larvae. The neuronal processes, labeled by znp-1 antibody, showed gaps and irregular arrangements in contrast to control larvae (Fig. 27A and A'). This could be a direct result of the gaps shown by the muscle fibers, since the neuronal processes would be innervating these muscles. The Dorsal Root Ganglia (DRGs) seem to be reduced in numbers or located at an ectopic location in *gum* mutants (Fig 27B and B') and the enteric neurons are missing. Some ectopic neurons were observed at the level of midline (arrows, Fig. 27B'). These could be either misplaced DRGs or precursors of enteric neurons that did not migrate to their correct destination.

Both the DRGs and the enteric neurons are neural crest derived tissues. Besides these, *gum* mutants showed defects in other neural crest derivatives like pigmentation and exhibited severe jaw malformations. *gum* mutant larvae showed less *crestin* positive cells and the cells seemed to be less migratory (Fig. 31). Migratory trunk neural crest cells in *gum* mutant larvae tended to stay close to the neural tube and were never observed taking the sub-dermal path while migrating ventrally (Fig 32). Cell migration is a complex phenomenon governed by several factors such as cell-cell adhesion, cell-ECM adhesion, guidance cues emanating from the destination of the migrating cell etc. In addition, in a developing embryo, many morphological changes are taking place and multiple cell populations are undergoing migration. The migrating cells must recognize their specific signal amid a large variety of signals

they might encounter. It is possible that the mutation in *gum* leads to a loss of a guidance cue or of another component of the neural crest migration pathway. This might also lead to ectopic DRGs and/or missing enteric neurons. Alternatively, a mutation in a cell-cell or cell-ECM adhesion protein may lead to an altered migration path. It is also possible that an ECM component serves as a guidance cue in this case as this can explain both the muscle as well as neural crest migration defects.

One way to study aberrant migration of neural crest cells would be to perform time-lapse imaging of neural crest cells expressing a fluorescent marker in *gum* mutant background. To achieve this, I outcrossed *gum* heterozygous fish into *-7.2kb sox10::EOS-FP* fish. *-7.2kb sox10::EOS-FP* (Takamiya, M. unpub.) is a transgenic line expressing the reporter EOS-FP (Nienhaus et al., 2006) under the control of the -7.2 kb *sox10* promoter (Hoffman et al., 2007) and is expressed by all neural crest cells. The *-7.2kb sox10::EOS-FP* fish in *gum* background are currently growing and will soon be ready for mating.

To understand the nature of the muscle and neuronal defects in *gum* mutants, we need to know the gene mutated in *gum* mutants. Therefore, a positional cloning approach was adopted to map the *gum* locus (in collaboration with Dr. Christelle Etard). By the time of writing this report, *gum* had been localized to a 2MB region on chromosome 14. Unfortunately, this region is too large and contains several genes to be tested by a candidate approach. Therefore, fine mapping of the locus is necessary and is currently underway.

4.2 Zebrafish as a model for muscle regeneration

In the last twenty years, the zebrafish has become an important vertebrate model organism to study development and disease. Recent studies show that it is also

an excellent model to study regeneration events. Zebrafish show exceptional regenerative abilities after damage to various tissues such as fin, heart, central nervous system (CNS), retina, and kidney (for recent reviews see, (Becker and Becker, 2008; Hitchcock and Raymond, 2004; Poss et al., 2003; Raya et al., 2004; Reimschussel, 2001)).However, so far no report has described muscle regeneration in fish.

In this study, I have tried to redress this issue by developing a model of inducible myopathy and performing a preliminary characterization of the putative muscle stem cells in the zebrafish. On one hand, this would allow us to harness the advantages of the zebrafish genetics and development and allow a possibility of *in vivo* imaging of regeneration. Live imaging would provide an increased temporal resolution of the events during regeneration, thus providing an opportunity to modulate these events and uncover their roles in regeneration. On the other hand, the use of zebrafish would facilitate drug/small molecule screening at an unprecedented rate to screen or at least pre-screen for potential modulators of muscle regeneration.

4.2.1 Galanthamine treatment: a conditional myopathy model

We report here the development of a conditional myopathy model of zebrafish: galanthamine treatment induces muscle degeneration and subsequent removal of galanthamine allows the injured muscle to regenerate. A previous study had demonstrated a loss of larval motility and muscle structure when acetylcholinesterase (*ache*) function was lost (Behra et al., 2002). The *ache* mutation can be phenocopied by application of acetylcholinesterase inhibitors such as galanthamine. I found that the removal of the inhibitor and a subsequent recovery period leads to a full functional recovery of the larvae. Therefore, I developed a treatment regime, where GAL application for up to 64 hours leads to complete

paralysis of treated larvae. Subsequent removal of GAL leads to a functional recovery of motility within 48-72 hours. As shown in section 3.3.2, birefringence measurements (Fig. 34), as well as electron microscopy (Fig. 35) observations, are consistent with the finding that GAL treatment causes muscle degeneration and that the muscles can regenerate following removal of embryos from the GAL containing medium and raising in fish water.

This approach has several important advantages over various techniques used in rodent muscle regeneration research. For example, methods of inducing focal injury in rodents include injection of cardiotoxin, a snake venom derived toxin that acts via compromising membrane permeability, injury induced by crushing, injury induced by application of dry ice and muscle overload by hanging. Of these, only cardiotoxin injection is a viable option for zebrafish larvae due to their small size. However, microinjections in older larvae are tedious and time consuming and it is not possible to perform them in a high throughput manner. Therefore, for induction of a systemic myopathy, GAL treatment is highly desirable as this can be performed in high numbers and automated if needed; a prerequisite to exploit the advantages of the zebrafish model system for drug screening.

4.2.2 Presence of putative muscle stem cells in zebrafish

Observation of electron micrographs obtained from 104 hpf larvae showed cells displaying typical characteristics of satellite cells: large nuclear to cytoplasmic ratio and lying adjacent to the muscle fiber under the basal lamina. These cells also express Pax7, the most commonly used marker for satellite cells and one that labels all satellite cells, as revealed by Immuno-electron microscopy (unpub. observations). This indicates that zebrafish, like mammals, might use stem cells for muscle

regeneration as opposed to the dedifferentiated tissue used by newts. Additionally, single fibers isolated from adult zebrafish have revealed associated satellite cells (Peter Zammit, pers. comm.).

To characterize zebrafish satellite cell distribution, a monoclonal antibody recognizing zebrafish Pax7 was used to ascertain the location of $Pax7^{+ve}$ cells at 24-75 hpf. As described before (section 3.2.6) $Pax7^{+ve}$ nuclei were observed at the superficial somite surface (Fig. 38 and 39). At 24 hpf there are two distinct classes of $Pax7^{+ve}$ nuclei: a larger number of weakly stained nuclei spread all over the superficial surface of the somite and a smaller number of very intensely stained nuclei. Given such striking differences in the intensity of staining and hence levels of Pax7 protein, one might speculate that there are two subclasses of $Pax7^{+ve}$ nuclei in the trunk at this stage. Indeed, it was shown recently that the fewer, higher intensity $Pax7^{+ve}$ cells, belonged to the neural crest lineage, as opposed to the more abundant, lower intensity $Pax7^{+ve}$ cells, that belonged to the somitic lineage (Hammond et al., 2007). The more intensely labeled $Pax7^{+ve}$ nuclei are lost in the *colourless* (*sox10*) mutants while low intensity $Pax7^{+ve}$ nuclei are not affected (Hammond et al., 2007). By 72 hpf, most $Pax7^{+ve}$ cells are lined along the dorsal and the ventral edges of the somite, and along the horizontal and vertical myosepta (Fig. 39). The $Pax7^{+ve}$ cells are rarely observed in the deeper myotome at this stage. Also, by 72 hpf, all trunk neural crest cells have migrated to their destination and most likely, differentiated. A review of the literature did not yield any reports of trunk neural crest cells still present at 72 hpf. Still the superficial $Pax7^{+ve}$ cells at 72 hpf show varying levels of Pax7 protein expression (as inferred by the intensity of antibody staining, color coded in Fig. 39). One possible explanation for this is that since Pax7 protein is required to maintain cells in an undifferentiated state, and at least some MRFs are known to directly

repress *pax7* transcription as well as Pax7 protein stability, the lower intensity Pax7^{+ve} cells might be the ones committed to differentiation. The Pax7^{+ve} cells at the superficial somite surface are quite flat, with oblong rather than spherical nuclei (Fig. 39), the orientation of these cells depends on their location; the ones at the myosepta are mostly perpendicular to the somite surface, while the ones superficial to the somites are parallel to the somite surface. Whether the cells at the superficial somite surface are more prone to differentiate vs. the cells at the myosepta, is however, not clear. These observations raise the questions: what is the lineage of these non neural crest Pax7^{+ve} cells and what fate awaits them. Recent evidence for the presence of a primitive dermomyotome in zebrafish, as discussed below, partly answers this question.

4.2.3 Presence of a dermomyotome in teleosts

The presence of Pax7^{+ve} cells at the superficial surface of the somite agrees with evidence for the presence of a functional dermomyotome in teleosts (For a review see (Stellabotte and Devoto, 2007)). The dermomyotome is a transient structure that, in amniotes, gives rise to both the myotome that generates the muscle, and the dermis that forms a layer of the skin. The amniote dermomyotome (section 1.4.3, Fig. 4) contributes cells to the primary myogenesis that gives rise to the initial muscle fibers in the somite as well as the secondary myogenesis that gives rise to the myogenic precursors for postnatal muscle growth as well as muscle satellite cells that serve as muscle stem cells.

The teleost dermomyotome was described as early as in the 19th century (Kaestner, 1892) in a manner similar to that of the amniote dermomyotome: by developmental state of origin, position, morphology, and the speculated fates of its

cells (Ramirez-Zarzosa et al., 1998; Veggetti et al., 1990; Waterman, 1969). Only recently has the teleost dermomyotome been shown to express the same markers as amniote dermomyotome, including *pax3*, *pax7*, *mesenchyme homeobox 1 (meox1)*, and *dachshund d (dachD)* (Devoto et al., 1996; Feng et al., 2006; Groves et al., 2005; Hammond et al., 2007; Hollway et al., 2007). In the teleosts, the primary myotome forms relatively early and independently of the dermomyotome. This is in contrast to the amniotes, where the first fibers elongate *after* the formation of the dermomyotome (section 1.4.3 and above). The first genetic evidence for the presence of a teleost dermomyotome came from the observations that the medial and the posterior cells of the epithelial somite express Myogenic Regulatory Factor (MRF) genes while the anterior cells don't; in zebrafish (Weinberg et al., 1996), herring, trout, pearlfish and carp (Cole et al., 2004; Delalande and Rescan, 1999; Steinbacher et al., 2006; Temple et al., 2001). In many teleosts, the *myoD* negative cells, anterior somitic cells yet uncommitted to myogenic fate, form a single row of cells at the anterior border of the somites (green cells, Fig. 58A). These cells are variously described as Anterior Border Cells (ABCs) (Stellabotte et al., 2007) or Row 1 cells (Hollway et al., 2007). In zebrafish and trout these ABCs subsequently start expressing the markers for dermomyotome, such as, pax3, *pax7*, *meox* and *dacD* (Groves et al., 2005; Hammond et al., 2007; Hollway et al., 2007; Steinbacher et al., 2007) while the posterior cells express myoD (blue cells, Fig. 58A). Single cell lineage tracing and time lapse microscopy have revealed that these cells move along the border of the somite to the lateral surface (Fig. 58A-C) (Hollway et al., 2007; Stellabotte et al., 2007). The ABCs move laterally (green cells, Fig. 58B) while the posterior cells elongate in the anterio-posterior direction (blue cells, Fig. 58B). By the time the segmentation ends (24 hours), these $Pax7^{+ve}$ ABCs are restricted to the surface of the somite and acquire flat

dermomyotomal cell morphology (Fig. 58C). Initially, the only non dermomyotomal fate of these is that of muscle fibers (Stellabotte et al., 2007) (green cells, dorsal view, Fig. 58D-F, transverse section, Fig. 58G, H). During early larval stage the dermomyotomal cells proliferate (Hammond et al., 2007; Hollway et al., 2007), and give rise to the secondary myotome, cells of the dorsal fin, and fin muscles (Hollway et al., 2007; Stellabotte et al., 2007). Given the existence of, and conserved gene expression patterns with amniotes in the zebrafish dermomyotome, one might speculate that this layer of $Pax7^{+ve}$ cells could serve as a source of satellite cells for adult muscle regeneration. Evidence from published reports suggests that the dermomyotomal layer of $Pax7^{+ve}$ cells remains proliferative through adulthood in zebrafish (Hammond et al., 2007; Hollway et al., 2007). This would also explain how fish sustain addition of muscle mass throughout life by hyperplasia (increase in fiber number) compared to the hypertrophic (increase of fiber size by addition of new cells) growth shown by mammals.

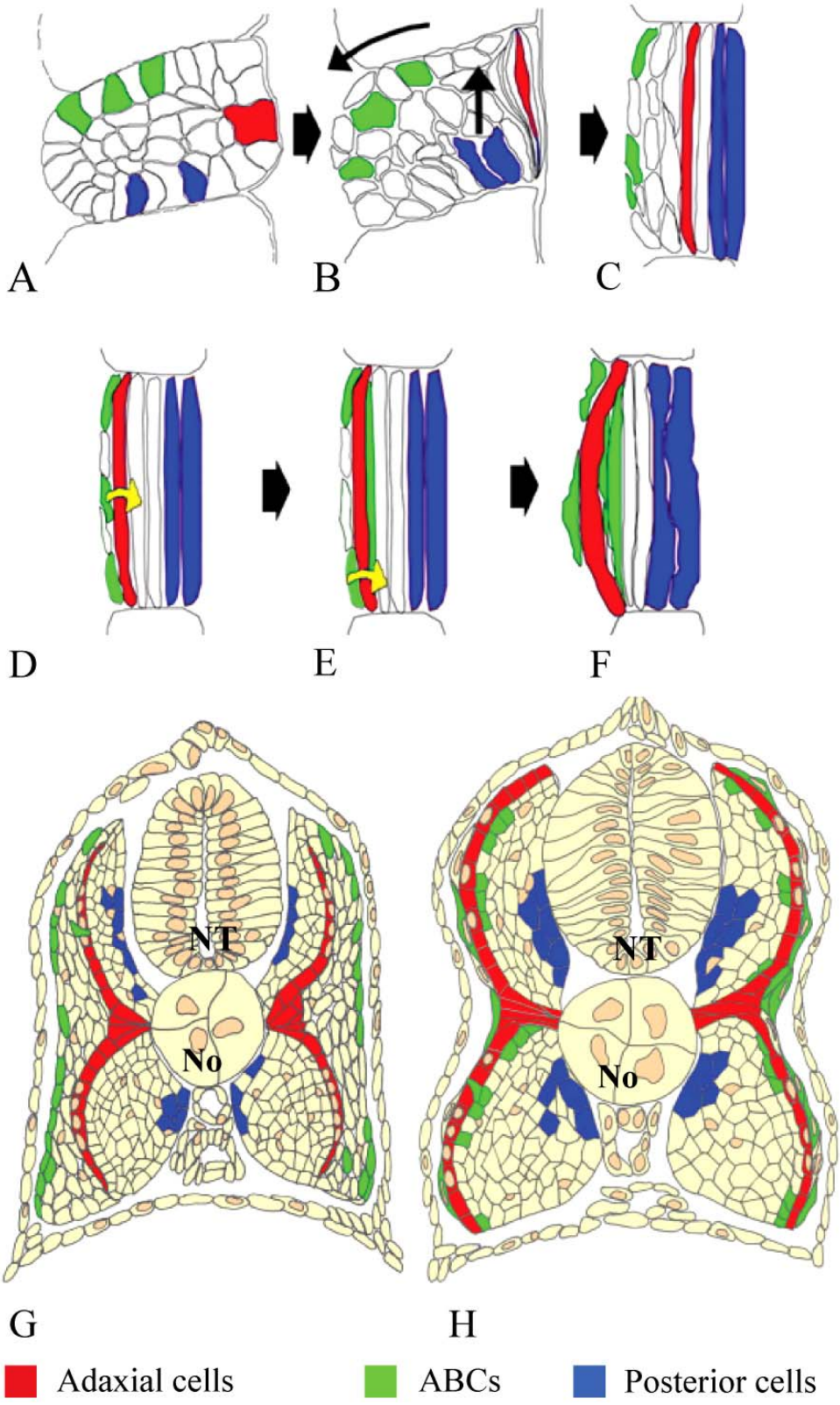
A
B
C
D
E
F
NT
No
NT
No
G
H
Adaxial cells
ABCs
Posterior cells

Figure 58: Dermomyotome and myotome morphogenesis (A-F) Schematic representation of somite cell movements and fates, viewed from dorsal (anterior is up and the midline is to the right). (A) In nascent somites, epithelial border cells surround a mesenchymal core. The anterior border cells (ABCs) are the anterior-most row of cells lateral to the adaxial cells (red) which line the notochord. (B-F) The fate of subsets of ABCs (green), posterior cells (blue), and adaxial cells (red) are shown once the somite loses its epithelial morphology. Adaxial cells elongate into slow muscle fibers (red) along the notochord, as posterior cells initiate elongation (blue), and ABCs (green) move laterally. At 24 hr, the posterior cells (blue) have elongated into medial fast fibers and a subset of the dermomyotome cells (green) have elongated medial to the superficial slow muscle layer (red). Some of the dermomyotome cells remain external to the myotome as a layer of flattened cells (green). (G, H) Schematics depicting transverse sections through the mid-trunk somite of an embryo partly through the segmentation period (20 hr in zebrafish, G), and at the end of the segmentation period (24 hr in zebrafish, H). Adaxial cells give rise to superficial slow fibers (red). ABCs give rise to dermomyotome cells on the external surface of the somite (green) at mid-segmentation stages and then to dermomyotome as well as lateral fast fibers by the end of the segmentation stage (green). Posterior cells (blue) have already elongated into muscle fibers at the 20-hr stage (G) and occupy distinct, medial positions in the 24 our myotome (H). Figure adapted from (Stellabotte et al., 2007) (A-F) and (Stellabotte and Devoto, 2007) (G, H).

4.2.4 Pax7 expression is perturbed in myopathic states

Comparison of three different myopathic states, namely GAL treatment and the myopathies induced by *steif* and *gum* mutations, with wild type sibling controls revealed subtle differences in the localization of $Pax7^{+ve}$ nuclei in the somites. GAL treated larvae and *steif* mutant larvae showed an increased number of $Pax7^{+ve}$ nuclei in the "inter-myosepta region" of the somite (Fig. 41A' and B'). In the wildtype larvae, the $Pax7^{+ve}$ nuclei are localized mostly to the boundaries of the somite, the horizontal and the vertical myosepta as well as the dorsal and the ventral edge of the myotome (Fig. 41A and B). One could therefore speculate that damage to muscle fibers causes these cells to move to the inter-myosepta region in an attempt to repair or regenerate damaged muscle fibers. This hypothesis can, to some extent, be supported by observing the localization of $Pax7^{+ve}$ nuclei in *gum* mutant larvae. Relative to *steif* mutants and GAL treated embryos, *gum* mutants show a milder

phenotype, with fibers detaching from the somite borders. The Pax7^{+ve} nuclei also tend to cluster around the somite borders in gum mutants, presumably in response to the detached muscle fibers (arrowheads, Fig. 41C'). However, further experimental proof is needed to validate the hypothesis that Pax7^{+ve} nuclei cluster around the site of damaged myofibers. One way to investigate this would be to cause focal injuries and then examine the behavior of Pax7^{+ve} cells during repair/regeneration process *in vivo*.

4.2.5 The number of proliferative Pax7^{+ve} cells increases dramatically in GAL treated larvae

One might expect that muscle injury would increase the number of Pax7^{+ve} cells. Surprisingly, GAL treated larvae showed a very slight, statistically insignificant, increase of total Pax7^{+ve} nuclei counted in four somites (n=6 larvae) despite the redistribution within the somite (discussed above). It is possible that upon muscle injury the rate of proliferation of Pax7^{+ve} cells increases to provide enough new cells to lead effective regeneration. Once the amplified cells enter the myogenic program, they would down-regulate *pax7* in order to differentiate into muscle fibers. Thus, the number of Pax7^{+ve} cells would remain constant, and only the turnover of these cells would increase. Indeed, an increased level of proliferative Pax7^{+ve} cells was observed upon GAL treatment (Fig. 42 A and B). Anti-Phospho-histone H3 antibody was used as a marker for proliferative Pax7^{+ve} cells. The increase in proliferative Pax7^{+ve} cells was around 80%, showing a very robust response to GAL treatment induced myopathy.

3-D rendering of confocal stacks showed that several of Pax7^{+ve}/PHH3^{+ve} cells were located in the deeper myotome that contains mature fast muscle fibers in a 72 hpf larva. This suggests that not only do Pax7^{+ve} cells undergo increased proliferation;

they also migrate to the deeper myotome, where most of the damaged muscles are and where therefore their differentiation is required. Thus, once these cells enter the myotome, they presumably undergo differentiation and downregulate *pax7* expression, thereby maintaining an almost constant number of total $Pax7^{+ve}$ cells. Because a majority of the $Pax7^{+ve}/PHH3^{+ve}$ dual labeled cells are observed deeper into the myotome, it can be concluded that the differentiation of the cells follows their amplification. It is not clear whether the amplification occurs at the site of muscle damage or along the migration to the site of damage. Further work is needed to find out whether these cells then go and fuse with damaged fibers or give rise to fibers *de novo*. Furthermore, it would be important to know when and precisely how they differentiate and if they need signals from the damaged cells for this. One way to address these questions is to have transgenic lines reporting the expression of genes in muscle differentiation pathway (*myf5, myoD, myogenin*). The *in vivo* imaging of these lines under conditions of muscle repair should yield information about kinetics of regeneration pathway. Additionally, blocking of genes upregulated in the microarray study (discussed below) in the background of these transgenic lines would provide information to the roles these genes play in the regeneration pathway.

Thus in summary, a drug inducible model of myopathy in zebrafish was developed and using this model it was found out that the zebrafish larvae mount a very robust regenerative response to this myopathy. The observations in this study revealed the presence of cells that show morphological hallmarks of mammalian satellite cells in the zebrafish. At 24 hpf, Pax7, a marker for satellite cells, labels nuclei at the somite surface. This is in agreement with recently published reports about the presence of a dermomyotome in zebrafish. By 72hpf, most $Pax7^{+ve}$ nuclei are restricted to somite borders. Subtle changes were observed in the localization of

$Pax7^{+ve}$ nuclei in myopathic states, presumably in response to damaged musculature. $Pax7^{+ve}$ cells also showed greatly increased proliferation in response to muscle damage, but not an overall increase in number of $Pax7^{+ve}$ cells, presumably due to $Pax7^{+ve}$ cells undergoing rapid differentiation into muscle fibers. The proliferative $Pax7^{+ve}$ cells were observed in the deeper myotome that contains only mature muscle fibers in healthy larvae.

One caveat for this study is that it was performed in relatively young animals. At this stage, most $Pax7^{+ve}$ cells are not fiber associated and therefore by definition *not* 'quiescent satellite cells'. Indeed, as has been stated above, $Pax7^{+ve}$ cells in the dermomyotome are proliferative. However, these cells have been shown to give rise to fiber associated satellite cells later (Hollway et al., 2007). This was also observed in the Pax7BAC::kikGR1 transgenic line that is being raised (Fig. 47). Zebrafish larvae transiently expressing Pax7BAC::kikGR1 initially show expression in dermomyotome cells. From day 5 onwards, fiber associated satellite cells could be observed in these larvae (Fig 47).

Since the focus of this study was young animals, this model could be useful for study of specification, proliferation, migration and differentiation of satellite cells. However, to study events involved in initial activation of satellite cells, one may need to study older larvae or adult fish.

4.3 Transcriptomics of GAL treated larvae

Tissue regeneration is a complex phenomenon with multiple signaling, cell migration, immune reaction and tissue remodeling events taking place simultaneously. Severe muscle injuries such as those induced by snake venom (for example, cardiotoxin, notexin or bupivacaine) used routinely to cause muscle injuries

in rodents lead to severe necrosis of the injected muscles. Soon after injury, cells involved in the inflammatory response, such as neutrophils and macrophages, infiltrate the injured area and clear away the muscle fibers damaged beyond repair (for a review see (Charge and Rudnicki, 2004)). During this period, satellite cells, which have been activated following muscle damage, must be prevented from undergoing apoptosis in response to the massive release of free radicals from the necrotic tissue. For these processes to act in a co-ordinate manner, numerous changes in gene expression levels must occur that would be reflected in the transcriptional profiling of the regenerating larvae. Therefore, with the hypothesis that the myopathic animals would increase expression of transcripts required for and facilitating regeneration, an unbiased genome wide expression profile was performed on GAL treated larvae compared to wildtype control larvae.

Initial microarray experiments were performed on custom build chips with oligos spotted onto glass slides at the in house microarray facility at FZK. The advantages of such an approach are readily available chips at a substantially lower cost than commercial alternatives, allowing a larger number of repeats and conditions. However, the initial experiments with custom made chips yielded very few differentially expressed genes. Therefore, commercially available chips from Agilent were used in subsequent experiments. Commercially available chips have better quality control and contain higher number of oligos (22k vs. 10k) spotted on them. However, a limitation of the application of microarray technology to the zebrafish is the still unfinished annotation of zebrafish genome. Hence, the 22k oligos represented on Agilent microarrays may not represent the full complement of zebrafish genes. For example, on comparing the genes upregulated in Sigma Compugen microarrays with the genes upregulated in the Agilent microarray, only 9 out of 13 upregulated genes

from the homemade array were found to be in the upregulated set from Agilent chips. The most prominent gene of these, *cardiomyopathy associated 1 (cmya1)* (discussed below), was not represented on Agilent microarrays. Here we discuss the categorization of upregulated genes according to the gene ontology (GO) class assigned to them and their possible roles in muscle regeneration followed by the most prominent upregulated genes upon GAL treatment that have been verified by ISH.

4.3.1 Genes upregulated upon GAL treatment in Agilent microarrays

To validate the hypothesis that the genes upregulated upon GAL treatment, and hence due to a myopathy, should be involved in muscle repair/regeneration it is important to compare our results with published microarray results in different models. A recent study, performed in mice, compared the effects of two different kinds of injuries; namely contractile overload induced injury (CI) with direct destruction of the muscle tissue (Freeze injury, FI), on the transcriptome (Warren et al., 2007). In total, 23 genes that were upregulated in the mouse study overlap with the upregulated genes in the GAL treated zebrafish larvae (corresponding to 25 zebrafish genes) (Table 7). The additional genes in zebrafish result because of gene duplications frequently seen in teleosts (Amores et al., 1998; Meyer and Schartl, 1999; Volff and Schartl, 2003). In several cases, a different member of the same gene family (Table yyy, shown in italics) represents the zebrafish genes. Despite differences in the mode of causing injury: the mouse study was performed on adult mice that were injured once, while the zebrafish study was performed on larval fish that were constantly under myopathic conditions; several common genes were upregulated. This indicates that there is a strong similarity in regenerative response to muscle damage at the transcriptional level. The mouse study also looked at the

relative timing of gene expression after injury induction. The earliest induced genes common with zebrafish study are the transcription factors *atf3*, *fos*, *C/EBP-delta*, *GADD45* and *btg2* and the stress responsive gene *xin* (*cmya1*, discussed later), that were induced within 6 hours of causing muscle injury. In contrast, the transcription of these genes was still upregulated in zebrafish at 3 dpf, after more than two days of treatment with GAL. This is because unlike CI or FI, GAL treatment causes persistent muscle damage. The expression of the other transcription factor common to both mouse and zebrafish study, *myogenin*, comes on relatively later in both CI and FI (on day 3 after induction of injury), as Myogenin is the MRF required for terminal differentiation of myoblasts.

Apart from transcriptional and stress response, the major response to myopathy is the immune response. Both the mouse study as well as GAL treated zebrafish larvae showed upregulation of immune responsive genes such as *TNF receptor 1* and *IRF7* and that of anti-apoptotic genes such as *bag3*, and *clusterin*. Of particular relevance is Bag3, an anti-apoptotic protein that is expressed predominantly in the muscle and localizes to the Z-discs. It is required for maintenance, but not development of striated muscles as mice with targeted knockout of *bag3* are born normal but show stunted growth, poor muscle maintenance and die by 4 weeks of age (Homma et al., 2006). In humans, mutations in *bag3* cause severe dominant childhood muscular dystrophy (Selcen et al., 2009). Bag3 acts as a co-chaperone by binding to Hsp70/Hsc70 and thereby modulating their chaperone activity (Takayama et al., 1999).

One prominent member of this list, cathepsin L (cathepsin La in zebrafish) is upregulated on day3 in CI and and on day1-day3 in FI groups, respectively. Recent work has shown that Cathepsin L proteolytically cleaved the N-terminus region of

Histone H3 during mouse embryonic stem cell differentiation, thus potentiating a role for chromatin modification during development and disease (Duncan et al., 2008). It might be a general phenomenon that Cathepsins could use for modulating chromatin structure of stem cells, including satellite cells.

Genes upregulated in (upto 3 days after injury) mouse model according to (Warren et al., 2007)	**CI**	**FI**	**Genes upregulated in zebrafish upon GAL treatment (3 dpf)**
Activating Transcription Factor 3	x	x	Activating Transcription Factor 3
FJB osteosarcoma oncogene	x	x	V-FOS FBJ Murine Osteosarcoma Viral Oncogene Homologue
Cardiac morphogenesis (xin)	x	x	Cardiomyopathy associated 1 (xin)
CCAAT/enhancer binding protein (C/EBP), Delta	x	x	CCAAT/enhancer binding protein (C/EBP), Delta
B-cell translocation gene 2	x	x	B-cell translocation gene 2
Pyruvate Dehydrogenase Kinase, isoenzyme 4	x	x	*Pyruvate Dehydrogenase Kinase, Isoenzyme 2*
Dusp1	x	x	*Dusp5*
GADD45, gamma	x	x	*GADD45 alpha, GADD45beta like*
Ras related associated with diabetes	x	x	ZGC:63471 (Ras-related associated with diabetes)
ankyrin repeat domain containing 10	x	x	*ankyrin repeat domain containing 9*
Thioredoxin 1	x	x	ZGC:92903 (Thioredoxin)
annexin A2	x	x	*annexin A2A*
Protein phosphatase 1 regulatory (inhibitor) subunit 14B	x	x	*Protein phosphatase 1 regulatory subunit 3C*
Cathepsin L	x	x	Cathepsin L, a
Bcl2 associated anthogene 3 (BAG3)	x		Bcl2 associated anthogene 3 (BAG3)
Clusterin	x		Clusterin
Socs3		x	Socs3a, Socs3b
Jun b oncogene		x	Jun B proto-oncogene, *Jun B proto-oncogene like*
arginase, 1 liver		x	*arginase, type II*
Capping protein (actin filament) gelsolin like		x	*Gelsolin (Amyloidosis, Finnish type)*
TNF receptor superfamily, member 1b		x	*TNF receptor superfamily, member 1a*
Myogenin	x	x	Myogenin
Interferon regulatory factor 7		x	Interferon regulatory factor 7

Table 7: The list of genes (left column) upregulated at different stages during the first 3 days of injury in the mouse model according to (Warren et al., 2007) compared with genes upregulated (right column) in GAL treated myopathy in zebrafish model. CI and FI represent the kind of muscle injury; that caused by contractile overload induced injury (CI) or freeze injury (FI). Red colour represents genes upregulated only on Sigma Compugen microarrays; green colour represents genes upregulated on Agilent microarrays while yellow colour represents genes upregulated in both sets of microarrays. See text for details.

In the GO analysis of gene upregulated upon GAL treatment, maximum numbers of genes (15) belonged to the 'receptor/signal transduction' class indicating heightened environmental stimuli that evoke response from the cells. Most notable amongst these are *angiopoietin like 7* (*angptl7*), *C-X-C Ligand 6*, and a member of the tetraspanin family zgc:100919 (discussed later). As discussed earlier, sever myopathy causes massive restructuring of the muscle tissue including but not limited to the muscle cells. The blood vessels/capillaries supplying muscles must be repaired as well. The upregulation of *angptl7* is indicative of the fact that such regeneration of blood vessels is occurring.

The other key categories of upregulated genes were: 'regulators of transcription' (most members of which were discussed above) with 13 members, enzymes (10 members), kinases/phosphatases (8 members). The high number of enzymes and kinase/phosphatases implicates a high degree of energy metabolism taking place in regenerating animals.

The novel genes identified in this study serve as a starting point for identification of new genes involved in muscle regeneration. Therefore, to get a better understanding of their spatio-temporal expression pattern as well as the changes caused in these by GAL treatment, I used *in situ* hybridization analysis of selected genes.

4.3.2 ISH verification of selected genes from the microarrays

4.3.2.1 cmya1

One of the most upregulated gene in response to GAL treatment was *cardiomyopathy associated 1* (*cmya1*) (section 3.3.1.1, Table 6). *cmya1* is a striated muscle specific gene first identified in a differential mRNA display screen in chicken (Wang et al., 1996). It was called *xin* and was shown to be responsible for cardiac morphogenesis in chicken (Wang et al., 1999). The Cmya1 protein localizes to intercalated discs of the heart and the myotendinous junctions in the skeletal muscles (Sinn et al., 2002). The characteristic feature of Cmya1 is the presence of several copies of a 16 amino acid repeating unit called the Xin repeat (Jung-Ching Lin et al., 2005; Pacholsky et al., 2004; Wang et al., 1999). The Xin repeat is an actin binding domain, and a minimum of 3 Xin repeats are required to bind actin filaments (Cherepanova et al., 2006; Pacholsky et al., 2004). The human Cmya1 protein contains a Mena/VASP-binding domain in the N terminal region and Filamin c binding regions in the C terminal region (van der Ven et al., 2006). The chick and the mouse *cmya1* genes also contain a putative DNA-binding domain (Wang et al., 1999). The mouse Cmya1 co-localizes with ß-catenin and N-cadherin throughout development and adulthood (Sinn et al., 2002).

Characterization of the zebrafish expression pattern of *cmya1* showed that it was expressed in newly developing muscle fibers. *cmya1* expression was also observed in the trunk muscles of GAL treated larvae, while the expression was at undetectable levels in wildtype untreated larvae. Therefore, it seems clear that *cmya1* is upregulated in response to muscle injury. The presence of multiple actin binding domains indicates a role for cytoskeletal organization for Cmya1. It is probable that Cmya1 also plays a role in conversion of the satellite cell cytoskeleton, which is that

of a motile non-contractile cell, into an organized array of actin and other sarcomeric proteins during differentiation. Transverse section as well as lateral view of GAL treated larvae stained for *cmya1* transcripts shows punctuate staining that might correspond to individual satellite cells (Fig. 49). However, co-localization of Pax7 antibody needs to be performed with *cmya1* ISH to definitely state this. Recently it has been reported that Cmya1 is expressed within satellite cells and within newly regenerated muscle fibers (Hawke et al., 2007). In this study, *cmya1* transcripts showed a >16 fold upregulation within 12 hours following muscle injury induced by cardiotoxin injection in mice. *In situ* hybridization with a probe specific to *cmya1* was used in conjunction with syndecan-4 (a marker for satellite cells) antibody to show colocalization of the two to muscle satellite cells. In the light of this report, the assumption that *cmya1* might be required for muscle regeneration by facilitating differentiation of satellite cells from motile to sessile, contractile myofibers gains support.

To understand the role that *cmya1* plays in muscle regeneration, a morpholino mediated approach to block *cmya1* translation was adopted. The MO-*cmya1* resulted in a muscle phenotype, with huge gaps in the myosepta (data not shown), unfortunately however, the control morpholino with 5bp mismatch also showed a strong though unrelated phenotype. A blast search of the control morpholino against the zebrafish genome did not yield any match. However, in the absence of a completely annotated genome sequence it is not possible to rule out the control morpholino targeting another transcript. Recently, it has been shown that certain morpholino exhibit off target neural apoptotic effects (Robu et al., 2007). These off target effects could be attenuated by co-injecting a morpholino against the tumor suppressor p53 (Robu et al., 2007). However, it was decided to generate a targeted

TILLING mutant in the *cmya1* locus and the TILLING mutation was requested from the Sanger Institute, UK. With the mutant available, it would be possible to perform a loss of function analysis of the *cmya1* gene and uncover its role in muscle regeneration and satellite cell biology.

4.3.2.2 zgc:100919

zgc:100919 is an as yet uncharacterized gene belonging to the tetraspanin superfamily. Tetraspanins are four pass transmembrane proteins characterized by two transmembrane extracellular loops, with both the N- and the C-termini lying on the intracellular side of the membrane. They are implicated in a diverse range of biological phenomena, including cell motility, metastasis, cell proliferation and differentiation (for review see (Hemler, 2005). The tetraspanins are associated with adhesion receptors of the integrin family and regulate integrin-dependent cell migration.

The zfin *in situ* expression pattern database shows that zgc:100919 is expressed in the migrating neural crest cells in the lateral pathway at 24-30 hpf. It is described that, by 48-60 hpf the staining is restricted to the pigment cells present along the dorsal and the ventral edge of the somite as well as along the midline. I was able to confirm this expression pattern, and in addition I observed that the GAL treatment increased expression of zgc:100919 in regenerating muscles (Fig. 51). On performing transverse sections (Fig. 52) of wildtype 72 hpf larvae through mid-trunk somites, the staining was seen in single cells on the surface of the somite (Fig. 52A and A'). Sometimes, staining was also observed in cells along the medial region of the horizontal myoseptum (Fig. 52A). Based on this myoseptal location, given that pigment cells are present only in the skin, one can assume that zgc:100919 is not

expressed in pigment cells. Upon GAL treatment, the expression of zgc:100919 is clearly observed in deeper fast muscle fibers (Fig. 52B, and B'). Since it was previously shown in this study that GAL treatment causes $Pax7^{+ve}$ cells to migrate into deeper myotome to cause muscle repair it is reasonable to hypothesize that zgc:100919 could be expressed by $Pax7^{+ve}$ cells. The expression of Pax7 at 72 hpf does look similar to the ISH expression pattern of zgc:100919 in the trunk. However, co-localization of the Pax7 antibody with zgc:100919 needs to be performed to test this hypothesis. Since tetraspanins are involved in cell adhesion and migration, and interaction with integrins, zgc:100919 might regulate migration of $Pax7^{+ve}$ cells upon GAL treatment.

4.3.2.3 zgc:103408 (muscle integrin binding protein)

Zgc:103408 is the zebrafish ortholog of human muscle integrin binding protein (MIBP). MIBP is known to interact with α7ß1 integrin and regulate cell adhesion and laminin matrix deposition (Li et al., 2003a). MIBP also increases the protein level and tyrosine phosphorylation of paxillin, an important signaling molecule involved in myogenic differentiation (Li et al., 2003a). It should be noted that α7ß1 integrin is expressed by satellite cells (Sacco et al., 2008). Therefore, it is likely that increased levels of MIBP in GAL treated larvae is indicative of myogenic precursors undergoing differentiation to repair or regenerate damaged/lost myofibers.

4.4 Generating tools for live imaging of muscle regeneration

4.4.1 The Tol2 transgenics

A major advantage of using zebrafish as a model organism is the live imaging possibilities it offers due to its relatively transparent larval stages and development outside the mother. In order to generate transgenic lines that report expression of markers specific for satellite cells, putative promoter sequences of pax7 (-3.3 kb), met (-5.3 kb), and myoD (-5 kb) were amplified and cloned into Tol2 expression system containing GFP as a reporter (as described in section 2.6). Transient expression of all these constructs yielded persistent GFP expression in muscle fibers, among other tissues (Fig. 45). Since the GFP is quite stable (Tombolini, 1997) the GFP observed in muscle fibers could be a remnant of the GFP that was expressed by myogenic precursors before they fused to form muscle fibers. However, the persistence of GFP to later stages could also mean that the *met* -5.3 kb upstream region is lacking enhancer elements that might be required to shut down *met* expression after progression of the satellite cell through differentiation and maturation into a muscle fiber. Indeed, similar persistent muscle fiber specific expression of GFP with a *myoD* -5kb::GFP construct (unpub. observations) and the *pax7* -3.3kb::GFP construct (data not shown) was observed. One drawback with the Tol2 system is the integration of multiple copies of inserts that could lead to integration site dependent effects on expression, resulting in ectopic expression that could require several generations of outcrosses to get a pure tissue specific line (unpublished observations). Taken together, to be able to track satellite cells *in vivo*, we were confronted with the following problems: a) less faithful expression with shorter constructs, b) how to ascertain fresh transcription of the transcription factor we were reporting, than the accumulated reporter protein, and c) how to discriminate a satellite cell amongst a

mass of muscle tissue that might retain fluorescent protein due to their long half life (so important for tracking cells over hours or even days).

4.4.2 BAC transgenics

To overcome the limitations of using shorter constructs imposed by Tol2 system I employed the following approach:

a) Bacterial Artificial Chromosomes (BACs) were tagged with reporters and injected into zebrafish embryos to generate transgenic lines. BACs are substantially larger (100-300kb) than promoter constructs and thus in all likelihood contain remote enhancers that may control spatio-temporal expression pattern of a gene. It has been well established that vertebrate *cis*-regulatory elements could be scattered over large distances. For example it has been shown that *myf5* is regulated by an enhancer -80kb upstream (Chen et al., 2007). Therefore BAC driven transgenes are generally more faithful than those driven by shorter constructs.

b) GFP is an extremely stable protein (Tombolini, 1997). Therefore, it would be difficult to distinguish the newly synthesized protein in response to muscle damage vs. the accumulated GFP that was transcribed before damage. Hence, to measure the transcriptional response of the gene to muscle damage, kikGR1 a yellow/green to red photoconvertible fluorescent protein, was used as a reporter. Complete photoconversion will therefore mark the accumulated fluorescent protein and any new fluorescence in the yellow/green channel should be a result of fresh transcriptional activity. Thus, kikGR1 could be used as a timer for recording the transcriptional activity of a gene in response to a stimulus. Using destabilized version of GFP, with a shorter half-life, was

considered initially but ultimately rejected, as the fluorescence of transiently expressing larvae was quite low. Therefore, the destabilized protein may be undetectable where a stable protein would yield a stronger signal.

c) KikGR1 could be easily photoconverted using a two-photon laser at 780nm. The advantage of using two photon over conventional confocal microscopy is that two-photon laser could specifically excite fluorescent proteins expressed by single cells buried deep in the tissue without exciting the cells in the planes above or below the cell. Therefore, a single cell could be optically highlighted, distinguished from the surrounding tissue, and followed over a course of time.

One significant drawback of using BACs is the reduced frequency of transgene insertion on account of substantially large insert size. However, pre screening of injected F_0 fish for good tissue specific expression generally results in a greater frequency of germline transmission.

5 Conclusion and outlook

There is an increasing need for better understanding of muscle regeneration in order to devise better therapies for patients suffering from myodegenerative diseases such as muscular dystrophies. With this study I have aimed at developing a zebrafish model for muscle regeneration to exploit the various advantages offered by this model.

Several different strategies were used in the present work; first, I used ENU mutagenesis screen to identify motility mutants that might have defective muscle maintenance, presumably due to ineffective repair. I isolated and characterized one such mutant that develops several neuronal and muscle defects. Several of these defects seem to result from neural crest tissues being mis-migrated or incorrectly specified. Second, I developed a zebrafish model for inducible myopathy by bath application of galanthamine hydrobromide (GAL), a blocker of acetylcholinesterase signaling. I found that zebrafish larvae showed a robust regeneration following muscle damage when the GAL was removed and the larvae were allowed to recover from muscle damage. Using electron microscopy and immunoelectron microscopy with Pax7 antibody, I identified zebrafish muscle satellite cells. I also identified a layer of $Pax7^{+ve}$ cells superficial to the somite that has been recently described as a primitive dermomyotome in teleosts. Upon GAL treatment induced muscle damage the $Pax7^{+ve}$ cells in the superficial layer become highly proliferative and are also observed in deeper myotome where normally only postmitotic muscle fibers are observed in healthy animals. Quantification of proliferative $Pax7^{+ve}$ cells showed an 80% increase in numbers upon GAL treatment. Third, an unbiased genome wide transcriptional profile of GAL treated animals vs. untreated animals was carried out to

identify transcripts upregulated during muscle regeneration. 95 genes were found to be upregulated in GAL treated animals and several of these genes are known to be involved in muscle development and maintenance. Some of these genes such as myogenin, *desmin* and *cmya1*, are expressed by satellite cells/myoblasts during differentiation. Others such as BAG3, Murf3 and Filamin C are required for muscle development, cytoskeletal organization and maintenance. Characterization of novel genes identified (such as zgc:100919) in the screen would give insights about muscle regeneration in zebrafish. Finally, I have also developed transgenic lines reporting the expression of Pax7 and Pax3 which could be used in long term fate mapping and in vivo imaging of satellite cells in zebrafish.

Further work in conjunction with the Pax7 and Pax3 transgenic lines could establish the putative roles of the genes identified in the microarray screen during muscle regeneration and satellite cell biology. On one hand this would help us design better strategies for muscle regeneration and high throughput screening platforms for drugs/bioactive molecules. On the other hand harnessing these tools would also shed light on the fundamental aspects of satellite cells biology.

Appendix A1

Genes upregulated upon GAL treatment in Agilent microarray

Zfin gene name	FC	P-value
myeloid cell leukemia sequence 1a (mcl1a)	1.71	0.0161
family with sequence similarity 46, member C (fam46c)	1.71	0.0035
calcium channel, voltage-dependent, gamma subunit 1 (cacng1)	1.72	0.0311
growth arrest and DNA-damage-inducible, alpha (gadd45a)	1.72	0.0278
calcitonin/calcitonin-related polypeptide, alpha (calca)	1.73	0.0260
membrane-spanning 4-domains, subfamily A, member 17A.5	1.73	0.0031
interferon regulatory factor 7 (irf7)	1.73	0.0192
foxo1a	1.74	0.0238
zgc:85866	1.75	0.0274
tumor necrosis factor receptor superfamily, member 1a	1.75	0.0099
EH-domain containing 2	1.76	0.0142
filamin C, gamma b	1.76	0.0073
v-jun sarcoma virus 17 oncogene homolog (avian) (jun)	1.76	0.0094
core promoter element binding protein (copeb)	1.76	0.0200
myeloid cell leukemia sequence 1b (mcl1b)	1.77	0.0095
zgc:77868	1.77	0.0367
zgc:56376	1.78	0.0518
zgc:92069	1.80	0.0010
v-jun sarcoma virus 17 oncogene homolog (avian) (jun)	1.80	0.0092
6-phosphofructo-2-kinase/fructose-2,6-biphosphatase 3	1.81	0.0086
keratin 18 (krt18)	1.81	0.0442
solute carrier family 16, member 9a (slc16a9a)	1.81	0.0053
RasGEF domain family, member 1Bb	1.81	0.0288
zgc:136256	1.81	0.0128
matrix Gla protein (mgp)	1.82	0.0142
arginase, type II	1.83	0.0210
annexin A2a (anxa2a)	1.83	0.0030
p4ha2	1.84	0.0066
similar to TRAF2 binding protein [Danio rerio] (XP_001340322)	1.84	0.0198
angiopoietin-like 7	1.85	0.0064
transducer of ERBB2, 1b (tob1b)	1.86	0.0037
Myogenin	1.86	0.0196
zgc:76966	1.86	0.0352
uncoupling protein 4 (ucp4)	1.88	0.0119
solute carrier family 25, member 25 (slc25a25)	1.89	0.0054
growth arrest and DNA-damage-inducible, beta like	1.89	0.0208
zgc:100919	1.91	0.0076
hspb1	1.91	0.0302
egl nine homolog 3 (C. elegans) (egln3)	1.91	0.0006
major vault protein	1.94	0.0043
peptide YYa	1.95	0.0137
zgc:103408 (Muscle integrin-binding protein) (MIBP)	1.96	0.0067
hypoxia induced gene 1 (hig1)	1.96	0.0055
p4ha1	1.98	0.0087
zgc:91870	2.00	0.0092
L-threonine dehydrogenase (tdh)	2.03	0.0105
zgc:92109	2.03	0.0139

hypoxia induced gene 1 (hig1)	2.04	0.0036
clusterin (clu)	2.06	0.0066
MAP kinase-interacting serine/threonine kinase 2	2.06	0.0108
heat shock protein 47 (hsp47)	2.08	0.0260
elongation factor-2 kinase (eef2k)	2.08	0.0038
zgc:56330	2.10	0.0043
major vault protein (mvp)	2.11	0.0026
zgc:91870	2.13	0.0105
CCAAT/enhancer binding protein (C/EBP), beta (cebpb)	2.14	0.0059
zgc:56330	2.15	0.0060
zgc:172053	2.15	0.0079
dual specificity phosphatase 5 (dusp5)	2.16	0.0123
major vault protein (mvp)	2.16	0.0024
zgc:103425 (CD151 molecule)	2.16	0.0026
B-cell translocation gene 2 (btg2)	2.16	0.0476
zgc:92069	2.17	0.0015
zgc:56330	2.17	0.0031
keratin 18 (krt18)	2.18	0.0035
FK506 binding protein 5 (fkbp5)	2.22	0.0185
complement component c3c	2.24	0.0005
Hsp47	2.38	0.0155
zgc:100859	2.38	0.0058
zgc:92903	2.40	0.0042
cathepsin L1, a (ctsl1a)	2.44	0.0099
zgc:103566	2.44	0.0036
XP_690732 : similar to chemokine CXC-like protein	2.44	0.0021
activating transcription factor 3 (atf3)	2.47	0.0094
complement factor B (cfb)	2.50	0.0005
zgc:85616	2.51	0.0061
tissue inhibitor of metalloproteinase 2, like (timp2l)	2.52	0.0038
complement component 6	2.56	0.0004
zgc:103438	2.61	0.0033
pyruvate dehydrogenase kinase, isoenzyme 2 (pdk2)	2.69	0.0385
parathyroid hormone 1 (pth1)	2.70	0.0107
zgc:103566	2.76	0.0031
LOC794635 similar to complement C4-2	2.78	0.0003
desmin	2.78	0.0010
zgc:92851	2.82	0.0019
heat shock protein 47 (hsp47)	2.86	0.0100
CCAAT/enhancer binding protein (C/EBP), delta	2.94	0.0100
alanine-glyoxylate aminotransferase (agxt)	3.09	0.0073
matrix metalloproteinase 9 (mmp9)	3.10	0.0095
jun B proto-oncogene (junb)	3.54	0.0013
heat shock protein 47 (hsp47)	3.73	0.0020
LOC557301	3.76	0.0000
jun B proto-oncogene, like (junbl)	3.85	0.0023
insulin-like growth factor binding protein 1 (igfbp1)	4.06	0.0134
zgc:123218	4.09	0.0009
Ras-related associated with diabetes	4.23	0.0039
SOCS-3b	4.52	0.0024
v-fos FBJ murine osteosarcoma viral oncogene homolog (fos)	4.64	0.0032
Fibronectin1b	5.19	0.0002

SOCS-3a	6.27	0.0012
heat shock protein HSPB11	7.95	0.0001

6 References

Adams, G. B., and Scadden, D. T. (2006). The hematopoietic stem cell in its place. Nat Immunol *7*, 333-337.

Adler, G., Hupp, T., and Kern, H. F. (1979). Course and spontaneous regression of acute pancreatitis in the rat. Virchows Arch A Pathol Anat Histol *382*, 31-47.

Alric, S., Froeschle, A., Piquemal, D., Carnac, G., and Bonnieu, A. (1998). Functional specificity of the two retinoic acid receptor RAR and RXR families in myogenesis. Oncogene *16*, 273-282.

Altman, N. (2005). Replication, variation and normalisation in microarray experiments. Appl Bioinformatics *4*, 33-44.

Amacher, S. L., Draper, B. W., Summers, B. R., and Kimmel, C. B. (2002). The zebrafish T-box genes no tail and spadetail are required for development of trunk and tail mesoderm and medial floor plate. Development *129*, 3311-3323.

Amores, A., Force, A., Yan, Y. L., Joly, L., Amemiya, C., Fritz, A., Ho, R. K., Langeland, J., Prince, V., Wang, Y. L., *et al.* (1998). Zebrafish hox clusters and vertebrate genome evolution. Science *282*, 1711-1714.

Amsterdam, A., Burgess, S., Golling, G., Chen, W., Sun, Z., Townsend, K., Farrington, S., Haldi, M., and Hopkins, N. (1999). A large-scale insertional mutagenesis screen in zebrafish. Genes Dev *13*, 2713-2724.

Amsterdam, A., and Hopkins, N. (2004). Retroviral-mediated insertional mutagenesis in zebrafish. Methods Cell Biol *77*, 3-20.

Amthor, H., Christ, B., and Patel, K. (1999). A molecular mechanism enabling continuous embryonic muscle growth - a balance between proliferation and differentiation. Development *126*, 1041-1053.

Aoyama, H., and Asamoto, K. (1988). Determination of somite cells: independence of cell differentiation and morphogenesis. Development *104*, 15-28.

Arnold, J. S., Werling, U., Braunstein, E. M., Liao, J., Nowotschin, S., Edelmann, W., Hebert, J. M., and Morrow, B. E. (2006). Inactivation of Tbx1 in the pharyngeal endoderm results in 22q11DS malformations. Development *133*, 977-987.

Asakura, A., Seale, P., Girgis-Gabardo, A., and Rudnicki, M. A. (2002). Myogenic specification of side population cells in skeletal muscle. J Cell Biol *159*, 123-134.

Aulehla, A., and Johnson, R. L. (1999). Dynamic expression of lunatic fringe suggests a link between notch signaling and an autonomous cellular oscillator driving somite segmentation. Dev Biol *207*, 49-61.

Bachrach, E., Li, S., Perez, A. L., Schienda, J., Liadaki, K., Volinski, J., Flint, A., Chamberlain, J., and Kunkel, L. M. (2004). Systemic delivery of human microdystrophin to regenerating mouse dystrophic muscle by muscle progenitor cells. Proc Natl Acad Sci U S A *101*, 3581-3586.

Bachrach, E., Perez, A. L., Choi, Y. H., Illigens, B. M., Jun, S. J., del Nido, P., McGowan, F. X., Li, S., Flint, A., Chamberlain, J., and Kunkel, L. M. (2006). Muscle engraftment of myogenic progenitor cells following intraarterial transplantation. Muscle Nerve *34*, 44-52.

Baldwin, G., Novitskaya, V., Sadej, R., Pochec, E., Litynska, A., Hartmann, C., Williams, J., Ashman, L., Eble, J. A., and Berditchevski, F. (2008). Tetraspanin CD151 Regulates Glycosylation of {alpha}3{beta}1 Integrin. J Biol Chem *283*, 35445-35454.

Barker, N., van Es, J. H., Kuipers, J., Kujala, P., van den Born, M., Cozijnsen, M., Haegebarth, A., Korving, J., Begthel, H., Peters, P. J., and Clevers, H. (2007). Identification of stem cells in small intestine and colon by marker gene Lgr5. Nature *449*, 1003-1007.

Barrantes, I. B., Elia, A. J., Wunsch, K., Hrabe de Angelis, M. H., Mak, T. W., Rossant, J., Conlon, R. A., Gossler, A., and de la Pompa, J. L. (1999). Interaction between Notch signalling and Lunatic fringe during somite boundary formation in the mouse. Curr Biol *9*, 470-480.

Barresi, M. J., Stickney, H. L., and Devoto, S. H. (2000). The zebrafish slow-muscle-omitted gene product is required for Hedgehog signal transduction and the development of slow muscle identity. Development *127*, 2189-2199.

Bassett, D. I., Bryson-Richardson, R. J., Daggett, D. F., Gautier, P., Keenan, D. G., and Currie, P. D. (2003). Dystrophin is required for the formation of stable muscle attachments in the zebrafish embryo. Development *130*, 5851-5860.
Baxendale, S., Davison, C., Muxworthy, C., Wolff, C., Ingham, P. W., and Roy, S. (2004). The B-cell maturation factor Blimp-1 specifies vertebrate slow-twitch muscle fiber identity in response to Hedgehog signaling. Nat Genet *36*, 88-93.
Becker, C. G., and Becker, T. (2008). Adult zebrafish as a model for successful central nervous system regeneration. Restor Neurol Neurosci *26*, 71-80.
Behra, M., Cousin, X., Bertrand, C., Vonesch, J. L., Biellmann, D., Chatonnet, A., and Strahle, U. (2002). Acetylcholinesterase is required for neuronal and muscular development in the zebrafish embryo. Nat Neurosci *5*, 111-118.
Behra, M., Etard, C., Cousin, X., and Strahle, U. (2004). The use of zebrafish mutants to identify secondary target effects of acetylcholine esterase inhibitors. Toxicol Sci *77*, 325-333.
Ben-Yair, R., Kahane, N., and Kalcheim, C. (2003). Coherent development of dermomyotome and dermis from the entire mediolateral extent of the dorsal somite. Development *130*, 4325-4336.
Ben-Yair, R., and Kalcheim, C. (2005). Lineage analysis of the avian dermomyotome sheet reveals the existence of single cells with both dermal and muscle progenitor fates. Development *132*, 689-701.
Benjamini, Y. a. H., Y (1995). Controlling the false discovery rate: A practical approach to multiple testing. J R Stat Soc *57*, 289-300.
Bessho, Y., Hirata, H., Masamizu, Y., and Kageyama, R. (2003). Periodic repression by the bHLH factor Hes7 is an essential mechanism for the somite segmentation clock. Genes Dev *17*, 1451-1456.
Bessho, Y., Sakata, R., Komatsu, S., Shiota, K., Yamada, S., and Kageyama, R. (2001). Dynamic expression and essential functions of Hes7 in somite segmentation. Genes Dev *15*, 2642-2647.
Bigot, A., Jacquemin, V., Debacq-Chainiaux, F., Butler-Browne, G. S., Toussaint, O., Furling, D., and Mouly, V. (2008). Replicative aging down-regulates the myogenic regulatory factors in human myoblasts. Biol Cell *100*, 189-199.
Birchmeier, C., and Brohmann, H. (2000). Genes that control the development of migrating muscle precursor cells. Curr Opin Cell Biol *12*, 725-730.
Bischoff, R., and Holtzer, H. (1970). Inhibition of myoblast fusion after one round of DNA synthesis in 5-bromodeoxyuridine. J Cell Biol *44*, 134-150.
Bladt, F., Riethmacher, D., Isenmann, S., Aguzzi, A., and Birchmeier, C. (1995). Essential role for the c-met receptor in the migration of myogenic precursor cells into the limb bud. Nature *376*, 768-771.
Blagden, C. S., Currie, P. D., Ingham, P. W., and Hughes, S. M. (1997). Notochord induction of zebrafish slow muscle mediated by Sonic hedgehog. Genes Dev *11*, 2163-2175.
Blanpain, C., and Fuchs, E. (2006). Epidermal stem cells of the skin. Annu Rev Cell Dev Biol *22*, 339-373.
Bodemer CW, E. N. (1959). Localization of newly synthesized proteins in regenerating newt limbs as determined by radioautographic localization of injected methionine-S35. Dev Biol *1*, 327–342.
Borycki, A. G., Mendham, L., and Emerson, C. P., Jr. (1998). Control of somite patterning by Sonic hedgehog and its downstream signal response genes. Development *125*, 777-790.
Bosch, M., Bagun, J., and Serras, F. (2008). Origin and proliferation of blastema cells during regeneration of Drosophila wing imaginal discs. Int J Dev Biol *52*, 1043-1050.
Boutet, S. C., Disatnik, M. H., Chan, L. S., Iori, K., and Rando, T. A. (2007). Regulation of Pax3 by proteasomal degradation of monoubiquitinated protein in skeletal muscle progenitors. Cell *130*, 349-362.
Brack, A. S., Conboy, M. J., Roy, S., Lee, M., Kuo, C. J., Keller, C., and Rando, T. A. (2007). Increased Wnt signaling during aging alters muscle stem cell fate and increases fibrosis. Science *317*, 807-810.

Brand-Saberi, B., Ebensperger, C., Wilting, J., Balling, R., and Christ, B. (1993). The ventralizing effect of the notochord on somite differentiation in chick embryos. Anat Embryol (Berl) *188*, 239-245.
Brand-Saberi, B., Muller, T. S., Wilting, J., Christ, B., and Birchmeier, C. (1996). Scatter factor/hepatocyte growth factor (SF/HGF) induces emigration of myogenic cells at interlimb level in vivo. Dev Biol *179*, 303-308.
Brawley, C., and Matunis, E. (2004). Regeneration of male germline stem cells by spermatogonial dedifferentiation in vivo. Science *304*, 1331-1334.
Brent, A. E., and Tabin, C. J. (2002). Developmental regulation of somite derivatives: muscle, cartilage and tendon. Curr Opin Genet Dev *12*, 548-557.
Bruckner, K., Perez, L., Clausen, H., and Cohen, S. (2000). Glycosyltransferase activity of Fringe modulates Notch-Delta interactions. Nature *406*, 411-415.
Bryson-Richardson, R. J., and Currie, P. D. (2008). The genetics of vertebrate myogenesis. Nat Rev Genet *9*, 632-646.
Buchberger, A., Freitag, D., and Arnold, H. H. (2007). A homeo-paired domain-binding motif directs Myf5 expression in progenitor cells of limb muscle. Development *134*, 1171-1180.
Buckingham, M., Bajard, L., Daubas, P., Esner, M., Lagha, M., Relaix, F., and Rocancourt, D. (2006). Myogenic progenitor cells in the mouse embryo are marked by the expression of Pax3/7 genes that regulate their survival and myogenic potential. Anat Embryol (Berl) *211 Suppl 1*, 51-56.
Buckingham, M., and Relaix, F. (2007). The role of Pax genes in the development of tissues and organs: Pax3 and Pax7 regulate muscle progenitor cell functions. Annu Rev Cell Dev Biol *23*, 645-673.
Cairns, J. (1975). Mutation selection and the natural history of cancer. Nature *255*, 197-200.
Camps, M., Nichols, A., and Arkinstall, S. (2000). Dual specificity phosphatases: a gene family for control of MAP kinase function. Faseb J *14*, 6-16.
Capdevila, J., Tabin, C., and Johnson, R. L. (1998). Control of dorsoventral somite patterning by Wnt-1 and beta-catenin. Dev Biol *193*, 182-194.
Caplan, A. I. (1991). Mesenchymal stem cells. J Orthop Res *9*, 641-650.
Carlson, B. M., and Faulkner, J. A. (1989). Muscle transplantation between young and old rats: age of host determines recovery. Am J Physiol *256*, C1262-1266.
Cerletti, M., Jurga, S., Witczak, C. A., Hirshman, M. F., Shadrach, J. L., Goodyear, L. J., and Wagers, A. J. (2008). Highly efficient, functional engraftment of skeletal muscle stem cells in dystrophic muscles. Cell *134*, 37-47.
Chalkley, D. (1954). A quantitative histological analysis of forelimb regeneration in triturus viridescens. Journal of Morphology *Volume 94*, 21 - 70.
Charge, S. B., and Rudnicki, M. A. (2004). Cellular and molecular regulation of muscle regeneration. Physiol Rev *84*, 209-238.
Chen, D., and McKearin, D. (2003). Dpp signaling silences bam transcription directly to establish asymmetric divisions of germline stem cells. Curr Biol *13*, 1786-1791.
Chen, W., Burgess, S., and Hopkins, N. (2001). Analysis of the zebrafish smoothened mutant reveals conserved and divergent functions of hedgehog activity. Development *128*, 2385-2396.
Chen, Y. H., Wang, Y. H., Chang, M. Y., Lin, C. Y., Weng, C. W., Westerfield, M., and Tsai, H. J. (2007). Multiple upstream modules regulate zebrafish myf5 expression. BMC Dev Biol *7*, 1.
Chenn, A., and McConnell, S. K. (1995). Cleavage orientation and the asymmetric inheritance of Notch1 immunoreactivity in mammalian neurogenesis. Cell *82*, 631-641.
Cherepanova, O., Orlova, A., Galkin, V. E., van der Ven, P. F., Furst, D. O., Jin, J. P., and Egelman, E. H. (2006). Xin-repeats and nebulin-like repeats bind to F-actin in a similar manner. J Mol Biol *356*, 714-723.
Chevallier, A., Kieny, M., and Mauger, A. (1977). Limb-somite relationship: origin of the limb musculature. J Embryol Exp Morphol *41*, 245-258.

Chiang, C., Litingtung, Y., Lee, E., Young, K. E., Corden, J. L., Westphal, H., and Beachy, P. A. (1996). Cyclopia and defective axial patterning in mice lacking Sonic hedgehog gene function. Nature *383*, 407-413.
Choi, S., Gustafson-Wagner, E. A., Wang, Q., Harlan, S. M., Sinn, H. W., Lin, J. L., and Lin, J. J. (2007). The intercalated disk protein, mXinalpha, is capable of interacting with beta-catenin and bundling actin filaments [corrected]. J Biol Chem *282*, 36024-36036.
Christ, B., Brand-Saberi, B., Grim, M., and Wilting, J. (1992). Local signalling in dermomyotomal cell type specification. Anat Embryol (Berl) *186*, 505-510.
Christ, B., Jacob, M., and Jacob, H. J. (1983). On the origin and development of the ventrolateral abdominal muscles in the avian embryo. An experimental and ultrastructural study. Anat Embryol (Berl) *166*, 87-101.
Christov, C., Chretien, F., Abou-Khalil, R., Bassez, G., Vallet, G., Authier, F. J., Bassaglia, Y., Shinin, V., Tajbakhsh, S., Chazaud, B., and Gherardi, R. K. (2007). Muscle satellite cells and endothelial cells: close neighbors and privileged partners. Mol Biol Cell *18*, 1397-1409.
Chuang, P. T., Kawcak, T., and McMahon, A. P. (2003). Feedback control of mammalian Hedgehog signaling by the Hedgehog-binding protein, Hip1, modulates Fgf signaling during branching morphogenesis of the lung. Genes Dev *17*, 342-347.
Chuang, P. T., and McMahon, A. P. (1999). Vertebrate Hedgehog signalling modulated by induction of a Hedgehog-binding protein. Nature *397*, 617-621.
Cinnamon, Y., Kahane, N., and Kalcheim, C. (1999). Characterization of the early development of specific hypaxial muscles from the ventrolateral myotome. Development *126*, 4305-4315.
Clayton, E., Doupe, D. P., Klein, A. M., Winton, D. J., Simons, B. D., and Jones, P. H. (2007). A single type of progenitor cell maintains normal epidermis. Nature *446*, 185-189.
Cohen, N., Kudryashova, E., Kramerova, I., Anderson, L. V., Beckmann, J. S., Bushby, K., and Spencer, M. J. (2006). Identification of putative in vivo substrates of calpain 3 by comparative proteomics of overexpressing transgenic and nontransgenic mice. Proteomics *6*, 6075-6084.
Cole, N. J., Hall, T. E., Martin, C. I., Chapman, M. A., Kobiyama, A., Nihei, Y., Watabe, S., and Johnston, I. A. (2004). Temperature and the expression of myogenic regulatory factors (MRFs) and myosin heavy chain isoforms during embryogenesis in the common carp Cyprinus carpio L. J Exp Biol *207*, 4239-4248.
Cole, S. E., Levorse, J. M., Tilghman, S. M., and Vogt, T. F. (2002). Clock regulatory elements control cyclic expression of Lunatic fringe during somitogenesis. Dev Cell *3*, 75-84.
Collier, J. R., McInerney, D., Schnell, S., Maini, P. K., Gavaghan, D. J., Houston, P., and Stern, C. D. (2000). A cell cycle model for somitogenesis: mathematical formulation and numerical simulation. J Theor Biol *207*, 305-316.
Collins, C. A., Olsen, I., Zammit, P. S., Heslop, L., Petrie, A., Partridge, T. A., and Morgan, J. E. (2005). Stem cell function, self-renewal, and behavioral heterogeneity of cells from the adult muscle satellite cell niche. Cell *122*, 289-301.
Conboy, I. M., Conboy, M. J., Smythe, G. M., and Rando, T. A. (2003). Notch-mediated restoration of regenerative potential to aged muscle. Science *302*, 1575-1577.
Conboy, M. J., Karasov, A. O., and Rando, T. A. (2007). High incidence of non-random template strand segregation and asymmetric fate determination in dividing stem cells and their progeny. PLoS Biol *5*, e102.
Cooke, J., and Zeeman, E. C. (1976). A clock and wavefront model for control of the number of repeated structures during animal morphogenesis. J Theor Biol *58*, 455-476.
Cornelison, D. D., Olwin, B. B., Rudnicki, M. A., and Wold, B. J. (2000). MyoD(-/-) satellite cells in single-fiber culture are differentiation defective and MRF4 deficient. Dev Biol *224*, 122-137.
Costa, M. L., Escaleira, R. C., Rodrigues, V. B., Manasfi, M., and Mermelstein, C. S. (2002). Some distinctive features of zebrafish myogenesis based on unexpected distributions of the muscle cytoskeletal proteins actin, myosin, desmin, alpha-actinin, troponin and titin. Mech Dev *116*, 95-104.

Cousins, J. C., Woodward, K. J., Gross, J. G., Partridge, T. A., and Morgan, J. E. (2004). Regeneration of skeletal muscle from transplanted immortalised myoblasts is oligoclonal. J Cell Sci *117*, 3259-3269.
Coutelle, O., Blagden, C. S., Hampson, R., Halai, C., Rigby, P. W., and Hughes, S. M. (2001). Hedgehog signalling is required for maintenance of myf5 and myoD expression and timely terminal differentiation in zebrafish adaxial myogenesis. Dev Biol *236*, 136-150.
Cowan, C. R., and Hyman, A. A. (2004). Asymmetric cell division in C. elegans: cortical polarity and spindle positioning. Annu Rev Cell Dev Biol *20*, 427-453.
Cui, X., Kerr, M. K., and Churchill, G. A. (2003). Transformations for cDNA microarray data. Stat Appl Genet Mol Biol *2*, Article4.
Curado, S., Anderson, R. M., Jungblut, B., Mumm, J., Schroeter, E., and Stainier, D. Y. (2007). Conditional targeted cell ablation in zebrafish: a new tool for regeneration studies. Dev Dyn *236*, 1025-1035.
Dale, J. K., Maroto, M., Dequeant, M. L., Malapert, P., McGrew, M., and Pourquie, O. (2003). Periodic notch inhibition by lunatic fringe underlies the chick segmentation clock. Nature *421*, 275-278.
Danpure, C. J., and Rumsby, G. (2004). Molecular aetiology of primary hyperoxaluria and its implications for clinical management. Expert Rev Mol Med *6*, 1-16.
Dastjerdi, A., Robson, L., Walker, R., Hadley, J., Zhang, Z., Rodriguez-Niedenfuhr, M., Ataliotis, P., Baldini, A., Scambler, P., and Francis-West, P. (2007). Tbx1 regulation of myogenic differentiation in the limb and cranial mesoderm. Dev Dyn *236*, 353-363.
Day, K., Shefer, G., Richardson, J. B., Enikolopov, G., and Yablonka-Reuveni, Z. (2007). Nestin-GFP reporter expression defines the quiescent state of skeletal muscle satellite cells. Dev Biol *304*, 246-259.
De Backer, F., Vandebrouck, C., Gailly, P., and Gillis, J. M. (2002). Long-term study of Ca(2+) homeostasis and of survival in collagenase-isolated muscle fibres from normal and mdx mice. J Physiol *542*, 855-865.
de Jong, J. L., and Zon, L. I. (2005). Use of the zebrafish system to study primitive and definitive hematopoiesis. Annu Rev Genet *39*, 481-501.
del Pozo, M. A., Balasubramanian, N., Alderson, N. B., Kiosses, W. B., Grande-Garcia, A., Anderson, R. G., and Schwartz, M. A. (2005). Phospho-caveolin-1 mediates integrin-regulated membrane domain internalization. Nat Cell Biol *7*, 901-908.
Delalande, J. M., and Rescan, P. Y. (1999). Differential expression of two nonallelic MyoD genes in developing and adult myotomal musculature of the trout (Oncorhynchus mykiss). Dev Genes Evol *209*, 432-437.
Dellavalle, A., Sampaolesi, M., Tonlorenzi, R., Tagliafico, E., Sacchetti, B., Perani, L., Innocenzi, A., Galvez, B. G., Messina, G., Morosetti, R.*, et al.* (2007). Pericytes of human skeletal muscle are myogenic precursors distinct from satellite cells. Nat Cell Biol *9*, 255-267.
Denetclaw, W. F., Jr., Berdougo, E., Venters, S. J., and Ordahl, C. P. (2001). Morphogenetic cell movements in the middle region of the dermomyotome dorsomedial lip associated with patterning and growth of the primary epaxial myotome. Development *128*, 1745-1755.
Denetclaw, W. F., Jr., Christ, B., and Ordahl, C. P. (1997). Location and growth of epaxial myotome precursor cells. Development *124*, 1601-1610.
Denetclaw, W. F., and Ordahl, C. P. (2000). The growth of the dermomyotome and formation of early myotome lineages in thoracolumbar somites of chicken embryos. Development *127*, 893-905.
Devoto, S. H., Melancon, E., Eisen, J. S., and Westerfield, M. (1996). Identification of separate slow and fast muscle precursor cells in vivo, prior to somite formation. Development *122*, 3371-3380.
Dhawan, J., and Rando, T. A. (2005). Stem cells in postnatal myogenesis: molecular mechanisms of satellite cell quiescence, activation and replenishment. Trends Cell Biol *15*, 666-673.
Dietrich, S., Schubert, F. R., Healy, C., Sharpe, P. T., and Lumsden, A. (1998). Specification of the hypaxial musculature. Development *125*, 2235-2249.

Dietrich, S., Schubert, F. R., and Lumsden, A. (1997). Control of dorsoventral pattern in the chick paraxial mesoderm. Development *124*, 3895-3908.
Dockter, J., and Ordahl, C. P. (2000). Dorsoventral axis determination in the somite: a re-examination. Development *127*, 2201-2206.
Dockter, J. L., and Ordahl, C. P. (1998). Determination of sclerotome to the cartilage fate. Development *125*, 2113-2124.
Doe, C. Q., and Bowerman, B. (2001). Asymmetric cell division: fly neuroblast meets worm zygote. Curr Opin Cell Biol *13*, 68-75.
Doetsch, F. (2003). A niche for adult neural stem cells. Curr Opin Genet Dev *13*, 543-550.
Dong, F., Sun, X., Liu, W., Ai, D., Klysik, E., Lu, M. F., Hadley, J., Antoni, L., Chen, L., Baldini, A.*, et al.* (2006). Pitx2 promotes development of splanchnic mesoderm-derived branchiomeric muscle. Development *133*, 4891-4899.
Doyon, Y., McCammon, J. M., Miller, J. C., Faraji, F., Ngo, C., Katibah, G. E., Amora, R., Hocking, T. D., Zhang, L., Rebar, E. J.*, et al.* (2008). Heritable targeted gene disruption in zebrafish using designed zinc-finger nucleases. Nat Biotechnol *26*, 702-708.
Draper, B. W., McCallum, C. M., Stout, J. L., Slade, A. J., and Moens, C. B. (2004). A high-throughput method for identifying N-ethyl-N-nitrosourea (ENU)-induced point mutations in zebrafish. Methods Cell Biol *77*, 91-112.
Draper, B. W., Stock, D. W., and Kimmel, C. B. (2003). Zebrafish fgf24 functions with fgf8 to promote posterior mesodermal development. Development *130*, 4639-4654.
Driever, W., and Fishman, M. C. (1996). The zebrafish: heritable disorders in transparent embryos. J Clin Invest *97*, 1788-1794.
Du, S. J., Devoto, S. H., Westerfield, M., and Moon, R. T. (1997). Positive and negative regulation of muscle cell identity by members of the hedgehog and TGF-beta gene families. J Cell Biol *139*, 145-156.
Dubrulle, J., McGrew, M. J., and Pourquie, O. (2001). FGF signaling controls somite boundary position and regulates segmentation clock control of spatiotemporal Hox gene activation. Cell *106*, 219-232.
Dubrulle, J., and Pourquie, O. (2004). fgf8 mRNA decay establishes a gradient that couples axial elongation to patterning in the vertebrate embryo. Nature *427*, 419-422.
Duncan, E. M., Muratore-Schroeder, T. L., Cook, R. G., Garcia, B. A., Shabanowitz, J., Hunt, D. F., and Allis, C. D. (2008). Cathepsin L proteolytically processes histone H3 during mouse embryonic stem cell differentiation. Cell *135*, 284-294.
Edmondson, D. G., and Olson, E. N. (1989). A gene with homology to the myc similarity region of MyoD1 is expressed during myogenesis and is sufficient to activate the muscle differentiation program. Genes Dev *3*, 628-640.
Emerson, C. P. (1990). Myogenesis and developmental control genes. Curr Opin Cell Biol *2*, 1065-1075.
Emery, A. E. (1991). Population frequencies of inherited neuromuscular diseases--a world survey. Neuromuscul Disord *1*, 19-29.
Epstein, J. A., Shapiro, D. N., Cheng, J., Lam, P. Y., and Maas, R. L. (1996). Pax3 modulates expression of the c-Met receptor during limb muscle development. Proc Natl Acad Sci U S A *93*, 4213-4218.
Ervasti, J. M., Ohlendieck, K., Kahl, S. D., Gaver, M. G., and Campbell, K. P. (1990). Deficiency of a glycoprotein component of the dystrophin complex in dystrophic muscle. Nature *345*, 315-319.
Esner, M., Meilhac, S. M., Relaix, F., Nicolas, J. F., Cossu, G., and Buckingham, M. E. (2006). Smooth muscle of the dorsal aorta shares a common clonal origin with skeletal muscle of the myotome. Development *133*, 737-749.
Etard, C., Behra, M., Fischer, N., Hutcheson, D., Geisler, R., and Strahle, U. (2007). The UCS factor Steif/Unc-45b interacts with the heat shock protein Hsp90a during myofibrillogenesis. Dev Biol *308*, 133-143.
Fan, C. M., Lee, C. S., and Tessier-Lavigne, M. (1997). A role for WNT proteins in induction of dermomyotome. Dev Biol *191*, 160-165.

Fan, C. M., Porter, J. A., Chiang, C., Chang, D. T., Beachy, P. A., and Tessier-Lavigne, M. (1995). Long-range sclerotome induction by sonic hedgehog: direct role of the amino-terminal cleavage product and modulation by the cyclic AMP signaling pathway. Cell *81*, 457-465.
Fan, C. M., and Tessier-Lavigne, M. (1994). Patterning of mammalian somites by surface ectoderm and notochord: evidence for sclerotome induction by a hedgehog homolog. Cell *79*, 1175-1186.
Fashena, D., and Westerfield, M. (1999). Secondary motoneuron axons localize DM-GRASP on their fasciculated segments. J Comp Neurol *406*, 415-424.
Feng, X., Adiarte, E. G., and Devoto, S. H. (2006). Hedgehog acts directly on the zebrafish dermomyotome to promote myogenic differentiation. Dev Biol *300*, 736-746.
Fielitz, J., Kim, M. S., Shelton, J. M., Latif, S., Spencer, J. A., Glass, D. J., Richardson, J. A., Bassel-Duby, R., and Olson, E. N. (2007a). Myosin accumulation and striated muscle myopathy result from the loss of muscle RING finger 1 and 3. J Clin Invest *117*, 2486-2495.
Fielitz, J., van Rooij, E., Spencer, J. A., Shelton, J. M., Latif, S., van der Nagel, R., Bezprozvannaya, S., de Windt, L., Richardson, J. A., Bassel-Duby, R., and Olson, E. N. (2007b). Loss of muscle-specific RING-finger 3 predisposes the heart to cardiac rupture after myocardial infarction. Proc Natl Acad Sci U S A *104*, 4377-4382.
Fisher, N. a. S., P (1985). Chi-plots for assessing dependence. Biometrica *72*, 253-265.
Fisher, N. a. S., P (2001). Graphical assessment of independence: is a picture worth 100 tests? Am Stat *55*, 233-239.
Flint, O. P., Ede, D. A., Wilby, O. K., and Proctor, J. (1978). Control of somite number in normal and amputated mutant mouse embryos: an experimental and a theoretical analysis. J Embryol Exp Morphol *45*, 189-202.
Forsberg, H., Crozet, F., and Brown, N. A. (1998). Waves of mouse Lunatic fringe expression, in four-hour cycles at two-hour intervals, precede somite boundary formation. Curr Biol *8*, 1027-1030.
Friedenstein, A. J., Piatetzky, S., II, and Petrakova, K. V. (1966). Osteogenesis in transplants of bone marrow cells. J Embryol Exp Morphol *16*, 381-390.
Fritz, A., Rozowski, M., Walker, C., and Westerfield, M. (1996). Identification of selected gamma-ray induced deficiencies in zebrafish using multiplex polymerase chain reaction. Genetics *144*, 1735-1745.
Fuchs, E., Tumbar, T., and Guasch, G. (2004). Socializing with the neighbors: stem cells and their niche. Cell *116*, 769-778.
Gajewski, M., Sieger, D., Alt, B., Leve, C., Hans, S., Wolff, C., Rohr, K. B., and Tautz, D. (2003). Anterior and posterior waves of cyclic her1 gene expression are differentially regulated in the presomitic mesoderm of zebrafish. Development *130*, 4269-4278.
Galloway, T. F., Kjorsvik, E., and Kryvi, H. (1999). Muscle growth and development in Atlantic cod larvae (Gadus morhua L.), related to different somatic growth rates. J Exp Biol *202*, 2111-2120.
Gayraud-Morel, B., Chretien, F., Flamant, P., Gomes, D., Zammit, P. S., and Tajbakhsh, S. (2007). A role for the myogenic determination gene Myf5 in adult regenerative myogenesis. Dev Biol *312*, 13-28.
Germanguz, I., Lev, D., Waisman, T., Kim, C. H., and Gitelman, I. (2007). Four twist genes in zebrafish, four expression patterns. Dev Dyn *236*, 2615-2626.
Gilboa, L., and Lehmann, R. (2006). Soma-germline interactions coordinate homeostasis and growth in the Drosophila gonad. Nature *443*, 97-100.
Giordani, J., Bajard, L., Demignon, J., Daubas, P., Buckingham, M., and Maire, P. (2007). Six proteins regulate the activation of Myf5 expression in embryonic mouse limbs. Proc Natl Acad Sci U S A *104*, 11310-11315.
Golding, J. P., Calderbank, E., Partridge, T. A., and Beauchamp, J. R. (2007). Skeletal muscle stem cells express anti-apoptotic ErbB receptors during activation from quiescence. Exp Cell Res *313*, 341-356.
Goldstein, B., and Hird, S. N. (1996). Specification of the anteroposterior axis in Caenorhabditis elegans. Development *122*, 1467-1474.

Golling, G., Amsterdam, A., Sun, Z., Antonelli, M., Maldonado, E., Chen, W., Burgess, S., Haldi, M., Artzt, K., Farrington, S.*, et al.* (2002). Insertional mutagenesis in zebrafish rapidly identifies genes essential for early vertebrate development. Nat Genet *31*, 135-140.
Goodell, M. A., Brose, K., Paradis, G., Conner, A. S., and Mulligan, R. C. (1996). Isolation and functional properties of murine hematopoietic stem cells that are replicating in vivo. J Exp Med *183*, 1797-1806.
Goodell, M. A., Rosenzweig, M., Kim, H., Marks, D. F., DeMaria, M., Paradis, G., Grupp, S. A., Sieff, C. A., Mulligan, R. C., and Johnson, R. P. (1997). Dye efflux studies suggest that hematopoietic stem cells expressing low or undetectable levels of CD34 antigen exist in multiple species. Nat Med *3*, 1337-1345.
Griffin, K. J., Amacher, S. L., Kimmel, C. B., and Kimelman, D. (1998). Molecular identification of spadetail: regulation of zebrafish trunk and tail mesoderm formation by T-box genes. Development *125*, 3379-3388.
Grifone, R., Demignon, J., Houbron, C., Souil, E., Niro, C., Seller, M. J., Hamard, G., and Maire, P. (2005). Six1 and Six4 homeoproteins are required for Pax3 and Mrf expression during myogenesis in the mouse embryo. Development *132*, 2235-2249.
Gros, J., Manceau, M., Thome, V., and Marcelle, C. (2005). A common somitic origin for embryonic muscle progenitors and satellite cells. Nature *435*, 954-958.
Gross, J. G., and Morgan, J. E. (1999). Muscle precursor cells injected into irradiated mdx mouse muscle persist after serial injury. Muscle Nerve *22*, 174-185.
Grounds, M. D., White, J. D., Rosenthal, N., and Bogoyevitch, M. A. (2002). The role of stem cells in skeletal and cardiac muscle repair. J Histochem Cytochem *50*, 589-610.
Groves, J. A., Hammond, C. L., and Hughes, S. M. (2005). Fgf8 drives myogenic progression of a novel lateral fast muscle fibre population in zebrafish. Development *132*, 4211-4222.
Gussoni, E., Soneoka, Y., Strickland, C. D., Buzney, E. A., Khan, M. K., Flint, A. F., Kunkel, L. M., and Mulligan, R. C. (1999). Dystrophin expression in the mdx mouse restored by stem cell transplantation. Nature *401*, 390-394.
Guyon, J. R., Kudryashova, E., Potts, A., Dalkilic, I., Brosius, M. A., Thompson, T. G., Beckmann, J. S., Kunkel, L. M., and Spencer, M. J. (2003). Calpain 3 cleaves filamin C and regulates its ability to interact with gamma- and delta-sarcoglycans. Muscle Nerve *28*, 472-483.
Hack, A. A., Lam, M. Y., Cordier, L., Shoturma, D. I., Ly, C. T., Hadhazy, M. A., Hadhazy, M. R., Sweeney, H. L., and McNally, E. M. (2000). Differential requirement for individual sarcoglycans and dystrophin in the assembly and function of the dystrophin-glycoprotein complex. J Cell Sci *113 (Pt 14)*, 2535-2544.
Haffter, P., Granato, M., Brand, M., Mullins, M. C., Hammerschmidt, M., Kane, D. A., Odenthal, J., van Eeden, F. J., Jiang, Y. J., Heisenberg, C. P.*, et al.* (1996). The identification of genes with unique and essential functions in the development of the zebrafish, Danio rerio. Development *123*, 1-36.
Haffter, P., and Nusslein-Volhard, C. (1996). Large scale genetics in a small vertebrate, the zebrafish. Int J Dev Biol *40*, 221-227.
Hall, T. E., Bryson-Richardson, R. J., Berger, S., Jacoby, A. S., Cole, N. J., Hollway, G. E., Berger, J., and Currie, P. D. (2007). The zebrafish candyfloss mutant implicates extracellular matrix adhesion failure in laminin alpha2-deficient congenital muscular dystrophy. Proc Natl Acad Sci U S A *104*, 7092-7097.
Halpern, M. E., Ho, R. K., Walker, C., and Kimmel, C. B. (1993). Induction of muscle pioneers and floor plate is distinguished by the zebrafish no tail mutation. Cell *75*, 99-111.
Hamade, A., Deries, M., Begemann, G., Bally-Cuif, L., Genet, C., Sabatier, F., Bonnieu, A., and Cousin, X. (2006). Retinoic acid activates myogenesis in vivo through Fgf8 signalling. Dev Biol *289*, 127-140.
Hammond, C. L., Hinits, Y., Osborn, D. P., Minchin, J. E., Tettamanti, G., and Hughes, S. M. (2007). Signals and myogenic regulatory factors restrict pax3 and pax7 expression to dermomyotome-like tissue in zebrafish. Dev Biol *302*, 504-521.

Hao, E., Tyrberg, B., Itkin-Ansari, P., Lakey, J. R., Geron, I., Monosov, E. Z., Barcova, M., Mercola, M., and Levine, F. (2006). Beta-cell differentiation from nonendocrine epithelial cells of the adult human pancreas. Nat Med *12*, 310-316.
Harburger, D. S., and Calderwood, D. A. (2009). Integrin signalling at a glance. J Cell Sci *122*, 159-163.
Hatta, K., Bremiller, R., Westerfield, M., and Kimmel, C. B. (1991). Diversity of expression of engrailed-like antigens in zebrafish. Development *112*, 821-832.
Hatta, K., Tsujii, H., and Omura, T. (2006). Cell tracking using a photoconvertible fluorescent protein. Nat Protoc *1*, 960-967.
Hawke, T. J., Atkinson, D. J., Kanatous, S. B., Van der Ven, P. F., Goetsch, S. C., and Garry, D. J. (2007). Xin, an actin binding protein, is expressed within muscle satellite cells and newly regenerated skeletal muscle fibers. Am J Physiol Cell Physiol *293*, C1636-1644.
Hay, E. D., and Fischman, D. A. (1961). Origin of the blastema in regenerating limbs of the newt Triturus viridescens. An autoradiographic study using tritiated thymidine to follow cell proliferation and migration. Dev Biol *3*, 26-59.
Hayashi, Y. K., Chou, F. L., Engvall, E., Ogawa, M., Matsuda, C., Hirabayashi, S., Yokochi, K., Ziober, B. L., Kramer, R. H., Kaufman, S. J.*, et al.* (1998). Mutations in the integrin alpha7 gene cause congenital myopathy. Nat Genet *19*, 94-97.
Heanue, T. A., Reshef, R., Davis, R. J., Mardon, G., Oliver, G., Tomarev, S., Lassar, A. B., and Tabin, C. J. (1999). Synergistic regulation of vertebrate muscle development by Dach2, Eya2, and Six1, homologs of genes required for Drosophila eye formation. Genes Dev *13*, 3231-3243.
Heasman, J. (2002). Morpholino oligos: making sense of antisense? Dev Biol *243*, 209-214.
Hemler, M. E. (2005). Tetraspanin functions and associated microdomains. Nat Rev Mol Cell Biol *6*, 801-811.
Henry, C. A., and Amacher, S. L. (2004). Zebrafish slow muscle cell migration induces a wave of fast muscle morphogenesis. Dev Cell *7*, 917-923.
Heslop, L., Beauchamp, J. R., Tajbakhsh, S., Buckingham, M. E., Partridge, T. A., and Zammit, P. S. (2001). Transplanted primary neonatal myoblasts can give rise to functional satellite cells as identified using the Myf5nlacZl+ mouse. Gene Ther *8*, 778-783.
Heydemann, A., Doherty, K. R., and McNally, E. M. (2007). Genetic modifiers of muscular dystrophy: implications for therapy. Biochim Biophys Acta *1772*, 216-228.
Heymann, S., Koudrova, M., Arnold, H., Koster, M., and Braun, T. (1996). Regulation and function of SF/HGF during migration of limb muscle precursor cells in chicken. Dev Biol *180*, 566-578.
Hill, A. J., Teraoka, H., Heideman, W., and Peterson, R. E. (2005). Zebrafish as a model vertebrate for investigating chemical toxicity. Toxicol Sci *86*, 6-19.
Hirsinger, E., Malapert, P., Dubrulle, J., Delfini, M. C., Duprez, D., Henrique, D., Ish-Horowicz, D., and Pourquie, O. (2001). Notch signalling acts in postmitotic avian myogenic cells to control MyoD activation. Development *128*, 107-116.
Hirsinger, E., Stellabotte, F., Devoto, S. H., and Westerfield, M. (2004). Hedgehog signaling is required for commitment but not initial induction of slow muscle precursors. Dev Biol *275*, 143-157.
Hitchcock, P. F., and Raymond, P. A. (2004). The teleost retina as a model for developmental and regeneration biology. Zebrafish *1*, 257-271.
Hoffman, E. P., Brown, R. H., and Kunkel, L. M. (1992). Dystrophin: the protein product of the Duchene muscular dystrophy locus. 1987. Biotechnology *24*, 457-466.
Hoffman, T. L., Javier, A. L., Campeau, S. A., Knight, R. D., and Schilling, T. F. (2007). Tfap2 transcription factors in zebrafish neural crest development and ectodermal evolution. J Exp Zoolog B Mol Dev Evol *308*, 679-691.
Holley, S. A., Geisler, R., and Nusslein-Volhard, C. (2000). Control of her1 expression during zebrafish somitogenesis by a delta-dependent oscillator and an independent wave-front activity. Genes Dev *14*, 1678-1690.

Hollway, G. E., Bryson-Richardson, R. J., Berger, S., Cole, N. J., Hall, T. E., and Currie, P. D. (2007). Whole-somite rotation generates muscle progenitor cell compartments in the developing zebrafish embryo. Dev Cell *12*, 207-219.
Hollway, G. E., and Currie, P. D. (2003). Myotome meanderings. Cellular morphogenesis and the making of muscle. EMBO Rep *4*, 855-860.
Hollway, G. E., Maule, J., Gautier, P., Evans, T. M., Keenan, D. G., Lohs, C., Fischer, D., Wicking, C., and Currie, P. D. (2006). Scube2 mediates Hedgehog signalling in the zebrafish embryo. Dev Biol *294*, 104-118.
Homma, S., Iwasaki, M., Shelton, G. D., Engvall, E., Reed, J. C., and Takayama, S. (2006). BAG3 deficiency results in fulminant myopathy and early lethality. Am J Pathol *169*, 761-773.
Huebsch, K. A., Kudryashova, E., Wooley, C. M., Sher, R. B., Seburn, K. L., Spencer, M. J., and Cox, G. A. (2005). Mdm muscular dystrophy: interactions with calpain 3 and a novel functional role for titin's N2A domain. Hum Mol Genet *14*, 2801-2811.
Huppert, S. S., Ilagan, M. X., De Strooper, B., and Kopan, R. (2005). Analysis of Notch function in presomitic mesoderm suggests a gamma-secretase-independent role for presenilins in somite differentiation. Dev Cell *8*, 677-688.
Huttner, W. B., and Kosodo, Y. (2005). Symmetric versus asymmetric cell division during neurogenesis in the developing vertebrate central nervous system. Curr Opin Cell Biol *17*, 648-657.
Ikeya, M., and Takada, S. (1998). Wnt signaling from the dorsal neural tube is required for the formation of the medial dermomyotome. Development *125*, 4969-4976.
Ingham, P. W., and Kim, H. R. (2005). Hedgehog signalling and the specification of muscle cell identity in the zebrafish embryo. Exp Cell Res *306*, 336-342.
Ingham, P. W., and McMahon, A. P. (2001). Hedgehog signaling in animal development: paradigms and principles. Genes Dev *15*, 3059-3087.
Ingham, P. W., and Placzek, M. (2006). Orchestrating ontogenesis: variations on a theme by sonic hedgehog. Nat Rev Genet *7*, 841-850.
Jarriault, S., Brou, C., Logeat, F., Schroeter, E. H., Kopan, R., and Israel, A. (1995). Signalling downstream of activated mammalian Notch. Nature *377*, 355-358.
Jiang, Y. J., Aerne, B. L., Smithers, L., Haddon, C., Ish-Horowicz, D., and Lewis, J. (2000). Notch signalling and the synchronization of the somite segmentation clock. Nature *408*, 475-479.
Johnson, R. L., Laufer, E., Riddle, R. D., and Tabin, C. (1994). Ectopic expression of Sonic hedgehog alters dorsal-ventral patterning of somites. Cell *79*, 1165-1173.
Jones, N. C., Tyner, K. J., Nibarger, L., Stanley, H. M., Cornelison, D. D., Fedorov, Y. V., and Olwin, B. B. (2005). The p38alpha/beta MAPK functions as a molecular switch to activate the quiescent satellite cell. J Cell Biol *169*, 105-116.
Joulia, D., Bernardi, H., Garandel, V., Rabenoelina, F., Vernus, B., and Cabello, G. (2003). Mechanisms involved in the inhibition of myoblast proliferation and differentiation by myostatin. Exp Cell Res *286*, 263-275.
Jouve, C., Palmeirim, I., Henrique, D., Beckers, J., Gossler, A., Ish-Horowicz, D., and Pourquie, O. (2000). Notch signalling is required for cyclic expression of the hairy-like gene HES1 in the presomitic mesoderm. Development *127*, 1421-1429.
Jung-Ching Lin, J., Gustafson-Wagner, E. A., Sinn, H. W., Choi, S., Jaacks, S. M., Wang, D. Z., Evans, S., and Li-Chun Lin, J. (2005). Structure, Expression, and Function of a Novel Intercalated Disc Protein, Xin. J Med Sci *25*, 215-222.
Kaestner, S. (1892). Ueber die allgemeine Entwicklung der Rumpf- und Schwanzmusculatur bei Wirbelthieren. Mit besonderer Beruecksichtigung der Selachier. Arch Anat Entwickelungsgesch *153–222*.
Kahane, N., Cinnamon, Y., Bachelet, I., and Kalcheim, C. (2001). The third wave of myotome colonization by mitotically competent progenitors: regulating the balance between differentiation and proliferation during muscle development. Development *128*, 2187-2198.

Kahane, N., Cinnamon, Y., and Kalcheim, C. (1998a). The cellular mechanism by which the dermomyotome contributes to the second wave of myotome development. Development *125*, 4259-4271.
Kahane, N., Cinnamon, Y., and Kalcheim, C. (1998b). The origin and fate of pioneer myotomal cells in the avian embryo. Mech Dev *74*, 59-73.
Kambadur, R., Sharma, M., Smith, T. P., and Bass, J. J. (1997). Mutations in myostatin (GDF8) in double-muscled Belgian Blue and Piedmontese cattle. Genome Res *7*, 910-916.
Karlstrom, R. O., Talbot, W. S., and Schier, A. F. (1999). Comparative synteny cloning of zebrafish you-too: mutations in the Hedgehog target gli2 affect ventral forebrain patterning. Genes Dev *13*, 388-393.
Karpowicz, P., Morshead, C., Kam, A., Jervis, E., Ramunas, J., Cheng, V., and van der Kooy, D. (2005). Support for the immortal strand hypothesis: neural stem cells partition DNA asymmetrically in vitro. J Cell Biol *170*, 721-732.
Kassar-Duchossoy, L., Gayraud-Morel, B., Gomes, D., Rocancourt, D., Buckingham, M., Shinin, V., and Tajbakhsh, S. (2004). Mrf4 determines skeletal muscle identity in Myf5:Myod double-mutant mice. Nature *431*, 466-471.
Kassar-Duchossoy, L., Giacone, E., Gayraud-Morel, B., Jory, A., Gomes, D., and Tajbakhsh, S. (2005). Pax3/Pax7 mark a novel population of primitive myogenic cells during development. Genes Dev *19*, 1426-1431.
Kawahira, H., Ma, N. H., Tzanakakis, E. S., McMahon, A. P., Chuang, P. T., and Hebrok, M. (2003). Combined activities of hedgehog signaling inhibitors regulate pancreas development. Development *130*, 4871-4879.
Kawakami, A., Nojima, Y., Toyoda, A., Takahoko, M., Satoh, M., Tanaka, H., Wada, H., Masai, I., Terasaki, H., Sakaki, Y*., et al.* (2005). The zebrafish-secreted matrix protein you/scube2 is implicated in long-range regulation of hedgehog signaling. Curr Biol *15*, 480-488.
Kawakami, K. (2007). Tol2: a versatile gene transfer vector in vertebrates. Genome Biol *8 Suppl 1*, S7.
Kawakami, K., Koga, A., Hori, H., and Shima, A. (1998). Excision of the tol2 transposable element of the medaka fish, Oryzias latipes, in zebrafish, Danio rerio. Gene *225*, 17-22.
Kawakami, K., and Shima, A. (1999). Identification of the Tol2 transposase of the medaka fish Oryzias latipes that catalyzes excision of a nonautonomous Tol2 element in zebrafish Danio rerio. Gene *240*, 239-244.
Kawakami, K., Shima, A., and Kawakami, N. (2000). Identification of a functional transposase of the Tol2 element, an Ac-like element from the Japanese medaka fish, and its transposition in the zebrafish germ lineage. Proc Natl Acad Sci U S A *97*, 11403-11408.
Kelly, R., Alonso, S., Tajbakhsh, S., Cossu, G., and Buckingham, M. (1995). Myosin light chain 3F regulatory sequences confer regionalized cardiac and skeletal muscle expression in transgenic mice. J Cell Biol *129*, 383-396.
Kelly, R. G., Jerome-Majewska, L. A., and Papaioannou, V. E. (2004). The del22q11.2 candidate gene Tbx1 regulates branchiomeric myogenesis. Hum Mol Genet *13*, 2829-2840.
Kerszberg, M., and Wolpert, L. (2000). A clock and trail model for somite formation, specialization and polarization. J Theor Biol *205*, 505-510.
Kidd, S., Lieber, T., and Young, M. W. (1998). Ligand-induced cleavage and regulation of nuclear entry of Notch in Drosophila melanogaster embryos. Genes Dev *12*, 3728-3740.
Kiel, M. J., He, S., Ashkenazi, R., Gentry, S. N., Teta, M., Kushner, J. A., Jackson, T. L., and Morrison, S. J. (2007). Haematopoietic stem cells do not asymmetrically segregate chromosomes or retain BrdU. Nature *449*, 238-242.
Kiger, A. A., Jones, D. L., Schulz, C., Rogers, M. B., and Fuller, M. T. (2001). Stem cell self-renewal specified by JAK-STAT activation in response to a support cell cue. Science *294*, 2542-2545.
Kimmel, C. B., Ballard, W. W., Kimmel, S. R., Ullmann, B., and Schilling, T. F. (1995). Stages of embryonic development of the zebrafish. Dev Dyn *203*, 253-310.
Kimmel, C. B., Hatta, K., and Eisen, J. S. (1991). Genetic control of primary neuronal development in zebrafish. Development *Suppl 2*, 47-57.

Kimmel, C. B., Kane, D. A., Walker, C., Warga, R. M., and Rothman, M. B. (1989). A mutation that changes cell movement and cell fate in the zebrafish embryo. Nature *337*, 358-362.
Kimmel, C. B., Warga, R. M., and Schilling, T. F. (1990). Origin and organization of the zebrafish fate map. Development *108*, 581-594.
Kmita, M., and Duboule, D. (2003). Organizing axes in time and space; 25 years of colinear tinkering. Science *301*, 331-333.
Koenig, M., Hoffman, E. P., Bertelson, C. J., Monaco, A. P., Feener, C., and Kunkel, L. M. (1987). Complete cloning of the Duchenne muscular dystrophy (DMD) cDNA and preliminary genomic organization of the DMD gene in normal and affected individuals. Cell *50*, 509-517.
Kopan, R., Schroeter, E. H., Weintraub, H., and Nye, J. S. (1996). Signal transduction by activated mNotch: importance of proteolytic processing and its regulation by the extracellular domain. Proc Natl Acad Sci U S A *93*, 1683-1688.
Kuang, S., Charge, S. B., Seale, P., Huh, M., and Rudnicki, M. A. (2006). Distinct roles for Pax7 and Pax3 in adult regenerative myogenesis. J Cell Biol *172*, 103-113.
Kuang, S., Gillespie, M. A., and Rudnicki, M. A. (2008). Niche regulation of muscle satellite cell self-renewal and differentiation. Cell Stem Cell *2*, 22-31.
Kuang, S., Kuroda, K., Le Grand, F., and Rudnicki, M. A. (2007). Asymmetric self-renewal and commitment of satellite stem cells in muscle. Cell *129*, 999-1010.
Kuang, S., and Rudnicki, M. A. (2008). The emerging biology of satellite cells and their therapeutic potential. Trends Mol Med *14*, 82-91.
Kumar, A., Velloso, C. P., Imokawa, Y., and Brockes, J. P. (2000). Plasticity of retrovirus-labelled myotubes in the newt limb regeneration blastema. Dev Biol *218*, 125-136.
Kuro-o, M., Matsumura, Y., Aizawa, H., Kawaguchi, H., Suga, T., Utsugi, T., Ohyama, Y., Kurabayashi, M., Kaname, T., Kume, E*., et al.* (1997). Mutation of the mouse klotho gene leads to a syndrome resembling ageing. Nature *390*, 45-51.
Laclef, C., Hamard, G., Demignon, J., Souil, E., Houbron, C., and Maire, P. (2003). Altered myogenesis in Six1-deficient mice. Development *130*, 2239-2252.
Langenau, D. M., Ferrando, A. A., Traver, D., Kutok, J. L., Hezel, J. P., Kanki, J. P., Zon, L. I., Look, A. T., and Trede, N. S. (2004). In vivo tracking of T cell development, ablation, and engraftment in transgenic zebrafish. Proc Natl Acad Sci U S A *101*, 7369-7374.
Langley, B., Thomas, M., Bishop, A., Sharma, M., Gilmour, S., and Kambadur, R. (2002). Myostatin inhibits myoblast differentiation by down-regulating MyoD expression. J Biol Chem *277*, 49831-49840.
Lansdorp, P. M. (2007). Immortal strands? Give me a break. Cell *129*, 1244-1247.
Le Grand, F., and Rudnicki, M. A. (2007). Skeletal muscle satellite cells and adult myogenesis. Curr Opin Cell Biol *19*, 628-633.
Lecourtois, M., and Schweisguth, F. (1998). Indirect evidence for Delta-dependent intracellular processing of notch in Drosophila embryos. Curr Biol *8*, 771-774.
Lee, C. S., Buttitta, L., and Fan, C. M. (2001). Evidence that the WNT-inducible growth arrest-specific gene 1 encodes an antagonist of sonic hedgehog signaling in the somite. Proc Natl Acad Sci U S A *98*, 11347-11352.
Lee, C. S., Buttitta, L. A., May, N. R., Kispert, A., and Fan, C. M. (2000). SHH-N upregulates Sfrp2 to mediate its competitive interaction with WNT1 and WNT4 in the somitic mesoderm. Development *127*, 109-118.
Leimeister, C., Dale, K., Fischer, A., Klamt, B., Hrabe de Angelis, M., Radtke, F., McGrew, M. J., Pourquie, O., and Gessler, M. (2000). Oscillating expression of c-Hey2 in the presomitic mesoderm suggests that the segmentation clock may use combinatorial signaling through multiple interacting bHLH factors. Dev Biol *227*, 91-103.
Lenhoff SG, L. H. (1986). Hydra and the birth of experimental biology, 1744: Abraham Trembley's Memoirs concerning the natural history of a type of freshwater polyp with arms shaped like horns. (Pacific Grove,
California: Boxwood Press).

Lepilina, A., Coon, A. N., Kikuchi, K., Holdway, J. E., Roberts, R. W., Burns, C. G., and Poss, K. D. (2006). A dynamic epicardial injury response supports progenitor cell activity during zebrafish heart regeneration. Cell *127*, 607-619.
Lewis, K. E., Concordet, J. P., and Ingham, P. W. (1999a). Characterisation of a second patched gene in the zebrafish Danio rerio and the differential response of patched genes to Hedgehog signalling. Dev Biol *208*, 14-29.
Lewis, K. E., Currie, P. D., Roy, S., Schauerte, H., Haffter, P., and Ingham, P. W. (1999b). Control of muscle cell-type specification in the zebrafish embryo by Hedgehog signalling. Dev Biol *216*, 469-480.
Li, J., Rao, H., Burkin, D., Kaufman, S. J., and Wu, C. (2003a). The muscle integrin binding protein (MIBP) interacts with alpha7beta1 integrin and regulates cell adhesion and laminin matrix deposition. Dev Biol *261*, 209-219.
Li, Y., Fenger, U., Niehrs, C., and Pollet, N. (2003b). Cyclic expression of esr9 gene in Xenopus presomitic mesoderm. Differentiation *71*, 83-89.
Li, Z., Mericskay, M., Agbulut, O., Butler-Browne, G., Carlsson, L., Thornell, L. E., Babinet, C., and Paulin, D. (1997). Desmin is essential for the tensile strength and integrity of myofibrils but not for myogenic commitment, differentiation, and fusion of skeletal muscle. J Cell Biol *139*, 129-144.
Lipton, B. H., and Schultz, E. (1979). Developmental fate of skeletal muscle satellite cells. Science *205*, 1292-1294.
Liu, H., Fergusson, M. M., Castilho, R. M., Liu, J., Cao, L., Chen, J., Malide, D., Rovira, II, Schimel, D., Kuo, C. J.*, et al.* (2007a). Augmented Wnt signaling in a mammalian model of accelerated aging. Science *317*, 803-806.
Liu, L., He, B., Liu, W. M., Zhou, D., Cox, J. V., and Zhang, X. A. (2007b). Tetraspanin CD151 promotes cell migration by regulating integrin trafficking. J Biol Chem *282*, 31631-31642.
Lo, D. C., Allen, F., and Brockes, J. P. (1993). Reversal of muscle differentiation during urodele limb regeneration. Proc Natl Acad Sci U S A *90*, 7230-7234.
Lopez-Onieva, L., Fernandez-Minan, A., and Gonzalez-Reyes, A. (2008). Jak/Stat signalling in niche support cells regulates dpp transcription to control germline stem cell maintenance in the Drosophila ovary. Development *135*, 533-540.
Lu, F. M., and Lux, S. E. (1996). Constitutively active human Notch1 binds to the transcription factor CBF1 and stimulates transcription through a promoter containing a CBF1-responsive element. Proc Natl Acad Sci U S A *93*, 5663-5667.
Lu, J., Webb, R., Richardson, J. A., and Olson, E. N. (1999). MyoR: a muscle-restricted basic helix-loop-helix transcription factor that antagonizes the actions of MyoD. Proc Natl Acad Sci U S A *96*, 552-557.
Lu, J. R., Bassel-Duby, R., Hawkins, A., Chang, P., Valdez, R., Wu, H., Gan, L., Shelton, J. M., Richardson, J. A., and Olson, E. N. (2002). Control of facial muscle development by MyoR and capsulin. Science *298*, 2378-2381.
Luo, R., An, M., Arduini, B. L., and Henion, P. D. (2001). Specific pan-neural crest expression of zebrafish Crestin throughout embryonic development. Dev Dyn *220*, 169-174.
Luz, M. A., Marques, M. J., and Santo Neto, H. (2002). Impaired regeneration of dystrophin-deficient muscle fibers is caused by exhaustion of myogenic cells. Braz J Med Biol Res *35*, 691-695.
MacRae, C. A., and Peterson, R. T. (2003). Zebrafish-based small molecule discovery. Chem Biol *10*, 901-908.
Marsh, J. L., and Theisen, H. (1999). Regeneration in insects. Semin Cell Dev Biol *10*, 365-375.
Mauro, A. (1961). Satellite cell of skeletal muscle fibers. J Biophys Biochem Cytol *9*, 493-495.
Mayer, U., Saher, G., Fassler, R., Bornemann, A., Echtermeyer, F., von der Mark, H., Miosge, N., Poschl, E., and von der Mark, K. (1997). Absence of integrin alpha 7 causes a novel form of muscular dystrophy. Nat Genet *17*, 318-323.

McClure, K. D., and Schubiger, G. (2007). Transdetermination: Drosophila imaginal disc cells exhibit stem cell-like potency. Int J Biochem Cell Biol *39*, 1105-1118.
McGrew, M. J., Dale, J. K., Fraboulet, S., and Pourquie, O. (1998). The lunatic fringe gene is a target of the molecular clock linked to somite segmentation in avian embryos. Curr Biol *8*, 979-982.
McKinnell, I. W., Ishibashi, J., Le Grand, F., Punch, V. G., Addicks, G. C., Greenblatt, J. F., Dilworth, F. J., and Rudnicki, M. A. (2008). Pax7 activates myogenic genes by recruitment of a histone methyltransferase complex. Nat Cell Biol *10*, 77-84.
McMahon, J. A., Takada, S., Zimmerman, L. B., Fan, C. M., Harland, R. M., and McMahon, A. P. (1998). Noggin-mediated antagonism of BMP signaling is required for growth and patterning of the neural tube and somite. Genes Dev *12*, 1438-1452.
McPherron, A. C., Lawler, A. M., and Lee, S. J. (1997). Regulation of skeletal muscle mass in mice by a new TGF-beta superfamily member. Nature *387*, 83-90.
McPherron, A. C., and Lee, S. J. (1997). Double muscling in cattle due to mutations in the myostatin gene. Proc Natl Acad Sci U S A *94*, 12457-12461.
Megeney, L. A., Kablar, B., Garrett, K., Anderson, J. E., and Rudnicki, M. A. (1996). MyoD is required for myogenic stem cell function in adult skeletal muscle. Genes Dev *10*, 1173-1183.
Meinhardt, H. (1986). Somites in Developing Embryos (eds Bellairs, R., Ede, D. A. & Lash, J. W.) In ((Plenum Publ. Corpl., USA, 1986).), pp. 179–191.
Mello, C. C., Draper, B. W., Krause, M., Weintraub, H., and Priess, J. R. (1992). The pie-1 and mex-1 genes and maternal control of blastomere identity in early C. elegans embryos. Cell *70*, 163-176.
Mello, C. C., Schubert, C., Draper, B., Zhang, W., Lobel, R., and Priess, J. R. (1996). The PIE-1 protein and germline specification in C. elegans embryos. Nature *382*, 710-712.
Meng, X., Noyes, M. B., Zhu, L. J., Lawson, N. D., and Wolfe, S. A. (2008). Targeted gene inactivation in zebrafish using engineered zinc-finger nucleases. Nat Biotechnol *26*, 695-701.
Meyer, A., and Schartl, M. (1999). Gene and genome duplications in vertebrates: the one-to-four (-to-eight in fish) rule and the evolution of novel gene functions. Curr Opin Cell Biol *11*, 699-704.
Miller, J. B., Teal, S. B., and Stockdale, F. E. (1989). Evolutionarily conserved sequences of striated muscle myosin heavy chain isoforms. Epitope mapping by cDNA expression. J Biol Chem *264*, 13122-13130.
Mokri, B., and Engel, A. G. (1975). Duchenne dystrophy: electron microscopic findings pointing to a basic or early abnormality in the plasma membrane of the muscle fiber. Neurology *25*, 1111-1120.
Molgo, J., Colasantei, C., Adams, D. S., and Jaimovich, E. (2004). IP3 receptors and Ca2+ signals in adult skeletal muscle satellite cells in situ. Biol Res *37*, 635-639.
Moloney, D. J., Panin, V. M., Johnston, S. H., Chen, J., Shao, L., Wilson, R., Wang, Y., Stanley, P., Irvine, K. D., Haltiwanger, R. S., and Vogt, T. F. (2000). Fringe is a glycosyltransferase that modifies Notch. Nature *406*, 369-375.
Montanaro, F., Liadaki, K., Volinski, J., Flint, A., and Kunkel, L. M. (2003). Skeletal muscle engraftment potential of adult mouse skin side population cells. Proc Natl Acad Sci U S A *100*, 9336-9341.
Montarras, D., Chelly, J., Bober, E., Arnold, H., Ott, M. O., Gros, F., and Pinset, C. (1991). Developmental patterns in the expression of Myf5, MyoD, myogenin, and MRF4 during myogenesis. New Biol *3*, 592-600.
Montarras, D., Morgan, J., Collins, C., Relaix, F., Zaffran, S., Cumano, A., Partridge, T., and Buckingham, M. (2005). Direct isolation of satellite cells for skeletal muscle regeneration. Science *309*, 2064-2067.
Morales, A. V., Yasuda, Y., and Ish-Horowicz, D. (2002). Periodic Lunatic fringe expression is controlled during segmentation by a cyclic transcriptional enhancer responsive to notch signaling. Dev Cell *3*, 63-74.
Morgan, J. E., Beauchamp, J. R., Pagel, C. N., Peckham, M., Ataliotis, P., Jat, P. S., Noble, M. D., Farmer, K., and Partridge, T. A. (1994). Myogenic cell lines derived from transgenic

mice carrying a thermolabile T antigen: a model system for the derivation of tissue-specific and mutation-specific cell lines. Dev Biol *162*, 486-498.
Morimoto, M., Takahashi, Y., Endo, M., and Saga, Y. (2005). The Mesp2 transcription factor establishes segmental borders by suppressing Notch activity. Nature *435*, 354-359.
Morin-Kensicki, E. M., and Eisen, J. S. (1997). Sclerotome development and peripheral nervous system segmentation in embryonic zebrafish. Development *124*, 159-167.
Morrison, S. J., Hemmati, H. D., Wandycz, A. M., and Weissman, I. L. (1995). The purification and characterization of fetal liver hematopoietic stem cells. Proc Natl Acad Sci U S A *92*, 10302-10306.
Mullins, M. C., Hammerschmidt, M., Haffter, P., and Nusslein-Volhard, C. (1994). Large-scale mutagenesis in the zebrafish: in search of genes controlling development in a vertebrate. Curr Biol *4*, 189-202.
Munsterberg, A. E., Kitajewski, J., Bumcrot, D. A., McMahon, A. P., and Lassar, A. B. (1995). Combinatorial signaling by Sonic hedgehog and Wnt family members induces myogenic bHLH gene expression in the somite. Genes Dev *9*, 2911-2922.
Munsterberg, A. E., and Lassar, A. B. (1995). Combinatorial signals from the neural tube, floor plate and notochord induce myogenic bHLH gene expression in the somite. Development *121*, 651-660.
Nagata, Y., Kobayashi, H., Umeda, M., Ohta, N., Kawashima, S., Zammit, P. S., and Matsuda, R. (2006a). Sphingomyelin levels in the plasma membrane correlate with the activation state of muscle satellite cells. J Histochem Cytochem *54*, 375-384.
Nagata, Y., Partridge, T. A., Matsuda, R., and Zammit, P. S. (2006b). Entry of muscle satellite cells into the cell cycle requires sphingolipid signaling. J Cell Biol *174*, 245-253.
Nagy, A., Rossant, J., Nagy, R., Abramow-Newerly, W., and Roder, J. C. (1993). Derivation of completely cell culture-derived mice from early-passage embryonic stem cells. Proc Natl Acad Sci U S A *90*, 8424-8428.
Nakano, Y., Kim, H. R., Kawakami, A., Roy, S., Schier, A. F., and Ingham, P. W. (2004). Inactivation of dispatched 1 by the chameleon mutation disrupts Hedgehog signalling in the zebrafish embryo. Dev Biol *269*, 381-392.
Nasevicius, A., and Ekker, S. C. (2000). Effective targeted gene 'knockdown' in zebrafish. Nat Genet *26*, 216-220.
Navarro, A., Anand-Apte, B., and Parat, M. O. (2004). A role for caveolae in cell migration. Faseb J *18*, 1801-1811.
Nienhaus, G. U., Nienhaus, K., Holzle, A., Ivanchenko, S., Renzi, F., Oswald, F., Wolff, M., Schmitt, F., Rocker, C., Vallone, B.*, et al.* (2006). Photoconvertible fluorescent protein EosFP: biophysical properties and cell biology applications. Photochem Photobiol *82*, 351-358.
Noctor, S. C., Martinez-Cerdeno, V., Ivic, L., and Kriegstein, A. R. (2004). Cortical neurons arise in symmetric and asymmetric division zones and migrate through specific phases. Nat Neurosci *7*, 136-144.
Nornes, S., Mikkola, I., Krauss, S., Delghandi, M., Perander, M., and Johansen, T. (1996). Zebrafish Pax9 encodes two proteins with distinct C-terminal transactivating domains of different potency negatively regulated by adjacent N-terminal sequences. J Biol Chem *271*, 26914-26923.
Norris, W., Neyt, C., Ingham, P. W., and Currie, P. D. (2000). Slow muscle induction by Hedgehog signalling in vitro. J Cell Sci *113 (Pt 15)*, 2695-2703.
Nystul, T., and Spradling, A. (2007). An epithelial niche in the Drosophila ovary undergoes long-range stem cell replacement. Cell Stem Cell *1*, 277-285.
Oates, A. C., and Ho, R. K. (2002). Hairy/E(spl)-related (Her) genes are central components of the segmentation oscillator and display redundancy with the Delta/Notch signaling pathway in the formation of anterior segmental boundaries in the zebrafish. Development *129*, 2929-2946.
Ochi, H., Pearson, B. J., Chuang, P. T., Hammerschmidt, M., and Westerfield, M. (2006). Hhip regulates zebrafish muscle development by both sequestering Hedgehog and modulating localization of Smoothened. Dev Biol *297*, 127-140.

Ochi, H., and Westerfield, M. (2007). Signaling networks that regulate muscle development: lessons from zebrafish. Dev Growth Differ *49*, 1-11.
Ogino, H., Satou, W., Fujii, M., Suzuki, T., He, Y., Michishita, E., and Ayusawa, D. (2002). The human MYOD1 transgene is suppressed by 5-bromodeoxyuridine in mouse myoblasts. J Biochem *132*, 953-959.
Ohlstein, B., and Spradling, A. (2007). Multipotent Drosophila intestinal stem cells specify daughter cell fates by differential notch signaling. Science *315*, 988-992.
Olguin, H. C., and Olwin, B. B. (2004). Pax-7 up-regulation inhibits myogenesis and cell cycle progression in satellite cells: a potential mechanism for self-renewal. Dev Biol *275*, 375-388.
Olguin, H. C., Yang, Z., Tapscott, S. J., and Olwin, B. B. (2007). Reciprocal inhibition between Pax7 and muscle regulatory factors modulates myogenic cell fate determination. J Cell Biol *177*, 769-779.
Olivera-Martinez, I., Coltey, M., Dhouailly, D., and Pourquie, O. (2000). Mediolateral somitic origin of ribs and dermis determined by quail-chick chimeras. Development *127*, 4611-4617.
Olivera-Martinez, I., Thelu, J., Teillet, M. A., and Dhouailly, D. (2001). Dorsal dermis development depends on a signal from the dorsal neural tube, which can be substituted by Wnt-1. Mech Dev *100*, 233-244.
Ordahl, C. P., Berdougo, E., Venters, S. J., and Denetclaw, W. F., Jr. (2001). The dermomyotome dorsomedial lip drives growth and morphogenesis of both the primary myotome and dermomyotome epithelium. Development *128*, 1731-1744.
Ordahl, C. P., and Le Douarin, N. M. (1992). Two myogenic lineages within the developing somite. Development *114*, 339-353.
Ozawa, E., Yoshida, M., Suzuki, A., Mizuno, Y., Hagiwara, Y., and Noguchi, S. (1995). Dystrophin-associated proteins in muscular dystrophy. Hum Mol Genet *4*, 1711-1716.
Pacholsky, D., Vakeel, P., Himmel, M., Lowe, T., Stradal, T., Rottner, K., Furst, D. O., and van der Ven, P. F. (2004). Xin repeats define a novel actin-binding motif. J Cell Sci *117*, 5257-5268.
Pallas, P. (1766). Miscellanea zoologica, quibus novae imprimis atque obscurae animalium species describuntur et observationibus iconibusque illustrantur. . . :. Hagae Comitum, apud Pterum van Cleef
Palmeirim, I., Henrique, D., Ish-Horowicz, D., and Pourquie, O. (1997). Avian hairy gene expression identifies a molecular clock linked to vertebrate segmentation and somitogenesis. Cell *91*, 639-648.
Panin, V. M., Papayannopoulos, V., Wilson, R., and Irvine, K. D. (1997). Fringe modulates Notch-ligand interactions. Nature *387*, 908-912.
Parker, M. H., Seale, P., and Rudnicki, M. A. (2003). Looking back to the embryo: defining transcriptional networks in adult myogenesis. Nat Rev Genet *4*, 497-507.
Partridge, T. A., Morgan, J. E., Coulton, G. R., Hoffman, E. P., and Kunkel, L. M. (1989). Conversion of mdx myofibres from dystrophin-negative to -positive by injection of normal myoblasts. Nature *337*, 176-179.
Peck AL, t. (1965). Historia Animalium. Vol 1. Cambridge: Harvard University Press.
Pereira, E. F., Hilmas, C., Santos, M. D., Alkondon, M., Maelicke, A., and Albuquerque, E. X. (2002). Unconventional ligands and modulators of nicotinic receptors. J Neurobiol *53*, 479-500.
Pestronk, A., Parhad, I. M., Drachman, D. B., and Price, D. L. (1982). Membrane myopathy: morphological similarities to Duchenne muscular dystrophy. Muscle Nerve *5*, 209-214.
Pisconti, A., Brunelli, S., Di Padova, M., De Palma, C., Deponti, D., Baesso, S., Sartorelli, V., Cossu, G., and Clementi, E. (2006). Follistatin induction by nitric oxide through cyclic GMP: a tightly regulated signaling pathway that controls myoblast fusion. J Cell Biol *172*, 233-244.
Polezhaev, A. A. (1992). A mathematical model of the mechanism of vertebrate somitic segmentation. J Theor Biol *156*, 169-181.
Poss, K. D., Keating, M. T., and Nechiporuk, A. (2003). Tales of regeneration in zebrafish. Dev Dyn *226*, 202-210.

Pourquie, O., Coltey, M., Teillet, M. A., Ordahl, C., and Le Douarin, N. M. (1993). Control of dorsoventral patterning of somitic derivatives by notochord and floor plate. Proc Natl Acad Sci U S A *90*, 5242-5246.
Pourquie, O., Fan, C. M., Coltey, M., Hirsinger, E., Watanabe, Y., Breant, C., Francis-West, P., Brickell, P., Tessier-Lavigne, M., and Le Douarin, N. M. (1996). Lateral and axial signals involved in avian somite patterning: a role for BMP4. Cell *84*, 461-471.
Price, F. D., Kuroda, K., and Rudnicki, M. A. (2007). Stem cell based therapies to treat muscular dystrophy. Biochim Biophys Acta *1772*, 272-283.
Prockop, D. J. (1997). Marrow stromal cells as stem cells for nonhematopoietic tissues. Science *276*, 71-74.
Ramirez-Zarzosa, G., Gil, F., Vazquez, J. M., Arencibia, A., Latorre, R., Lopez-Albors, O., Ortega, A., and Moreno, F. (1998). The post-larval development of lateral musculature in gilthead sea bream Sparus aurata (L.) and sea bass Dicentrarchus labrax (L.). Anat Histol Embryol *27*, 21-29.
Rando, T. A., Disatnik, M. H., Yu, Y., and Franco, A. (1998). Muscle cells from mdx mice have an increased susceptibility to oxidative stress. Neuromuscul Disord *8*, 14-21.
Ratajczak, M. Z., Majka, M., Kucia, M., Drukala, J., Pietrzkowski, Z., Peiper, S., and Janowska-Wieczorek, A. (2003). Expression of functional CXCR4 by muscle satellite cells and secretion of SDF-1 by muscle-derived fibroblasts is associated with the presence of both muscle progenitors in bone marrow and hematopoietic stem/progenitor cells in muscles. Stem Cells *21*, 363-371.
Raya, A., Consiglio, A., Kawakami, Y., Rodriguez-Esteban, C., and Izpisua-Belmonte, J. C. (2004). The zebrafish as a model of heart regeneration. Cloning Stem Cells *6*, 345-351.
Réaumur, R. (1712). Sur les diverses reproductions qui se font dans les écrevisses, les omars, les crabes, etc. et entr'autres sur celles de leurs jambes et de leurs écailles. Mém Acad Roy Sci, 223–245.
Reese, K. J., Dunn, M. A., Waddle, J. A., and Seydoux, G. (2000). Asymmetric segregation of PIE-1 in C. elegans is mediated by two complementary mechanisms that act through separate PIE-1 protein domains. Mol Cell *6*, 445-455.
Reimschussel, R. (2001). A fish model of renal regeneration and development. Ilar J *42*, 285-291.
Relaix, F., Montarras, D., Zaffran, S., Gayraud-Morel, B., Rocancourt, D., Tajbakhsh, S., Mansouri, A., Cumano, A., and Buckingham, M. (2006). Pax3 and Pax7 have distinct and overlapping functions in adult muscle progenitor cells. J Cell Biol *172*, 91-102.
Relaix, F., Polimeni, M., Rocancourt, D., Ponzetto, C., Schafer, B. W., and Buckingham, M. (2003). The transcriptional activator PAX3-FKHR rescues the defects of Pax3 mutant mice but induces a myogenic gain-of-function phenotype with ligand-independent activation of Met signaling in vivo. Genes Dev *17*, 2950-2965.
Relaix, F., Rocancourt, D., Mansouri, A., and Buckingham, M. (2005). A Pax3/Pax7-dependent population of skeletal muscle progenitor cells. Nature *435*, 948-953.
Rios, R., Carneiro, I., Arce, V. M., and Devesa, J. (2002). Myostatin is an inhibitor of myogenic differentiation. Am J Physiol Cell Physiol *282*, C993-999.
Robert, V., Massimino, M. L., Tosello, V., Marsault, R., Cantini, M., Sorrentino, V., and Pozzan, T. (2001). Alteration in calcium handling at the subcellular level in mdx myotubes. J Biol Chem *276*, 4647-4651.
Robu, M. E., Larson, J. D., Nasevicius, A., Beiraghi, S., Brenner, C., Farber, S. A., and Ekker, S. C. (2007). p53 activation by knockdown technologies. PLoS Genet *3*, e78.
Rodaway, A., Takeda, H., Koshida, S., Broadbent, J., Price, B., Smith, J. C., Patient, R., and Holder, N. (1999). Induction of the mesendoderm in the zebrafish germ ring by yolk cell-derived TGF-beta family signals and discrimination of mesoderm and endoderm by FGF. Development *126*, 3067-3078.
Rossant, J. (2008). Stem cells and early lineage development. Cell *132*, 527-531.
Rowlerson A, V. A., ed. (2001). Cellular mechanisms of post-embryonic muscle growth in aquaculture species. (San Diego: Academic Press).

Roy, S., Wolff, C., and Ingham, P. W. (2001). The u-boot mutation identifies a Hedgehog-regulated myogenic switch for fiber-type diversification in the zebrafish embryo. Genes Dev *15*, 1563-1576.
Rudnicki, M. A., Schnegelsberg, P. N., Stead, R. H., Braun, T., Arnold, H. H., and Jaenisch, R. (1993). MyoD or Myf-5 is required for the formation of skeletal muscle. Cell *75*, 1351-1359.
Sabourin, L. A., Girgis-Gabardo, A., Seale, P., Asakura, A., and Rudnicki, M. A. (1999). Reduced differentiation potential of primary MyoD-/- myogenic cells derived from adult skeletal muscle. J Cell Biol *144*, 631-643.
Sacco, A., Doyonnas, R., Kraft, P., Vitorovic, S., and Blau, H. M. (2008). Self-renewal and expansion of single transplanted muscle stem cells. Nature.
Sadeh, M., Czyewski, K., and Stern, L. Z. (1985). Chronic myopathy induced by repeated bupivacaine injections. J Neurol Sci *67*, 229-238.
Sambrook, J. a. R. D. (2001). Molecular Cloning: A Laboratory Manual (Third Edition)).
Sampaolesi, M., Blot, S., D'Antona, G., Granger, N., Tonlorenzi, R., Innocenzi, A., Mognol, P., Thibaud, J. L., Galvez, B. G., Barthelemy, I.*, et al.* (2006). Mesoangioblast stem cells ameliorate muscle function in dystrophic dogs. Nature *444*, 574-579.
Sampaolesi, M., Torrente, Y., Innocenzi, A., Tonlorenzi, R., D'Antona, G., Pellegrino, M. A., Barresi, R., Bresolin, N., De Angelis, M. G., Campbell, K. P.*, et al.* (2003). Cell therapy of alpha-sarcoglycan null dystrophic mice through intra-arterial delivery of mesoangioblasts. Science *301*, 487-492.
Sanchez Alvarado, A., and Tsonis, P. A. (2006). Bridging the regeneration gap: genetic insights from diverse animal models. Nat Rev Genet *7*, 873-884.
Sawada, A., Shinya, M., Jiang, Y. J., Kawakami, A., Kuroiwa, A., and Takeda, H. (2001). Fgf/MAPK signalling is a crucial positional cue in somite boundary formation. Development *128*, 4873-4880.
Scaal, M., and Christ, B. (2004). Formation and differentiation of the avian dermomyotome. Anat Embryol (Berl) *208*, 411-424.
Schauerte, H. E., van Eeden, F. J., Fricke, C., Odenthal, J., Strahle, U., and Haffter, P. (1998). Sonic hedgehog is not required for the induction of medial floor plate cells in the zebrafish. Development *125*, 2983-2993.
Schier, A. F., and Talbot, W. S. (2005). Molecular genetics of axis formation in zebrafish. Annu Rev Genet *39*, 561-613.
Schubert, W., Sotgia, F., Cohen, A. W., Capozza, F., Bonuccelli, G., Bruno, C., Minetti, C., Bonilla, E., Dimauro, S., and Lisanti, M. P. (2007). Caveolin-1(-/-)- and caveolin-2(-/-)-deficient mice both display numerous skeletal muscle abnormalities, with tubular aggregate formation. Am J Pathol *170*, 316-333.
Seale, P., Sabourin, L. A., Girgis-Gabardo, A., Mansouri, A., Gruss, P., and Rudnicki, M. A. (2000). Pax7 is required for the specification of myogenic satellite cells. Cell *102*, 777-786.
Sekimizu, K., Nishioka, N., Sasaki, H., Takeda, H., Karlstrom, R. O., and Kawakami, A. (2004). The zebrafish iguana locus encodes Dzip1, a novel zinc-finger protein required for proper regulation of Hedgehog signaling. Development *131*, 2521-2532.
Selcen, D., Muntoni, F., Burton, B. K., Pegoraro, E., Sewry, C., Bite, A. V., and Engel, A. G. (2009). Mutation in BAG3 causes severe dominant childhood muscular dystrophy. Ann Neurol *65*, 83-89.
Shefer, G., Van de Mark, D. P., Richardson, J. B., and Yablonka-Reuveni, Z. (2006). Satellite-cell pool size does matter: defining the myogenic potency of aging skeletal muscle. Dev Biol *294*, 50-66.
Shimada, M., Yokosawa, H., and Kawahara, H. (2006). OMA-1 is a P granules-associated protein that is required for germline specification in Caenorhabditis elegans embryos. Genes Cells *11*, 383-396.
Shin, J., Park, H. C., Topczewska, J. M., Mawdsley, D. J., and Appel, B. (2003). Neural cell fate analysis in zebrafish using olig2 BAC transgenics. Methods Cell Sci *25*, 7-14.

Shinin, V., Gayraud-Morel, B., Gomes, D., and Tajbakhsh, S. (2006). Asymmetric division and cosegregation of template DNA strands in adult muscle satellite cells. Nat Cell Biol *8*, 677-687.
Sieger, D., Tautz, D., and Gajewski, M. (2003). The role of Suppressor of Hairless in Notch mediated signalling during zebrafish somitogenesis. Mech Dev *120*, 1083-1094.
Sinn, H. W., Balsamo, J., Lilien, J., and Lin, J. J. (2002). Localization of the novel Xin protein to the adherens junction complex in cardiac and skeletal muscle during development. Dev Dyn *225*, 1-13.
Smith, G. H. (2005). Label-retaining epithelial cells in mouse mammary gland divide asymmetrically and retain their template DNA strands. Development *132*, 681-687.
Smythe, G. M., Davies, M. J., Paulin, D., and Grounds, M. D. (2001). Absence of desmin slightly prolongs myoblast proliferation and delays fusion in vivo in regenerating grafts of skeletal muscle. Cell Tissue Res *304*, 287-294.
Solnica-Krezel, L., Schier, A. F., and Driever, W. (1994). Efficient recovery of ENU-induced mutations from the zebrafish germline. Genetics *136*, 1401-1420.
Solter, D. (2006). From teratocarcinomas to embryonic stem cells and beyond: a history of embryonic stem cell research. Nat Rev Genet *7*, 319-327.
Song, X., Wong, M. D., Kawase, E., Xi, R., Ding, B. C., McCarthy, J. J., and Xie, T. (2004). Bmp signals from niche cells directly repress transcription of a differentiation-promoting gene, bag of marbles, in germline stem cells in the Drosophila ovary. Development *131*, 1353-1364.
Spallanzani, L. (1769). Prodromo di un opera da imprimersi sopra la riproduzioni animali (An essay on animal reproduction). London: T Becket & de Hondt.
Spana, E. P., Kopczynski, C., Goodman, C. S., and Doe, C. Q. (1995). Asymmetric localization of numb autonomously determines sibling neuron identity in the Drosophila CNS. Development *121*, 3489-3494.
Spence, M. S., Yip, J., and Erickson, C. A. (1996). The dorsal neural tube organizes the dermamyotome and induces axial myocytes in the avian embryo. Development *122*, 231-241.
Spradling, A., Drummond-Barbosa, D., and Kai, T. (2001). Stem cells find their niche. Nature *414*, 98-104.
Steinbacher, P., Haslett, J. R., Obermayer, A., Marschallinger, J., Bauer, H. C., Sanger, A. M., and Stoiber, W. (2007). MyoD and Myogenin expression during myogenic phases in brown trout: a precocious onset of mosaic hyperplasia is a prerequisite for fast somatic growth. Dev Dyn *236*, 1106-1114.
Steinbacher, P., Haslett, J. R., Six, M., Gollmann, H. P., Sanger, A. M., and Stoiber, W. (2006). Phases of myogenic cell activation and possible role of dermomyotome cells in teleost muscle formation. Dev Dyn *235*, 3132-3143.
Stellabotte, F., and Devoto, S. H. (2007). The teleost dermomyotome. Dev Dyn *236*, 2432-2443.
Stellabotte, F., Dobbs-McAuliffe, B., Fernandez, D. A., Feng, X., and Devoto, S. H. (2007). Dynamic somite cell rearrangements lead to distinct waves of myotome growth. Development *134*, 1253-1257.
Stickney, H. L., Barresi, M. J., and Devoto, S. H. (2000). Somite development in zebrafish. Dev Dyn *219*, 287-303.
Stoick-Cooper, C. L., Weidinger, G., Riehle, K. J., Hubbert, C., Major, M. B., Fausto, N., and Moon, R. T. (2007). Distinct Wnt signaling pathways have opposing roles in appendage regeneration. Development *134*, 479-489.
Straub, V., Donahue, K. M., Allamand, V., Davisson, R. L., Kim, Y. R., and Campbell, K. P. (2000). Contrast agent-enhanced magnetic resonance imaging of skeletal muscle damage in animal models of muscular dystrophy. Magn Reson Med *44*, 655-659.
Stromblad, S., Fotedar, A., Brickner, H., Theesfeld, C., Aguilar de Diaz, E., Friedlander, M., and Cheresh, D. A. (2002). Loss of p53 compensates for alpha v-integrin function in retinal neovascularization. J Biol Chem *277*, 13371-13374.
Strome, S. (2005). Specification of the germ line. WormBook, 1-10.

Strome, S., and Wood, W. B. (1983). Generation of asymmetry and segregation of germ-line granules in early C. elegans embryos. Cell *35*, 15-25.
Struhl, G., and Adachi, A. (1998). Nuclear access and action of notch in vivo. Cell *93*, 649-660.
Tajbakhsh, S., and Buckingham, M. (2000). The birth of muscle progenitor cells in the mouse: spatiotemporal considerations. Curr Top Dev Biol *48*, 225-268.
Tajbakhsh, S., Rocancourt, D., Cossu, G., and Buckingham, M. (1997). Redefining the genetic hierarchies controlling skeletal myogenesis: Pax-3 and Myf-5 act upstream of MyoD. Cell *89*, 127-138.
Takayama, S., Xie, Z., and Reed, J. C. (1999). An evolutionarily conserved family of Hsp70/Hsc70 molecular chaperone regulators. J Biol Chem *274*, 781-786.
Takke, C., and Campos-Ortega, J. A. (1999). her1, a zebrafish pair-rule like gene, acts downstream of notch signalling to control somite development. Development *126*, 3005-3014.
Tallafuss, A., and Eisen, J. S. (2008). The Met receptor tyrosine kinase prevents zebrafish primary motoneurons from expressing an incorrect neurotransmitter. Neural Develop *3*, 18.
Tatsumi, R., Liu, X., Pulido, A., Morales, M., Sakata, T., Dial, S., Hattori, A., Ikeuchi, Y., and Allen, R. E. (2006). Satellite cell activation in stretched skeletal muscle and the role of nitric oxide and hepatocyte growth factor. Am J Physiol Cell Physiol *290*, C1487-1494.
Taupin, P., and Gage, F. H. (2002). Adult neurogenesis and neural stem cells of the central nervous system in mammals. J Neurosci Res *69*, 745-749.
Temple, G. K., Cole, N. J., and Johnston, I. A. (2001). Embryonic temperature and the relative timing of muscle-specific genes during development in herring (Clupea harengus L.). J Exp Biol *204*, 3629-3637.
Tennyson, C. N., Klamut, H. J., and Worton, R. G. (1995). The human dystrophin gene requires 16 hours to be transcribed and is cotranscriptionally spliced. Nat Genet *9*, 184-190.
Tombolini, R. U., A; Davey, M E; de Bruijn, F J; Jansson, J K (1997). Flow cytometric and microscopic analysis of GFP-tagged Pseudomonas fluorescens bacteria. FEMS Microbiol Ecol *22*, 17–28.
Tosney, K. W., Dehnbostel, D. B., and Erickson, C. A. (1994). Neural crest cells prefer the myotome's basal lamina over the sclerotome as a substratum. Dev Biol *163*, 389-406.
Traver, D., Paw, B. H., Poss, K. D., Penberthy, W. T., Lin, S., and Zon, L. I. (2003). Transplantation and in vivo imaging of multilineage engraftment in zebrafish bloodless mutants. Nat Immunol *4*, 1238-1246.
Treier, M., O'Connell, S., Gleiberman, A., Price, J., Szeto, D. P., Burgess, R., Chuang, P. T., McMahon, A. P., and Rosenfeld, M. G. (2001). Hedgehog signaling is required for pituitary gland development. Development *128*, 377-386.
Troyanskaya, O., Cantor, M., Sherlock, G., Brown, P., Hastie, T., Tibshirani, R., Botstein, D., and Altman, R. B. (2001). Missing value estimation methods for DNA microarrays. Bioinformatics *17*, 520-525.
Tsutsui, H., Karasawa, S., Shimizu, H., Nukina, N., and Miyawaki, A. (2005). Semi-rational engineering of a coral fluorescent protein into an efficient highlighter. EMBO Rep *6*, 233-238.
Tulina, N., and Matunis, E. (2001). Control of stem cell self-renewal in Drosophila spermatogenesis by JAK-STAT signaling. Science *294*, 2546-2549.
Turner, P. R., Fong, P. Y., Denetclaw, W. F., and Steinhardt, R. A. (1991). Increased calcium influx in dystrophic muscle. J Cell Biol *115*, 1701-1712.
Urasaki, A., Morvan, G., and Kawakami, K. (2006). Functional dissection of the Tol2 transposable element identified the minimal cis-sequence and a highly repetitive sequence in the subterminal region essential for transposition. Genetics *174*, 639-649.
Ustanina, S., Carvajal, J., Rigby, P., and Braun, T. (2007). The myogenic factor Myf5 supports efficient skeletal muscle regeneration by enabling transient myoblast amplification. Stem Cells *25*, 2006-2016.

van der Ven, P. F., Ehler, E., Vakeel, P., Eulitz, S., Schenk, J. A., Milting, H., Micheel, B., and Furst, D. O. (2006). Unusual splicing events result in distinct Xin isoforms that associate differentially with filamin c and Mena/VASP. Exp Cell Res *312*, 2154-2167.
van Eeden, F. J., Granato, M., Schach, U., Brand, M., Furutani-Seiki, M., Haffter, P., Hammerschmidt, M., Heisenberg, C. P., Jiang, Y. J., Kane, D. A.*, et al.* (1996). Mutations affecting somite formation and patterning in the zebrafish, Danio rerio. Development *123*, 153-164.
van Raamsdonk, W., van't Veer, L., Veeken, K., Heyting, C., and Pool, C. W. (1982). Differentiation of muscle fiber types in the teleost Brachydanio rerio, the zebrafish. Posthatching development. Anat Embryol (Berl) *164*, 51-62.
Vandebrouck, A., Ducret, T., Basset, O., Sebille, S., Raymond, G., Ruegg, U., Gailly, P., Cognard, C., and Constantin, B. (2006). Regulation of store-operated calcium entries and mitochondrial uptake by minidystrophin expression in cultured myotubes. Faseb J *20*, 136-138.
Vasyutina, E., and Birchmeier, C. (2006). The development of migrating muscle precursor cells. Anat Embryol (Berl) *211 Suppl 1*, 37-41.
Veggetti, A., Mascarello, F., Scapolo, P. A., and Rowlerson, A. (1990). Hyperplastic and hypertrophic growth of lateral muscle in Dicentrarchus labrax (L.). An ultrastructural and morphometric study. Anat Embryol (Berl) *182*, 1-10.
Volff, J. N., and Schartl, M. (2003). Evolution of signal transduction by gene and genome duplication in fish. J Struct Funct Genomics *3*, 139-150.
Volonte, D., Liu, Y., and Galbiati, F. (2005). The modulation of caveolin-1 expression controls satellite cell activation during muscle repair. Faseb J *19*, 237-239.
von Hofsten, J., Elworthy, S., Gilchrist, M. J., Smith, J. C., Wardle, F. C., and Ingham, P. W. (2008). Prdm1- and Sox6-mediated transcriptional repression specifies muscle fibre type in the zebrafish embryo. EMBO Rep *9*, 683-689.
Wagner, J., Schmidt, C., Nikowits, W., Jr., and Christ, B. (2000). Compartmentalization of the somite and myogenesis in chick embryos are influenced by wnt expression. Dev Biol *228*, 86-94.
Wagner, K. R. (2002). Genetic diseases of muscle. Neurol Clin *20*, 645-678.
Wagner, K. R., Fleckenstein, J. L., Amato, A. A., Barohn, R. J., Bushby, K., Escolar, D. M., Flanigan, K. M., Pestronk, A., Tawil, R., Wolfe, G. I.*, et al.* (2008). A phase I/IItrial of MYO-029 in adult subjects with muscular dystrophy. Ann Neurol *63*, 561-571.
Wahl, M. B., Deng, C., Lewandoski, M., and Pourquie, O. (2007). FGF signaling acts upstream of the NOTCH and WNT signaling pathways to control segmentation clock oscillations in mouse somitogenesis. Development *134*, 4033-4041.
Wallace, G. Q., and McNally, E. M. (2008). Mechanisms of Muscle Degeneration, Regeneration, and Repair in the Muscular Dystrophies. Annu Rev Physiol.
Wallace, H., Maden, M., and Wallace, B. M. (1974). Participation of cartilage grafts in amphibian limb regeneration. J Embryol Exp Morphol *32*, 391-404.
Wang, D. Z., Hu, X., Lin, J. L., Kitten, G. T., Solursh, M., and Lin, J. J. (1996). Differential displaying of mRNAs from the atrioventricular region of developing chicken hearts at stages 15 and 21. Front Biosci *1*, a1-15.
Wang, D. Z., Reiter, R. S., Lin, J. L., Wang, Q., Williams, H. S., Krob, S. L., Schultheiss, T. M., Evans, S., and Lin, J. J. (1999). Requirement of a novel gene, Xin, in cardiac morphogenesis. Development *126*, 1281-1294.
Warren, G. L., Summan, M., Gao, X., Chapman, R., Hulderman, T., and Simeonova, P. P. (2007). Mechanisms of skeletal muscle injury and repair revealed by gene expression studies in mouse models. J Physiol *582*, 825-841.
Waterman, R. E. (1969). Development of the lateral musculature in the teleost, Brachydanio rerio: a fine structural study. Am J Anat *125*, 457-493.
Watterson, R. L., Fowler, I., and Fowler, B. J. (1954). The role of the neural tube and notochord in development of the axial skeleton of the chick. Am J Anat *95*, 337-399.

Weinberg, E. S., Allende, M. L., Kelly, C. S., Abdelhamid, A., Murakami, T., Andermann, P., Doerre, O. G., Grunwald, D. J., and Riggleman, B. (1996). Developmental regulation of zebrafish MyoD in wild-type, no tail and spadetail embryos. Development *122*, 271-280.
Wellik, D. M. (2007). Hox patterning of the vertebrate axial skeleton. Dev Dyn *236*, 2454-2463.
Westerfield, M. (2000). The zebrafish book. A guide for the laboratory
use of zebrafish (Danio rerio), 4th ed. edn: Eugene: University of Oregon Press.).
Westhusin, M. (1997). From mighty mice to mighty cows. Nat Genet *17*, 4-5.
Whitfield, T. T., Granato, M., van Eeden, F. J., Schach, U., Brand, M., Furutani-Seiki, M., Haffter, P., Hammerschmidt, M., Heisenberg, C. P., Jiang, Y. J*., et al.* (1996). Mutations affecting development of the zebrafish inner ear and lateral line. Development *123*, 241-254.
Widmann JJ , F. H. (1975). The regenerative response of Kupffer cells and endothelial cells after partial hepactomy. In: Lesch R, Reutter W. editors. Liver regeneration after experimental injury. (New York: Stratton Intercontinental Medical Book Corp.).
Williams, B. A., and Ordahl, C. P. (1997). Emergence of determined myotome precursor cells in the somite. Development *124*, 4983-4997.
Wilm, T. P., and Solnica-Krezel, L. (2005). Essential roles of a zebrafish prdm1/blimp1 homolog in embryo patterning and organogenesis. Development *132*, 393-404.
Wolff, C., Roy, S., and Ingham, P. W. (2003). Multiple muscle cell identities induced by distinct levels and timing of hedgehog activity in the zebrafish embryo. Curr Biol *13*, 1169-1181.
Wolff, C., Roy, S., Lewis, K. E., Schauerte, H., Joerg-Rauch, G., Kirn, A., Weiler, C., Geisler, R., Haffter, P., and Ingham, P. W. (2004). iguana encodes a novel zinc-finger protein with coiled-coil domains essential for Hedgehog signal transduction in the zebrafish embryo. Genes Dev *18*, 1565-1576.
Wolpert, L., Hicklin, J., and Hornbruch, A. (1971). Positional information and pattern regulation in regeneration of hydra. Symp Soc Exp Biol *25*, 391-415.
Woods, I. G., and Talbot, W. S. (2005). The you gene encodes an EGF-CUB protein essential for Hedgehog signaling in zebrafish. PLoS Biol *3*, e66.
Wozniak, A. C., and Anderson, J. E. (2007). Nitric oxide-dependence of satellite stem cell activation and quiescence on normal skeletal muscle fibers. Dev Dyn *236*, 240-250.
Wright, W. E., Sassoon, D. A., and Lin, V. K. (1989). Myogenin, a factor regulating myogenesis, has a domain homologous to MyoD. Cell *56*, 607-617.
Wyttenbach, A., Sauvageot, O., Carmichael, J., Diaz-Latoud, C., Arrigo, A. P., and Rubinsztein, D. C. (2002). Heat shock protein 27 prevents cellular polyglutamine toxicity and suppresses the increase of reactive oxygen species caused by huntingtin. Hum Mol Genet *11*, 1137-1151.
Xie, T., and Spradling, A. C. (2000). A niche maintaining germ line stem cells in the Drosophila ovary. Science *290*, 328-330.
Yamada, M., Tamura, Y., Sanzen, N., Sato-Nishiuchi, R., Hasegawa, H., Ashman, L. K., Rubinstein, E., Yanez-Mo, M., Sanchez-Madrid, F., and Sekiguchi, K. (2008). Probing the interaction of tetraspanin CD151 with integrin alpha 3 beta 1 using a panel of monoclonal antibodies with distinct reactivities toward the CD151-integrin alpha 3 beta 1 complex. Biochem J *415*, 417-427.
Yamashita, Y. M., Fuller, M. T., and Jones, D. L. (2005). Signaling in stem cell niches: lessons from the Drosophila germline. J Cell Sci *118*, 665-672.
Yamashita, Y. M., Mahowald, A. P., Perlin, J. R., and Fuller, M. T. (2007). Asymmetric inheritance of mother versus daughter centrosome in stem cell division. Science *315*, 518-521.
Yang, L., Kemadjou, J. R., Zinsmeister, C., Bauer, M., Legradi, J., Muller, F., Pankratz, M., Jakel, J., and Strahle, U. (2007). Transcriptional profiling reveals barcode-like toxicogenomic responses in the zebrafish embryo. Genome Biol *8*, R227.
Yang, X. H., Richardson, A. L., Torres-Arzayus, M. I., Zhou, P., Sharma, C., Kazarov, A. R., Andzelm, M. M., Strominger, J. L., Brown, M., and Hemler, M. E. (2008). CD151 accelerates

breast cancer by regulating alpha 6 integrin function, signaling, and molecular organization. Cancer Res *68*, 3204-3213.
Yang, X. M., Vogan, K., Gros, P., and Park, M. (1996). Expression of the met receptor tyrosine kinase in muscle progenitor cells in somites and limbs is absent in Splotch mice. Development *122*, 2163-2171.
Yang, Y. H., Dudoit, S., Luu, P., Lin, D. M., Peng, V., Ngai, J., and Speed, T. P. (2002). Normalization for cDNA microarray data: a robust composite method addressing single and multiple slide systematic variation. Nucleic Acids Res *30*, e15.
Yao, S. N., and Kurachi, K. (1993). Implanted myoblasts not only fuse with myofibers but also survive as muscle precursor cells. J Cell Sci *105 (Pt 4)*, 957-963.
Yoshida, M., Suzuki, A., Yamamoto, H., Noguchi, S., Mizuno, Y., and Ozawa, E. (1994). Dissociation of the complex of dystrophin and its associated proteins into several unique groups by n-octyl beta-D-glucoside. Eur J Biochem *222*, 1055-1061.
Yoshida, S., Nabeshima, Y., and Nakagawa, T. (2007a). Stem cell heterogeneity: actual and potential stem cell compartments in mouse spermatogenesis. Ann N Y Acad Sci *1120*, 47-58.
Yoshida, S., Sukeno, M., and Nabeshima, Y. (2007b). A vasculature-associated niche for undifferentiated spermatogonia in the mouse testis. Science *317*, 1722-1726.
Zammit, P. S., Golding, J. P., Nagata, Y., Hudon, V., Partridge, T. A., and Beauchamp, J. R. (2004). Muscle satellite cells adopt divergent fates: a mechanism for self-renewal? J Cell Biol *166*, 347-357.
Zammit, P. S., Heslop, L., Hudon, V., Rosenblatt, J. D., Tajbakhsh, S., Buckingham, M. E., Beauchamp, J. R., and Partridge, T. A. (2002). Kinetics of myoblast proliferation show that resident satellite cells are competent to fully regenerate skeletal muscle fibers. Exp Cell Res *281*, 39-49.
Zammit, P. S., Partridge, T. A., and Yablonka-Reuveni, Z. (2006). The skeletal muscle satellite cell: the stem cell that came in from the cold. J Histochem Cytochem *54*, 1177-1191.
Zon, L. I., and Peterson, R. T. (2005). In vivo drug discovery in the zebrafish. Nat Rev Drug Discov *4*, 35-44.